8-2016

The Development of Polyurethane-based Solid-to-Solid Phase Change Materials for Thermal Energy Storage Applications

Claire Kway Poh
Clemson University

THE DEVELOPMENT OF POLYURETHANE-BASED SOLID-TO-SOLID PHASE CHANGE MATERIALS FOR THERMAL ENENRGY STORAGE APPLICATIONS

A Dissertation
Presented to
the Graduate School of
Clemson University

In Partial Fulfillment
of the Requirements for the Degree
Doctor of Philosophy
Materials Science and Engineering

---

by
Claire Kway Poh
August 2016

Accepted by:

Dr. Philip J. Brown
Dr. Olin Thompson Mefford, IV
Dr. Vincent Blouin
Dr. William Pennington

ABSTRACT

This work investigated and characterized the structure-property relationship of a polyurethane-based block copolymer and the thermal energy storage properties obtained through the solid-to-solid phase transition of a PCM polyol polymer that undergoes a thermal transition at low temperatures. The chemical and physical factors that influence or dictated the microphase separation between the urethane "hard" segment block and the polyol "soft" segment block of conventional polyurethanes how the resulting changes in phase morphology effects the crystallization behavior of the "soft" component, which in this dissertation is analogous to the PCM polymer component was analyzed. The urethane HS group behaves as a cross-link and restricts PCM polymer chain mobility, thereby the PCM can no longer translate freely and instead exhibits a solid-to-solid phase transition. The introduction of HS cross-link exhibits a behavior known as the HS chain-end effect, in which HS constrictions cause the PCM polymer to become partially crystalline. The extent to which PCM crystallization is limited by the HS chain end effect can vary depending on HS structural factors, such molecular architecture and HS composition. The HS chain end effect was quantified for the following HS structural variables; HS cross-link nature, diisocyanate molecular geometry, HS chain length to characterize and compare how each factor limits PEG PCM polymer crystallization. By doing so in a systematic manner, the optimal configuration for an effective PU-SSPCM can be determined. To examine HS cross-link nature, an analogous linear and a non-linear PU-SSPCM polymer, were compared to determine differences in final thermal

energy storage properties. The effects of diisocyanate molecular geometry was investigated by comparing the thermal energy storage properties of a series of PU-SSPCMs varied only by its diisocyanate component. The considered diisocyanates were selected based on specific structural moieties that affect the structural regularity, rigidity, and symmetry of the HS. The chain length of the hard segment component influence on thermal energy storage properties was also investigated by varying the proportions of urethane HS concentration and PCM polymer concentrations. HS cross-link nature, the HS diisocyanate component, and HS chain length are considered chemical level factors since they can be controlled during synthesis. On the physical level, the possibility of a connection between the degree of phase separation and thermal energy storage properties were explored. This relationship was investigated by measuring thermal energy storage properties of PU-SSPCMs with a high, medium, and low degree of phase separation. Varying HS crystallization by cooling rates from a homogeneous melt state was used to obtain different levels of phase separation.

Thermal energy storage properties were measured using Differential Scanning Calorimetry experiments. Supplemental information about the chemical structure of the synthesized polyurethane-based solid-to-solid phase change materials (PU-SSPCM) was analyzed by FTIR analysis techniques. The phase morphology and the degree of phase separation prevalent in the prepared samples was characterized by FTIR, TGA, and DSC techniques.

DEDICATION

This work is dedicated to my family, friends and co-workers, without whom I would never have come this far.

To my mom, Cecile Chenault Poh, for the support and encouragement you have provided through all the years. Without you, I would never have had the confidence necessary to achieve my goals.

To my dogs, Hobie and Pippa, for the ability to relax and laugh at my struggles and enjoy the perspective of those who have been where I am and those who have seen so much more.

To my friends and lab mates, for allowing me to vent, being understanding and sharing the incredible journey that is Graduate School. You made this process not only more enjoyable, but also more entertaining and livable.

ACKNOWLEDGEMENTS

First off, a special thank you to my advisor Dr. Brown and to Dr. Mefford. Also a big thank you to Kate Stevens, Joel Barden and Eliza Allen for helping me with my defense. Justin and Nicole for their encouragement and support. My mom and my dogs Pippa and Hobie.

List of Abbreviations

PCM - phase change material

SSPCM - solid-to-solid phase change material

PU-SSPCM - polyurethane-based solid-to-solid Phase Change Materials

HS - hard segment

SS - soft segment

PU - polyurethane

TES - Thermal energy storage

PEG - Poly(ethylene glycol) Mn= {2000, 3000, 6000 g/mol}

BDO - 1,4-Butane Diol

HMDI 1,6-Diisocyanatohexane

DIDD 1,12-Diisocyanatododecane

PDI 1,4-Phenylene Diisocyanate

TDI 2,4-Tolylene Diisocyanate

BICH 1,3-Bis(isocyanatomethyl)cyclohexane

MDI 4,4'-Methylenebis(phenyl isocyanate

TABLE OF CONTENTS

LIST OF TABLES

LIST OF FIGURES

Chapter 1 INTRODUCTION

A phase change material is a substance that undergoes a reversible change of state with the capacity to store a significant amount of heat per unit volume, while maintaining a constant temperature.[1-3] Unlike conventional sensible heat storage materials such as water or rocks, PCMs are a "latent" heat storage (LHS) and can store 15 times more thermal energy per unit volume without changing temperate.[4] The mechanism by which PCM exhibit latent heat storage properties is illustrated in Figure 1.1.

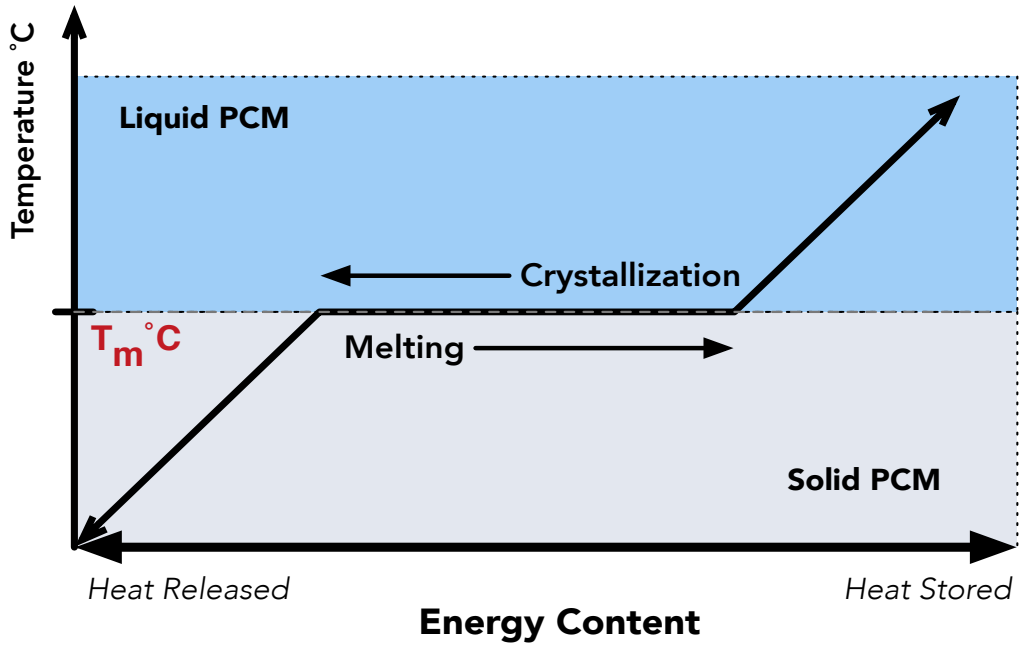

Figure 1.1: The phase change mechanism that facilitates latent heat storage properties

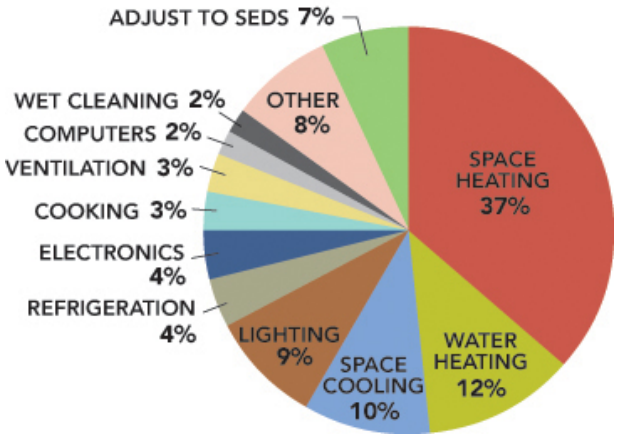

Figure 1.2: Building Site Energy Consumption by end use (Source: EIA, Annual Energy Outlook 2012 and Appendix 2010 U.S. Buildings Energy End-Use Splits, by Fuel Type (Quadrillion Btu)[13] (see Appendix I for data)

PCMs' unique properties have been harnessed for a wide array of applications that require temperature regulation functionality and energy storage; such applications include textiles[5-7], electronic devices[8], greenhouses[9] and solar panel systems [10]

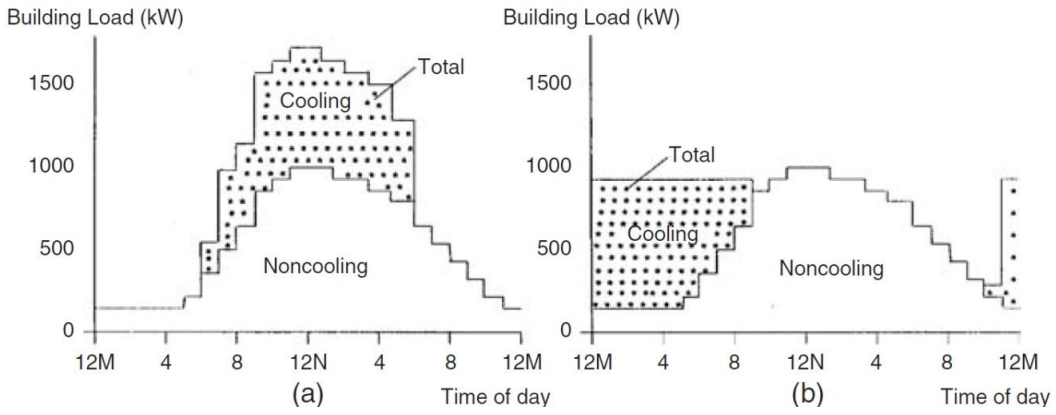

Figure 1.3: (a) Case with PCM TES system (b) Case with no PCM TES system (Source: Niraj 2014; Reprinted with permissions from Clemson University. July 7, 2016.

It is vitally indispensable that modern society conserve and reduce our reliance on oil. The way we manage natural resources now could have irremediable repercussions in the future. The building sector leads the world in energy consumption, accounting for 40% of global primary energy consumption.[11,12]The integration of Phase Change Materials (PCMs) into building envelopes has been found to be an effective method for improving thermal mass. According to Figure 1.2, almost 50% of the energy consumed by buildings is attributed to space conditioning.[13] Figure 1.4 shows two cases; one for buildings that utilized PCM thermal energy storage (TES) properties and one that did not. It can be seen that a reduction peak-hour cooling loads and shifting peak demand times was observed for the case with PCM.[14] Therefore, this study shows that utilizing PCM in building systems can significantly improve building energy efficiency and reduce energy consumption.[15]

PCM-enhanced building materials improve the thermal mass of a building material, without needing additional material and thus are an advantage over conventional

materials. is ad the ability to reduce energy consumption for space conditioning and reduce peak load, improvement of occupant comfort, compatibility with traditional technologies, and potential for applications in retrofit projects.[16] Preliminary studies have identified the potential energy-savings of integrating solid-liquid PCM (SLPCM) in building materials such as bricks, wall-board, flooring,[1,4,15,17-19] which is why interest in developing enhanced-PCM building materials technology has accelerated over the last decade.[4,15]

Issues with solid-liquid PCM

Phase change materials are classified according to their phase transition; a solid-solid PCM (SSPCM) or solid-liquid PCM (SLPCM).[3,10,20,21,16] The majority of PCM field application testing in buildings have focused on solid-liquid PCM (SLPCM). The biggest issue with SLPCM is that it needs a secondary container to prevent leaking and contamination problems. If the PCM leaks or contaminates its surroundings, it will no longer be effective.[10,16] Microencapsulation methods are commonly used to mitigate this problem. Recently, a life cycle analysis study shows microencapsulated PCMs are infeasible energy saving devices and have a payback of 7 years.[22] As a result, there has been growing interest in polymer-based PCMs that exhibit a solid-to-solid phase transition.

1.2. SOLID-TO-SOLID PCM

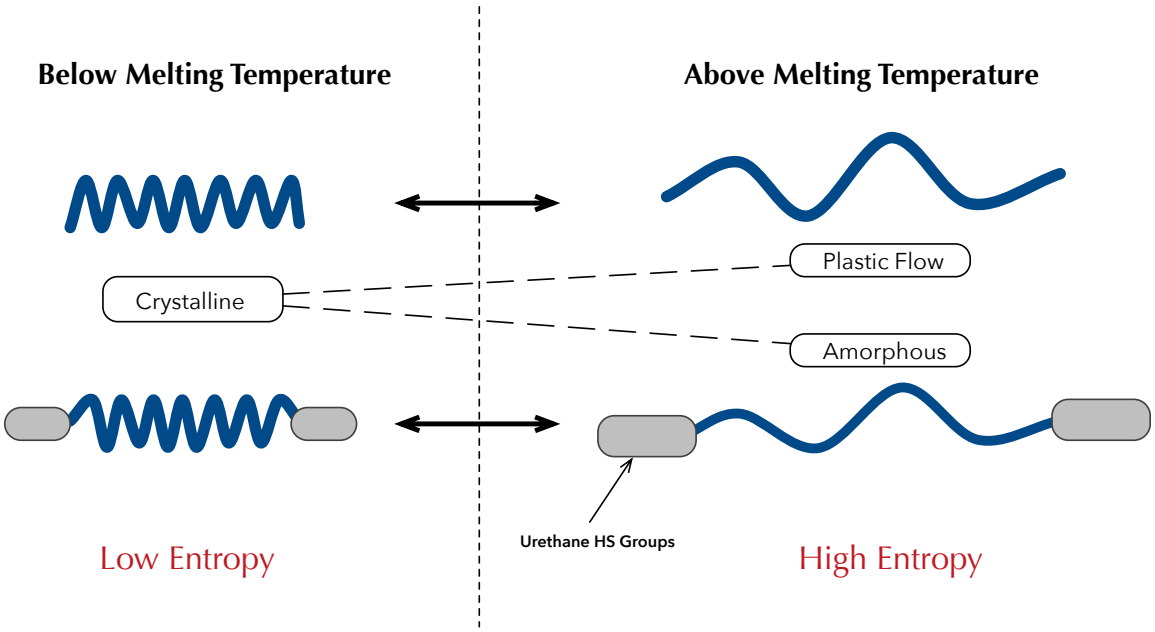

Figure 1.4: Solid-to-Solid Phase Transition Mechanism that demonstrates latent heat storage properties due to changes in entropy.

Solid-to-Solid PCM (SSPCM) store or deliver thermal energy by means of a solid-to-solid phase transition and do not generate liquid or gases.[10,21] SSPCMs are favored over traditional solid-liquid PCMs (SLPCMs) because they maintain a solid framework throughout their phase transition.[10,16,21] Therefore, unlike solid-liquid PCMs, SSPCMs do not require a secondary containment device. Instead SSPCMs can be directly incorporated into or processed in a series with a secondary material of any arbitrary shape.[23] As a result, SSPCMs are associated with simpler fabrication steps[24] and lower initial manufacturing costs,[25] implying lower embodied energy, which is more beneficial for overall primary energy consumption on a global scale. For these reasons, a faction of authors have focused their attention on developing novel types of solid-to-solid PCMs for thermal energy storage applications.[24,26-29]

The essential configuration of polymer-based SSPCMs consists of a typical solid-liquid PCM polymer that is covalently bonded to a secondary thermally labile structure.[20] The attachment to the HS prevents the dissolution of the PCM polymer so it can no longer translate freely.[30,31] As a result, the PCM polymer remains in the amorphous state and exhibits TES properties as it transitions between a crystalline and amorphous state. The entropic change between a crystalline "ordered" state to a "disordered" amorphous state facilitates the storage and release of thermal energy. This dynamic behavior is illustrated in Figure 1.4. This behavior can be vaguely represented by the Gibbs free energy equation $\Delta G=\Delta H-T\Delta S$; at equilibrium $\Delta G=0$, $\Delta H=-T\Delta S$, ΔH is enthalpy of fusion, T is temperature, and ΔS is change in entropy.[32] It can be seen that an increase in ΔS will lead to an increase in ΔH. The introduction of the HS cross-link responsible for the solid-to-solid phase transition. Consequently, the PCM polymer becomes only semi-crystalline.[31,33] The mobility of the PCM polymer chain segments in the vicinity of the HS cross-links are restricted.[26]. As a result the central portion of the PCM polymer chain demonstrates greater chain mobility than the other portion of the PCM polymer chain. The middle portion can undergo vibrational and rotational motion, which is enough chain mobility for neighboring polymer chains to align, orient to form a PCM crystalline structure.[30 31,33]

Polyurethane-based solid-to-solid PCMs

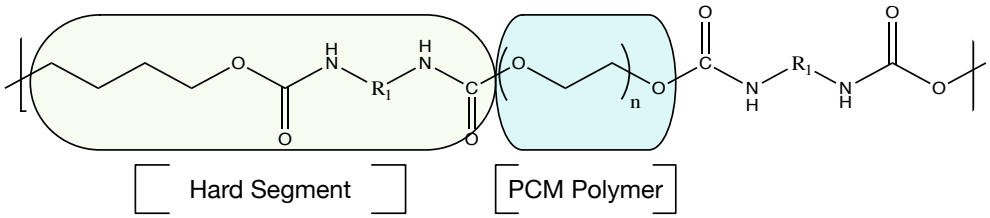

Figure 1.5: PU-SSPCM Primary Chain structure and the Hard Segment and PCM Polymer Components

Earlier studies have presented a variety of novel types of polymer-based SSPCMs (pSSPCMs). Recently, polyurethane-based SSPCMs (PU-SSPCMs) have attracted a great deal of attention as a more viable option for commercial use as an energy saving device. In a PU-SSPCMs urethane groups are used to restrict the chain movement of the PCM polymer. In conventional polyurethanes (PUs), the urethane group is referred to as the "hard" segment (HS) domain because it is rigid and demonstrates a thermal transition at elevated temperatures.[35] Meanwhile, the polyol component is called the “soft” segment (SS) and demonstrates a thermal transition at low temperatures. PU-SSPCMs are analogous to conventional segmented polyurethane (SPU) materials in terms of structure. For the purpose of this dissertation the "soft" segment (SS), is equivalent to and referred to as the PCM polymer, and the urethane group is referred to as the HS. Figure 1.5 shows the primary chain structure of a PU-SSPCM and the HS and PCM polymer components. It is assumed that the chain movement of the PCM polymer ultimately dictates heat storage properties, since chain mobility determines the crystallization behavior of the soft segment chain in the segmented polyurethane elastomer. At the HS urethane group cross-linking is introduced. The HS cross-link is responsible for maintaining the solid framework as the PCM polymer undergoes its phase transition.[26,30,31]

Table 1.1 Criteria for practical PCM

General Criteria of PCM for Effective Thermal Energy Storage Systems			
Thermal Properties	Physical Properties	Kinetic Properties	Chemical Properties
Good Heat Transfer (thermal conductivity)	Manageable phase transition	No Super-cooling	Long-term Stability
High Latent Heat of Fusion, Enthalpy, ΔH (J/g)	High Density	Crystallization	Compatible with Construction Materials
Phase-transition temperature PTT) matches operating conditions	Small Volume Change	Uniform Melting and Crystallization Behavior	Non-toxic
	Non-volatile		Non-Hazard
			Flame Resistant

Table 1.1 lists the criteria for the phase change characteristics for effective PCMs in building applications. Thus far, an assortment of PU-SSPCM compositions have been presented that demonstrate a broad range of enthalpy values and phase transition temperatures. Consequently, the structure-property relationship for PU-SSPCMs is ill-defined and it is hard to ascertain what structure would give rise to desired phase change characteristics listed in 1.1. It has been noticed that the the phase transition temperature can be lowered to ambient temperatures by lowering the PEG molecular weight [25,31,34] Consequently, lower molecular weight also leads to a less thermal energy storage capacity.

The Chain end effect

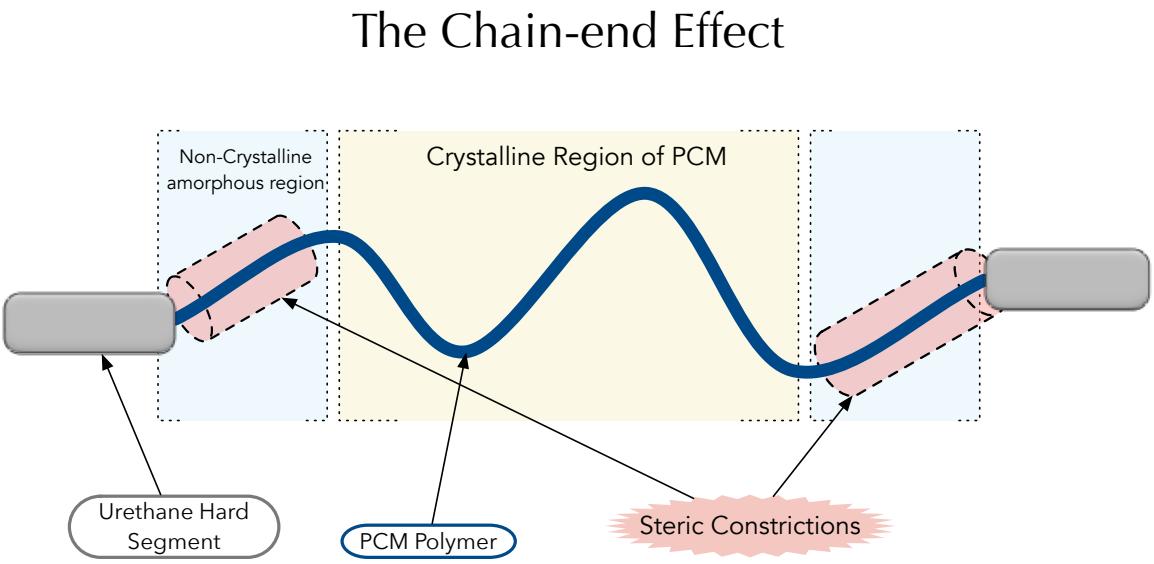

Figure 1.6: Illustration of the Hard Segment Chain-end effect shows how it limits PCM crystallization.

One behavioral trend that has consistently been observed in most SSPCM systems, and is universal to model polymer networks, is the limiting effect cross-links have on PCM polymer crystallization. In regular PU materials the mobility of the central portion of the polymer chains in model networks has been shown to be higher than that of the units attached to the cross-links[35-37], [38] Illustrated in Figure 1.6, the HS Chain end effect is observed when a portion of the PCM chain segments have a restricted mobility due to their vicinity to the hard segment regions and therefore behave as non-crystalline amorphous chain segments in the continuous PCM phase domain.[37,39] The remaining crystalline portion is responsible for the PCM latent heat storage properties. Therefore, thermal energy storage properties depends on the number of PEG chain units the HS chain-end effect prevents from participating in crystallization.[25,34]. It has been found that there may be a connection between the composition of the hard segment and the magnitude in which enthalpy and the PCM crystalline region is reduced by the chain-end

effect.[34],[40] Alkan's results revealed that aliphatic HS restricted a lesser portion of PCM polymer chain mobility, compared to aromatic HS.[34]This was an extraordinary finding, because it shows that it may be possible the HS chain end's limiting effect on PCM crystallization could be reduced by modifying HS composition. Based on these findings it is inferred that, a HS composition that restricts the least number of PCM chain segments will have the largest PCM crystalline region, and will exhibit maximum heat storage capacity.

Thus, the characterization of the relationship between structure and the chain end effect could lead to determining what configuration demonstrates the least chain end effect behavior, and maximum thermal energy storage properties. Furthermore, it may also be determined what the optimal configuration is for a PU-SSPCM that exhibits thermal energy storage (TES) properties suitable for building applications.

1.2.2. STRUCTURAL FACTORS KNOWN TO INFLUENCE CONVENTIONAL POLYURETHANE MATERIALS IN LITERATURE

There has been extensive amount of research on the complex structure-property relationship SPU materials. Unfortunately, the majority of research on the connection between PU micro- and macrostructure and final properties is primarily focused only on mechanical properties. [37,41,42] It is well known the final properties of SPU elastomers are largely determined by its heterogeneous phase morphology. Phase separation behavior is connected to the characteristics and the organization of the hard and soft phase domains, which is determined by the composition of the HS and SS.[41,43,44] The HS diisocyanate

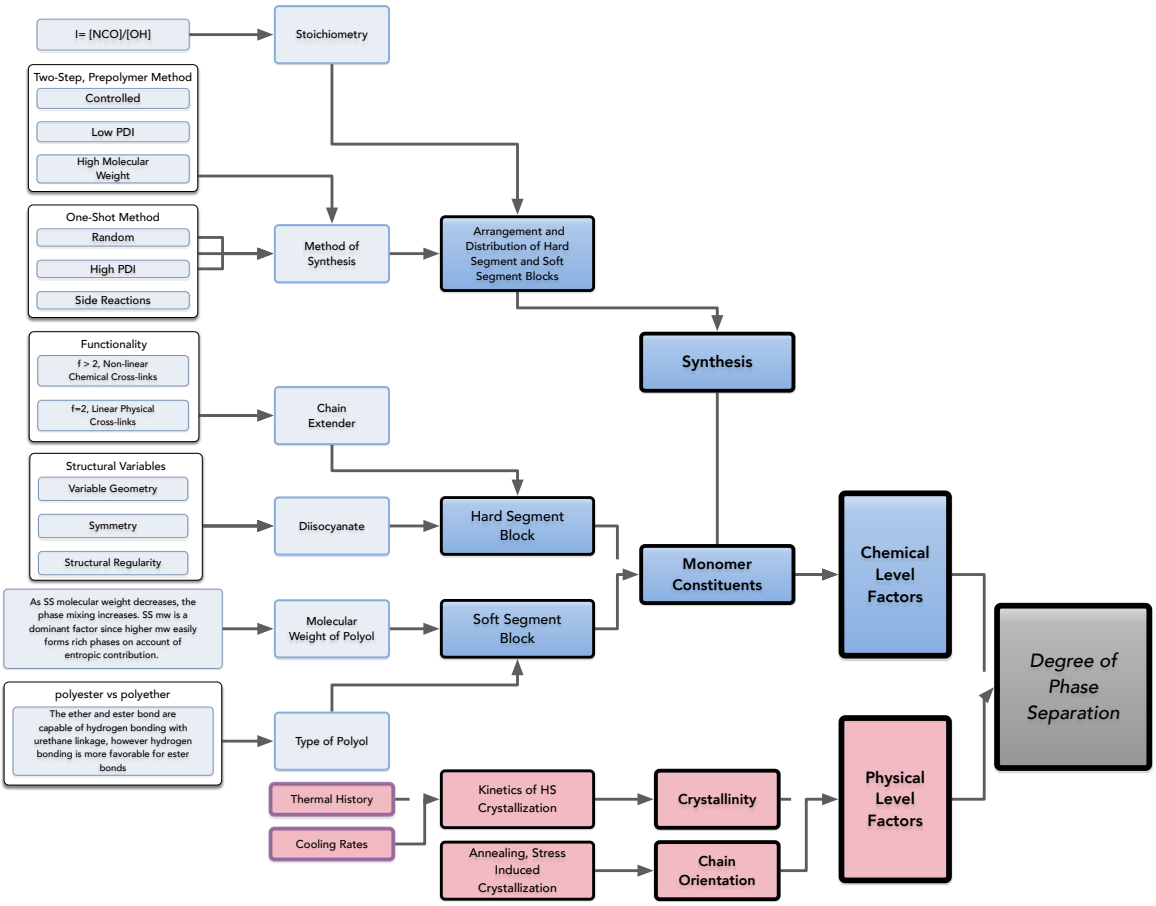

Figure 1.7: SPU Chemical and Physical level variables that directly influence phase separation, thus final properties.

component controls the HS urethane groups ability to form hydrogen bonds. The formation of physical cross-links depends on the strength of hydrogen bond. Which is why if a diisocyanate has weak inter-urethane hydrogen bond interaction, these polyurethanes will demonstrate poor phase separation.[42] Figure 1.7 shows a flow chart of SPU property-determining parameters at the chemical and physical level and how each factor relates to phase separation behavior. Many researchers have focused on the effect of soft segment (SS) type and length, hard segment (HS) type and length, hard domain crystallinity and the extent of microphase segregation on structure-function relationships in segmented polyurethanes from a mechanical property standpoint [45]. Ultimately, PU's phase separation strongly depends on the hydrogen bond formation between the urethane linkages, which is why an enhancement in hard domain crystallinity is observed when

hard segment content is increased. [42]It also depends on the SS type and molecular weight. Typically, as the SS molecular weight decreases, the phase mixing increases. [45-47] PEG PCM crystallization is only observed in the soft domain if the polyol chain is long enough to fold and form crystalline lamella.

In this dissertation, the information found in conventional PU literature is related to structural factors that caused a change in %SS crystallinity was extrapolated and were used as the key research objectives of this dissertation.

a) PU-SSPCM molecular architecture: Linear vs Non-Linear

Amongst the PU-SSPCMs published thus far, both linear and non-linear molecular architecture have been presented. Linear PU-SSPCMs have a linear chain structure and rely on hydrogen bonded urethane HS groups that act as physical cross-links to support the materials solid framework. Whereas, the non-linear PU-SSPCMSs have a multi-functional urethane HS that forms a chemically cross-linked network. The HS acts as a junction point that anchors that prevents the dissolution of the PCM polymer.[37] Earlier studies presenting linear, non-linear, and the thermoplastic non-linear PU-SSPCMs showed no significant difference in the enthalpy values reported. This is unusual considering the drastic dissimilar molecular structures. Since there is no apparent trend in enthalpy data that points to a specific structural feature that directly influences TES properties, it is difficult to assess the connection between molecular structure and thermal energy storage properties. Therefore, the relationship between underlying structural-level factors and their final thermal energy storage properties still remain unclear. On account

of inconsistencies between the handful of PU-SSPCM studies it is impossible to distinguish how the molecular architecture relates to the phase transition behavior of the PCM polymer and the amount of heat it absorbs and releases as it transitions between and amorphous and crystalline state.

For regular PUs the introduction chemical cross-links alter the materials physical properties. PU's with a chemically cross-linked PU-SSPCMs are considered thermosets. Thermoset PU-SSPCMs have a homogeneous morphology and thermal heating cannot destroy their network structure.[18,21,25] On the other hand, physically cross-linked PUs behave as thermoplastics (TPU). [18,21,25,26] The introduction of chemical cross-links converts the PU elastomers morphology from a heterogeneous to a homogeneous morphology. Therefore, TPU elastomers have a separate hard and soft phase domain that can repeatedly be melted and re-cooled.[23,26,30,31,34,48-50] The dramatic change in physical properties that occurs as a result of different HS cross-link nature indicates there may also be a similar effect on TES properties and the crystallization behavior of PEG PCM. There has yet to be a study that investigates the influences molecular architecture on TES properties. Compared to the other PU-SSPCMs, Yanshan[50] presented a PU-SSPCMS with a interpenetrating network (IPN) structure. Apart from the other studies, Yanshan's demonstrated dramatically lower phase transition temperatures (PTT), but high enthalpy values with a PEG molecular weight of 6000 g/mol. It is in agreement amongst authors that an enthalpy value of at least 100 J/g is necessary to be considered an effective poly-SSPCM TES system.[30,31] However, to achieve such a high enthalpy value PEG PCM molecular weights of 6,000-10,000 $gmol^{-1}$ must be used. Consequently, the range of

phase transition temperatures (PTT) associated with these molecular weights are significantly higher than human comfort temperatures ($T_{m,c}$=19-25˚C).[26,31,49] Figure 1.3 shows the results from an energy simulation study that indicated the PCM phase transition temperature should be related to the climate-specific optimal temperature, to achieve maximum thermal energy storage performance. According to these results it is imperative the phase transition of the PCM polymer be observed at human comfort temperatures to be considered an effective energy saving device for building applications. At this point, it is not conclusive whether or not the IPN molecular architecture is the attributing factor for low PTT. Thus, further study comparing this relationship would be worthwhile, in addition to understanding how the chain end effect differs according to chain network molecular architecture.

b) Diisocyanate Molecular Geometry

Furthermore, a few authors have identified a link between HS configuration and soft segment (SS) crystallization. Alkan[34] is the only author to have demonstrated there may be a correlation between the number of PCM chain segments the HS chain end effects prevents from participating in crystallization and the molecular geometry of the HS's diisocyanate component. Alkan quantified the chain end effects observed in a series of PUPCMs prepared with 1,6 Hexamethylene Diisocyanate (HDI), 2,4-Tolyene Diisocyanate (TDI) and IPDI as the diisocyanates HS component, combined with PEG (M_n= 1,000, 6,000 and 10,000 g/mol) as the PCM polymer component. He found that the chain end effect was more prominent in the PU-SSPCM samples prepared with larger,

rigid aromatic diisocyanates compared to those prepared with aliphatic diisocyanates. Alkan attributed this difference to varied diisocyanate structural features that alters the range of interaction between PCM polymer chains. [34]

It is well known from conventional PU literature that the diisocyanate component dictates that chemical nature of the HS.[41,42] Therefore, the diisocyanate component governs the ability of the HS to form hydrogen bonds, which directly impacts the materials phase separation behavior. Because the details of the phase morphology determine a PU materials final properties, the molecular geometry of the diisocyanate also strongly influences final properties. Prisacariu[41]demonstrated that even the slighted change in a diisocyanates molecular structure can cause profound changes in PU final properties

c) Ratio of Percent Hard Segment Content (%HSC) and Soft Segment Content (%SSC)

In addition to HS composition, the length of the HS chain segments also plays a strong role on phase separation behavior and final properties. It is known that varying the ratio of the percentage of hard segment content (%HSC) and percent soft segment content (%SSC) changes the level of phase mixing in the material. It could be easily disputed that common PU parameters such as degree of phase separation and the weight proportion of hard and soft segments, which were also not addressed in earlier PU-SSPCM studies, could be impacting the PCM heat of enthalpy values. There has yet to be a PU-SSPCM study that has investigated the impact of diisocyanates and %HSC. Results obtained from X-Ray, and atomic force microscopy (AFM) methods demonstrated that an increase in the soft segment molecular weight contributed to increased incompatibility between the

hard and soft domains. Therefore, microphase separation is enhanced with increasing soft segment chain molecular weight because higher molecular weights easily form rich phases on account of entropic contribution[51-53]. Which is why, an enhancement in hard domain crystallinity is observed when hard segment content is increased. Crystallization is only observed in the soft domain if the polyol chain is long enough to fold and form crystalline lamella.

Considering, the nature of the HS cross-link, diisocyanate molecular geometry, and the ratio of %HSC and %SSC are all factors that play a dominant role in determining final properties in regular PU materials. It is reasonable to presume they could also play a strong role in determining thermal energy storage properties.

It is highly likely that discrepancies in the results are attributed to variations in synthesis conditions, diisocyanate composition, nature of network structure, processing conditions etc., all of which are examples of the underlying factors that are well-known to strongly influence PU final properties.[54]

d) Kinetics HS crystallization

The development of a phase separated morphology driven by both thermodynamics and kinetic factors.[37,55-57] While thermodynamic factors are mostly related to the chemical nature of the HS and SS, kinetic factors are associated with the crystallization mechanisms of the hard and soft segment and are controlled at the physical level. [37] This varies from the aforementioned factors (HS cross-link, diisocyanate molecular geometry, and the ratio of %HSC and %SSC), which are chemical level factors, since they are

determined during synthesis. Equal to chemical level factors, the degree of phase separation and final properties of segmented polyurethanes can be controlled kinetically through post-processing treatments such as annealing and stress-induced crystallization. [58-60] Since, each of these factors play a role in determining the final properties of conventional polyurethanes, it is necessary to gain a better understanding of how these factors influence PU-SSPCM thermal energy storage properties, which is determined by the crystallization of the PCM Polymer.

The confinement effect

Besides the chain-end effect, a second effect that limits SS crystallization has been noted in literature. The confinement effect is observed when PEG PCM chains become confined by the HS phase domain and an interphase region that serves as a boundary between the PCM and HS domains appears. It has been observed in literature that this confinement of SS chain into their own phase domain creates greater restriction on SS chain mobility. Consequently, a reduction in %SS crystallinity is observed.[45,51,61] the underlying behavior responsible for the drop in soft segment crystallinity with highly phase-separated systems has been attributed to an increase in the ratio of non-crystalline SS chain units to crystalline SS units.[45,51,61]

The confinement effect is observed when there is a decline in SS crystallinity due to raising the level of phase segregation. Thus, the confinement effect is only noticeable in well-organized phase separated polyurethanes. [45,51,61] With increasing phase segregation, the HS domain will eventually start to confine the SS phase domain, which results in the

formation interphase boundary region. The illustration in Figure 1.9 shows the interphase boundary region located between the HS and SS/PCM phase. This is a co-continuous region made up of HS phase dispersed within the soft phase matrix. In this region the trapped SS chains is immobilized by the HS and the HS act as an impurity and disrupts the crystallization of the dispersed SS chains. Consequently, the size of the SS crystalline region is reduced. The size of the interphase boundary region increases with higher degrees of phase separation, which implies that as the separation between the SS and HS phase domain structures develop, the confinement effect becomes more prominent. The connection between degree of phase separation and SS crystallinity has been investigated in previous literature.

Hood measured the morphological changes that take place when selectively controlling the crystallization of the HS, by cooling rate. [62,63] Hood found that compared quench cooled, slowly cooled samples demonstrated a measurable decline in SS crystallinity and concluded that better packed highly crystalline HS crystals exhibit a stronger confinement effect.[61] This result suggested that a sample with a high degree of phase separation and highly crystalline HS enhanced the restriction of soft segment chain motion. [61] DSC Analysis results reported by Korley[45] indicated minimal phase-mixing between the hard and soft domains, which suggests the primary limitation to soft segment crystallization is domain confinement, inhibiting the growth of large, well-ordered soft segment crystallites. [41–45,61]

On the other hand, Petrovic [52] found that shorter SS chain lengths exhibited greater amorphous regions than highly phase-mixed PUs, which led him to believe that soft

segment mobility is mostly limited by the attached hard segment rather than phase mixing. Therefore, according to Petrovic the reduction in soft segment crystallinity is a result of the chain-end effect rather than the confinement effect.

In this dissertation the limitation the confinement effect has on PCM crystallization will be compared to the HS Chain end effects. Both limitations originate from different structural parameters, therefore each behaviorally effect must be studied individually.

Need for systematic study

Polyurethanes are complex materials which implies that PU-SSPCM are as well; however, failure to consider important parameters that have been proven to govern the final properties of polyurethane elastomers in the study of PU-SSPCM points to a gap in knowledge that needs to be addressed in future work. The purpose of this dissertation is to systematically describe and examine the structure-property relationship of PU-SSPCMs.

Critical to material optimization is developing an understanding of the relationship between structure and function. It is important to systematically study each factor since there are numerous cases where the underlying factors do not display their effects independently. Since the effect of each factor is certain to depend on the level of the others, the experiment is bound to yield an inaccurate image of the effect of each factor and is incapable of detecting the effect of the inter-dependence of both (or other) factors. Because the effects of these factors are not independent, the levels of the other factors must be examined by varying all factors simultaneously. Experimental setup yields

information revealing the connection between compositional factors and soft segment crystallinity that has been documented in conventional polyurethane literature.

1.3. RESEARH APPROACH

Until now, previous PU-SSPCMs that have been investigated were studied as a typical PCMs and not as polyurethane. It is well known polyurethanes have a complex structure-property relationship. There are certain factors on the chemical and physical level that have a powerful impact on the final properties of a polyurethane. Therefore, it doesn't make sense why the same factors would not be considered when analyzing the thermal energy storage properties of a PU-SSPCM. Owning to the fact that PU-SSPCMs have the same basic structure as regular segmented polyurethane, it is logical to believe that similar factors will have the same effects on PU-SSPCM thermal energy storage properties. The purpose of this dissertation is to systematically identify and characterize the relationship between a PU-SSPCMs structural configuration and its thermal energy storage properties based on PU structural factors that have been found to provoke a change in SS crystallinity. The information gained from identifying the connection between PU chemical and physical structural factors and SS crystallization, will point to what the most optimal PU-SSPCM configuration looks like.

Although the majority of PU structure-property studies focused on how altering SS crystallinity affects mechanical properties, the idea that same underlying factors used to provoke a change in SS crystallization could also be linked to thermal energy storage properties in PU-SSPCMs was further explored in this dissertation. The structural

variables studied in this research were specifically selected based on research findings from literature on conventional polyurethanes. The structural variables considered in this dissertation are as follows; HS cross-link nature, PEG PCM molecular weight, diisocyanate composition, ratio of %HSC and %SSC, and the kinetics of HS crystallization. Each of these factors were found to play some sort of role in influencing the final properties of conventional polyurethanes, therefore, it is necessary to gain a better understanding of how these factors influence phase change enthalpy of the soft segment (SS).

Research Goals

The goal of this research is to quantify the heat storage capacity of a family of PU-based SSPCMs and uncover the driving chemical and physical factors that cause a change in the thermal energy storage properties. The chemical and physical factors this research focuses on were selected based on findings reported in conventional polyurethane literature, which suggested that a parameter that led to an increase in soft segment crystallinity was observed.

Contribution

Previous work on PU-SSPCMs have only dealt with estimating thermal energy store properties using DSC methods, whereas our study takes a more in-depth look at the systematic relationships between the underlying factors that could have an impact on PCM polymer phase transition behavior. Also New correlations were developed between

PU property-governing factors and the thermal energy storage properties of PU-SSPCMs. Overall, the information obtained from these studies will reveal optimal design parameters for developing SSPCM polyurethane elastomers. This dissertation is an extension of the current literature on PU-SSPCMs that incorporates a systematic investigation of the underlying factors that have been identified in conventional polyurethane literature, to modulate soft segment crystallization. The findings of this work will uncover the path to defining the optimal configuration of a PU-SSPCM that exhibits maximum thermal energy storage properties.

Organization of this dissertation

This dissertation is organized in a manner that presents research findings as a series of studies. Each chapter focuses on one of the four structural factors and analyzes the effect on the crystallization and melting behavior of the PEG phase change component. It is expected that by understanding of how the components of a PU-SSCM structural system is related to PEG PCM crystallization, it will be easier to ascertain the optimal polyurethane molecular architecture that will provide the ultimate thermal energy storage properties.

Each of these parameters was studied systematically in order to determine the direct connection with thermal energy storage properties. This dissertation presents the work done and is organized such that an entire chapter is dedicated to one parameter. A final chapter will present a conclusion based on the results of all the chapter studies.

In Chapter 4 the effects of the nature of the network structure on thermal energy storage properties will be discussed. In previous literature, a hyperbranched PU-SSPCM, and a linear PU-SSPCM, comparative to a segmented polyurethane, both showed excellent results. However, the hyperbranched PU-SSPCM contains chemical cross-linking, while the segmented polyurethane consists of physical cross-links. It remains unclear the effect cross-linking has on thermal energy storage properties. Therefore, in chapter 4, one set of thermoset PU-SSPCM and one set of thermoplastic SSPCM were synthesized. Each set contained a counterpart sample made from the same diisocyanate monomer and PEG molecular weight. With the same constituents, the comparison of PEG crystallization behavior between a thermoset and thermoplastic can be attributed to the nature of the cross-link with confidence. Differential Scanning Calorimetry (DSC) techniques were used to analyze the crystallization behavior of the PEG PCM polymer. Furthermore, chemical analysis of both materials was carried out using FTIR techniques.

In Chapter 5, chemically cross-linked and physically cross-linked PU-SSPCMs, varied by their diisocyanate components will be fabricated. The diisocyanate components were selected to represent the following diisocyanate structural moieties: size, rigidity/flexibility, and symmetry, all of which are known to cause property changes in polyurethanes. Using DSC methods, the soft segment crystallinity was measured according to the diisocyanate structural variables. From the results, information on the influence structural composition has upon thermal energy storage properties was gained. Furthermore, conditions for synthesis and characterization of the bulk polymer are discussed.

In Chapter 6, samples with physical cross-links are further investigated. A series of samples varied by hard segment content were prepared. Enthalpy values were measured accordingly, using DSC methods. The results from this chapter provide a greater understanding regarding the optimal composition parameters for developing PU-SSPCM with favorable thermal energy storage properties.

Chapter 7 investigates the impact of the degree of phase separation between the hard and soft block on heat storage properties. TES properties were interpreted by measuring soft segment crystallinity using DSC methods. The degree of phase separation was determined by FTIR and glass transition.

Chapter 2 LITERATURE REVIEW

This literature review is organized into four sections. The first section is an overview of phase change materials (PCMs); first, an explanation of the functional thermal energy storage (TES) properties of PCMs is discussed, followed by a brief summary on the history of PCM research and the various applications that have utilized PCM properties. Third, a brief synopsis on the concept of PCM-enhanced building materials and a run-down of the field application studies that have demonstrated energy saving benefits, from implementing PCMs into building envelopes is provided. Finally, a discussion on the feasibility of solid-liquid PCM (SLPCM), the microencapsulation method used to mitigate issues with fabrication, and a life cycle analysis outlook on the feasibility of microencapsulated PCMs as an energy-saving device is provided. The second section will focus on polymer-based solid-to-solid PCMs (pSSPCMs). Here, a rundown of the existing literature published on shape-stable PCMs, composite SSPCMs, and polyurethane-based solid-to-solid PCMs (PU-SSPCM) is provided. The scope of this dissertations' research interest is focused on polyurethane-based SSPCMs (PU-SSPCMs); therefore, in this section a critical analysis of a selection of studies that have presented various novel types of PU-SSPCM systems are discussed in great detail. Here, discrepancies in experimental design, interesting findings, common trends in results, and gaps of knowledge are all highlighted. The critical analysis discussed here contributed to shaping the motivation for this dissertation. The third section is centered on conventional polyurethane (PU) materials. The main hypothesis of this dissertation was developed based on an extrapolation of information found in conventional PU literature. Thus, in

this section, key experimental findings acquired from an assortment of PU literary sources, about PU complex structure-property relationship, is summarized. Following that, evidence pointing to certain underlying factors that have been identified to modulate soft segment (SS) crystallization is outlined to provide the premise that leads to the conjectures of chemical and physical-level parameters impact on thermal energy storage properties this dissertation investigates. The fourth and final section is dedicated to clarifying terminology for the purposes of this dissertation.

2.1.MOTIVATION

Acknowledging that our finite energy resources, namely coal, oil, and natural gas, can by no means meet our needs for the future, has led to a search for efficient, economical and feasible sources of energy. In 2010 the United States accounted for 19% of the world's energy consumption; only 1% less than China. Considering that China makes up 20% of the world's population and the U.S. only makes up 4.6%, on average the U.S. consumes 30% more energy per person than any other country in the world. In Figure 1.1, it can be seen that the building sector (commercial and residential buildings) account for 41.5% of primary energy consumption in the U.S. Of the energy sources used by the U.S. buildings sector, 75% came from fossil fuels, 16% from nuclear generation, and 9% from renewables (See Appendix 1.1.8). The average life span of a residential home or commercial building could be anywhere from 10 to 200 or more years. Therefore, there are long lasting repercussions involved with energy inefficient buildings.

The infrastructure and the energy of new construction will dictate the size and shape of a building. Estimates from the 2010 Residential Energy Consumption Survey (RECS) show that 48% of energy consumption in U.S. homes in 2009 was for heating and cooling (Figure 1.1). There are long lasting repercussions to not meeting the lowered energy consumption requirements. Energy consumption in buildings has garnered interest in using thermal energy storage for space heating, hot water, cooling, and air-conditioning.

2.2. THERMAL ENERGY STORAGE

The idea of increasing the thermal mass of a building envelope as a means to regulate the thermal condition of our living environment is a design technique that dates back 2000 years. Thick stonewalls and ceramic tiles to store heat under the floor were used by the Romans as a means to create 'thermal mass'. The Eskimos built igloos out of compressed snow to trap indoor heat and shield them from harsh outdoor temperatures.[14] The working principle of a thermal mass is that during the warmer days, the mass absorbs the heat (charging), keeping the internal space cooler than outside while during the night, when the outdoor temperature falls, the mass dissipates the heat indoors (discharging) to maintain the indoor temperatures at a comfortable level. Figure 2.2 shows a comparison of peak load periods for a high thermal mass wall and low thermal wall with the external temperature. The change in temperature from day to night is known as the dinaural temperature variation. It can be seen that the dinaural temperature curve for the low thermal mass temperature wall, lags behind the curve of the high thermal mass wall and has a slightly lower peak temperature. This demonstrates that the indoor temperature of a

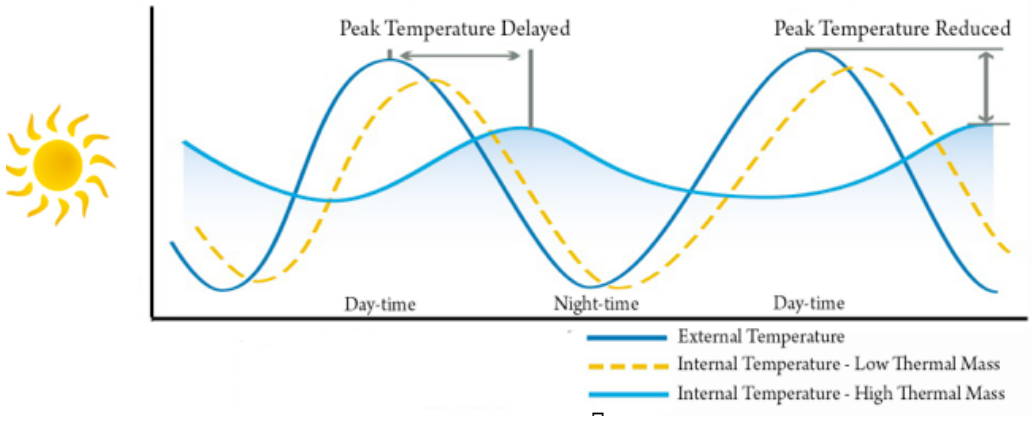

Figure 2.1: Indoor temperature fluctuations of a Low thermal mass envelope vs. a high thermal mass

room with a high thermal mass wall was less influenced by external temperature changes than the low mass wall. To counter balance this thermal lag, excess energy is needed to regulate temperature in order to maintain thermal comfort. [64]

The use of thermal energy storage (TES) systems in building envelopes provides a way to increase thermal mass without having to increase the amount of material used. Thermal energy storage (TES) strategies operate on the working principle that during the day, which is considered the "off-peak" period, as the temperature rises, excess thermal energy is stored as latent heat, and then at night released during the "on-peak" period when the temperature is cooler.[65] The use of a TES system in this manner counter-balances the thermal lag so that a constant indoor temperature is observed. (See Figure 2.4) As a result, the demand for electricity to power heating, ventilating and air-conditioning (HVAC) systems for space heating, hot water, cooling and air-conditioning is reduced and the overall building energy performance is improved. [18,64]

As shown in Figure 2.5, the reversible storage of thermal energy can be obtained through chemical or physical processes (Dincer, 2011; Mehling, 2008; Lane, 1983). In order for a system to retrieve the stored energy and use it for many continuous cycles (charging and discharging), these methods need to be reversible.

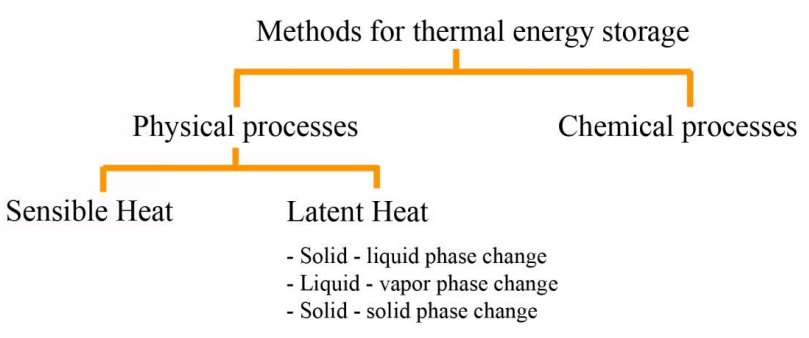

Figure 2.2: Possible methods for reversible storage of thermal energy

2.3. PHASE CHANGE MATERIALS (PCM)

A phase change material is a substance that undergoes a reversible change of state with the capacity to store a significant amount of heat per unit volume, while maintaining a constant temperature.[1-3] Unlike conventional sensible heat storage materials such as water or rocks, PCMs are classified as "latent" heat storage (LHS) and can store 15 times more thermal energy per unit volume without changing temperature.[4] PCM's ability to store thermal energy over extended periods of time without requiring additional power (depending on the mass, volume, heat load and latent heat of fusion values) are harnessed and employed in various applications associated with temperature regulation.

Theoretically, the benefits of using PCM-based TES systems in buildings is that it helps, a) maintain constant temperatures indoors and b) shift energy consumption from periods of peak electricity rates to periods of lower rates accompanied by the additional advantage of lower demand charges.

PCM-enhanced building materials improve the thermal mass of building, thus introducing several advantages over conventional materials.[2] As shown Figure 1.3, the peak load periods of a building with and without a PCM TES system. It can be seen that the PCM TES systems provide enough storage capacity to shift the heating and cooling demands to later time periods when electricity prices are lower than PCM.

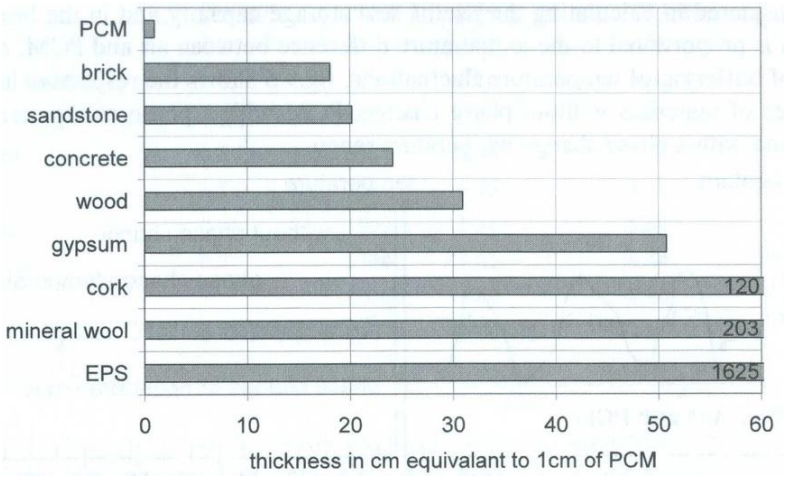

Figure 2.3: Necessary layer thickness of different building materials to store as much heat as a 1 cm thick layer of PCM. (Source: Niraj 2014[66])

Figure 2.4 shows the required thickness of other construction materials to store an equivalent amount of thermal energy that a 1 cm thick layer of PCM is able to absorb. The PCM in this particular comparison is capable of storing 130 MJ/m^3 at a temperature difference of 4 Kelvin.[67] A significant difference in wall thickness between PCM wall thickness and the other regular building materials is quite noticeable. It took

approximately 18 cm of brick and 24 cm of concrete to store an equivalent amount of energy to 1cm PCM. This shows that the same insulative properties can be obtained without having to use bulkier materials. Apart from that, PCMs are more appealing because they exhibit latent heat thermal energy storage (LHTES) properties, whereas bricks and concrete demonstrate sensible heat storage. Therefore, the thickness of PCM walls in tandem with its LHTES properties indicates PCM to be a viable option for improving building energy efficiency [67].

2.3.1. HISTORY OF PCMS IN BUILDINGS

The "Dover House" constructed in Boston in 1948, was the first passive solar house that employed Glauber's salt (Sodium sulfate decahydrate " Na_2SO_4 $10H_2O$) as the Phase Change Material. [64] In the Dover house, the solar panels with Glauber's salt sat directly behind a bank of eighteen windows that lined the second story of the south-facing wall. [64] In 1974, NSF awarded a contract to the Dow Chemical Company, to identify materials that could be used as PCMs in buildings. It was estimated nearly 20,000 materials that could be used as a PCM. Thus there is an immense variability in the types of PCMs available for use as thermal energy storage. [64] Today many advances have been made in PCM research, technology, and the utilization of their unique properties in applications other than buildings. Existing literature on PCMs can roughly be divided into three categories. The majority of literature on PCMs has dealt primarily with:

1.The chemical makeup and thermo-physical properties of existing PCMs.

2.Integration of PCM in building materials.

3.Experimental and numerical studies on the performance of PCMs within the building environment.

The chemical makeup and thermo-physical properties of existing PCMs

The vast spectrum of PCMs available makes it necessary to classify them in an orderly fashion. Because the two most important criteria of phase change materials, the melting temperature and energy absorbed, depend on molecular bonds, they have been classified primarily based on their chemical makeup.[21]

Many substances have been explored as potential PCMs.[10,21] A number of authors have reported comprehensive lists of possible candidates for latent heat storage, covering a wide range of temperatures.[16,18,21] The listed PCMs are classified according to their phase transition as a solid-liquid PCM (SLPCM) or a solid-solid PCM (SSPCM) and categorized as either an organic, inorganic, polymeric, or eutectic PCM.[20,3,10,21,16]

A. Organic PCMs - These PCMs are then classified as paraffin (alkanes) and non-paraffin (non-alkanes).

B. Inorganic PCMs - These PCMs are grouped as salt hydrates and metallics.

C. Eutectics - Eutectics are proportional mixtures of organic-organic, inorganic-inorganic or inorganic-organic PCMs.

Table 2.1: Comparison of organic, inorganic and eutectic PCMs. (Adapted from: Zalba, 2003[16])

Organics	Inorganics	Eutectics
Advantages	Advantages	Advantages
No corrosives	Greater phase change enthalpy	No phase separation
Low or none undercooling		
Chemical and thermal stability		
Disadvantages	Disadvantages	Disadvantages
Lower phase change enthalpy	Undercooling	Lack of test data
Low thermal conductivity	Corrosion	of thermophysical
Inflammability	Phase separation	properties
	Phase segregation, lack of thermal stability	

A complete review of the types of materials used as PCMs, their classification, characteristics, advantages and disadvantages, and the various experimental techniques used to determine the behavior of these materials in melting and solidification, are discussed in Zalba 2003[16] Table 2.1 provides a comprehensive list of properties that characterize a PCM substance as either organic, inorganic, or eutectic.

Each type of PCM has desirable and undesirable properties when it comes to their applicability in buildings. [16,18,21,67-69] The selection of a PCM for latent heat thermal energy storage systems needs to fulfill certain requirements and exhibit various beneficial thermo-physical properties as well. In great detail, the requirements and selection criteria for the practical use of PCMs have been outlined by in literature[13,16,67-69]. A summarized list of the general criteria of properties necessary for practical PCMs according is given in Table 1.1

The practicality of PCMs depends on whether they meet the thermo-physical properties required of the target application. The operating temperature of the application should be matched with the transition temperature of the PCM, in order to obtain effective thermal energy storage properties. According to the American society of heating, refrigerating,

and air-conditioning engineers (ASHRAE)[70] the comfortable room temperature for a single office is listed as 21.1°C (70°F). Therefore, a PCM with a phase transition close to human comfort temperature (20°C) must be selected for building applications. The latent heat should be as high as possible, especially on a volumetric basis, to minimize the physical size of the heat stored. High thermal conductivity would assist the charging and discharging of the energy storage.

Also, long-term phase stability during phase transition is key for obtaining meaningful TES properties. Small volume changes on phase transformation and small vapor pressure at operating temperatures to reduce the containment problem. Super-cooling has been a troublesome aspect of PCM development, particularly for salt hydrates. Super-cooling of more than a few degrees will interfere with proper heat extraction from the store, and super-cooling of 5–10˚C can prevent it entirely. Besides properties that impact PCM's utility as a TES, it is also necessary for the PCM to be chemically stable. PCM can suffer from degradation by loss of hydration, chemical decomposition, or incompatibility with materials of construction. PCMs should be non-toxic, non-flammable, and non-explosive for safety. Economically, low-cost and large-scale availability of the phase change materials are also very important.[1,3,4 ,2,18,21]

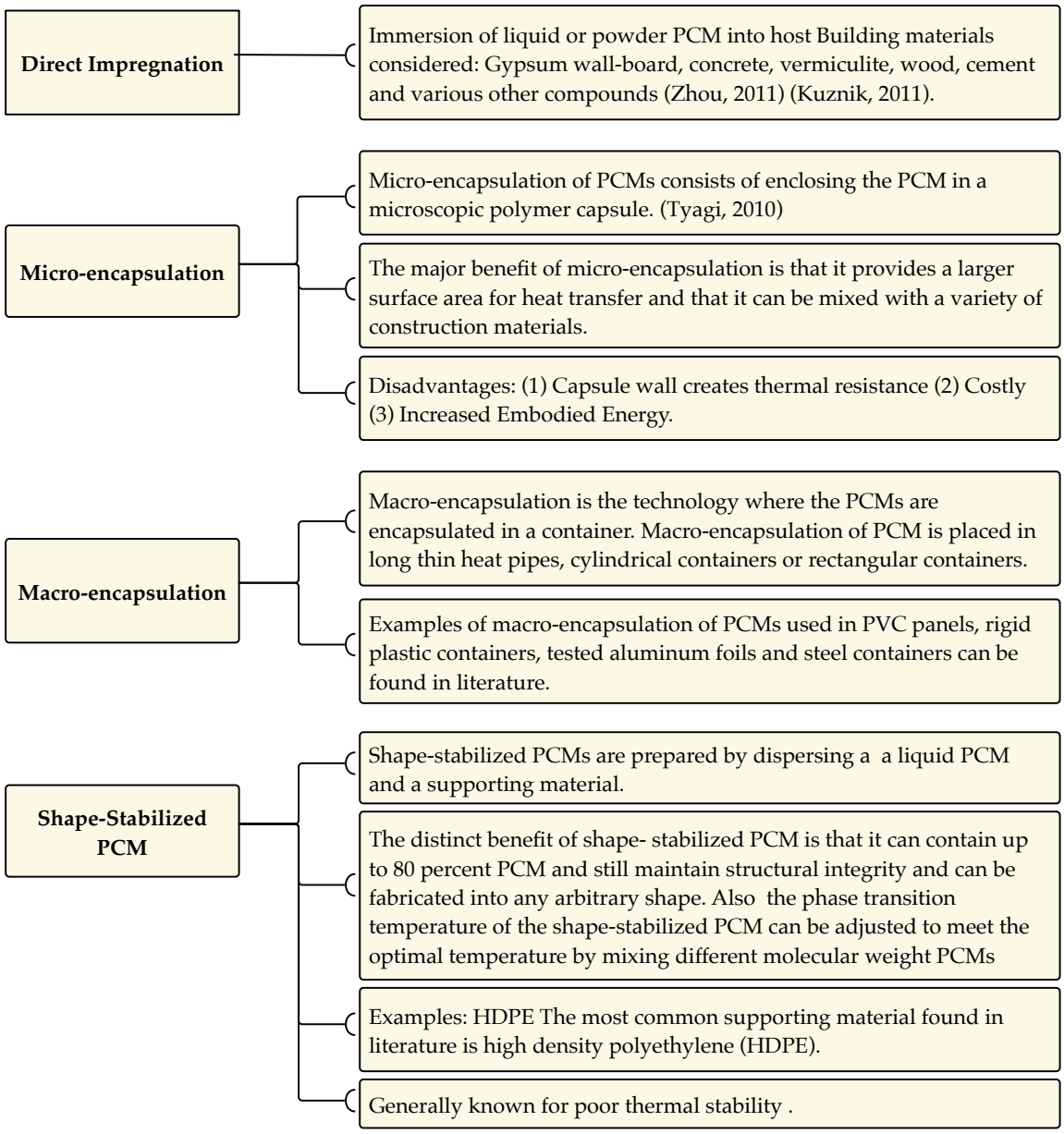

Figure 2.4: Methods for integrating PCMs into building materials

A large part of this work includes field application studies in which PCMs are used to enhance the thermal mass of regular building materials such as gypsum wallboard, insulation, bricks, concrete blocks etc. On account of PCMs and the continuous changes in their phase of state, one of the biggest issues is finding a proper containment device

that will prevent the PCM from leaking or becoming contaminated. In order for a PCM to be beneficial as thermal energy storage, it must be contained in one centralized place and must be compatible with the secondary building material it is being utilized with or be completely isolated from it. Therefore, a variety of methods for the incorporation of PCMs into regular construction materials have been a widely researched topic.

An overview of the main methods used to integrate PCM into regular building materials and their associated advantages and disadvantages are discussed. is summarized in Figure 2.6. The four primary containment methods depicted in Figure 2.9 include a) direct impregnation b) micro-encapsulation c) macro-encapsulation d) shape-stabilized methods. [18]

PCMs latent heat storage properties are best taken advantage of by direct integration into interior building materials. The system found to be most effective includes a carrier building material with good thermal conduction, combined with the enormous surface to volume ratio and the high storage capacity of PCM.[21] Until recently, PCMs that exhibit a solid-to-liquid phase transition have been the primary focus of field application studies. The application of solid-liquid PCM is limited due to leakage and contamination problems. If PCM leaks or contaminates its surroundings, it will no longer be effective.[10,16] To mitigate this problem, microencapsulation technology has been the most commercially viable method used to resolve these issues.[71] Microencapsulated PCM (mPCM) works by using a polymer or inorganic microcapsule shell to isolate the PCM from the supporting material.

Numerous studies have shown that implementing building materials such as bricks, wallboard, insulation, or concrete enhanced with mPCMs into a building envelope provide effective means for reducing energy consumption.[10,18 16,72] However, several consequences to the microencapsulation method have been noticed, questioning its feasibility; 1) heat storage capacity is compensated because the microcapsule shell increases the thermal resistance between PCMs and the environment[71] and 2) added fabrication steps that increase initial energy and economic costs.[10,16]

Experimental and numerical studies on the performance of PCMs within the building environment.

There are a large number of parameters that affect energy consumption in buildings and make the process of selecting the type and amount of PCM challenging. The thermal performance of a building is dependent on many factors. The envelope characteristics such as the building geometry, orientation, construction type, placement and size of windows, the thermo-physical properties of the construction materials, their interaction with outdoor conditions, plus indoor control strategies such as the HVAC schedules and set-point temperatures are a few parameters that, in tandem, determine the amount of heating or cooling required to maintain comfortable indoor living conditions. This is why numerical modeling systems are necessary for estimating the percent saving in energy consumption brought about by PCMs. Numerous evaluations have been carried out on the performance of PCM in buildings. These evaluations, both experimental and numerical, can be further divided into two categories:

1)Active incorporation - the use of PCMs working in conjunction with air conditioning systems.

2)Passive incorporation - the use of PCMs in buildings without resorting to the utilization of additional air-conditioning to heat or cool the PCM.

It is clear that there are many factors to consider when incorporating PCMs into a building envelope. Numerous experimental and numerical studies on the performance of PCMs within the building environment have been carried out. A great deal of effort has been put toward computer models and simulations, to determine where the primal spot to incorporate the PCM and where its thermal energy storage properties will be the most advantageous. Niraj[73] made an attempt to assess theoretically the energy performance of PCM boards for a simple building in 15 different climates in the United States. Climate specific regions require PCMs that can offer a range of phase transition temperatures; a PCM used in Tucson, AZ would not be effective in Antarctica. The application of PCM wallboards in those buildings demonstrated significant benefits in terms of annual energy savings.

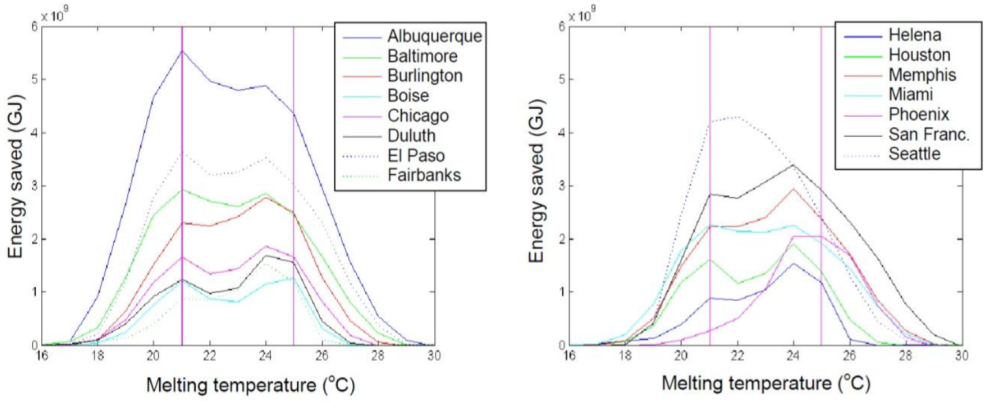

Figure 2.5: Energy saved as function of PCM's melting temperature for the 15 climates (set point temperatures: 21˚C and 25˚C) (Source: Niraj 2012[66]; Reprinted with permissions from Clemson University. July 8, 2016.)

The results from a melting temperature sensitivity study, shown in Figure 2.7, by Niraj[66] show that the optimum temperature is an important factor in determining the energy saving potential of the PCM board. It can be seen that a slight divergence from the optimum temperatures for each climate can reduce the energy saving potential by 5-10 percent.

2.3.2. LIFE CYCLE ANALYSIS OF PCM

A material selection decision should not only capture the functional performance required but should also consider the economic, social, and environmental impacts originated during the product life cycle.[74] Most field application studies studying PCM-enhanced building envelopes have reported only on energy consumption during the use stage and have failed to look at the energy consumed on a global scale. Recently, an interesting concept known as the "cradle" to "grave" model demonstrated the need to evaluate the environmental impact of a product or material on a broader scale in order to obtain true energy saving benefits. This model is based on life-cycle assessment (LCA); a methodology used to quantify the lifetime environmental impact of a product, starting from raw material extraction till the end of its life. Figure 2.8 shows a diagram of the life cycle stages and the energy impacts that are factored into tabulating the energy consumed

over a products lifetime.

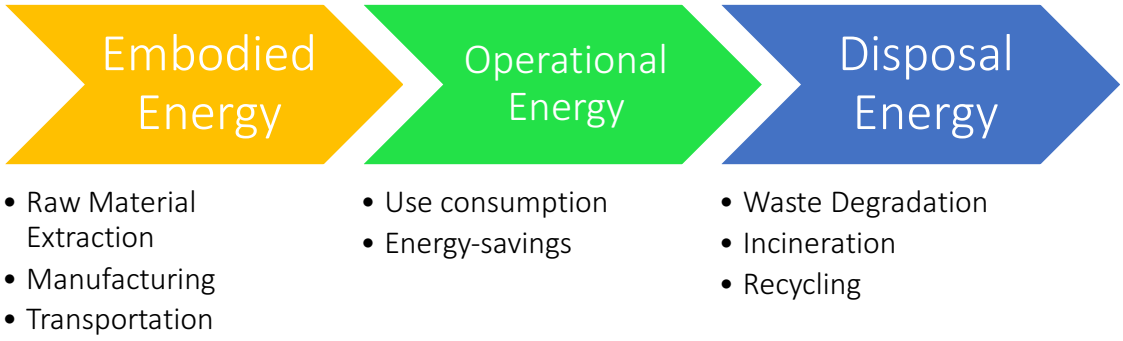

Figure 2.6: Diagram of Energy Consumption during Life Cycle Stages

As for reducing building energy consumption, through life-cycle assessment, the infeasibility of energy-saving technologies with an embodied energy that exceeds the potential energy-saving benefits by greater than a 2-5 year payback has been realized.[3,16,18] Recently, this is an issue recognized for microencapsulated PCM. It has been found that the extra energy used for manufacturing and fabrication adds tremendous costs to the overall energy being used.[71, 75]

Table 2.2: Annual electric energy consumption (kWh) for each cubicle

Annual electric energy consumption (kWh)	**REF**	**PU**	**PU + PCM**
Summer period (4 months)	219	98	83
Winter period (4 months)	2393	1504	1504
Total for a whole year	2612	1602	1587

DeGracia studied the environmental impact of including phase change materials (PCM) in a typical Mediterranean building. In this work, a life cycle assessment (LCA) was used to analyze whether the energy savings due to the inclusion of PCM was large enough to balance the environmental impact originated during the manufacturing of PCM.[76] Table

2.2 shows the comparison of energy consumption of a PCM integrated into polyurethane insulation from deGracia's study.[76] According to this table, over the course of the whole year, PU+PCM reduced energy consumption by less than 0.01%. Considering the added embodied energy of PCM, the impact its addition made on energy consumption was not significant enough to be considered a feasible energy saving material. However, the efficiency of PCMs is conditional; these values are based on just one hypothetical scenario; in another scenario with different conditions the implementation of PCM might be more impactful. DeGracia's experiments concluded that for such a system, when considering summer conditions all year around and a lifetime of the building of 100 years, the use of PCM reduced the overall impact by more than 10%, which would take 60 years to payback. Therefore, it is clear from this study that the inclusion of mPCM ended up costing more energy than is saved.[76]

As a supplement to this dissertation, a life cycle assessment (LCA) based on a hypothetical building system with a PCM-enhanced gypsum wallboard is provided in Chapter 9. This LCA study was conducted in order to estimate the energy payback of paraffin mPCMs. Through which, the embodied energy of a microencapsulated PCM was calculated. From the results of the LCA, it was found that other containment methods, besides microencapsulation, should be considered for integrating PCM into building

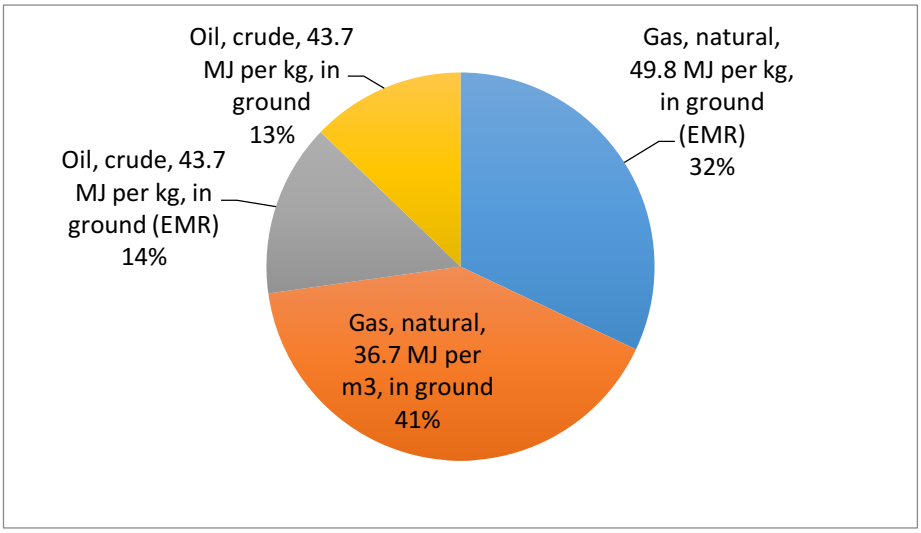

materials due to the processes contribution to the embodied energy. Figure 2.12 shows the manufacturing steps for producing a polyol PCM and Figure 2.13 shows a breakdown of the sources of energy consumed during manufacturing of 1kg of Polyol PEG.

Figure 2.7: Embodied Energy of Polyol PCM (MJ/kg) (Source: Athena Life Cycle Inventory Database)

Here an overview of the study is provided. The life cycle assessment was performed using the Athena Software. The study was based on a 12'ft by 12'ft block of gypsum drywall with 30% paraffin mPCM and 70% gypsum by volume. The energy consumed during each stage of production, starting from raw material extraction, was tabulated.

Energy consumption values were obtained from a database of life cycle assessments. It was found that it would take ~69.0 MJ of energy to produce 200g of mPCM. Provided that the latent heat of fusion PCM is 151 kJ/kg, which would be 100% efficiency performance and the PCM is activated 200 days per year, it was estimated the payback would be around 10.75 years. Based on this analysis, a payback of 8.2 to 10.75 MJ/kg years for 30g of paraffin mPCM in gypsum wallboard.

2.4.POLYMER-BASED SOLID-TO-SOLID PHASE CHANGE MATERIALS (PSSPCM)

2.4.1. OVERVIEW OF POLYMER-BASED SSPCM

A polymer-based Solid–solid PCM (pSSPCM) exhibits latent heat storage properties in the same manner as solid–liquid polymer PCMs (SLPCM), except these materials do not change into a liquid state at their melting temperatures. Instead, the PCM polymer transitions from a crystalline to an amorphous state. Through the entropy change that occurs as the PCM polymer transitions from an "ordered" crystalline state to a "disordered" amorphous state is the mechanism by which latent heat storage properties are observed (See Figure 1.4).[31,30,71,77]

Their basic configuration is comprised of a PCM polymer that serves as the "working" component and a secondary component that is responsible for maintaining the solid framework. The fabrication of pSSPCMs involves the chemical fixation of the chain-ends of a SLPCM polymer PCM to a secondary component that is thermally stable, well above the melting temperature of the SLPCM polymer.[30,71,77] Once the chain ends are fixed, the dissolution of the SLPCM polymer is prevented. The covalent bond between, anchors the chain ends so that its chain movement is restricted and the polymer can no longer translate freely. However, the SLPCM polymer may still demonstrate vibrational and rotational motion, which is enough chain mobility to allow extended chain crystals to form. Thus, PU-SSPCMs are essentially semi-crystalline materials. A variety of chemical

methods have been used to fix PCM polymer chain ends; the most common include grafting, blocking, and cross-linking copolymerization.[20]

2.4.2. ADVANTAGES AND DISADVANTAGES OF PU-SSPCMS

Polymer-based SSPCMs are advantageous among all of the PCMs due to the following reasons: (1) no leakage of melted PCM during phase change process; (2) no extra fabrication steps, which implies lower embodied energy and initial costs;[16] (3) no liquid or gas generation during phase change, therefore small volume change;[10,21] (4) Can be directly incorporated into or in a series with a material for direct use;[24] and can be processed into arbitrary shapes.[23 24,26,31]

On the other hand, a drawback to pSSPCMs that has greatly limited their application is that they generally exhibit their phase transition at temperatures much higher than the temperature range required for building applications. A common finding in literature has shown that the phase transition temperature can be lowered by decreasing the molecular weight of the PEG PCM polymer, however at the same time this would lead to lower enthalpy values, low transition enthalpy and unstable thermal property that greatly limit their applications. In recent years, several attempts have been made to lower phase transition temperatures.[31,78,33]

2.4.3. POLYURETHANE-BASED SSPCM

Thus far, a handful of papers have proposed various types of novel PU-SSPCMs systems. However, there are quite a few discrepancies between these papers which makes their

comparison rather complex. Therefore, to simplify the discussion on this body of work and make it easy to refer to common trends each PU-SSPCM study is organized into a table format that summarizes their composition, molecular architecture, respective thermal energy storage properties, and the DSC method parameters followed. See Table 2.3 [26,30,31,34,48-50]

As can be seen in Figure 2.8, PU-SSPCMs block copolymer configuration is made up of

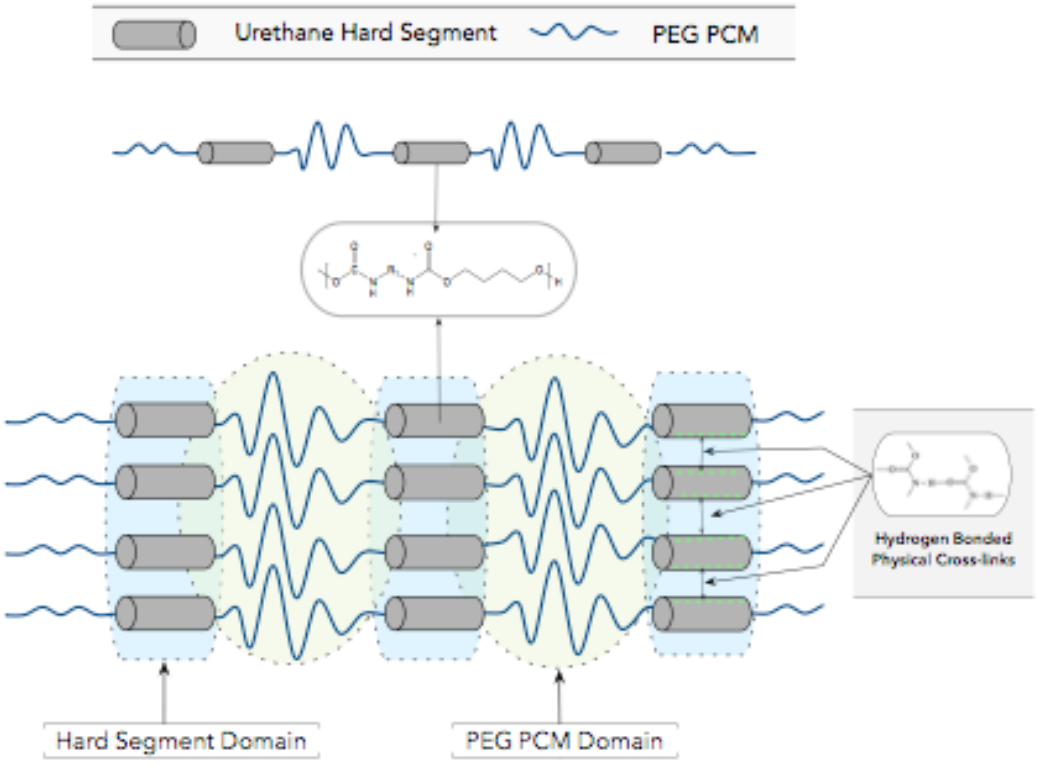

Figure 2.8: Schematic of PCM polymer segment and the urethane hard segment (HS)

alternating urethane and PCM polymer chain segment. The urethane group is called the "hard" segment (HS) and includes a diisocyanate (DI) and chain extender (CE). The urethane HS is responsible for preventing the dissolution of the PCM polymer. The PCM

chain is equivalent to the low temperature “soft” segment component in conventional segmented polyurethane materials (SPU).

Table 2.3: Summary of PU-SSCM Literature

Author	MATERIAL MONOMER COMPONENTS	Sample Name	ΔH_m (J/g)	T_m °C	DSC Method: heat/cool rate (°C/min)	first heat run? (y/n)	Molecular Architecture	%SSC
Su 2006	**PCM Polymer:** Polyethylene glycol (PEG, M_n=10,000 g/mol) **Diisocyanate:** 4,4'-Diphenylmethane diisocyanate (MDI) **Chain Extender:** 1,4-Butane diol (BDO) **Polymerization Solvent:** N,N-dimethylformamide (DMF)	PUPCM	138.7	65.3	Heating rate of 10°C/min, over the temperature range of 0°C to 100 °C.	No	**Linear**	88.70%
Alkan 2012	**PCM Polymer:** Polyethylene glycol (PEG, M_n = 1000, 6000, & 10,000 g/mol) **Diisocyanate:** 1,6'-Hexamethylene diisocyanate (HMDI), Isophorone diisocyanate (IPDI), and 2,4'-Toluene diisocyanate (TDI) **Chain Extender:** none **Polymerization** N,N-dimethylformamide (DMF)	HMDI-1000 HMDI-6000 HMDI-10000 IPDI-6000 IPDI-10000 TDI-6000 TDI-10000	109.0 176.0 171.0 166.0 169.0 161.0 162.0	19.0 59.9 57.7 57.4 58.8 57.0 57.1	Heated from 0°C to 80°C at a rate of 2°C/min	No	**Linear**	Unk
Meng 2008	**PCM Polymer:** Polyethylene glycol (PEG, M_n= 3,400 g/mol) **Diisocyanate:** Isophorone diisocyanate (IPDI) **Chain Extender:** 1,4-Butanediol (BDO) **Polymerization Solvent:** N,N-dimethylformamide (DMF)	Cycle 1 Cycle 2 Cycle 3 Cycle 4 Cycle 5	121.0 90.0 115.0 99.0 99.0	51.0 46.9 46.9 46.9 46.9	First heated from 0 to 100°C at a rate of 1°C/min and kept at 100°C for 1 min, and then cooled to 0°C at the cooling rate of 1°C/min. Same cycle was repeated five times.	No	**Linear**	Unk
Li 2007	**PCM Polymer:** Polyethylene glycol (PEG, M_n=10,000 g/mol) **Diisocyanate:** 4,4'-Diphenylmethane diisocyanate (MDI) **Chain Extender:** Pentaerythritol (PE) (tetrafunctional) **Polymerization Solvent:** N,N-dimethylformamide (DMF)	PUPCM	153.0	58.7	Samples were heated from room temperature to 100°C at a heatng rate of 10°C/min	No	**Non-Linear: Star-block Copolymer**	94.64%
Cao 2006	**PCM Polymer:** Polyethylene glycol (PEG, M_n = 6,000 g/mol) **Diisocyanate:** 4,4'-Diphenylmethane diisocyanate(MDI) **Chain Extender:** Boltorn® H20 **Polymerization Solvent:** N,N-dimethylformamide (DMF)	HB-PUPCM:90 HB-PUPCM:80 HB-PUPCM:70 HB-PUPCM:60	138.2 118.1 102.8 91.2	67 66.4 62.2 57.5	First heated from -50 to 150°C at a rate of 10°C/ min. Second, at the same rate sample was heated again to 250°C. Enthalpy was recorded on second scan.	Yes	**Non-Linear: Hyper-branched**	90% 80% 70% 60%
Cao 2007	**PCM Polymer:** Polyethylene glycol (PEG, M_n = 6,000) **Diisocyanate:** Toluene-2,4-diisocyanate (2,4-TDI) **Chain Extender:** Boltorn® H30 **Polymerization Solvent:** N, N-dimethylformamide (DMF)	HB-PUPCM	124.8	66.6	First heated from -50 to 150°C at a rate of 10°C/ min. Second, at the same rate sample was heated again to 200°C. Enthalpy was recorded on second scan.	Yes	**Non-Linear: Hyper-branched**	90%
Liao 2010	**PCM Polymer:** Polyethylene glycol (PEG, M_n = 6,000 g/mol) and Pentaerythritol (PE) **Diisocyanate:** Liquefaction modified 4,4'-diphenylmethane diisocyanate (L-MDI, with 23 wt% **Chain Extender:** Boltorn® H20 **Polymerization Solvent:** N,N-dimethylformamide (DMF)	HBPU D-HBPU	115.7 125.0	55.7 59.0	First heated to 120° C, held for 5 min then cooled to -20 °C at a rate of 10°C/ min. Second, at the same rate, sample was heated from -20 to 120°C. Enthalpy was recorded on second scan.	No	**Non-Linear: Hyper-branched**	90% 90%
Xi 2009	**PCM Polymer:** Polyethylene glycol monomethyl ether (MPEG, M_n = 1000, 2000, 5000 g/mol) **Diisocyanate:** 2,4'-Toluene diisocyanate (TDI) **Chain Extender:** "PD" and Phenylethylene (PE) **Polymerization Solvent:** Tetrahydrofuran (THF), Acetone, N-hydroxymethylacrylamide (NMA), and azodiisobutyronitrile (AIBN)	MGPM: 71% MDPM: 64% MGPM: 53% MGPM: 46% MGPM: 38%	108.5 90.3 75.9 53.4 47.2	57.7 55.8 55.4 54.0 53.2	A heating/cooling rate of 10°C/min over the different temperature range (0–200 °C, -50 to 100, then cooled to -50 °C)	Yes	**Linear**	71% 64% 53% 46% 38%
Xi 2012	**PCM Polymer:** Polyethylene glycol (PEG, M_n = 6,000) and MPEG (M_n = 4000 g/mol) **Diisocyanate:** 4,4'-Diphenylmethane diisocyanate (MDI) **Chain Extender:** Novel tetrahydroxy compound (THCD) **Polymerization Solvent:** Tetrahydrofuran (THF) and N,N-dimethylformamide (DMF)	TPUPCM	137.4 J/g	56.1	DID NOT SPECIFY HEAT/COOL RATE. Thermal cycling testing of 100 consecutive heating and cooling cycles (in the temperature interval 0–100°C, maintained at approximately 15 and 25 min, respectively.)	No	**Non-Linear: graft-comb network**	
Yanshan 2014	**PCM Polymer:** Modified copolymer Polyethylene glycol (PEG, Mn = 1000, 2000 4000, 6000, & 10000 g/mol) (MFPEG) **Cross-linking agent** Formaldehyde **Chain Extender:** Melamine **Polymerization Solvent:** Water	MFPEG1000 MFPEG2000 MFPEG 4000 MFPEG6000 MFPEG10000	82.7 85.3 97.9 103.9 96.2	25.96 28.3 35.31 36.88 32.3	Samples were heated from 10–90°C at a rate of 10°C/min under a nitrogen atmosphere.	No	**Non-Linear: IPN Network**	

Distinction between molecular structures of PU-SSPCMs

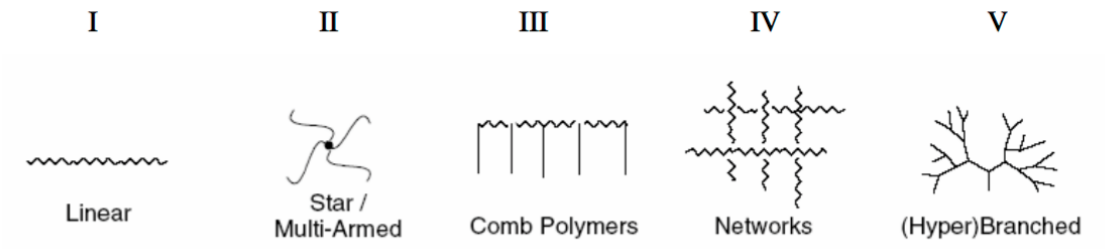

Figure 2.9: Schematic of the four main types of polymer architectures: (I) Linear, (II) graft star-block, (III) graft comb, (IV) Interpenetrating network (IPN) (V) Hyper-branched.

According to Table 2.4, the monomer constituents of each of PU-SSPCM listed vary by either it's diisocyanate, PEG molecular weight, or chain extender component. It is based on the functionality of these monomer constituents that determines its molecular architecture. Figure 2.9: Schematic of the four main types of polymer architectures: (I) Linear, (II) graft star-block, (III) graft comb, (IV) Interpenetrating network (IPN) (V) Hyper-branched. schematically shows the four main types of polymer molecular architectures.

2.4.4. LINEAR PU-SSPCMS

In Table 2.4, the linear PU-SSPCMs studied by Alkan[34], Su[31], and Meng[79] were based on the same linear alternating block copolymer structure. (Figure 2.8) which consists of a diisocyanates and chain extender HS blocks and PCM polymer SS block. According to Table 2.4, the listed linear PU-SSPCM varied by either its diisocyanate, PEG molecular weight or chain-extender monomer reagent. In order to obtain a linear structure, it was

necessary that during polymerization that ratio of NCO and OH groups be maintained at a 1:1 stoichiometric and that all of the monomer reagents used be bifunctional (f= 2). Most authors used used a bi-functional (f=2) chain extender, 1,4-Butane diol (BDO) to obtain a linear chain structure; except for Alkan who did not use a chain extender at all.[34]

These linear PU-SSPCMs rely on a physically cross-linked network to maintain its solid framework that allows it to exhibit a solid-to-solid phase transition. The physically cross-linked network is made up a urethane-rich crystalline structure that is formed as a result of secondary hydrogen bonding interaction between neighboring urethane groups. The physical cross-links demonstrate a glass and melting transition at elevated temperatures (>100˚C), while the PEG PCM polymer demonstrates its glass transition and a thermal transition around ambient temperatures depending on its molecular weight (<100˚C) [37,42]. The significantly higher melting temperature of the physical cross-link is the reason why these material remain in the solid state as the PEG PCM polymer cycles through its phase transition at temperatures less than 100˚C. [31,34,48]

Thermal Energy Storage Properties of Linear PU-SSCM

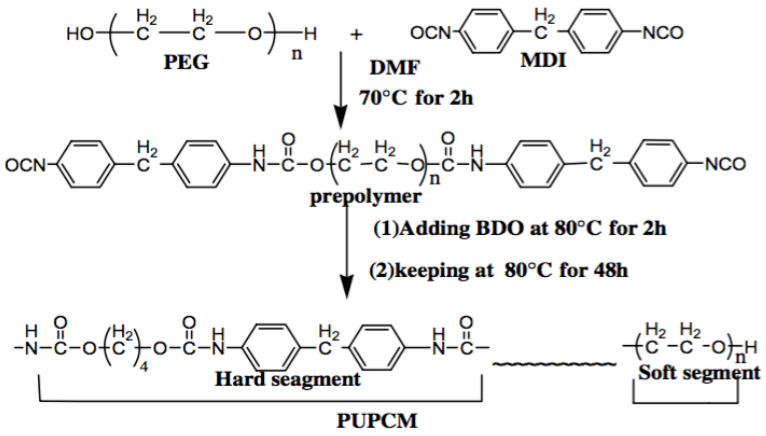

Figure 2.10: Schematic of Reaction scheme for Su's Linear PU-SSPCM prepared with MDI and PEG M_n= 10,000 g/mol (Source: Su 2006[31]; Reprinted with permissions from Springer. July 7, 2016.)

Su and Liu prepared a PU-SSPCM with MDI and PEG M_n=10,000 g/mol and a 1,4 butane idol (BDO) chain extender and reported an enthalpy value of 138.7 J/g. [31] A schematic of the reaction scheme for Su's linear PU-SSPCM is shown in Figure 2.10. Meng studied a similar PU-SSPCM system, with a phase change enthalpy of ~110J/g but instead used IPDI as the diisocyanate and a PEG molecular weight of M_n=3400 g/mol.[80] Alkan prepared 3 sets of PU-SSPCMs with HMDI, TDI, and IPDI combined with a series of PEG molecular weights M_n= 1000, 6000, 10,000 g/mol. [34]The results from Alkan's studied demonstrated how PU-SSPCM thermal energy storage properties vary according to the composition of its diisocyanate and PEG molecular weight components. Alkan noticed PU-SSPCMs prepared with higher PEG molecular weights also showed higher enthalpy values. However, it can also be seen that with higher molecular weight, higher phase transition temperatures were also observed. When comparing the enthalpy values of PU-SSPCMs prepared with the same PEG molecular weight, Alkan found that the PCMs with aromatic diisocyanates, TDI and IPDI, demonstrated lower enthalpy values,

compared to the PCMs prepared with aliphatic HMDI.[34] Alkan attributed this observation to the aromatic diisocyanates creating a larger steric effect that inhibited crystallization of a greater portion of the PEG PCM chain. Compared to aliphatic diisocyanates, aromatic diisocyanates are bulkier and more rigid because they are unable to assume multiple conformational arrangements. Thus, due to the inherent structural characteristics of aromatic diisocyanates, the range of PEG chain interaction was reduced more so than the smaller aliphatic diisocyanates. As a result, the PU-SSPCMs prepared with larger, more rigid aromatic diisocyanates exhibited lower thermal energy storage properties. The results from Alkan's study provided evidence that there might be a correlation between the structural characteristics of diisocyanates, PEG molecular weight and thermal energy storage properties. However, Alkan failed to consider other factors underlying HS configuration. The HS component in the samples he studied were not prepared with a chain extender nor were they prepared with a weight ratio high enough to produce physical cross-links, which explains why not all of the samples Alkan studied exhibited a solid-to-solid phase transition. Secondly, Alkan did not consider the possibility that phase separation may have been a factor affecting his results. It is highly likely that the lower enthalpic values observed for the samples prepared with larger aromatic diisocyanates is not solely attributed to the diisocyanate molecular structure but rather as a result of phase mixing. In addition to the chemical level factors that impact soft segment crystallization through the chain-end effect, some authors have assumed a strong link between the degree of phase separation and soft segment crystallinity.

Linear PU-SSPCMs are Thermoplastic Polyurethanes with a Heterogeneous Phase Morphology

The linear PU-SSPCMs are considered to be a thermoplastic polyurethane material. Therefore, they are expected to demonstrate thermal reversible properties, and will exhibit a phase separation between the PCM polymer and urethane hard segments. However, the appearance of a heterogeneous phase structure depends on the ratio of HS and soft segment (SS) content that makes up a polyurethanes chain structure. [37] It also depends on processing treatments.[54] According to the Koberstein model[57], a critical hard segment content (%HSC) of at least 30% to observe a two-phase system [37]. Alkan [34], Su[31], nor Meng[79] specified what the percent of HS content was in the samples they prepared.

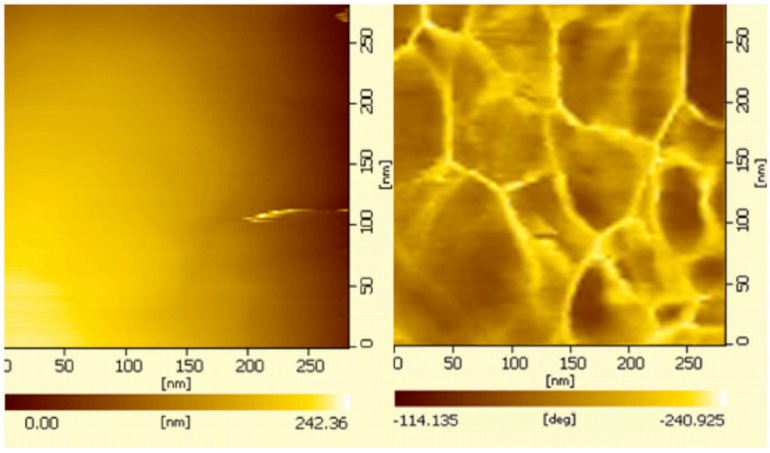

Figure 2.11: Tapping mode atomic force microscopy 'height' and 'phase' images of PEGPU (left: height image, right: phase image) (Source: Meng 2008; Reprinted with permissions from Springer. July 7, 2016.)

The atomic force microscopy (AFM) phase images Meng took showed evidence of phase separation indicating that the HS physically cross-linked network confined the PEG PCM chain that resembled the typical microencapsulation technique used for containing

SLPCM. [79] Although it was not specified, the AFM phase images prove that Meng's sample was comprised of at least 30% HS content. These phase images are given in Figure 2.11.

It has also been noted for regular polyurethane materials that a chain extender is an essential component of the HS for observing phase separation. The purpose of a chain extender is to help form physical cross-links by increasing hydrogen bonding strength between urethane HS.[81,82] Without a chain extender the fiber axis that serves to stabilize the structure of the hard segment physical cross-links will be offset and thus inadequate packing of urethane hard segments will be observed. [44]

However, it was noticed that Alkan did not use a chain extender in the preparation of his materials. Alkan[34] reported that a solid-to-solid phase change was observed for all PCMs prepared with aliphatic HMDI, however the PCMs prepared with aromatic diisocyanates (IPDI and TDI) and PEG M_n=6000 and 10,000 g/mol only demonstrated a solid-to-solid phase change. The PCMs prepared with IPDI, TDI and PEG M_n=1000g/mol demonstrated a solid-to-liquid phase transition. While, Alkan attributed this observation to the large steric effects caused by aromatic diisocyanates rigid molecular structure, it is more likely that this occurred because a chain extender was not used.[34] Based on polyurethane literature, it is known without a chain extender a HS with aromatic diisocyanates does not have enough structural regularity to form physical cross-links.[81] It is likely that even the PCM Alkan prepared that did exhibit solid-to-solid phase change behavior, it's solid framework was held together by PEG chain entanglements and not physical cross-links. This should be addressed in future work.

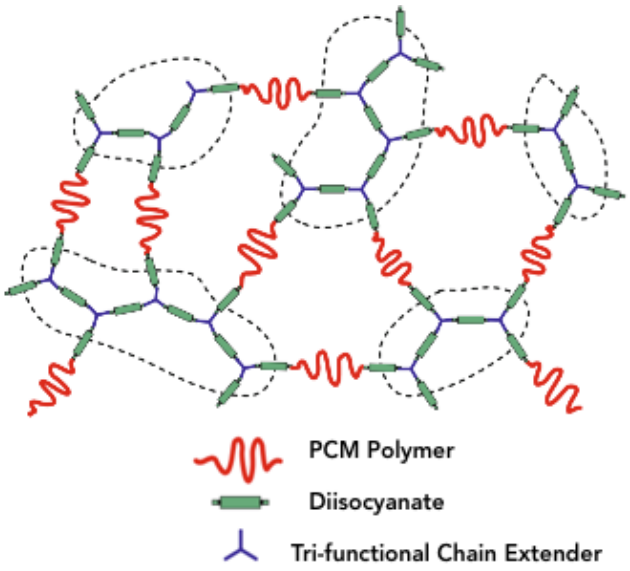

Figure 2.12: Diagram of PU-SSPCM with tri-functional chain extender

Mostly from the results presented in Alkan's study, a correlation between the structural characteristics of diisocyanates, PEG molecular weight and thermal energy storage properties can be noticed. From the comparison of enthalpy values reported by Su[28], Alkan[34] and Meng[30](See Table 2.4), all of which used different diisocyanate reagents, quite a bit of variation in enthalpy values can be seen. This indicates that the diisocyanates may have a significant effect on TES properties. Alkan's findings suggests that modifying the structural geometry of the diisocyanate component will also cause a significant change in phase change properties in PU-SSPCMs. While, his study provided great insight, he failed to address other typical factors known to affect SS crystallization in regular PU materials such as, HS length, the degree of phase separation and HS content[45,51,61,83,84].

Overall, the results from Alkan[34] and the others mentioned studies on linear PU-SSPCMs did not provide enough conclusive evidence to proves this as they have failed to address

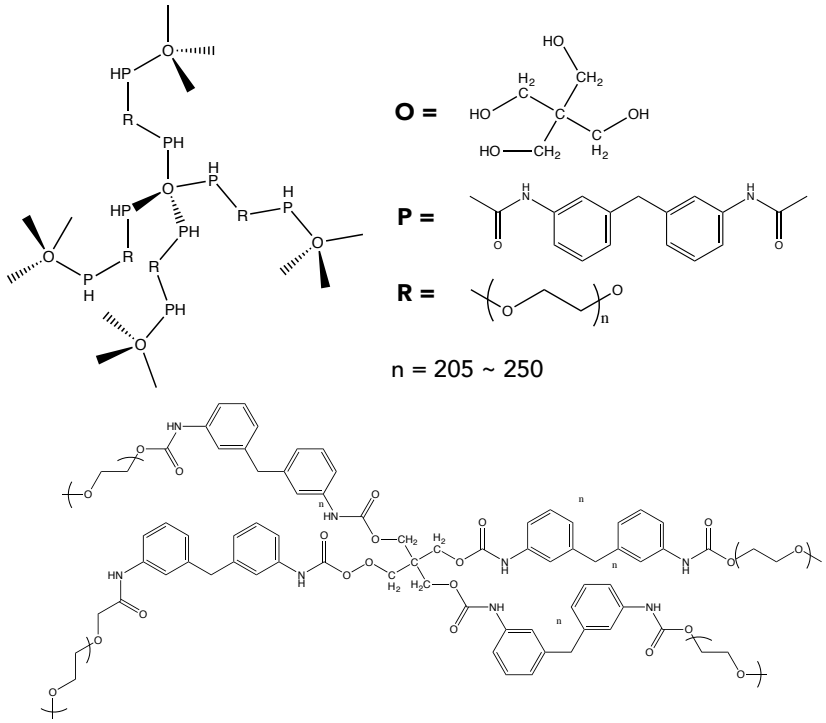

Figure 2.13: Li 2007 Star-like PEG/MDI/PE copolymer PU-SSPCM (Adapted from Li 2007; Reprinted with permissions from Springer. July 7, 2016.)

important factors related to phase separation and the percentage of HS content. Thus, more information on the connection between diisocyanate structure and PEG chain crystallization is needed to correlate PU-SSPCM microstructure influence on thermal energy storage properties.

2.4.5. NON-LINEAR PU-SSPCM

Non-linear PU-SSPCMs demonstrate the same HS-PCM block copolymer system as linear thermoplastic PU-SSPCM. Except that, as far as we know, because of its structure, non-linear PU-SSPCMS do not form physical cross-links. As highlighted in Table 2.4, the non-linear PU-SSPCMs were also varied by PEG molecular weights, diisocyanate, and chain extender monomer reagents. While the linear PU-SSPCMs only used reagents

with a functionality equal to 2, non-linear PU-SSPCMs prepared by Cao[26], Liao[49], Li[24], Xi[29] and Yanshan[50] used multi-functional reagent ($f < 2$) in the HS have to create a non-linear PU-SSPCM systems with unique molecular architectures like the ones shown in Figure 2.9: II - V. When a chain extender is used with a functionality equal to 3 or more, the primary chain structure is no longer linear. Instead, a network polymer structure like the one depicted in Figure 2.15. In the non-linear structure, each HS (diisocyanate + chain extender) has three-arms and three PCM polymer attached. Consequently, these non-linear PU materials no longer rely forming hydrogen bonded physical cross-links to maintain its solid framework. Instead, these materials attribute its structural integrity to the diisocyanates junction point which serves as the point of cross-link for more than two PCM polymer chains. It is assumed that the multifunctional HS cross-link alone is thermally labile enough to maintain the solid framework above 100˚C so that a solid-to-solid phase transition is observed. Li prepared a PU-SSPCM with a star-like molecular architecture (Figure 2.11: II) cross-linked network PU-SSPCM using a tetrafunctional chain extender called pentaerythritol (PE) along with, MDI (4,4'-diphenylmethane diisocyanate) and PEG M_n = 10,000 g/mol.[24] The molecular structure of Li's star-block PU-SSPCM is depicted in Figure 2.13.

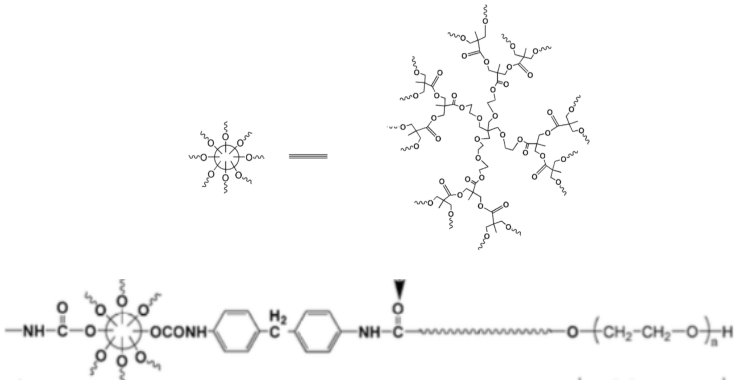

Figure 2.14: Schematic of Hyper-branched PU-SSPCM (HB-PUPCM) prepared by Cao. (Source Cao 2006[26]; Reprinted with permissions from Elsevier. July 7, 2016.)

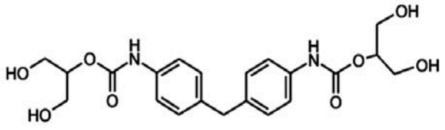

Chemical Formula: $C_{21}H_{26}N_2O_8$
Molecular weight: 434.4397

'THCD' chain extender

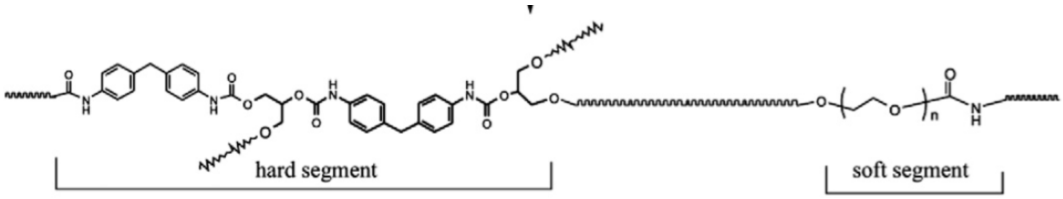

Figure 2.15: Chain Structure pf Xi's Comb PU-SSPCM (Source: Xi 2012[29]; Reprinted with permissions from Elsevier. July 7, 2016.)

Liao and Cao[26,32,49,85]have published a series of papers on a hyperbranched PU-SSPCM, in which different generations of the multifunctional reagent Boltorn® were used as a chain extender to formulate two versions of PU-SSPCM with a hyperbranched molecular architecture similar the one illustrated in Figure 2.9:V. Figure 2.16 shows a schematic of the synthesis scheme Cao and Liao followed to prepare these hyper-branched PU-SSPCM (HB-PUPCM. Liao's PU-SSPCM was prepared with PEG M_n=6000 g/mol, MDI

and Boltorn® H20, which was used as the multi-function reagent to create the hyper branched network. To improve enthalpy and thermal resistance the polymer was doped with other PCMs like polyethylene (PE). As for Cao[26,32], he prepared two different hyper-branched PU-SSPCM; one with third generation Boltorn® H30 and MDI, and the other with second generation Boltorn® H20. PEG molecular weight and 2,4-TDI were selected as the PCM soft segment and the diisocyanate hard segment. A melt enthalpy of 75 J/g was observed for Liao's PU-SSPCM. Whereas, Cao's PU-SSPCM demonstrated a lesser melt enthalpy of 124.8 J/g and 118.1 J/g for the latter PU-SSPCM. Liao's PU-SSPCM was doped with other PCMs like polyethylene (PE) to improve enthalpy and thermal resistance; which is the main reason it shows higher enthalpy.

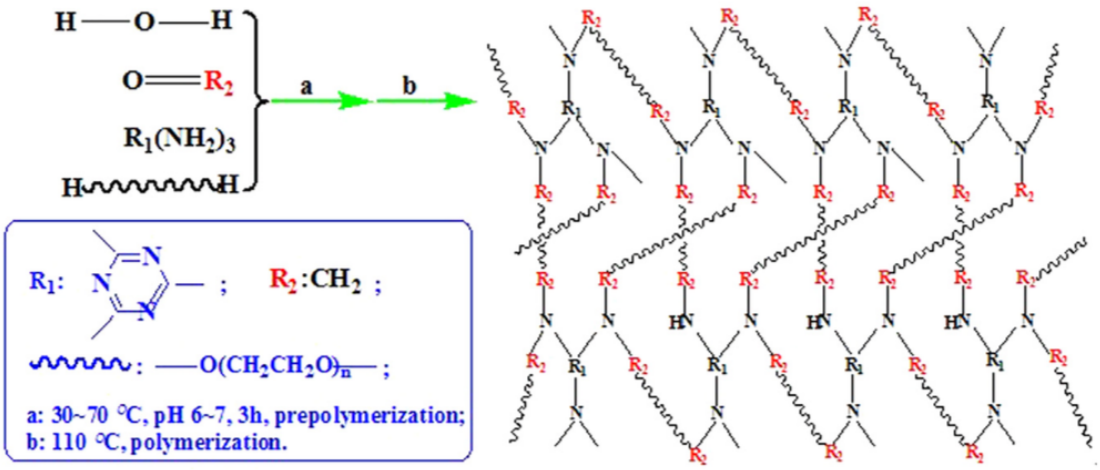

Figure 2.16: Synthesis scheme to network structure of Yanshan's IPN PU-SSPCM; Reprinted with permissions from Elsevier. July 7, 2016.)

Xi 2012[29] derived a novel tetra-functional chain extender named "THCD", which stands for tetra-hydroxy compound, to prepare a PU-SSPCM with a graft-comb molecular architecture. (Figure 2.9: III.) The molecular structure of THCD is shown in Figure 2.15, respectively. PEG M_n = 6,000 g/mol and a secondary copolymer monomer containing

polyethylene glycol monomethyl ether (MPEG) modified with a vinyl group was used as the phase change unit. A series of synthesis steps were followed to combine the PEG copolymer PCM with THCD and MDI.

Yanshan[50] prepared a non-linear PU-SSPCM with a molecular architecture is similar to the sketch of a interpenetrating network (IPN) network polymer drawn in (Figure 2.9: IV.). Yanshan's IPN PU-SSPCM consisted of a melamine/formaldehyde chemically cross-linked network that was formed through amine–aldehyde condensation reaction and aldolization mechanism. Its three dimensional cross-linked network serves as the HS component that maintains the materials solid framework. The molecular structure of this IPN PU-SSPCM is shown in Figure 2.16. Typically, phase separation is prevented in materials with 3-D IPN molecular architectures because the HS cross-links are immobilized and so the HS remain dispersed throughout the soft segment phase[86]. Therefore, in result to its IPN cross-linked structure Yanshan's PU-SSPCM is assumed to have a homogeneous morphology.

Non-linear PU-SSPCMs are Thermoplastic and demonstrate Heterogeneous Morphology

While all of the non-linear PU-SSPCM studies summarized Table 2.4 have a chemically cross-linked network structure, some of these PU-SSPCMs were found to still demonstrate a heterogeneous morphology. The AFM phase images shown in Figure 2.17 taken by Li and Cao of their star-block and hyper branched PU-SSPCM, showed separate phase domains between the branched "hard" block structure and the PCM PEG "soft" chains PCM chain. This indicated that although they are non-linear, there is a level of phase separation present in these PU-SSPCMs, which implies that they are thermoplastic

non-linear PU-SSPCMs. Of the PU-SSPCMs listed in Table 2.4 the ones with a star-block, graft-comb, and hyper-branched molecular architectures were found to demonstrate a heterogeneous phase morphology. This was an interesting observation considering that phase separation is still observed despite having a chemically cross-linked network structure. Only Yanshan's[50]IPN PU-SSPCM demonstrated a homogeneous morphology, and thus can be classified as a thermoset PU-SSPCM. The status of the PU-SSPCMs linearity and whether a homogeneous or heterogeneous morphology was specified in Table 2.4

There has yet to be any study that correlates phase morphology to the thermal energy storage properties of PU-SSPCM. However, the a IPN PU-SSPCMs Yanshan[50] prepared with this IPN chemically cross-linked PU-SSPCMs prepared by values. Of all the studies mentioned, Yanshan's IPN PU-SSPCM demonstrated the lowest enthalpy (ΔH_m = 103 J/g). However, the melting temperatures were dramatically lower than the other PU-SSPCM system. The melting temperatures observed were between 25-36˚C, whereas close to the temperature range required for building applications.

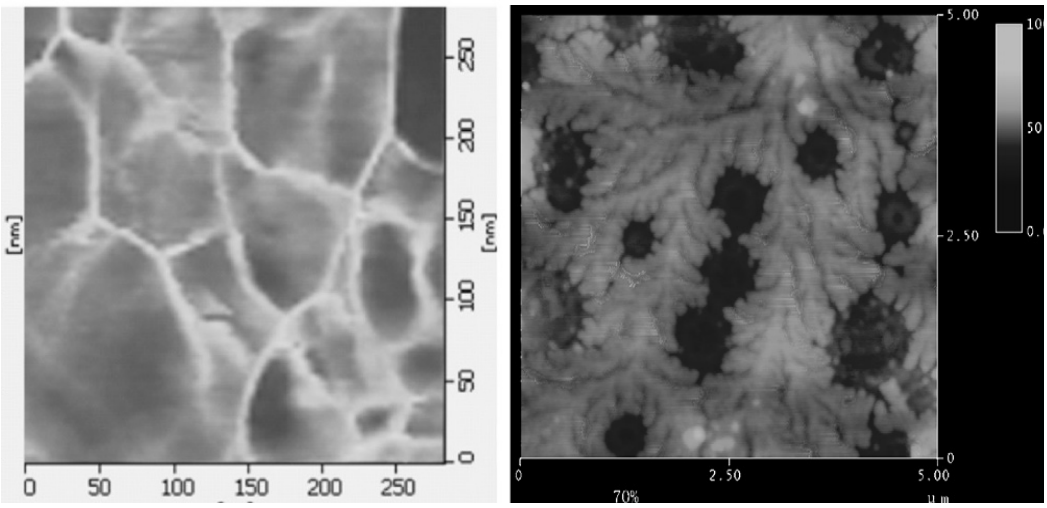

Figure 2.17: AFM phase images of Meng's linear PU-SSPCM (IPDI/PEG-3400/BDO) (left) and Cao's Hyperbranched (HB-PUPCM) (MDO/ PEG-10000/ Boltorn®) (right); Reprinted with permissions from Elsevier. July 7, 2016.)

While it is unknown if the lower observed temperature range has something to do with its different HS composition or its chemically cross-linked network molecular architecture, based on the fact that Yanshan's PU-SSPCM differs from the others listed in Table 2.4 because a) it has a chemically cross-linked network and b) instead of a urethane HS primary chain structure it has a biuret HS chain structure, which is a by-product of urethanes, strongly indicates it may be possible to lower phase transition temperature by altering the PU-SSPCM microstructure. However, first the connection between microstructure and thermal energy storage properties must be defined. However, because this is the first bit of information that gives some indication the phases transition temperature could be lowered by modifying the microstructure it is necessary might be changed to lower phases transition temperature. In order to determine how we might get the root why the thermoset IPN PU-SSPCM demonstrated such as drastic drop in phase transition temperature

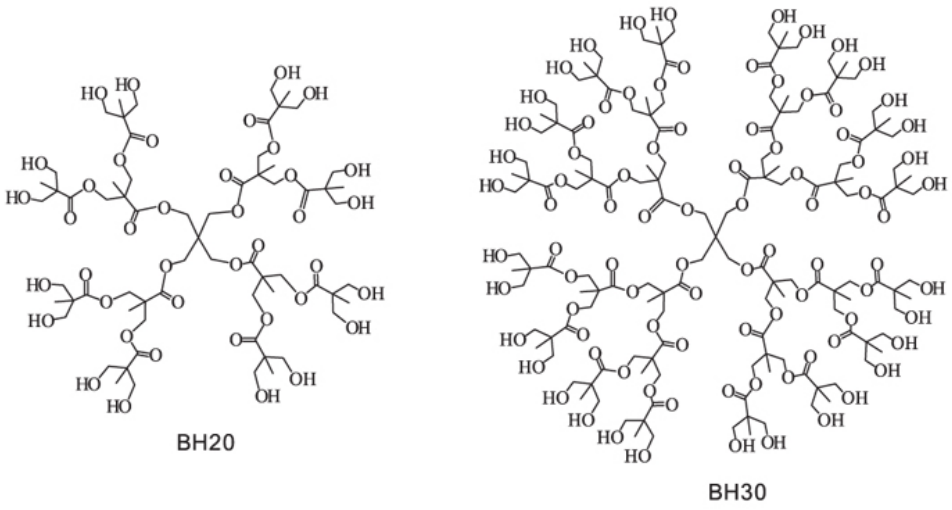

Figure 2.18: Boltorn® H20 (left) H30 (right)(Source Cao 2006 and 2007; Reprinted with permissions from Elsevier. July 7, 2016.)

2.4.6. CHAIN EXTENDER FUNCTIONALITY AND THERMAL ENERGY STORAGE PROPERTIES

The studies on linear PU-SSPCM showed indication of a strong relationship between the diisocyanates component and thermal energy storage properties. However, for the non-linear PU-SSPCMs the same notion that different monomer constituents or in this case different molecular architectures causes a significant change in thermal energy storage properties is not apparent based on enthalpy values given Table 2.4. The comparison of thermal energy storage properties between PU-SSPCM with different molecular architecture reveals a significant difference in enthalpy values (See Table 2.4) Therefore, it is difficult to determine any correlation between molecular architecture and thermal energy storage properties.

Considering that the functionality of the chain-extender determines how many arms of PCM chain branches, it seemed logical to believe that higher enthalpy values would be

observed for PU-SSPCMs with higher chain extender functionality because they can accommodate a greater number of PEG chains and a higher ratio of PCM chain concentration would give rise to more PEG chain crystallization. The chain extenders used by Cao to prepare a hyperbranched PCM were Boltorn® H3O , which has a functionality of 32 and Boltorn® H2O that has a functionality of 16 (shown in Figure 2.18) Considering that Cao's HB-PUPCM prepared with Boltorn® H3O could accommodate 2 time more PCM PEG polymer chains than the H20 version and 4 times more than Li[24] and Xi's [29] tetra-functional PU-SSPCMs, it was expected that Cao's Boltorn® H30 HB-PUPCM would demonstrate the highest enthalpy values, followed by the HB-PUPCM prepared with Boltorn®H2O. However, the enthalpy values given in Table 2.4 showed that Cao's Boltorn® H30 version hyper-branched SSPCM actually demonstrated lower enthalpy values (ΔH_m = 124.8 J/g) than Li's (ΔH_m =153 J/g) and Xi's (ΔH_m =137.4) tetra-functional PU-SSPCM. Because no significant variation between the PU-SSPCM prepared with polyfunctional Boltorn® - and tetra-functional (PE and THCD) chain extenders was observed it contradicted this notion that a higher ratio of PEG PCM chains did not lead to higher enthalpy values.

Compared to the other non-linear PU-SSPCM studied by Yanshan[50], which has a IPN molecular architecture and a homogeneous morphology so it did not need a chain extender, Yanshan's demonstrated the lowest enthalpy values (ΔH_m = 103 J/g), but only slightly lower than the others. However, as far as the phase transition temperatures observed for each study, Yanshan's was dramatically lower than the other PU-SSPCM system. The melting temperatures observed were between 25-36˚C, whereas the others

were all observed at temperatures between 50-65˚C. The temperatures Yanshan observed were significantly closer to the temperature range required for building applications. Based on the fact that Yanshan's PU-SSPCM differs from the others listed in Table 2.4 because a) it has a chemically cross-linked network and b) instead of a urethane HS primary chain structure it has a biuret HS chain structure, a by-product of urethanes, indicates there is a possibility that its molecular architecture is the reason why lower phase transition temperatures were observed. This is the first bit of information that gives some indication the phases transition temperature could be lowered by modifying the microstructure. At this point it is unknown if the lower observed temperature range has something to do with its different HS composition or its chemically cross-linked network molecular architecture. Thus, before this claim can be made, first the connection between microstructure and thermal energy storage properties must be defined.

2.4.7. INCONSISTENT MONOMER COMPONENTS

The PU-SSPCM studies summarized in Table 2.4 are not only inconsistent in their monomer components (PEG molecular weight, diisocyanates, and chain extender), but also in their molecular architectures. Based on the inconsistencies in their configurations, it is difficult to ascertain the optimal SSPCM configuration that will produce maximum thermal energy storage capacity at phase transition temperatures suitable for building applications. It is well-known that modifying PU materials by altering the PEG molecular weights and type diisocyanate components will cause profound changes in the materials final properties. However, because it is not fully understood how each monomer

component affects the crystallization of the PEG PCM chain. Therefore, the enthalpy values reported are not comparable.

2.4.8. THE CHAIN-END EFFECT

The extent to which the hard and soft phases are defined depends on the microstructure of the material. The HS component is made up of a diisocyanate and a chain extender. (Figure 2.8) The diisocyanate composition plays a key role in determining the degree of phase separation; its molecular structure determines the hydrogen bond strength of the HS physical cross-links, as well as the rate at which the HS diffuses through the soft phase. The slightest change in diisocyanate structure can have a profound change in PU final properties.

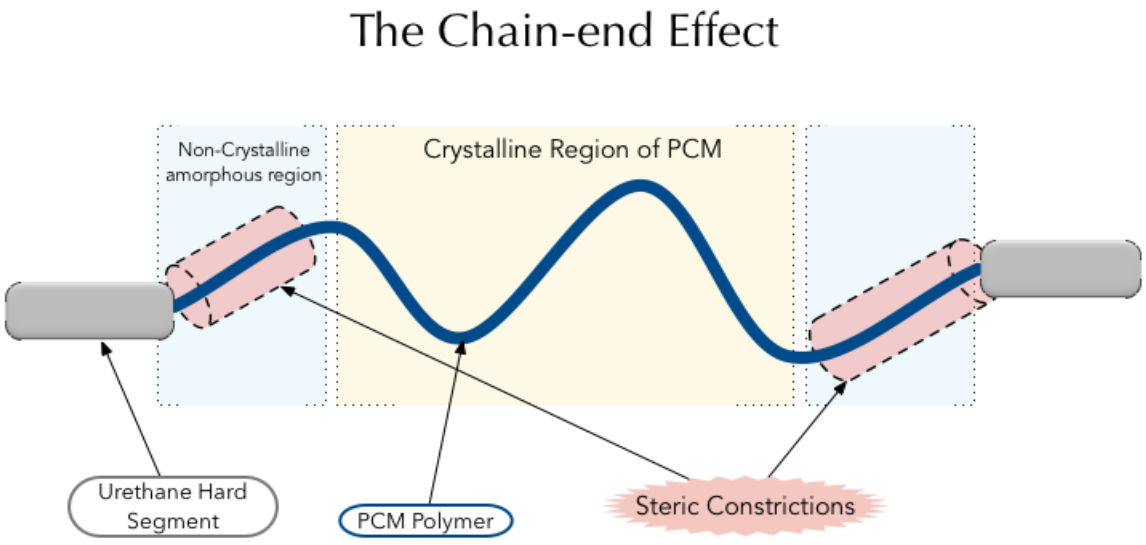

Figure 2.19: Diagram of the HS Chain-End effect

The HS cross-link act as a junction point that prevents the dissolution of PCM chains and is crucial to observing a solid-to-solid phase transition temperature. It has been noticed that a cross-linked PCM polymer will demonstrate lower enthalpy and phase transition temperatures than its pure state; This decline is associated with an increase in the ratio of non-crystalline to crystalline PCM chain units. The appearance of non-crystalline PCM chain unit is attributed to HS steric constrictions that prevents the arrangement and orientation of near-by chain units. This behavior is also observed in regular PU materials and is known as the HS Chain-end effect. The degree to which HS steric hindrance constrictions suppress PCM chain crystallization varies according to the composition and configuration of the HS[54]. It is assumed there is a connection between thermal energy storage properties and the composition and configuration of the HS cross-link. Therefore, A PU with a HS configuration that exhibits less steric constrictions would have a higher ratio of crystalline chain units than non-crystalline and thus would be ideal for obtaining maximum thermal energy storage properties

Crystallization in Polymer Cross-linked Networks

It is well known that the manner in which polymer networks crystallize is different from that of linear polymers. [87]In the case of un-cross-linked polymers, kinetic factors play a dominant role in the formation of lamella [88]. Which is the opposite for the crystallization in polymer networks, which is usually presumed as mostly controlled by thermodynamic factors. [36] Thermoplastic and thermoset SPUs are essentially partially crystalline cross-

linked networks. Therefore, the crystallization of the soft segment chain should be viewed in the same way as polymer network crystallization.

The mobility of the central portion of the soft segment chains in SPU model networks has been shown to be higher than that of the units attached to the cross-links [37]. HS steric constrictions prevent the movement of SS end chain units so they can no longer participate in crystallization. As a result, the outside portion of PCM polymer chains behaves as a non-crystalline amorphous region that form a interphase boundary region between the hard and soft phase domains. The cooperative motions of the amorphous chains units can be observed as a glass transition step. With the increase in non-crystalline amorphous chain-units there is a decrease in crystalline chain units that leads to a decline in soft segment crystallinity. This HS-SS chain-end effect is similar to behavior observed in other conventional cross-linked polymer networks. Flory[55] studied the thermodynamics of a crystallization network and pointed out that a reduction in crystalline melting temperature would be expected to decrease as the ratio of crystalline to amorphous volume decreased, because the disruptive effect of increased cross-linking reduces the ability of the chains to form crystallites [55] Consequently, the arrangement and orientation of PEG molecules are partially suppressed by the disruptive effect and the crystalline regions become smaller, which causes the transition point and enthalpy to fall to a certain degree. In a paper by Qiao, the crystallization of a PEG hydrogel cross-linked by chain scission was investigated. The end-linked PEG had a well-defined chain length, with known cross-linking functionality so that the pure steric effect of the cross-link could be realized. The strength of the steric effect was determined by the reduction is

crystallinity. Therefore, lower PEG molecular weights were observed to experience the strongest steric effect. This work determined that the cross-links acts as an impurity and disturbs the crystallization course allowing only a portion of the PEG chain to crystallize, as well as that a minimum chain length is required for crystalline to form. Flory's disruptive effect, Qiao's steric effect, and the SPU chain-end effect all have different names but are describing the same behavior.

Qiao[89] pointed out that a minimum molecular weight is necessary for crystallization to take course or else the chain won't be long enough to fold or crystallize. The same holds true for SPU, the SS molecular weight must typically be greater than 400g/mol to obtain a semi-crystalline material[24]. There is a contention on what the optimal molecular weight between cross-links is that will yield a notable enthalpy. Qiao[90] reported that when Molecular Weight decreases to 1000, The reason for this is that the motion of the chains of PEG is restricted by the cross-links and the molecular chain of PEG is not long enough to fold and to crystallize and crystallinity can no longer be detected. [91](Qiao et al.) In Jiang's study maximum crystallinity is achieved when the degree of polymerization is 227. Therefore, the ratio of chain units able to crystallize shrink with lower PEG molecular weights. At the critical molecular weight, no heat of enthalpy is observed since there are no chain units available for crystallization. Depending the distribution of molecular weight, extended chain crystals is the initial crystal formed and the only crystal type formed. Lamella thickness corresponds to whether extended chain or chain-folded crystals are formed[92].

For SSPCM to be used as an efficient TES in building applications a notable enthalpy value generated from a phase transition in the ambient temperature range must be obtained. The main technical problem is that only low PEG molecular weight SSPCM operate at ambient temperatures. Unfortunately, shorter PEG chains experience the strongest steric effect so chain segments are able to crystallize and a smaller enthalpy value is observed. The idea is to identify the molecular configuration that demonstrates the least steric effects, so that low PEG chain molecular weight can be used to achieve a phase transition that occurs at ambient temperatures.

Jiang [25]observed that enthalpy was measure for different PEG chain molecular weights for 80% PEG. Jiang's results observed a maximum enthalpic value for a molecular weight of 10,000 g/mol. This indicates that maximum crystallinity is achieved when the degree of polymerization is 227. Molecular Weight threshold PEG stores latent heat at different temperatures depending upon their average molecular weight. This plateau in PTT and enthalpy occurs when molecular reaches a threshold value. It can be seen that the phase change temperature of the used polymer is increased strongly when the molecular weight is increased from 1000 g/mol to 6,000 g/mol, but there only a small increase when the molecular weight reaches above 6000 to 10,000. The same tendency was observed for the enthalpy. Alkan's study revealed the melting temperature as a function of diisocyanate is invariant above 6000g/mol, but shows a significant variation in phase transition temperature for molecular weights between 1000 and 6000 g/mol. The same tendency was observed for the enthalpy.

Beech [92]discussed the interfacial free energy of low molecular weight PEO. In this paper Flory's theory was slightly modified to include chain folding to more accurately estimate the interfacial energy of PEO for both folded and extended chain crystals. It was noticed in this paper that the distribution of molecular weight correlates to the melting temperature and to obtain the most accurate value the weight average distribution must be calculated. Molecular weights around 3700 that have a wide distribution will crystallize in both extended-chain and chain folding. While a molecular weight of 4000 with a narrow distribution will crystallize only by extended chain folding. Chains that are longer than 6000 molecular weight will crystallize by chain folding and extended chain. When chains begin to chain fold, the interfacial free energy decreases by 1kcal. For molecular weights from 1000 to 6000 /mol, if there is a narrow distribution, will crystallize by extended chain and the interfacial energy increases from 1-3kcal. When the molecular weight of the PEO chain is or is greater than 6000 g/mol, less variation in melting temperature is seen because the interfacial energy is decreasing. Between 1000-6000 g/mol, only increase by 1 kcal because PEG can only crystallize by extended-chain. Therefore, the larger variation in interfacial energy for extended chain crystallites explains why a larger variation in enthalpy is noticed for less than 6000 g/mol. The plateau in enthalpy for PEG molecular weights above 6000g/mol is be attributed to entanglements formed.[87,92-94]

2.4.9. DSC METHOD PARAMETERS

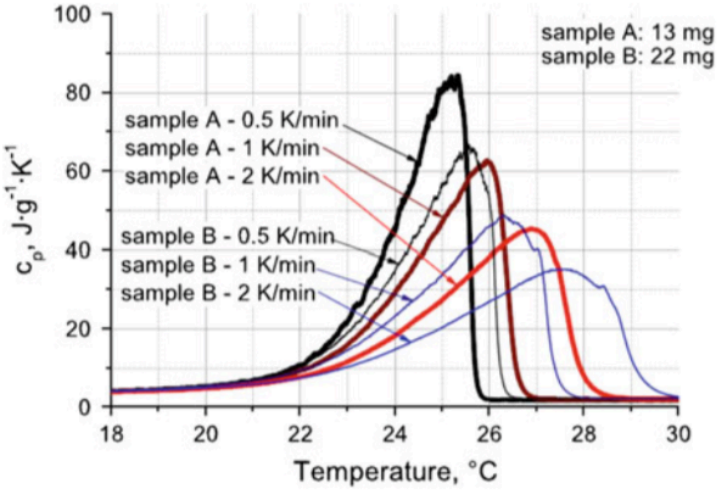

Figure 2.21: Effect of different sample masses and different heating rates. Reprinted with permissions from Kosny 2012. July 7, 2016.

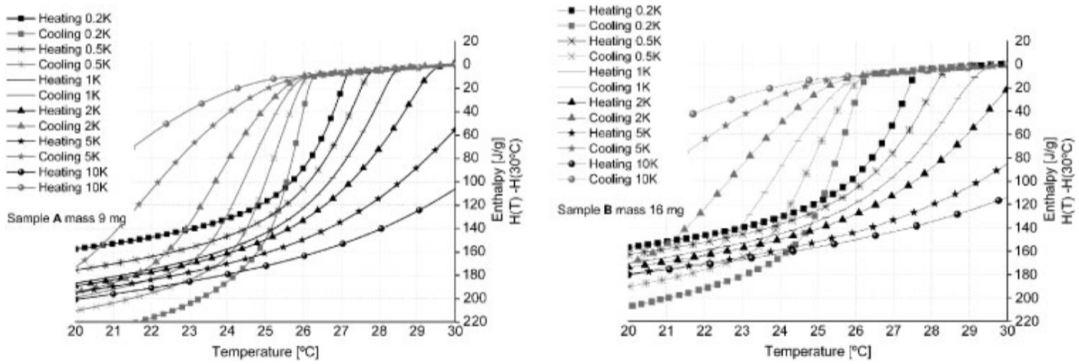

Figure 6. Results obtained with the dynamic method at different heating/cooling rates for sample A (left) and sample B (right).

Figure 2.20: DSC results from different heating/cooling rates. Reprinted with permissions from Mehling 2008. July 7, 2016.

The majority of literature on PCMs use DSC methods to estimate their thermal energy storage properties. It can be seen in Table 2-4 that the heat/cool rate varied between studies. Different heat and cooling rates describe different thermal profiles. [Therefore, the experimental configuration and the DSC parameters were far from optimal for evaluating their TES properties in building environments. Su and Lu[31] reported enthalpy values that were measured at a rate of 10˚C/min, while Alkan[34] recorded the heat of enthalpy values at a heat/cool rate of 2˚C/min, within relatively equal temperature ranges. When the enthalpy–temperature relationship of a PCM is determined using dynamic heating or cooling, the enthalpy values from heating/cooling are systematically shifted to higher/lower temperatures. The reason is that too high heating rates lead to a temperature gradient in the sample and the heat-flux signal therefore originates not from the sample at one temperature, but from a temperature range.[95] Therefore, the enthalpic values of these two studies are not comparable because they are describing two different thermal profiles, which would demonstrate different heat of enthalpy values and melting temperatures. To estimate the thermal energy properties that reflect indoor temperature fluctuations, a heat/cool rate of 2˚C/min is appropriate. In addition to different heat-cool rates, only some of the literature measured enthalpy after being heated to homogeneous melt. This would also have an effect on the enthalpy of heat values measured; however, no author has yet considered these variables in their results or noted them in the experimental design. In Figure 2.20 the thermal profile of the same sample was measured using different rates. It can be seen that the DSC curves were different for each rate. The DSC measures heat flow as a function of sample mass and scan rate. Slower heating and

cooling rates more evenly affect the sample and lead to better resolution. Therefore, it is clear that the heat storage properties of PU-SSPCMs, are not comparable unless the enthalpy of heat and melting temperature were measured at the same rate. In addition to that only some of the literature measured enthalpy after being heated to homogeneous melt. This also would have an effect on the enthalpy of heat values measured. Therefore, it can be assumed that most of the enthalpy values reported in Table 2.4 is not reliable data.

The discrepancies found in earlier PU-SSPCM studies highlight the need for a systematic investigation of the effect the molecular architecture has on PCM polymer crystallization. By comparing the TES properties of a PU-SSPCM with opposing cross-link natures that form the HS junction point that attaches PCM chains, the difference in chain-end effects that disrupt PEG chain crystallinity can be identified.

2.5. SEGMENTED POLYURETHANE ELASTOMERS

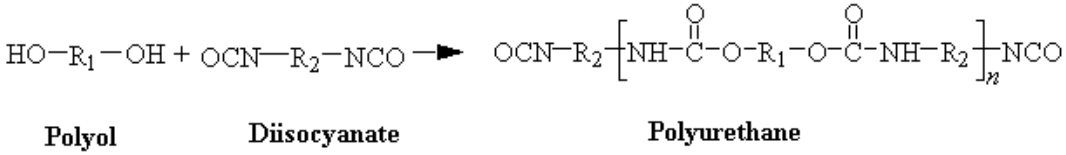

Figure 2.23: The formation of urethane groups through the polyaddition reaction of diisocyanate and polyol monomers.

Polyurethanes (PU) are a broad class of polymers with an unlimited number of structures. The only general requirement is the presence of a urethane group, (–NHCO−O–) in its

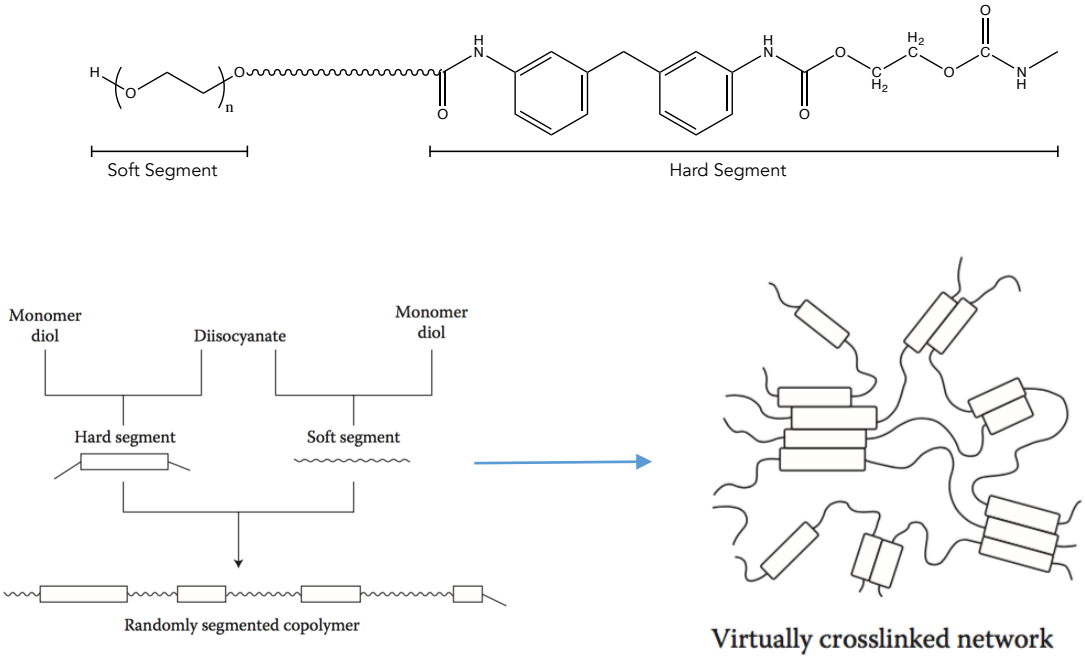

Figure 2.22: Schematic of typical block copolymer SPU made of alternating Soft Segment (SS) and Hard Segment (HS).

primary chain with a more or less frequency. PU elastomers are based on three monomers: (1) an isocyanate source, (2) a macrodiol, and (3) a chain extender. As shown in Figure 2.23, urethane groups are typically formed by a reaction between isocyanate (–NCO) and hydroxyl groups (-OH). More specifically, Segmented Polyurethane (SPU) elastomers are a unique type of PUs that is obtained by reacting polyols and chain

extenders with diisocyanates. SPUs have a -(AB-) type block copolymer structure that consists of alternating rigid and flexible blocks termed “hard segment” (HS) and “soft segment” (SS). Typically, the A "soft" segment (SS) component is generally a high molecular weight polyol or a macrodiol and the B ”hard" segment (HS) component is built from a diisocyanate monomer and a chain extender. [37]The reaction between diisocyanate (NCO) group. This is shown in Figure 2.22.[54] The origin of the HS and SS names stems from the A and B block components demonstrating separate thermal transitions. The SS usually has its glass transition below ambient temperature and the HS is frequently a relatively rigid aromatic molecule with the glass transition above ambient temperature.[37,96,97]

Polyol

Table 2.4: Examples of Polyether and Polyester Polyols

Polyol	Structure
Polyethylene oxide (PEO)	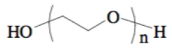
Polypropylene oxide (PPO)	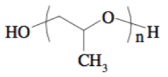
Polytetramethylene oxide (PTMO)	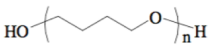
Polyethylene adipate (PEA)	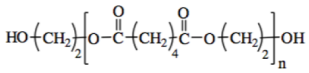
Polytetramethylene adipate (PTMA)	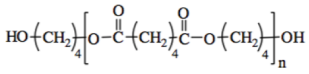
Polycaprolactone (PCL)	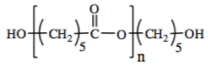

Polyols are used as the macrodiol component. Polyols are hydroxyl terminated macromolecules, with molecular weights ranging from 250 to 10,000 g/mol. The structure of polyol is an important factor in determining the properties of polyurethane. A list of polyols used for the manufacture of polyurethanes is given in Table 2.4. Typically, the polyols used are either hydroxyl terminated polyethers and hydroxyl terminated polyesters.

$$\text{Hydroxyl value (mg KOH/g)} = \frac{56.1 \times \text{functionality}}{\text{molecular weight}} \times 1000 \qquad \textbf{Equation (2.1)}$$

Polyols are characterized by their hydroxyl value, which is related to its molecular weight and functionality as follows.

Diisocyanate Component

The diisocyanate (DI) component can be either aromatic or aliphatic. PUs prepared with aliphatic DI will display profoundly different final properties from PUs[41]. The chain extender (CE) is typically a short chain diol the CE, but can also be a diamine

Chain-extender

The chain extender is an essential component of the hard segment. The introduction of a chain extender increases the HS length. It serves to stabilize the structure of the hard segment's physical cross-links by increasing hydrogen-bonding strength. Without a chain extender, the HS fiber axis is offset, as a result, inadequate chain packing of urethane hard segments will be observed.[98] HS groups without a CE are unable to pack as closely and has less inter-chain interaction than a HS that includes a chain extender. PUs with only a diisocyanate and polyol generally have very poor physical properties and often does not exhibit microphase separation.[54] Typical chain extenders have low molecular weights (M_w) of < 400 and are bifunctional intermediates designed to react with the isocyanate groups to become part of the HS. Either diols or diamines can be used to produce urethane or urea-based hard segments. The choice of chain extender and diisocyanate determines the characteristics of the hard segment and to a large extent the physical properties of polyurethane. Examples of common diol chain extenders are listed in

Table 2.5.

Table 2.5: Examples of Chain Extenders

(EG) (ethylene glycol)	$HO-(CH_2)_2-OH$
(BG or BDO) (butylene glycol)	$HO-(CH_2)_4-OH$
(DEG) (diethylene glycol)	$HO-(CH_2)_2-O-(CH_2)_2-O$

The presence of the urethane groups makes the HS prone to forming Hydrogen bond. SPU are held together by both covalent and and hydrogen bonds. In addition to the thermodynamic incompatibility between the HS, the attractive H bond forces causes neighboring HS groups to self-associate. As a result, SS are excluded and eventually the ordered HS chains form their own phase domain. As shown in Figure 2.28, HS hydrogen bonds form linear hydrogen bonds in either a parallel or an antiparallel fashion, which can lead up to infinite stacks of hydrogen bonded arrays. The hydrogen-bonded urethane groups act as physical cross-links and act as a virtually cross-linked network are responsible for the structural integrity of the material.[37] (See Figure 2.28) Details of the phase domain structure formed is dependent on the strength of hydrogen bond interaction between urethane groups[37].

Nature of HS Cross-link

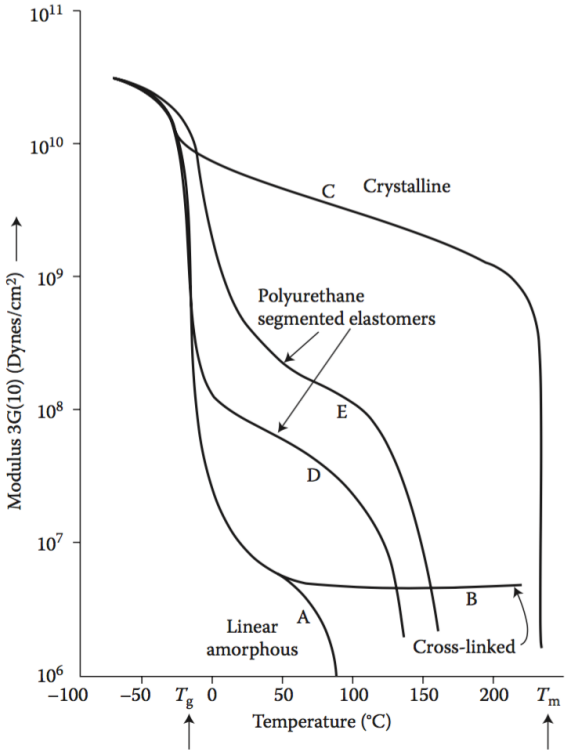

Figure 2.24: Thermal behavior in Polyurethane Elastomers. Reprinted with permission from Michael Szycher, P. D. *Szycher's Handbook of Polyurethanes,*

The hydrogen bonding interaction that forms the HS crystallites and behave as "physical

Table 2.6: Effects of Cross-linking on Mechanical Properties in Polyurethanes Reprinted with permission from Michael Szycher, P. D. *Szycher's Handbook of Polyurethanes, Second Edition*; CRC Press, 2012. Copyright 2000 American Chemical Society.")

Low Cross-Linking of Polyether Urethane Elastomers

MW between cross-links	2500	4500	8500	12,500
Tensile strength (psi)	200	220	130	160
Ultimate elongation (%)	110	190	260	310
Glass transition (°C)	–59	–59	–59	–59
Swelling in benzene (%)	294	342	384	467

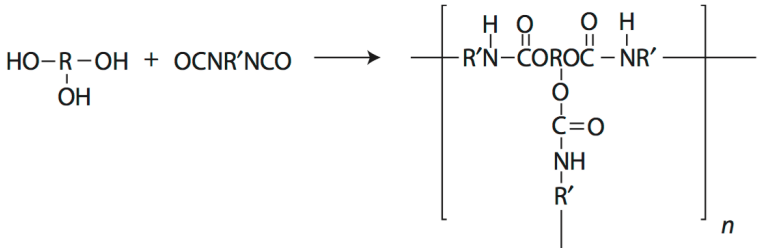

Figure 2.25: Use of trifunctional or higher-functional polyols.

cross-links" formed, is responsible for the structural integrity of the SPU material; however, the HS cross-link may be of a chemical or physical nature.[40] A physical cross-link can be defined as a non-covalent bond that is stable under one condition but not under another.[99] PU elastomers with physical cross-links behave like cross-linked elastomers at ambient temperatures but as linear polymers at elevated temperatures, having reversible properties as the temperature is raised or lowered. These materials are called thermoplastic elastomers. As shown in Figure 2.24, chemical crosslinks are introduced to the urethane HS, the polyurethane material becomes a thermoset and can no longer be destroyed by thermal treatment.[37,40,100-101] The introduction of chemical cross-links immobilizes the hard segment so that the polymer has a homogeneous morphology.[102 40,103] *Cross-linking* increases the degree of cross-linking and leads to an

increase in rigidity, softening point, and modulus of elasticity for amorphous polymers, thus reducing elongation and swelling by solvents. [104] As shown in Table 2.6, increasing the density of chemical cross-links, which can be observed by a lower molecular weight between cross-links, M_c, leads to higher the elastic properties. [103,104] Chemical cross-links are often deliberately added into polyurethane materials to increase mechanical properties such as, tensile strength and hardness, while elongation is decreased. [100,103,105] Most often, the introduction of chemical cross-links takes place at the urethane HS through the use of a tri- or multifunctional reagents, as shown in Figure 2.25, or by increasing isocyanate content to invoke chain-branching through allophanate and isocyanurate linkages. [106] [104]Depending on the chemical composition and the amount of cross-linking and branching, it is possible to obtain products ranging from soft elastomers to hard resinous materials. [104]

2.5.2. DEGREE OF PHASE SEPARATION]

The extent to which the A and B block segments are separated is dependent on its monomer constituents; the type of diisocyanate, polyol and chain extender employed and their arrangement along the primary chain structure affect hydrogen bond formation between the urethane linkages. Equally important is the post-processing treatment, which controls the kinetics of phase separation.[40,107] The combinations of isocyanate and macrodiol reagents, and the synthesis reactions routes and post processing have direct impact on micro-phase structure.[37,108]

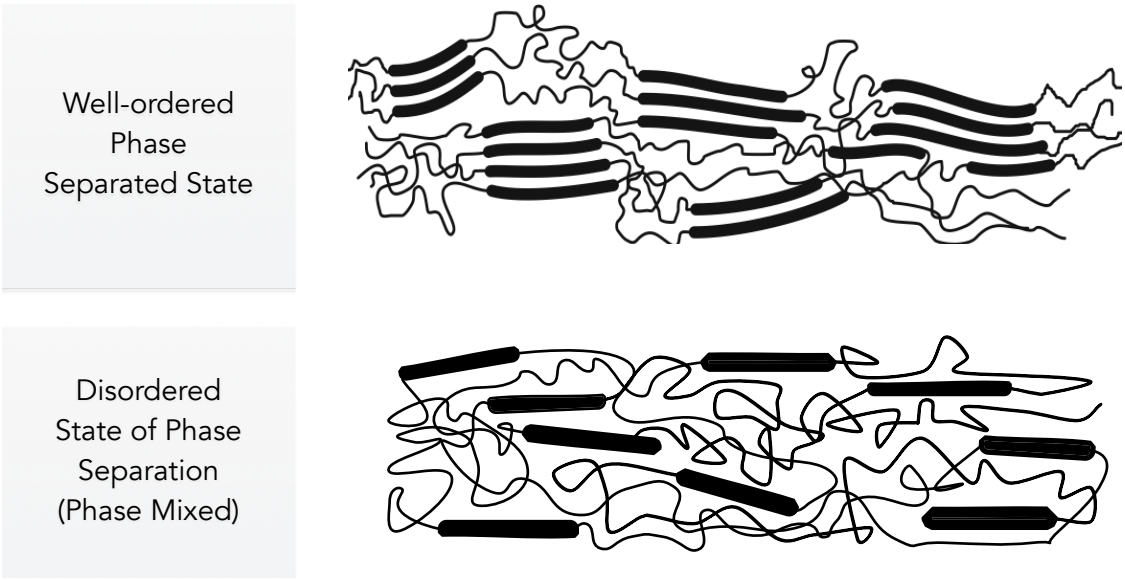

Figure 2.26: Comparison of a disordered state to a well-ordered phase separated state.

In the solid state, unique elastomeric properties are observed due to microdomain formation. Different degrees of phase separation can give rise to a wide realm of properties.[4,109] Characteristics and the organization of the hard and soft phase domains is connected is linked to microstructural and macrostructural factors. Much work has been done to characterize this unique structure-property relationship, however, this work is predominantly conducted for effects on mechanical properties.

The degree of phase separation between the 'hard" and "soft" domain's influence on mechanical properties has been extensively studied. Generally, PUs are materials that have uniform and organized phase morphologies and tend to demonstrate higher tensile strength. The increase in tensile strength stems from physical cross-links formed by the hydrogen bonded hard segments. On the other hand, PUs with less complete phase

separated systems have lesser physical cross-links because the hard segment is dispersed throughout the soft matrix. In result, poorer tensile strength is observed [110].

Chemical and Physical Variable Factors That Determine Degree of Phase Separation

Modifications made to the molecular structure and concentration one of three main PU components: polyol, diisocyanate and chain extender can have a profound effect on the final properties of polyurethanes. The mechanical properties of polyurethane are strongly governed on the extent of microphase separation and the details of the hard and soft phase domain structures. At a primary level the morphology is controlled by the chemical nature of monomers, molecular weight and distribution of hard and soft segments, crosslinking, and degree of branching. At a secondary level, the morphology is controlled by the three dimensional chain orientations and crystallinity.

The strength of the hydrogen bond is dependent on inter-chain interaction, which can be altered by the structural regularity of the diisocyanate hard segment, the chain sequence organization of the polyol and urethane blocks, and the molecular weight of the polyol chain. [61] In addition, physically processing treatments that determine the kinetic of HS chain ordering plays an equally strong role in governing the degree of phase separation. During cooling and above a critical order-disorder temperature, there is spontaneous segregation of SS and HS phase separation to form micro-domains by spinodal decomposition. The degree to which the hard and soft phase domains are established depends on the time order of several events; diffusion rate, crystallization of the hard segment block and/or vitrification.[61]

Synthesis and Phase Separation

The organization of hard and soft segment and thus phase separation, is strongly affected by the method of synthesis. Polyurethanes that are perfectly alternating chain sequences lead to better packing and crystallization of the hard segment. A high order of hard segment crystalline regions will exhibit the highest degree of phase separation and that high degree transpires into superior physical properties.[111,54,112,113] It is much easier for chains with high sequential ordering to form hard segment physical cross-links, thus PUs with more organized chain structures tend to demonstrate higher degrees of phase separation and more organized domain structures [42,111] Therefore, the selection of the appropriate synthesis method is vitally important, as it determines the addition sequence of reactants [37,54]. The preparation of PUs can be differentiated according to the medium of preparation (bulk, solution, water) and the addition sequence of reactants (one-step or prepolymer synthesis routes).[54] Therefore, the method of synthesis used to prepare SPU materials can be used to dictate its microstructure and control its final properties.

Soft Segment Molecular Weight and Phase Separation

Many researchers have focused on the effect of soft segment (SS) type and length, hard segment (HS) type and length, hard domain crystallinity, and the extent of microphase segregation on structure-function relationships in segmented polyurethanes from a mechanical property standpoint.[45] Results obtained from X-ray, and AFM methods demonstrated that an increase in the soft segment molecular weight contributed to increased incompatibility between the hard and soft domains. Therefore, microphase

separation is enhanced with increasing soft segment chain molecular weights because higher molecular weights easily form rich phases on account of entropic contribution, [37,51,52,114]which is why, an enhancement in hard domain crystallinity is observed when hard segment content is increased. Crystallization is only observed in the soft domain if the polyol chain is long enough to fold and form crystalline lamella.

The composition of the SS chain is also linked to determining phase separation behavior. Generally, more complete phase separations are seen for polyether PUs than polyester PUs, because polyester soft segment chains are more susceptible to hydrogen bonding interactions[42]. The attractive forces between ester and urethane groups promote phase mixing; however, the non-polar polyether group's incompatibility with urethane groups further drives the phase separation.[54]

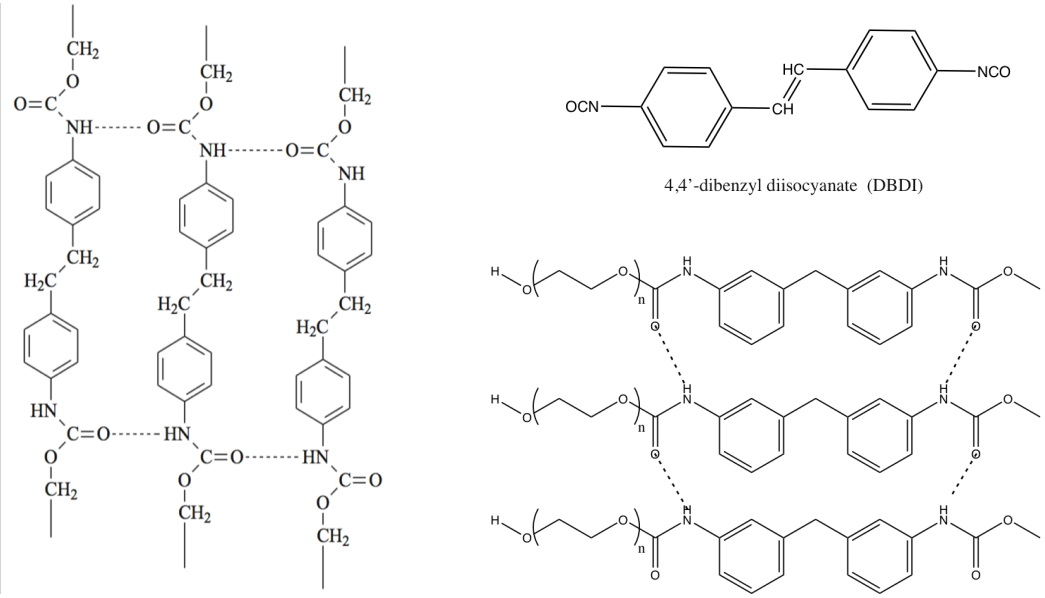

Figure 2.27: Hydrogen bond interaction between 4,4' DBDI HS (left) packs more closely than 4,4'-MDI (right) because of extra methyl group.

Hard Segment Composition and Phase Separation Behavior

The degree of phase separation obtained stems from the strength of inter-urethane hydrogen bonds that make up the physically cross-linked network. The ability of the HS to form hydrogen bonds is dictated by the chemical nature of the diisocyanates. Numerous studies have established that the chemical nature of diisocyanates has a direct effect upon the phase separation behavior, and the details of the domain structure, which ultimately determine macroscopic properties[42].

There are a wide variety of diisocyanate structural moieties variables (aliphatic, aromatic, size, variable geometry, symmetry), which can greatly influence the degree of phase separation and organization of the hard domain structure that will alter the way the hard and soft domain interact, resulting in profound changes to final PU properties.

A) **Extended linear "anti" DBDI position**

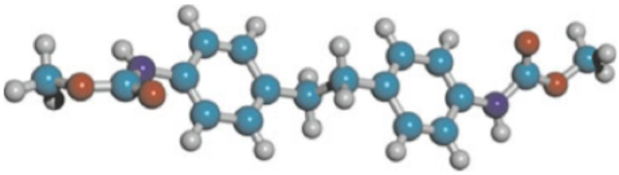

B) **Contorted "syn" DBDI position**

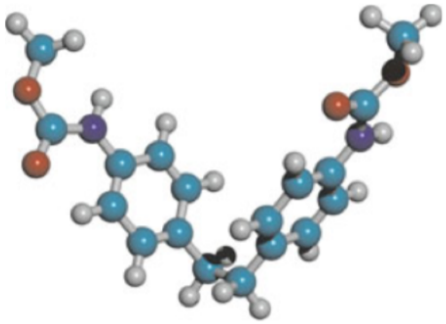

C) **Conventional rigid 4,4-diphenylmethane diisocyanates (MDI) non-crystallizing**

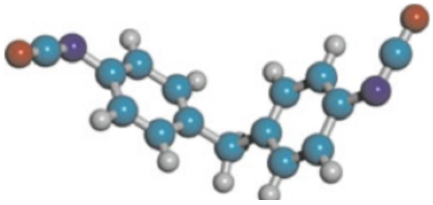

Figure 2.28: "anti" and "syn" conformation arrangements of DBDI vs MDI (Source: Prisacariu 2003[54]; Reprinted with permissions from Springer. July 7, 2016.)

Unlike aromatic diisocyanates, aliphatic have a high degree of chemical and structural regularity favorable for crystallization, and thus lead to stronger hydrogen bonding.[101] Stronger interaction between urethane groups, promote a greater degree of phase separation, [58] which is why polyurethanes with aliphatic HS, typically have more complete phase separations.[115] [61] Additionally, linear aliphatic diisocyanates impart greater flexibility in the HS because it can assume multiple conformation arrangements compared to an aromatic diisocyanate HS. [115,116]

The connection between diisocyanate structural features and physical properties has been the central focus of Prisacariu's'[54] research. For example, the hydrogen bonds of PUs

prepared with DBDI and MDI were compared. It can be seen in Figure 2.28, DBDI's structure has an ethylene bridge between the phenol rings that introduces a variable geometry into the hard segment due to the possibility of internal rotation of this DI around the -CH_2-CH_2 ethylene bridge, leading to the appearance of both "anti" and "syn" rotational conformations.[41] X-ray diffraction spectrums for PUs with DBDI showed a fiber repeat distance expected for a fully extended chain. This indicated that the rigid MDI formed only half of the potential hydrogen bonds of DBDI. However, MDI forms only half of the potential hydrogen bonds as DBDI. X-ray diffraction shows a hexagonal lattice crystalline system. DBDI's ability to assume multiple conformational arrangements leads to greater packing and inter-chain hydrogen bonding. MDI on the other hand, is intrinsically kinked in shape, reducing conformational mobility and thereby hindering close packing and achievement of hydrogen bonding[41,111].

Furthermore, Priscariu[111] studied how flexibility of the HS determined the rate of phase separation for a PU with an aliphatic HDI coupled with BDO, compared to an aromatic MDI and BDO HS. HDI's multiple conformational arrangements were ascribed to introducing greater flexibility to the HS. The HDI-BDO PU produced a well-defined phase domain structure, which indicated that the flexible HS allows more compact packing and surface area for crystallization between the HS blocks as well as allowing it to diffuse faster into separate phase domains[61, 58,115]. Prisacariu[42] observed a greater degree of phase separation for diisocyanates with multiple spatial arrangements because of their variable geometry and because of their ability to diffuse more rapidly through the soft domain matrix.

Furthermore, the symmetry of the diisocyanates chemical structure will have a direct effect on the micro-phase separation, as studies have shown that DI symmetry plays a role in the micro-phase morphology of polyurethanes.[117] Numerous studies have shown that DI symmetry plays a role in the micro-phase morphology of polyurethanes. [117] In their work, polyurethanes that were prepared by using symmetrical diisocyanates such as 1,4-phenylene diisocyanate (PPDI), 1,6-hexamethylene diisocyanate (HDI) and 1,4-cyclohexyl diisocyanate (CHDI), all showed microphase morphology, where ribbon-like hard segments percolated through the soft segment matrix. [60,118]

On the other hand polyurethanes based on unsymmetrical diisocyanates such as bis(4-isocyanatocyclohexyl)methane (HMDI), 2,6- and 2,4-toluene diisocyanate (TDI), MDI and 1,3-phenylene diisocyanate (MPDI), did not display microphase morphology at room temperature. In contrast to their urethane counterparts, all polyether ureas, regardless of the structure or symmetry of the diisocyanate displayed microphase morphology at room temperature. Their study shows the important role of hard segment symmetry on the microphase morphology of polyurethanes.[117]

Yilgor studied the influence of hydrogen bonding and diisocyanate symmetry on microphase morphology. Their study on non-chain extended, segmented polyether urethanes showed some interesting results regarding the microphase separation in these polymers. His study shows the important role of hard segment symmetry on the microphase morphology of polyurethanes.[117] He also found that symmetric diisocyanate showed microphase morphology, while polyurethanes based on unsymmetrical diisocyanates did not display microphase morphology at room temperature. [119]

Kinetics of HS Crystallization

The diisocyanates chemical structure governs the rigidity and structural regularity for HS crystallization that will feed into the three dimensional chain orientation and hard segment crystallinity properties that influence polyurethane morphology at the secondary level. Flexible hard segments are able to percolate through the soft segment matrix much more quickly than rigid HS which can lead to a higher degrees of phase separation.[117] Morphology is determined by the crystallization mechanisms of the hard and soft segment. The nature of the crystallization process is governed by both thermodynamics and kinetics. Crystallinity and chain orientation are macroscopic factors that influence the morphology and final properties of segmented polyurethanes, and can be controlled through post-processing treatments that affect crystallinity and molecular chain orientation such as annealing and stress-induced crystallization which are kinetically controlled [46, 47, 51]. The development of hard segment crystallinity depends on intermolecular interaction between chains and the time allotted for crystallization to occur. Slower cooling rates allow better-packed, more perfect hard segment crystalline structures to form. Highly crystalline hard segments will enhance the exclusion of soft segment chains to produce well-defined phase domain structures. Hood measured the morphological changes that take place when selectively controlling the crystallization of either the HS or SS, by tailoring the SPU composition. He found that compared to quench cooling, slow cooling rates produce a greater reduction in soft domain crystallinity because highly crystalline hard segments enhance the restriction of soft segment chain

motion, which results in a fewer number of soft segment PEG chains active for crystallization.

2.5.3. SYNTHESIS

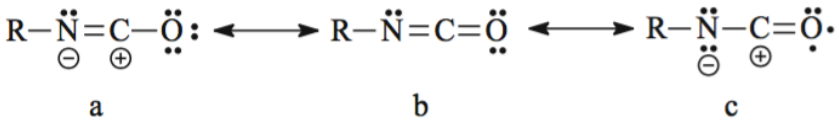

Figure 2.29: Resonance structure of isocyanate group

The first essential component of a PU is the isocyanate. Molecules that contain two isocyanate groups are called diisocyanates. They are compounds containing the isocyanate group (–NCO) that combine with hydroxyl (-OH) groups to form a urethane (-NHC=OO-). The diisocyanate can be aromatic or aliphatic. The structure, substituents, and steric effect can influence the reactivity of the isocyanate.[106,120] Aromatic isocyanates are more reactive than aliphatic isocyanates due to negative charge delocalization. Substitution on the aromatic ring can affect delocalization of the negative charge in the case of aromatic isocyanates. Electron withdrawing groups on the -ortho or -para position can increase the reactivity of the NCO group, while an electron-donating group will have the opposite effect on the reactivity of isocyanate. The electronic structure of the isocyanate group can be represented by resonance structures and is shown in Figure 2.32[121]. The high reactivity of isocyanate toward nucleophilic reagents is mainly due to the pronounced electropositive character of the carbon atom caused by the delocalization of electrons onto oxygen, nitrogen and aromatic groups.[120]

The chemical composition of PU materials can be expressed by its stoichiometry; $N_{diisocyanate} = N_{polyol} + N_{chain\text{-}extender}$ (N is number of moles). Varying the stoichiometric ratio alters the fraction of HS. By changing the formulation, PU materials can be produced with properties ranging from soft to relatively hard-reinforced rubber elastomers. In order to obtain a linear thermoplastic PU material with high molecular weight, equal molar quantities of isocyanate [-NCO] and hydroxyl groups [-OH]. [37,117,121] If the NCO/OH ratio is greater than 1, this leads to the formation of allophanate and/or biuret chain branching. Figure 2.30shows the theoretical relationship between molecular weight and NCO/OH ratio.

Stoichiometric Index Equation $$I = \left(100 \times \left[NCO\right]\right) \div \left(\left[OH\right]_p + \left[OH\right]_{ce}\right)$$

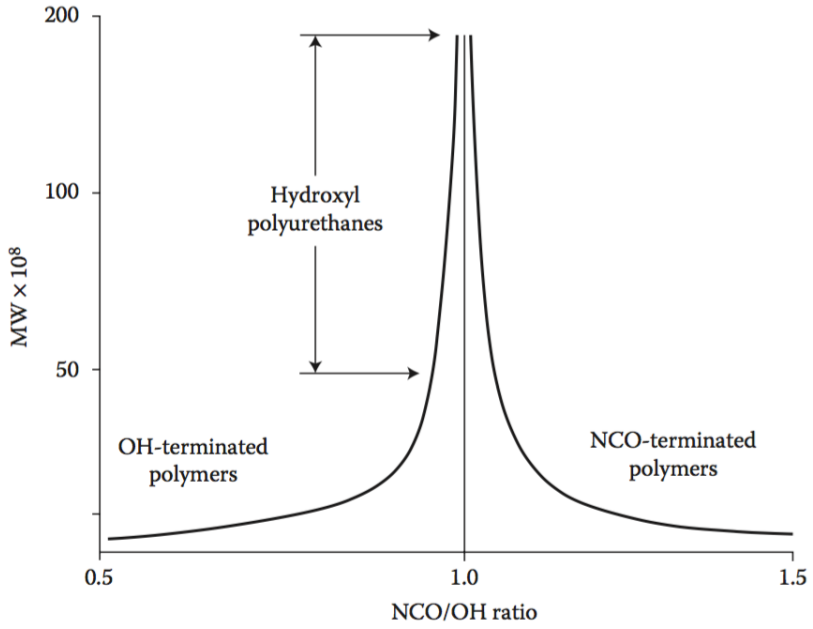

Figure 2.30: The theoretical relationship between molecular weight and NCO/OH ratio. Reprinted with permission from Michael Szycher, P. D. *Szycher's Handbook of Polyurethanes, Second Edition*; CRC Press, 2012. Copyright 2000 American Chemical Society."

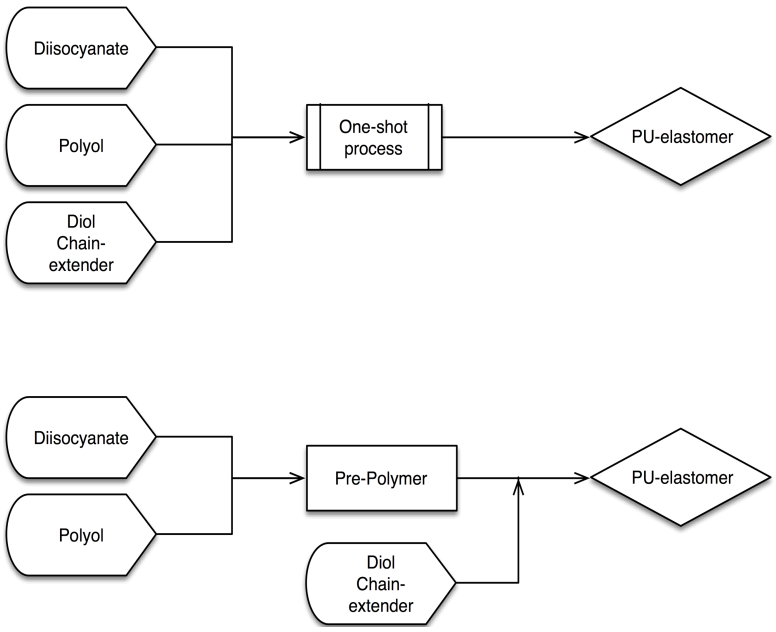

Figure 2.31: One shot and Two-step Method routes for the Synthesis of Polyurethane elastomers.

The diisocyanate-diol reaction route is classified as an addition reaction and proceeds with the formation of no by-product. This reaction is highly sensitive, therefore the reaction conditions strongly influence the microstructure and molecular weight of the polyurethane product yield.

Synthesis Methods

The preparation of PUs can be differentiated according to the medium of preparation (bulk, solution, water) and the addition sequence of reactants (one-step or prepolymer synthesis routes).[54]

As previously mentioned, perfectly alternating chain sequences lead to better packing and crystallization of the hard segment, which indicates a high degree of phase separation that transpires into superior physical properties.[54,112,113] Therefore, because the method of

synthesis determines the addition sequence of reactants, selecting the appropriate synthesis method is important.[37,54] One-step and two-step synthesis routes are the two most commonly used method of synthesis. Statistically, the one-shot method produces polymers with random chain sequences and a high molecular weight distribution, whereas the pre-polymer method has less side reactions and produces polymers with a regular structural arrangement of blocks and a PDI of ~2; the pre-polymer method produces a more regular structural arrangement of blocks.[106,112]

One Shot Method

The one-shot method of synthesis involves adding all of the monomer reagents (PEG, DI and chain extender diol) simultaneously. Typically, when polymerization commences, there is a slightly favored reaction between the -OH of the chain extender and the diisocyanate. Once polymerization commences, the -OH end hydroxyl groups of the polyol and chain extender compete for isocyanate groups. Typically, there is a slightly favored reaction between the -OH of the chain extender and the diisocyanate. As a result, this difference in reactivity between –OH Hydroxyl groups and -NCO isocyanate groups affect the sequence of hard segments in the polymer chain.

Two-Step Method

The two-step method involves first forming a diisocyanate end-capped pre-polymer; the SS polyol is reacted with diisocyanate in a 2:1 NCO/OH ratio. Second, a short diol chain extender is added to form the hard segment and increase the molecular weight. Generally,

the pre-polymer method tends to produce more regular polymers because the extra pre-polymer step end-caps the PEG chain with the diisocyanate and then connects these oligomers with the chain extender. The two-step method is better for obtaining a linear polyurethane polymer with a PDI of ~2, whereas, the one-shot method is not controlled enough to yield regular block sequences, therefore the polymers obtained typically have a much broader PDI.[122] Synthesis of polyurethanes will never result in the same product. Synthetic polymers such as PEG are typically polydispersed. [106]Thus, it is expected that slight discrepancies in data collection may be the result of synthesis conditions as it is impossible to synthesize identical perfect polymers.[100]

Side Reaction

The dimerization and trimerization of the diisocyanate will throw off the stoichiometric balance[121]. Aromatic isocyanates are easily dimerized at low temperatures, especially in the presence of acidic or basic catalysts. Dimerization and trimerization of diisocyanate

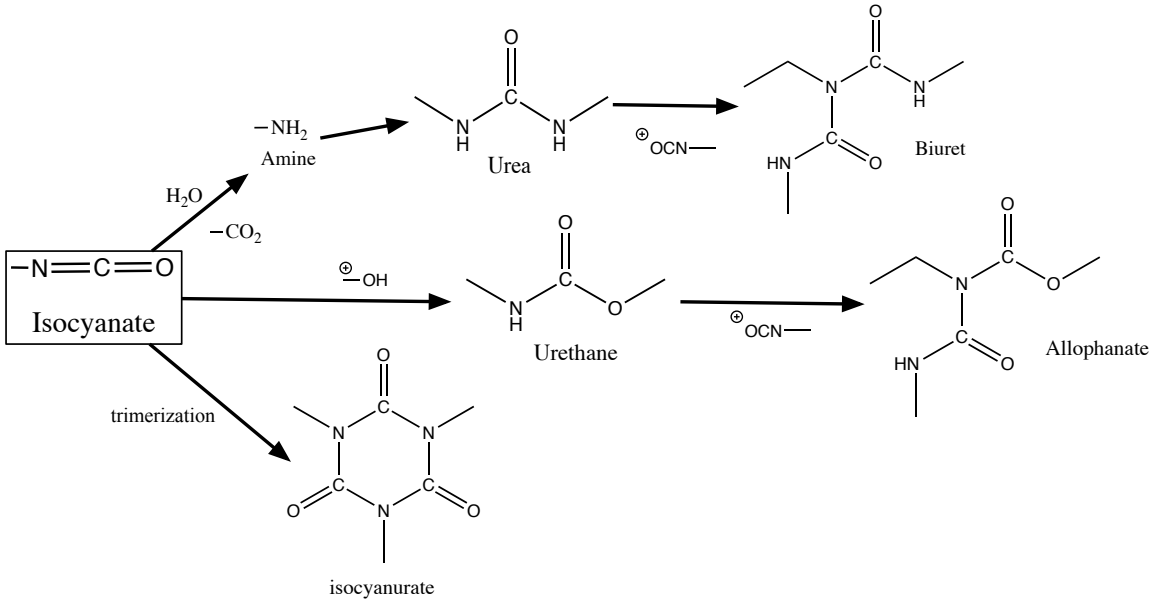

Figure 2.32: Scheme of possible side reaction routes.

can hinder the formation of high molecular weight linear polyurethanes by throwing off the stoichiometric balance ratio of the isocyanate and hydroxyl groups.[37,123] This can also lead to potential introduction of branching or crosslinking sites in the polymer chain. [124] On account of the many potential side reactions that can occur to consume excess diisocyanate, the free content of NCO must be accurately determined so that the correct adjustments of NCO/OH ratio can be made to produce a polyurethane material with the desired properties.[37,124] Chain branching is a consequence of excessive diisocyanate groups. The free remaining isocyanate groups attach to the urethane amine groups to form allophanate linkages or possibly urea groups if water is present in the system.[106]

3.1.3.1.1 Allophanate

According Figure 2.34, the reaction of the free remaining excess isocyanate groups with a urethane group to form an allophanate, leads to chain branching or crosslinking of the polyurethane[121]. When a polyurethane is formed in the presence of excess polyisocyanate, the urethane group itself can supply an active hydrogen to react with the isocyanate, thus forming a branch point. Obviously, a diisocyanate could similarly form a cross-link between two vicinal polyurethane chains. These cross-links are not as stable as the conventional cross- links formed from polyfunctional polyols and polyisocyanates; allophanate cross-links are thermally labile and open quite easily at higher temperature. [123]

3.1.3.1.2 Biuret

When polyurea is formed in the presence of excess polyisocyanate, the urea group

can supply active hydrogens to react with the isocyanate, thus forming a branch point. [120,125] Urea formed in this reaction could also act as a potential crosslinking site by reacting with the isocyanate to form a biuret. It has been reported that the relative rate of reaction of an isocyanate with a urea is much faster than with a urethane.

3.1.3.1.3 Isocyanurate

In the right conditions, excess isocyanate forms cyclic trimers that are called isocyanurate.[124] When the isocyanate is a diisocyanate or higher polyisocyanate, these isocyanurate rings act as extremely stable cross-links in the polyurethane network. Isocyanurate are frequently used to produce polyurethane of thermal stability. [120,124]

Often, these side reactions can be avoided by the use of moderate reaction temperatures (100-140°C) and the use of no catalyst.[126]

Reaction Variables to avoid side reactions

High Purity Reagents:Careful control of reaction variables is vitally important in the synthesis of linear polyurethane materials with high molecular weights. High Purity is essential if high molecular weight linear polyurethanes are to be obtained. Therefore, (a) acidic and basic impurities should be avoided and (b) monofunctional impurities should be avoided as they would act as chain stoppers, thereby resulting in low molecular weight polymer.126 Water may also be considered an impurity; its presence in the reaction system would upset the reactant balance by terminating isocyanate groups. The presence of water first

causes the formation of unstable carbamic acid, which then disintegrates into amine and carbon dioxide. The formation of gas gives rise to foam production. Further reaction between amine and isocyanate leads to the formation of urea groups.124The addition of 0.4 mole-% of water to the reaction can cause a decrease in inherent viscosity from 1.0 to 0.33.126 Therefore, having an anhydrous reaction system is vitally important. Water content should be below 0.1%, to prevent side reactions from occurring. Thus, it is recommended that prior to synthesis procedures the diisocyanate, macrodiol, and short chain diol reactants are de-moisturized to eliminate any absorbed moisture that might lead to adventitious crosslinking

Polymerization Solvent:

The purpose of the polymerization solvent is to provide a nonreactive medium in which the diisocyanate, the diol, and the precipitate polyurethane product are soluble. The polymerization solvent impacts the yield polymer molecular weight and molecular weight distribution of the final polymer.[112] Thus, active hydrogen or polar solvents should be avoided. Lyman demonstrated how the appropriate solvent can enhance the lifetime of the growing polymer chain by minimizing side reactions. In this study Lyman found that the polymerization solvent 50/50 di-methyl sulfoxide/4-methylpentanone-2, demonstrated minimal side reactions, and consistently yielded high molecular weight precipitates with narrow molecular weight distributions, compared to other commonly used solvents such as xylene, or nitrobenzene.[112]

Temperature and Time:

Although the diisocyanate-diol reaction is exothermic, additional heat must be applied if high molecular weight polyurethanes are to be obtained. Temperatures of about 110 to 140°C were found to be most satisfactory for polymerizations.[112,113,126] (Reaction times of the order of 1-2 hours were found necessary to obtain high molecular weight polyurethanes. Long term heating, however, often resulted in degradation of the polyurethane.

In conclusion, in order for the polymer to be genuinely thermoplastic, adventitious crosslinking by the action of absorbed moisture must be avoided, and excess isocyanate groups which means the stoichiometric proportions, must be maintained at I=100 and the reaction system must be as anhydrous as possible.

Chapter 3 EXPERIMENTAL

3.1.CHEMICAL REAGENTS USED

Reagent:	Dimethyl Sulfoxide (DMSO)
Chemical Formula:	C_2H_6OS
Grade:	ACS reagent 99.9%
Company Identification:	Sigma Aldrich
MSDS Name:	Dimethyl Sulfoxide
Catalog Number:	67-68-5

Reagent:	Methyl Isobutyl Ketone (MIBK)
Chemical Formula:	$(CH_3)_2\ CHCH_2\ COCH_3$
Grade:	ACS reagent 98.5%
Company Identification:	Sigma Aldrich
MSDS Name:	4-Methyl-2-pentanone, Methyl Isobutyl Ketone
Catalog Number:	108-10-1

Reagent:	Acetone
Chemical Formula:	$(CH_3)_2CO$
Grade:	ACS reagent, 99.5%
Company Identification:	Sigma Aldrich
MSDS Name:	Acetone
Catalog Number:	67-64-1

Reagent:	Dibutyltin Dilaurate (DBDL)
Chemical Formula:	$C_{32}H_{64}O_4Sn$
Grade:	95% purity
Company Identification:	Sigma Aldrich
MSDS Name:	Dibutyltin Dilaurate
Catalog Number:	77-58-7

Reagent:	Methanol
Chemical Formula:	CH_4O
Grade:	ACS reagent 99.8%
Company Identification:	Sigma Aldrich
MSDS Name:	Methanol
Catalog Number:	67-56-1

Experimental procedures and chemical reagents that are common to all chapters are outlined in this section. Specific research details are described within its respective chapter.

3.2.MONOMERS USED FOR SYNTHESIS

Polyethylene glycol (PEG) molecular weights M_n= 2000, 3000, 6000 g/mol of BioUltra grade was purchased from Sigma Aldrich (CAS No. 25322-68-3). Prior to synthesis, PEG was heated to 100˚C for 3 hours and purged in nitrogen overnight to eliminate water content and achieve high molecular weight polymers. Reaction systems must contain less than 0.5% water to avoid side reactions[122].

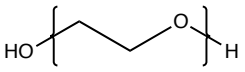

PCM Polyol: Poly(ethylene glycol) (PEG), Mn= {2000, 3000, 6000 g/mol}

Chemical Formula: $C_2H_6O_2$
Exact Mass: 62.04
Molecular Weight: 62.07
m/z: 62.04 (100.0%), 63.04 (2.2%)
Elemental Analysis: C, 38.70; H, 9.74; O, 51.55

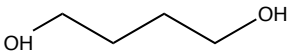

Chain Extender: 1,4-Butane Diol (BDO) Mn=90.12 g/mol

Chemical Formula: $C_4H_{10}O_2$
Exact Mass: 90.07
Molecular Weight: 90.12
m/z: 90.07 (100.0%), 91.07 (4.3%)
Elemental Analysis: C, 53.31; H, 11.18; O, 35.51

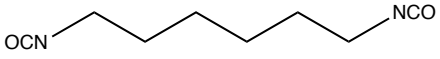

1,6-Diisocyanatohexane (HMDI) OCN(CH2)6NCO Mn =168.19 g/mol purchased from Sigma Aldrich, puriss GC grade 98% (CAS No. 822060).

Chemical Formula: $C_8H_{12}N_2O_2$
Exact Mass: 168.09
Molecular Weight: 168.20
m/z: 168.09 (100.0%), 169.09 (8.7%)
Elemental Analysis: C, 57.13; H, 7.19; N, 16.66; O, 19.02

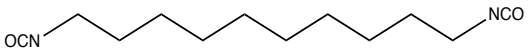

1,12-Diisocyanatododecane (DIDD) C14H24N2O2 Mn=252.35 g/mol, purchased from Sigma Aldrich, GC grade 96.5% purity (CAS No.13879 351).

Chemical Formula: $C_{12}H_{20}N_2O_2$
Exact Mass: 224.15
Molecular Weight: 224.30
m/z: 224.15 (100.0%), 225.16 (13.0%)
Elemental Analysis: C, 64.26; H, 8.99; N, 12.49; O, 14.27

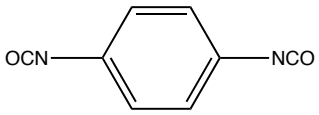

1,4-Phenylene Diisocyanate (PDI) C8H4N2O2 Mn=160.13 g/mol, purchased from Sigma Aldrich (CAS No. 104-49-4).

Chemical Formula: $C_8H_4N_2O_2$
Exact Mass: 160.03
Molecular Weight: 160.13
m/z: 160.03 (100.0%), 161.03 (8.7%)
Elemental Analysis: C, 60.01; H, 2.52; N, 17.49; O, 19.98

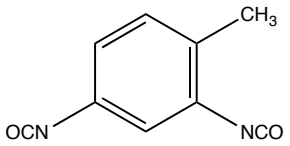

2,4-Tolylene Diisocyanate (2,4-TDI) C9H6N2O2 Mn=174.16 g/mol, purchased from Sigma Aldrich, technical grade 80% purity (CAS No. 584-84-9).

Chemical Formula: $C_9H_6N_2O_2$
Exact Mass: 174.04
Molecular Weight: 174.16
m/z: 174.04 (100.0%), 175.05 (9.7%)
Elemental Analysis: C, 62.07; H, 3.47; N, 16.09; O, 18.37

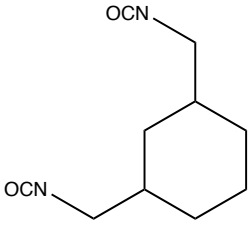

1,3-Bis(isocyanatomethyl)cyclohexane (BICH) C6H10(CH2NCO)2 Mn=194.23 g/mol, purchased from Sigma Aldrich, GC grade 98.5%,purity mix of cis- and trans-isomers (CAS No.38661722).

Chemical Formula: $C_{10}H_{14}N_2O_2$
Exact Mass: 194.11
Molecular Weight: 194.23
m/z: 194.11 (100.0%), 195.11 (10.8%)
Elemental Analysis: C, 61.84; H, 7.27; N, 14.42; O, 16.47

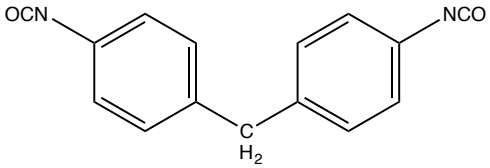

4,4'-Methylenebis(phenyl isocyanate (MDI) CH2(C6H4NCO)2 Mn=250.25g/mol, purchased from Sigma Aldrich 98% purity (CAS No. 101- 68-8).

Chemical Formula: $C_{15}H_{10}N_2O_2$
Exact Mass: 250.07
Molecular Weight: 250.26
m/z: 250.07 (100.0%), 251.08 (16.2%), 252.08 (1.2%)
Elemental Analysis: C, 71.99; H, 4.03; N, 11.19; O, 12.79

The chain extender used was Butane Diol (BDO) $C_4H_{10}O_2$ purchased from Sigma Aldrich and was Reagent Plus 99% grade (CAS No. 110-63-4).

3.3. FABRICATION OF SAMPLES

Samples were formulated in a three-neck, 500mL, ChemGlass round bottom flask equipped with a Teflon-coated magnetic stir bar. A picture of this set up is shown in Figure 3.2. It is vitally important moisture be eliminated from reaction system to avoid side reactions.[124] As side reactions can interfere with polymerization and prevent high molecular weights from being obtained. Therefore, careful consideration was taken to eliminate excess water content in the reaction system. Thus, to obtain higher regularity of structure, polymerization should be carried out in solution. In dimethyl sulfoxide, dimethylacetamide, tetramethylene sulfone, and dimethylsulfoxide/4-methylpentanone (50/50), side reactions are minimized. Generally, reaction in solution is "cleaner," with less chance of allophanate formation, which causes branching and increase in viscosity[121]. Lyman [122] showed that a 50:50 solvent solution of dimethyl sulfoxide (DMSO) and 4-methylpentanone-2 (MBK) (50/50) minimize adventitious cross-linking. In a typical reaction, initially an end-capped prepolymer was formed initially by reacting PEG {M_n= 2000g/mol} (30g) with a diisocyanate monomer in 50:50 DMSO and MIBK (100mL). The monomer reagents were combined in a 2:1 [NCO]/[OH] stoichiometric ratio. To determine the quantity mass of reactants needed Using the equivalent weight of the prepolymer (EW_{pp}) was calculated using . The mass amounts used varied according to PEG molecular weight, the molecular weight of the diisocyanate type, and the desired HS concentration. The prepolymer solution was left to react for about 20-30 minutes and was followed by the addition of 1,4-Butane Diol (BDO). More BDO and diisocyanate were added to build up the chain to the desired hard segment content. The reaction vessel was

placed in a heated oil bath temperatured at 120˚C. During the reaction, the vessel was vacuum-sealed and purged with nitrogen to isolate excess moisture from the system. The reactants were stirred vigorously and allowed to react for a predetermined time. Typically, the reaction took 1-1.5 hours. Afterwards, the polymer was precipitated with distilled water and heated in the oven at 65˚C. Therefore, this solution was selected as the solvent medium to carry out the reaction. 24 hours prior to the reaction, reagents were heated to 100˚C and purged in nitrogen overnight to remove water content. By minimizing the presence of water, we were able to avoid adventitious side reactions that would inhibit yield and molecular weight of the polymer.

Equation 2: Stoichiometric Index

$$I = \left(100 \times \left[NCO\right]\right) \div \left(\left[OH\right]_{p} + \left[OH\right]_{ce}\right)$$

[NCO] = equivalents of NCO groups from diisocyanate; $[OH]_{PEG}$ = equivalents of OH groups from macrodiol; $[OH]_{CE}$ = equivalents of OH groups from chain extender.

Equation 4: Equivalent weight of prepolymer

$$EW_{pp} = \frac{(\boldsymbol{n_{NCO}} \times \boldsymbol{FW_{DI}}) + \boldsymbol{FW_{PEG}}}{\boldsymbol{n_{NCO-OH}}} = EW_{PEG} + EW_{DI} + EW_{CE}$$

Equation 5: Mass total of prepolymer

$$\boldsymbol{m_{tot}} = (\boldsymbol{n_{DI}} \times \boldsymbol{FW_{DI}}) + \boldsymbol{FW_{PEG}}$$

m_{tot} total mass of prepolymer, n_{NCO-OH} is the difference in the number of moles of NCO groups and number of –OH groups, n_{DI} is the number of moles of diisocyanate, FW_{DI} is the formula weight of diisocyanate, FW_{PEG} is the formula weight of PEG, EW_{NCO} is the equivalent weight of the diisocyanate, EW_{BDO} is

the equivalent weight of the 1,4 Butane diol chain extender, EW_{pp} is the equivalent weight of the prepolymer, f is the functionality.

$$n_{NCO} = f_{DI} \times n_{DI}$$

n_{NCO} number moles of [–NCO] group.

$$n_{OH} = f_{PEG} \times n_{PEG}$$

number moles of $[-OH]_{PEG}$ groups

$$n_{NCO-OH} = n_{NCO} - n_{OH}$$

n_{NCO-OH} is the moles of unreacted isocyanate (NCO) groups

Equation 6: Equivalent weight of PEG, –OH groups, $EW_{PEG} = \frac{n_{PEG} \times FW_{PEG}}{f_{PEG}}$

Equation 7: Equivalent weight of isocyanate groups –NCO, $EW_{NCO} = \frac{n_{NCO} \times FW_{NCO}}{f_{NCO}}$

Equation 8: Equivalent weight of BDO chain extender

$EW_{BDO} = \frac{n_{BDO} \times FW_{BDO}}{f_{BDO}}$ f is the functionality of the monomer, n is the number of moles, FW is the formula weight

Equation 9: Cross-linking polyfunctional equation

$$\begin{cases} 1 \times PEG \\ + \\ 2 \times DI \end{cases} \xrightarrow{yields} -[\![DI - PEG - DI]\!] -$$

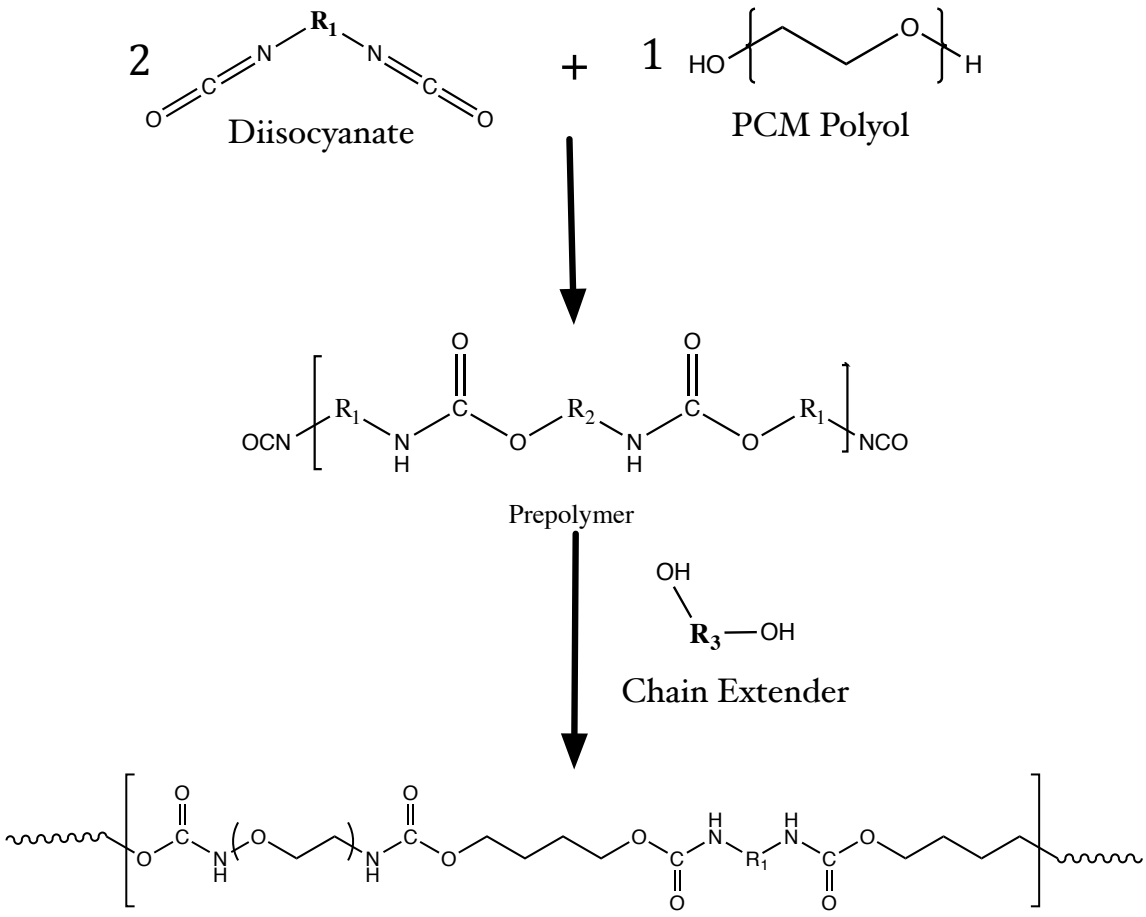

Figure 3.1: Reaction Route of two-step polymer synthesis

$$\text{eqn (1.1)} \%HS \frac{(n+1)M_{DI}+nM_{CE}}{(n+1)M_{DI}+nM_{CE}+M_{PEG}}$$

It has been that the hard-segment molecular weight, M_n(HS), depends on the soft segment molecular weight, $M_n(SS)$, and SSC. They are related by the expression:

$$\overline{M}_n(\text{HS}) = \overline{M}_n(\text{SS}) \times (100 - \text{SSC})/\text{SSC} \quad \text{eqn (1.2): Hard Segment}$$

3.3.1. LINEAR THERMOPLASTIC PU-SSPCM SAMPLES

Careful stoichiometric calculations and preparation steps to avoid adventitious water were carried out to control the molecular weight and the HS/SS distribution.

The reaction vessel was placed in a heated oil bath thermostated at 120˚C. During the reaction, the vessel was vacuum-sealed and purged with nitrogen to isolate the system from excess moisture. The reactants were stirred vigorously and allowed to react for a predetermined time. Typically, the reaction took 1-1.5 hours. Afterwards, the polymer was precipitated with distilled water and heated in the oven at 65˚C. 24 hours prior to the reaction reagents were heated to 100˚C and purged in nitrogen overnight to remove water content. By minimizing the presence of water, adventitious side reactions that would inhibit yield and molecular weight of the polymer were avoided.

Figure 3.2: Setup of Reaction vessel used in synthesis of samples

Literature shows that the alternating chain structure of thermoplastic polyurethanes is more organized and closer to the "ideal" chain structure when synthesis procedures are conducted in this manner.[1,19,21] Prior to synthesis, steps were taken to dehydrate the diisocyanate, PEG and BDO monomer reagents. This included purging the 50:50 DMSO-MBK and dissolved PEG solution with nitrogen for 1 hour and heating the PEG monomer overnight in an oven at 100˚C. An offset in the stoichiometric balance or the presence of moisture in the reaction system could potentially lead to side reactions that would reduce product yield and the final polymer molecular weight. It could also lead to adventitious cross-linking, which would mean the product would no longer be thermoplastic. Therefore, these were vital procedures to the synthesis of thermoplastic PU-SSPCMs. However, it should be noted that it is impossible to obtain a polyurethane material with an "ideal" perfectly alternating chain structure and it is impossible to obtain a polyurethane material with the exact same chain structure when prepared at different

times and places.[20] Therefore, slight discrepancies in data could be attributed to slight differences in chain structure that originate from synthesis proceedings. Thus, in order to obtain higher regularity of structure, polymerization should be carried out in solution. Solution polymerization, however, also has some disadvantages. Lyman[25]found a considerable effect of solvent on yield and molecular weight of MDI/ethylene glycol polyurethanes due to various kinds of polymer-solvent interactions. Apparently, the extent of side reactions governed the molecular weight obtained. In dimethyl sulfoxide, tetramethylene sulfone and dimethyl sulfoxide/4-methylpentanone-2 (50/50), these reactions are apparently minimized. Generally, reaction in solution is "cleaner" with less chance of allophanate formation, which causes branching and molecular weight increase. Higher dilution favors cyclization and decrease in molecular weight.[26] Increase in molecular weight may be obtained by introducing branching by the addition of a small amount of tri- or polyfunctional components (polyols). Frequently, commercial polyols have somewhat higher functionality than two.[2 37]

Sample Nomenclature

A code system for naming each sample was used to keep track of the combinations of diisocyanate, PEG molecular weights, and the nature of cross-link. The series of samples prepared with a I=100 ratio were labeled with a Y and the series of PU-SSPCMs prepared with excess diisocyanate (I=150) were labeled with an X. The code system is ordered in the following fashion: [X or Y + Diisocyanate. + PEG molecular weight- percent hard segment content (%HSC)] (an example of a sample name is YDIDD2000-34 or XPDI

2000). The codes refer, first to the linearity of the sample; X represents thermoset PU-SSPCMs and Y- designates thermoplastic PU-SSPCMs.

3.4.CHARACTERIZATION OF HEAT STORAGE PROPERTIES BY DSC

Differential Scanning Calorimetry (DSC) measurements were carried out on a TA Instruments Q1000 DSC. It was calibrated using an Indium test. All samples of about 5-10mg were prepared in aluminum metal pans and tested in air. Results were analyzed through TA Instruments Universal Analysis 2000 V4.7A software. Prior to use, the calorimeter was calibrated with mercury and indium standards; an empty aluminum pan was used as reference.

DSC Experimental Design Setup

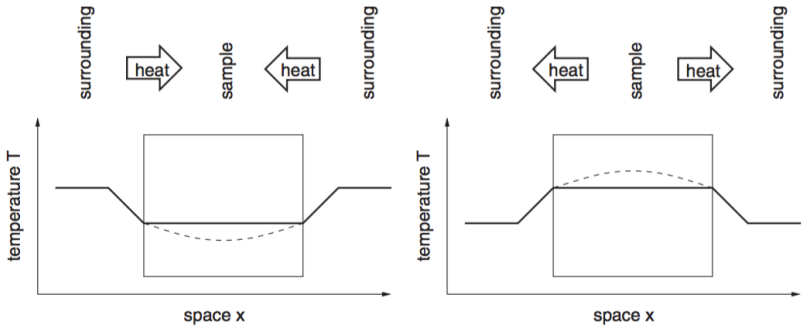

Figure 2. Sketch of the temperatures inside the sample during heating (left) and cooling (right). In the calculation of the thermal effect, the temperature of the material is assumed to be the same throughout the whole sample (solid lines). In reality, due to heat transfer limitations, the temperature is not uniform (dashed lines).

Figure 3.3

For a successful design of PCM systems, the specific enthalpy should be known with an uncertainty dh smaller than 10% of h_m and ΔT smaller than 0.5 K, as shown in

DSC Analysis was used to evaluate the thermal energy stored and released by a PEG PCM polymer in a thermoset and in a thermoplastic polyurethane-SSPCM system.

PEG is the “working” phase change component. Therefore, only the thermal transitions demonstrated by the PEG chain segment is attributed to thermal energy storage properties. Generally, PEG with molecular weights of 2000-6000g/mol melt and crystallize between 0˚C and 80˚C. The thermal regulation of indoor room temperatures is the primary application target for SSPCMs. DSC experimental methods were designed to simulate temperature changes in a building environment, in order to obtain an accurate profile of thermal energy storage properties. Room temperature fluctuations occur in small 1-2˚C degree increments. Therefore, a heat and cool rate of 2˚C/min was used. Method parameters for thermoplastic PU-SSPCM samples included a prior step in which samples were heated to homogeneous melt state and then cooled at 20˚C/min to 70˚C. The melting temperature at which the homogeneous melt state was reached differed for each sample. The temperature was determined by either POM hot stage experiments or the final melt temperature of the endothermic peak >100˚C that was observed during the

DSC initial heat run. Heating sample to a homogeneous melt destroyed all HS domain order established during synthesis. This heating step was necessary to eliminate any variation in the samples phase domain morphology, as this may affect results. By cooling all samples at 20˚C/min, a baseline degree of phase separation was established in all thermoplastic samples. This step is not necessary for thermoset XPCM samples because they are thermosets and do not melt nor contain a phase separated morphology.

For the purpose of evaluating thermal energy storage properties only the

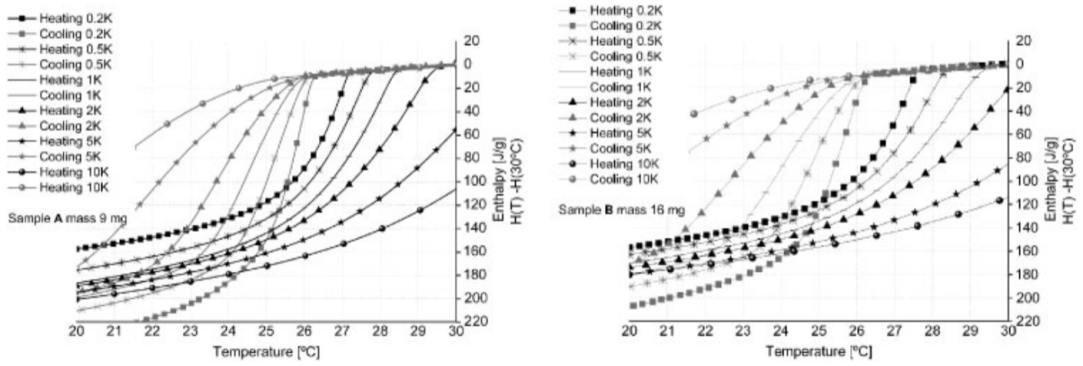

Figure 6. Results obtained with the dynamic method at different heating/cooling rates for sample A (left) and sample B (right).

crystallization and melting behavior of the PEG PCM component was of interest. Therefore, enthalpy values were measured only within a temperature window of 0-70˚C

$$X_{C_{PEG}}(\%) = \frac{\Delta H_{m_{PCM}}}{\Delta H^{0}_{m_{PEG}} \times SSC\%} \times 100$$

were considered to gain an accurate profile of the heat storage characteristics of each sample. Particularly for applications in the building sector, where temperature changes of the PCM are often only a few degrees, accurate data is of crucial interest [95]. For

successful designs of PCM systems for building applications, a heating and cooling rate of 2˚C/min was selected to obtain accurate ΔH and temperature data in these conditions. For the purpose of evaluating thermal energy storage properties, only the enthalpy values of the soft segment component were measured. Therefore, only the temperature window in which PEG soft segment chains crystallize and melt was of interest to gain an accurate profile of the heat storage characteristics of each sample.

Equation 10: $\%X_c$ is percent crystallinity

X_c% values is the % crystallinity of the PEG PCM polymer and can be used to approximate the size of the PCM crystalline region. Theoretically, the percent ratio of non-crystalline can be quantified by the expression: 100% - X_c% = % non-crystalline PCM.

Melting temperature (T_m) is the extrapolated onset peak maximum. ΔH_m is measured over the temperature range melting occurred. ΔH_m is proportional to crystalline content. Enthalpy is the heat energy required for melting or heat energy released upon crystallization.

$$\Delta H = C_p \Delta T$$

3: Enthalpy of fusion, ΔH (J/g) is proportional to specific heat. C_p is specific heat (J/g˚C) PCMs exhibits latent heat storage so no change is temperature occurs. Thus, if ΔT is 1, is can be seen that ΔH and specific heat is equivalent. Specific heat is how much heat must

be absorbed to increase depended on the amount of heat capacity the sample absorbs and releases as it transitions between a crystalline and amorphous state.

3.5.QUANTIFYING THE HS CHAIN-END EFFECT

Magnitude of reduction in enthalpy to approximate HS chain end effect

The magnitude of reduction in melt enthalpy values after HS are introduced can be expressed as: $|\Delta H| = |100\%$ Crystalline PEG - $\Delta H_{m,PCM}|$. Theoretically, $|\Delta H|$ can be used to describe the degree to which PEG PCM crystallization is limited by HS chain end effects as it quantifies the portion of non-crystalline amorphous PEG PCM chain. $X_c\%$ values represents the PEG PCM polymer percent crystallinity and can be used to describe the size of the crystalline region. The equation below was used to quantify the HS Chain-end effect

$$|\Delta H| = |\Delta H_{PEG,m} - \Delta H_{PCM,m}|$$

Baseline shift at glass transition ΔCp to approximate HS Chain end effect

There is a possibility a number of the PEG PCM chains that make up the non-crystalline region were not prevented from participating in crystallization solely on account of HS chain end effects, but by phase mixing. PCM polymer crystallization is disrupted when; a) PCM chain segments that are trapped in the HS phase become immobilized. b) HS when mixed in the PCM phase, acts as an impurity to PCM chain. The limitation on PCM polymer crystallization due to phase mixing is separate from the limiting effects introduced by HS steric restrictions. Therefore, while the limitation on PCM

crystallization can be represented by |ΔH| values, this value is linked to both non-crystalline PCM chain trapped in the interphase boundary region and non-crystalline PCM restricted by the HS chain end. With that said, the use of |ΔH| values may not be the most accurate method for describing the HS chain end effects.

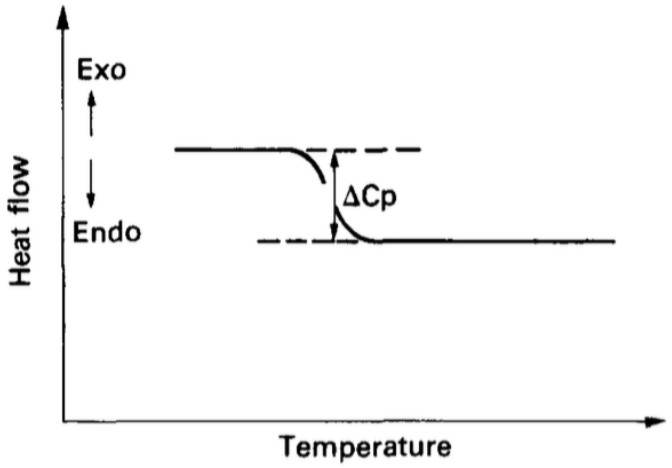

Figure 3.4: Determination of the heat capacity step from initial heat DSC Curves.

The baseline shift at glass transition is quantified by ΔC_p and is proportional to the mass of segments taking part in the glass transition. It is a common practice to use ΔC_p values to approximate the size of the amorphous region, assuming that the PCM chain units immobilized by phase mixing do not participate in cooperative motion.[34] Soft segments dissolved in the hard phase are not expected to contribute to ΔC_p, since their mobility is restricted. Therefore, because the presence of hard blocks as impurities in the soft phase do not affect its heat-capacity determination, ΔC_p is a better approximation of the HS chain end effect.

Approximating the Degree of Phase Mixing with Glass transition temperature

Equation 11: Fox Copolymer Equation

$$\frac{1}{T_g} = \frac{w_1}{T_{g_1}} + \frac{w_2}{T_{g_2}}$$

Generally, when using Differential Scanning Calorimetry (DSC) experiments to evaluate phase separation in PU materials, the behavior of the HS and SS phase domains is based on Fox's copolymer equation (equation 10).[34] Where w_1 and Tg_1 are weight fractions of the soft and hard segments, and Tg_1 and Tg_2 are their glass transitions, respectively. The Fox equation can be used to predict the amount of the hard segments in the soft phase or vice versa by selecting a shifted glass transition (Tg) value either of the soft or hard phase.

An interphase layer has a Tg, which is a function of the relative amounts of the compounds. Since the phase mixing is partial, three separate phase transitions usually occur. In the mixing of the flexible soft phase with the hard phase, which introduces much free volume, should lower Tg of the hard phase.[34] The amount of mixed material is small compared to the mass of pure phases, so that the third Tg is not observable. Typically, some increase of the soft segment glass transition and some decrease of the hard segment glass transition is observed. A third glass transition ($T_{g,mix}$) is from the boundary interphase layer, which is a transition phase made up of mixed SS and HS. When HS is mixed in the SS, the SS $T_{g,SS}$ will shift to a higher temperature depending on the amount of HS present. Thus, $T_{g,mix}$ is the glass transition of an interphase layer is

often a function of the relative amounts of the HS and SS polymers and appear merged as one glass transition. Due to the fact that phase mixing is typically only partial, $T_{g,mix}$is not usually observed.

Using the Tg shift method to approximate the degree of phase separation requires both an accurate Tg, and the corresponding thermal expansion of the two phases, which is rather difficult to determine in the case of hard segments, due to the fact that phase mixing is typically only partial, $T_{g,HS}$ is not usually observed. Another approach to estimate the PUs amount of phase mixing is based on measuring the specific heat, ΔC_p, at the glass transition temperature and comparing it with the $\Delta C_p^{\ 0}$ for the pure component the degree of phase mixing can be represented by the ratio $\Delta C_p(Tg)/\Delta C^{\circ}p(Tg)$. Unlike the Tg shift method, which only indicates the phase composition relatively, quantitative information can easily be obtained through the ΔC_p measurement. Therefore, The determination of phase separation by this ΔC_p, measurement can be more accurate than that from the T_g, shift in the case of polyurethanes[52]

$$\Delta Cp(Tg)/\Delta C^{\circ}p(Tg).$$

Equation 12: Ratio approximates level of phase mixing

Petrovic proposed that that the degree of phase separation could be measured by the magnitude of enthalpy jump at the glass transition and the shift of the $T_{g,SS}$ of the soft and hard segments.[52] The enthalpy jump ΔC_p, at the glass transition has been applied to the study of segmented polyurethanes.[39] The underlying idea in this method is that ΔC_p, at T_g proportional to the mass of the polymer chains taking part in the transition, assuming that the chains of the soft phase mixed with the hard phase will be immobilized and will not

participate in the cooperative motions at the glass transition of the pure soft phase.[52] The assumption is made that ΔC_p, of the hard phase in the region of measurement is negligible and *can* be ignored because phase mixed or dispersed soft segments do not relax at the same temperature as the continuous soft phase.

Camberlin[39] showed that a quantitative evaluation of the degree of phase segregation in segmented linear polyurethanes and polyurethane can be made by measuring the heat capacity change ΔC°_{p} at the glass transition of the soft phase. The ratio $\Delta Cp/\Delta C^{\circ}_{p}$ corresponds to the percent segregation of the soft phase. This amount of PCM chains outside the continuous PCM phase domain, can be expressed as (ΔC°_{p} - $-\Delta C_p$) and used to quantify the amount of PCM segments trapped in the hard domains and/or dispersed in the interphase boundary region. The heat capacity change ΔC_p

per gram of soft segment in the polyurethane was compared with ΔC°_{p} for the pure PEG PCM polymer was measured; ΔC_p is equivalent to ΔC°_{p} per gram of soft segments at the glass transition in totally phase-separated polyurethane. ΔC_p values per gram of soft segments in homopolymer and in the phase separated polyurethanes must be similarly estimated. According to literature 1.54 J/g˚C is the standard heat capacity for a PEG homopolymer.[81] This value was used as ΔC°_{p} of the pure PEG polymer

3.6.FOURIER TRANSFORM INFRARED SPECTROSCOPY (FTIR)

The Fourier Transform Infrared Spectroscopy using attenuated transmission reflection (ATR) transmittance on a Nicolet Magna IR Spectrometer 550 set, equipped with a diamond material contact ATR accessory. The spectra were recorded in the range 600-

4000 cm^{-1}, with normal resolutions at 4 cm^{-1}. Background spectra were collected before each absorbance spectra were recorded. 16 interferrograms scans were collected. An ATR correction and a baseline correction were made for each sample spectra using Omnic analysis software. Prior to experiments, samples were stored in a desiccator and purged with N_2, 24 hours.

3.7.THERMAL GRAVIMETRIC ANALYSIS (TGA)

Thermal gravimetric analysis (TGA) was used to determine the thermal stability of the prepared solid-solid PCMs. Approximately 5mg of sample was measured in a platinum pan using a TA Instruments Q5000 TGA. TGA scans were collected in air at 20 ^{o}C/min to detail thermal degradation up to 200℃ and up to 400 ^{o}C. The weight loss was recorded as temperature increased. As mentioned in the literature review the ability to endure melt processing is a criterion for the utility of SSPCM in building applications. Therefore, determining samples are thermally stabile at 200 ^{o}C was pertinent to this study. On top of that, making sure the samples were non-volatile was vitally important for DSC instrument and DSC experiments carried out up to 250^{o}C.

3.8.POLAR OPTICAL MICROSCOPY (POM)

Polar optical microscopy (POM) images were taken on a James Swift Microscope (England). A Hot Stage by Mettler Toledo PP82HT and a FP90 Central Processor equipped with a Beltram polarizing lens was used. Samples were mounted on a slide and

heated up to 250˚C at 20˚C/min or until the sample showed signs of degradation. Images of the samples were taken at 25˚C, 100˚C, and 250˚C.

Chapter 4 THE EFFECT OF CROSS-LINK NATURE ON THERMAL EVERGY STORAGE PROPERTIES

4.1.INTRODUCTION

As outlined in the introduction, this dissertation is organized into four chapters in which each chapter will focus on one of the four chemical and physical factors that govern polyurethane properties; cross-link nature, diisocyanate composition, hard segment content, and the kinetics of HS crystallization are the factors. In this chapter the effect of cross-link nature on thermal energy storage (TES) properties is explored.

In the literature review section, a series of earlier studies on PU-SSPCMs were outlined in Table 2.4. As discussed previously, some of the PU-SSPCM materials listed have a linear chain structure and some have a non-linear molecular architecture, but either demonstrate thermoplastic or thermoset behavior. In Table 2.4 a summary of phase change characteristics reported by previous PU-SSPCM studies is given. It can be seen that there is no significant difference in enthalpy values (ΔH_m) despite having dissimilar molecular architectures. Unfortunately, no distinction can be made on how a PU-SSPCM's molecular architecture influences its thermal energy storage properties.

Amongst the PU-SSPCMs discussed in Chapter 2, only Yanshan's IPN PU-SSPCM[50] and Alkan's linear PU-SSPCM[34] made with HMDI and PEG M_n =1000 g/mol (HMDI-1000,

T_m=19˚C)[34] have demonstrated phase transition temperatures the closest to the temperature range required for building applications. It makes sense that Alkan's HMDI-1000 PU-SSPCM demonstrated a low melting temperature, because it was prepared with a low molecular weight PEG. Thus far, Yanshan is the only author to present a PU-SSPCM with a IPN molecular architecture. Thus far, Yanshan' IPN PU-SSPCM is the only one to demonstrate a solid-to-solid phase transition at temperatures near human comfort temperatures (18-30˚C). It is unknown why Yanshan's IPN PU-SSPCM demonstrated markedly lower PTT than the other PU-SSPCMs. At this point, this is the only PU-SSPCM studied with a IPN 3-D chemically cross-linked network. Therefore, it may be speculated that the lower phase transition temperature is attributed to its IPN molecular architecture (See Figure 2.9). It is possible a chemically cross-linked network exhibits a chain end effect that limits PEG PCM crystallization to a lesser extent than trifunctional HS cross-links or linear physical cross-link. Because Yanshan used a higher PEG molecular weight (M_n=6000 g/mol) was used this raises questions on whether this PU-SSPCM IPN molecular structure is the root cause for observing lower phase transition temperatures. The PU-SSPCM developed by Yanshan[50] differed from the other PU-SSPCMs mentioned because its non-linear molecular architecture is a three dimensional interpenetrating network (IPN), and can be classified as a thermoset polyurethane, whereas the other PU-SSPCMs discussed reported melting temperatures of at least 50˚C and were thermoplastic.

The final properties exhibited by a polyurethane elastomer with a chemically cross-linked network is significantly different from a PU with physically cross-linked network, even if

both PU materials are comprised of the same monomer constituents. [127] Polyurethanes with a chemically cross-linked network are classified as a thermoset, and PUs with a physically cross-linked network are known as thermoplastics.[34] Thermoset PUs cannot be broken down by thermal treatment.[34] The introduction of chemical cross-link immobilizes the hard segment so that it remains stagnant and dispersed within the soft segment matrix [102] In result, thermoset materials demonstrate a homogenous morphology. [86] On the other hand, polyurethanes with a linear chain structure form hydrogen bonded physical cross-links that can continuously be melted and re-cooled. Depending on the strength hydrogen bond, these thermoplastic PU materials exhibit a heterogeneous morphology. [128]

Chemical cross-links are often deliberately added in polyurethane materials to increase mechanical properties. Kothandaraman[103] found that increasing chemical cross-linking in polyurethanes led to an increase in tensile strength and hardness, while elongation decreased. [103] Methods used to introduce chemical cross-links include increasing the functionality of hydroxyl containing compounds, such as tri- or multifunctional reagents, or by increasing isocyanate (NCO) content to form branched or cross-linked polymers. [103] Considering the profound effect the introduction of chemical cross-links has on polyurethane materials' mechanical properties denotes the possibility of thermoset and thermoplastic PU-SSPCMs would demonstrate different thermal energy storage properties. If this were the case, it would explain why Yanshan's IPN PU-SSPCM[50] demonstrated its solid-to-sold thermal transition at much lower temperature compared to the other thermoplastic PU-SSPCMs discussed. Thus, it may be speculated that the drop

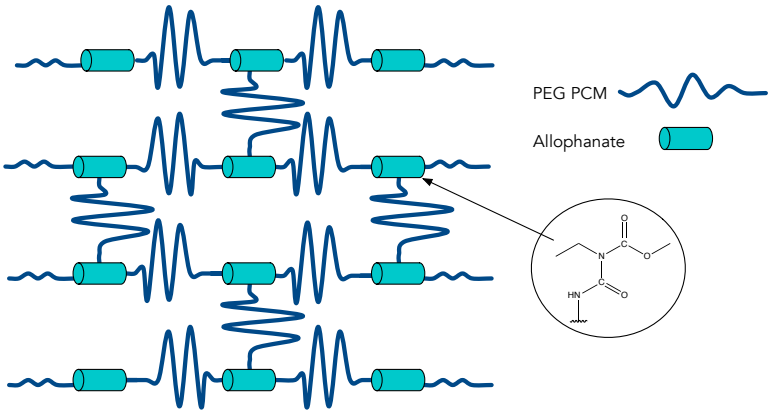

Figure 4.1: Schematic of Chemically Cross-linked PU-SSPCM (XPCM)

in melting temperatures observed is connected to the 3-D chemical cross-linked network and it homogeneous morphology. There has yet to be a study that has investigated the relationship between PU molecular architecture and soft segment thermal properties, the majority of polyurethane literature focuses on resulting mechanical property behavior. [129] There also has yet to be a study PU-SSPCMs that compares the thermal energy storage properties of a non-linear thermoset PU-SSPCM with a chemically cross-linked network to a linear thermoplastic PU-SSPCM with a physically cross-linked network.

One of the objectives of this chapter study is to establish a methodology for the fabrication of a PU-SSPCM thermoset and PU-SSPCM thermoplastic that are analogous because they are derived from the same monomer components, yet differ by the nature of their cross-linked networks.

In this chapter a family of chemically cross-linked PU-SSPCMs with a three dimensional molecular network architecture was prepared by modifying the stoichiometric balance between NCO and OH groups to drive allophanate formation. Figure 4.1 illustrates the molecular architecture of a PU-SSPCM with a chemically cross-linked network. Previously shown in, Figure 2.11 depicts the molecular architecture of a physically cross-

linked PU-SSPCM. In this chapter a full characterization and analysis of the prepared samples was carried out. FTIR techniques were used to verify that the reactions during sample synthesis went to full completion and to confirm that the prepared samples were comprised of a cross-linked network with opposing chemical natures. The melting and crystallization behavior was analyzed using Polarized Optical Microscopy (POM) equipped with a hot stage. Optical images of the samples were taken to verify that the samples were exhibiting solid-to-solid phase transitions. DSC Analysis was used to describe the crystallization and melting behavior of chemically cross-linked (XPCM) and physically cross-linked (Y-PCM) PU-SSPCM samples prepared with the following series of PEG molecular weights (M_n= 2000, 3000, 6000 g/mol) and the following diisocyanates: 1,6-Diisocyanatohexane (HMDI), 1,4-Phenylene diisocyanate (PDI), and 4,4-Methylenebis (phenyl isocyanate) (MDI). Only the thermal transitions demonstrated by the PEG PCM polymer were considered, since PEG is the "working" phase change component. The measured melt enthalpy values (ΔH_m) were used to quantify the HS chain end effect and the percent crystallinity (X_c%), which were used to evaluate the thermal energy storage properties of analogous non-linear thermoset and a linear thermoplastic PU-SSPCM.

The results obtained in this work helped to clarify the role the cross-link nature factor has on PEG PCM crystallization. Additionally, the results of this work indirectly reveal how the chain-end effects observed for different HS composition cause change in PEG PCM chain mobility, which then varies thermal energy storage properties.

4.2.EXPERIMENTAL

Further details related to reagents, synthesis set-up, experimental setup, instrumentation, calibration and parameters is discussed in the experimental section in Chapter 3.

4.2.1. FABRICATION OF PU-SSPCM SAMPLES

A family of thermoset and a family of thermoplastic PU-SSPCMs were prepared with the following diisocyanate monomers: 1,6-Diisocyanatohexane (HMDI), 1,4-Phenylene diisocyanate (PDI), and 4,4-Methylenebis (phenyl isocyanate) (MDI). Each diisocyanate was combined with a series of PEG molecular weights (M_n= 2000, 3000, 6000 g/mol). Further details on the polymerization reaction, synthesis procedures and the reagents can be found in Chapter 3.

Sample Nomenclature

Samples were named according to cross-link nature, diisocyanate, and PEG molecular weights. The series of samples prepared with a I=100 ratio were labeled with a Y and the series of PU-SSPCMs prepared with excess diisocyanate (I=150) were labeled with an X. A code-naming system was used to keep track of the combinations of The codes followed the indicated pattern: *[Y + Diisocyanate + PEG molecular weight]* and refers to, the physical cross-link (Y), the abbreviation of the diisocyanate used and the PEG molecular weight. Similarly, for the chemically cross-linked samples, the indicated code pattern was used: *[X + Diisocyanate name + PEG molecular weight].* A list of the samples considered and their nomenclature is given in Table 4.1.

Table 4.1: List of PU-SSPCM Samples Prepared

Diisocyanate	(abbv.)	PEG MW (g/mol)	[Nomenclature]
1,6-Diisocyanatohexane	(HMDI)	Poly(ethylene glycol) (PEG), Mn= {2000}	XHMDI 2000
1,6-Diisocyanatohexane	(HMDI)	Poly(ethylene glycol) (PEG), Mn= {3000}	XHMDI 3000
1,6-Diisocyanatohexane	(HMDI)	Poly(ethylene glycol) (PEG), Mn= {6000}	XHMDI 6000
1,6-Diisocyanatohexane	(HMDI)	Poly(ethylene glycol) (PEG), Mn= {2000}	YHMDI 2000
1,6-Diisocyanatohexane	(HMDI)	Poly(ethylene glycol) (PEG), Mn= {3000}	YHMDI 3000
1,6-Diisocyanatohexane	(HMDI)	Poly(ethylene glycol) (PEG), Mn= {6000}	YHMDI 6000
1,4-Phenylene Diisocyanate	(PDI)	Poly(ethylene glycol) (PEG), Mn= {2000}	XPDI 2000
1,4-Phenylene Diisocyanate	(PDI)	Poly(ethylene glycol) (PEG), Mn= {3000}	XPDI 3000
1,4-Phenylene Diisocyanate	(PDI)	Poly(ethylene glycol) (PEG), Mn= {6000}	XPDI 6000
1,4-Phenylene Diisocyanate	(PDI)	Poly(ethylene glycol) (PEG), Mn= {2000}	YPDI 2000
1,4-Phenylene Diisocyanate	(PDI)	Poly(ethylene glycol) (PEG), Mn= {3000}	YPDI 3000
1,4-Phenylene Diisocyanate	(PDI)	Poly(ethylene glycol) (PEG), Mn= {6000}	YPDI 6000
4,4'-Methylenebis(phenyl isocyanate)	(MDI)	Poly(ethylene glycol) (PEG), Mn= {2000}	XMDI 2000
4,4'-Methylenebis(phenyl isocyanate)	(MDI)	Poly(ethylene glycol) (PEG), Mn= {3000}	XMDI 3000
4,4'-Methylenebis(phenyl isocyanate)	(MDI)	Poly(ethylene glycol) (PEG), Mn= {6000}	XMDI 6000
4,4'-Methylenebis(phenyl isocyanate)	(MDI)	Poly(ethylene glycol) (PEG), Mn= {2000}	YMDI 2000
4,4'-Methylenebis(phenyl isocyanate)	(MDI)	Poly(ethylene glycol) (PEG), Mn= {3000}	YMDI 3000
4,4'-Methylenebis(phenyl isocyanate)	(MDI)	Poly(ethylene glycol) (PEG), Mn= {6000}	YMDI 6000

Y-PU-SSPCM Synthesis Conditions

All samples in the Y-PCM set were prepared using a weight ratio of 40% HS and 60% SS-PEG. The polymerization reaction route was conducted in two steps, and followed the reaction scheme shown in Figure 3.1. The polymerization procedures followed are identical to the solution polymerization method described by Lyman.[112] A 50:50 DMSO/DMA solution was selected as the solvent medium because it has been found to minimize side reactions and lead to higher precipitate yields of the polyurethane product.[112]

First, in a typical reaction, 30g of PEG (Mn= 2000, 3000 and 6000 g/mol) were added to 100mL of 50:50 DMSO:MBK solution. The mixture was stirred vigorously and heated to 60-70˚C. After the PEG was fully dissolved, the diisocyanate monomer was added in a 2:1 ratio [NCO]/[OH] to form an isocyanate capped prepolymer. After 10-15 minutes, 2 moles of 1,4-Butane Diol (BDO) was added to the prepolymer solution, followed by another 2 moles of diisocyanate. This chain build-up sequence continued until the HS molecular weight amounted to approximately 40% of the entire polymer's molecular weight. The HS reagents (diisocyanate and BDO) were added sequentially to maintain a

Table 4.2: Molar Compositions of XPCM and YPCM PU-SSPCM

	Moles of DI	Moles of PEG		Moles of DI	Moles of PEG	Moles of CE
XHMDI 2000	12	1	**YHMDI 2000**	0	1	5
XHMDI 3000	16	1	**YHMDI 3000**	8	1	7
XHMDI 6000	32	1	**YHMDI 6000**	16	1	15
XPDI 2000	12	1	**YPDI 2000**	6	1	5
XPDI 3000	16	1	**YPDI 3000**	8	1	7
XPDI 6000	32	1	**YPDI 6000**	16	1	15
XMDI 2000	9	1	**YMDI 2000**	4.5	1	3.5
XMDI 3000	13	1	**YMDI 3000**	6.5	1	5.5
XMDI 6000	24	1	**YMDI 6000**	12	1	11

DI - Diisocyanate

DI - Diisocyanate, CE - Chain Extender

*For the series of thermoset sample (XPCM) the amount of NCO groups were calculated to have a excess of .5 [NCO] groups.

stoichiometric ratio of 1.0 [NCO/OH] during polymerization. The mass of diisocyanate and 1,4 butane diol (BDO) reagents were carefully calculated according to diisocyanate

and PEG molecular weights (M_n=2000, 3000, and 6000 g/mol). Table 4.2 summarizes the molar compositions used to produce all of the samples considered in this chapter.

Once all of the HS reactants were added, the reaction system was stirred vigorously for a predetermined amount of time to allow all of reagents to react. Typically, the reaction took 1-1.5 hours. Afterwards, the polymer was precipitated with distilled water and heated in the oven at 65˚C. 24 hours prior to the reaction, reagents were heated to 100˚C and purged in nitrogen overnight, to remove water content. By minimizing the presence of water, adventitious side reactions that would inhibit yield and molecular weight of the polymer were avoided.

X-PU-SSPCM Synthesis Conditions

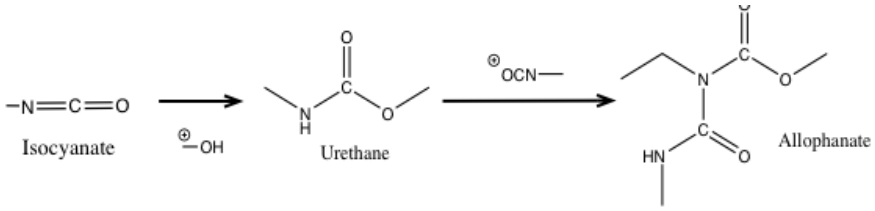

Figure 4.2: Schematic of Allophanate Formation.

The family of XPCM thermoset PU-SSPCM samples were prepared by modifying the stoichiometric balance of the polymerization reaction to facilitate branching. The formation of allophanate groups in the sample was induced by increasing the number of

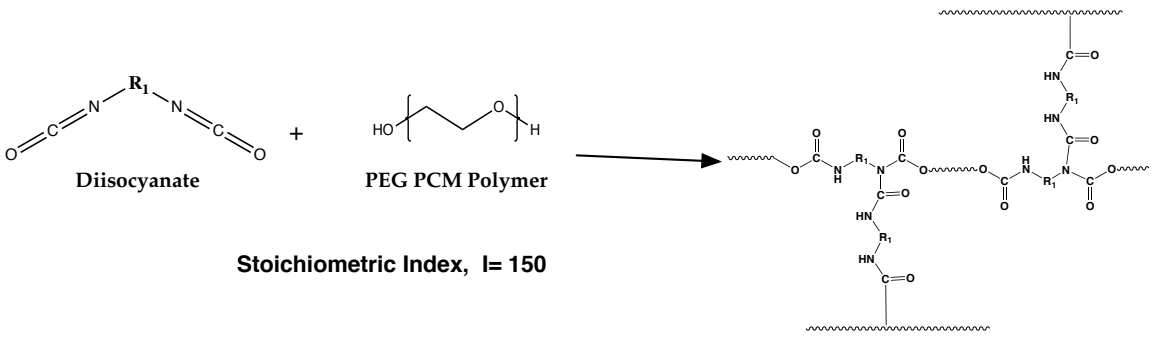

Figure 4.3: Schematic of Chemically Cross-linked PU-SSPCM with Allophanate Chain Branching

isocyanate groups present in the reaction ([NCO/OH] > 1) and carrying the reaction out at a higher curing temperature. See Figure 2.30: The theoretical relationship between molecular weight and NCO/OH ratio. Allophanate groups are formed from excess isocyanate groups reacting with urethane groups (see Figure 4.2): (1) and isocyanate group as a result of trimerization of the isocyanate (2) allophanate formation is the favorable reaction in the uncatalyzed reaction system, whereas trimerization is favored under basic catalyst conditions [106].

The XPCM samples were formulated in a three-neck 500mL ChemGlass round bottom flask equipped with a Teflon-coated magnetic stir bar. The reaction route of synthesis followed is schematically shown in a typical reaction, 30g of PEG (Mn= 2000, 3000 and 6000 g/mol) was added to 100mL of acetone and stirred while being heated to 50-60˚C. Once the PEG dissolved, the diisocyanate monomer was added, all at once. The mass amount of diisocyanate reagent needed to maintain a stoichiometric ratio of 1.5 in the reaction, varied by PEG molecular weight and diisocyanate type. The reactants were stirred vigorously, and allowed to react until a solid gel mass was formed. On average, the reaction would take 30 minutes to 1 hour. After cooling, the sample was washed with distilled water and stored in a nitrogen-purged environment. A schematic of a chemically cross-linked PU-SSPCM is shown in Figure 4.3.

While maintaining a balance between NCO and OH groups is key for obtaining a linear polymer, the same consideration for stoichiometric balance was not necessary in preparing a set of PU-SSPCM samples with a 3-D chemically cross-linked network. The reagents were added simultaneously during the polymerization of XPCM samples,

whereas for the polymerization of PCM samples, the monomer reagents were added consecutively in order to obtain an alternating polymer sequence and avoid side reactions.

4.2.2. ANALYSIS OF THERMAL ENERGY STORAGE PROPERTIES BY DIFFERENTIAL SCANNING CALORIMETRY (DSC)

DSC measurements were carried out on a TA Instruments Q1000. All samples of about 5-10mg were prepared in aluminum metal pans and tested in air. Results were analyzed through TA Instruments Universal Analysis 2000 V4.7A software. A more detailed description of instrumentation and method parameters can be found in the experimental section (Chapter 3).

The method parameters for the physically cross-linked (Y-PCM) set of samples included a preliminary heating step, in which samples were heated to 250˚C. Heating sample to a homogeneous melt to destroy any HS domain ordering from synthesis. The initial heat step was necessary to eliminate any variation in the samples phase domain morphology, as this may affect results. DSC curves from the initial heat step were used to characterize the level of phase separation present in the sample. By cooling all samples at 20 ˚C/min, a baseline degree of phase separation was established in all thermoplastic samples. This step is not necessary for XPCM samples because they are thermosets and do not melt nor contain a phase separated morphology. Multiple runs of bulk polymer were conducted to

increase validity of measurements and to ensure the bulk polymer was uniform throughout.

The temperature was determined by either POM hot stage experiments or the final melt temperature of the endothermic peak >100˚C that was observed during the DSC initial heat run.

4.2.3. FTIR BY ATR

FTIR analysis techniques were used to verify synthesis proceedings were successfully carried out and to confirm the XPCM samples were comprised of a allophanate chemically cross-linked network and the YPCM samples were linear polyurethane materials. A more detailed description of instrumentation, sample preparation and method parameters can be found in the experimental section (See Chapter 3).

4.2.4. POLAR OPTICAL MICROSCOPY (POM) ANALYSIS

A more detailed description of instrumentation and method parameters can be found in the experimental section (See Chapter 3).

4.2.5. TGA

Thermal Gravimetric Analysis (TGA) was used to determine the thermal stability of the prepared solid-solid PCMs. See Chapter 3.

4.3.RESULTS SECTION

4.3.1. SYNTHESIS OF SAMPLES

In this work, we sought to establish a methodology for the synthesis of two sets of polyurethane SSPCM elastomers with the same monomer constituents, but opposing cross-link natures. Two sets of polyurethane based SSPCMs with different cross-link natures were prepared and characterized. To alter the nature of the HS cross-link from linear physical cross-links to chemical cross-links formed by allophanate branching, the stoichiometric ratio of hydroxyl to isocyanate groups was adjusted to 1.5.

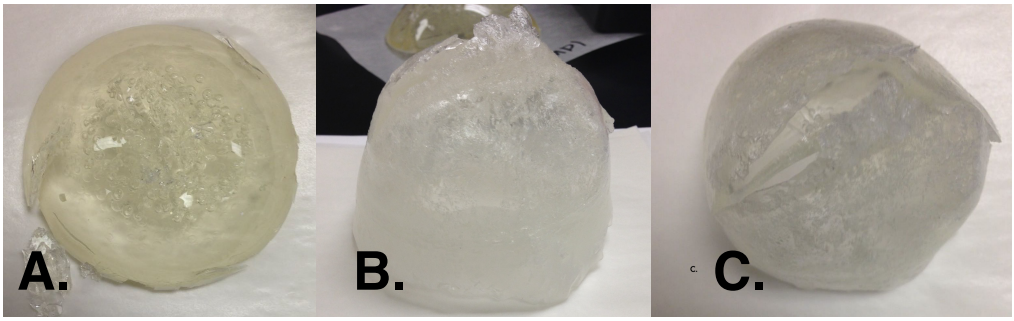

Figure 4.4: Images of resulting non-linear polymer from synthesis A) XPDI 2000 B) XPDI 3000 C) XPDI 6000

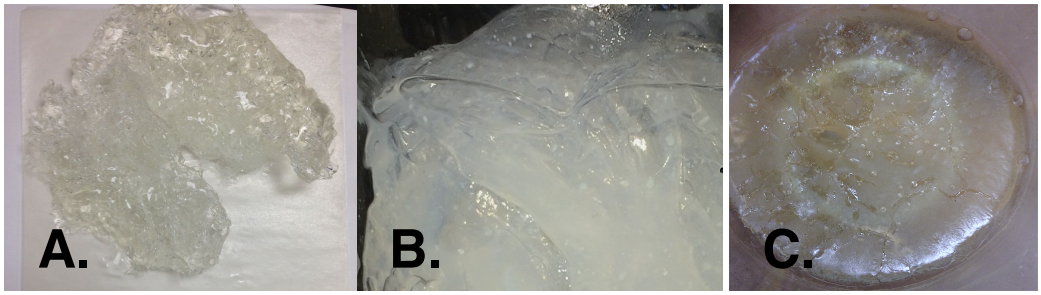

Figure 4.5: Images of resulting non-linear polymer from synthesis A) XHMDI 2000 B) XHMDI 3000 C) XHMDI 6000

Physically cross-link, thermoplastic (YPCM) samples

The addition of the water altered the solubility interaction between the DMSO:MIBK solvent and the product polymer; as a result the polymer product is forced to precipitate. After adding the water, the reaction solution turned a white color instantly. This change in color indicated a polymer was precipitating and suggested that the monomer reagents had successfully polymerized.

It was noticed that the samples did not initially precipitate fully, instead the resultant polymer remained in a white solution form for a long period of time (approx. 24 hours). It wasn't until all of the solvent and water evaporated from the bulk polymer that it began to show signs of solidarity. Normally, this could take 1-3 days depending on the sample. We attempted to speed up this process by putting the samples in an oven at 100˚C, but found that subjecting the samples to heat over an extended period of time caused them to yellow and degrade faster. Therefore, to avoid degradation the samples were left in a nitrogen purged vacuum chamber at ambient conditions for a few days before testing to allow water and DMSO:MBK solution to vaporize. It was observed that the more residual DMSO-MBK solvent present in the solution kept the polymer in a semi-soluble state. Therefore, when adding water must make sure to stir vigorously so the polymer precipitates and gets fully rid of 50:50 DMSO:MBK solvent. The physical cross-links formed by inter-urethane hydrogen bonding is responsible for the solid framework of these materials. Therefore, precipitation also relies kinetically on the HS urethane groups finding its corresponding neighbors and forming a HS crystallite micro-domain

Non-Linear Chemically Cross-linked PU-SSPCM (XPCM)

Images of a selection of the resulting polymer products from the synthesis of non-linear PU-SSPCMs (XPCM) prepared with a stoichiometric index of I=150 is shown in Figure 4.4 and Figure 4.5

This family of samples labeled as XPCM and were prepared with a stoichiometric ratio I=150. The excess diisocyanate groups reacted with an amine in t urethane HS to form allophanate chain branches. [37,100,106,129-132] The quantity of reagents used to prepare the set of XPCM and Y-PCM samples are listed in Table 4.2: Molar Compositions of XPCM and YPCM PU-SSPCM.

Synthesis of polyurethanes never results in the same product. Thus, it is expected that slight discrepancies in data collection may be the result of synthesis conditions as it is impossible to synthesize perfectly identical polymers.[100] Figure 4.6 shows the polymer products from synthesis of a linear thermoplastic PU-SSPCMs.

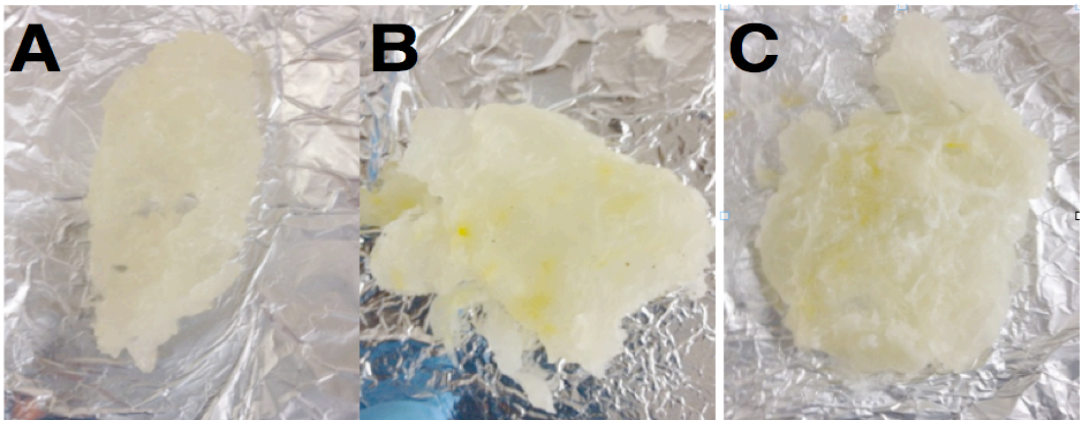

Figure 4.6 Images of result thermoplastic polymer from synthesis of A) YHMDI 2000 B) YHMDI 3000 C) HMDI 6000.

All samples of the XPCM series were transparent, whereas all the Y-PCM series were opaque due to porosity of the same as a result of processing. Samples prepared with aromatic diisocyanates, PDI and MDI, showed signs of yellowing. Overtime, the

yellowing increased considerably. It is known that aromatic diisocyanates are prone to UV degradation and so it is common for aromatic SPU materials to have a yellowish tint.[106,122,132,133] Other samples showed only spots of discoloration. This could be attributed to thermal instability, degradation, and exposure to impurities.

4.3.2. FTIR RESULTS

FTIR analysis was used to characterize the composition of the prepared PU-SSPCM samples. It was necessary to confirm that during synthesis, 1) the polymerization of diisocyanate and PEG monomers converted to urethanes, 2) the monomers fully reacted, thus, no residual diisocyanate and hydroxyl groups remained, and 3) no side reaction interference occurred.

Figure 4.7-4.24 the IR spectra of all XPCM samples and Y-PCM samples are overlaid with its respective pure PEG molecular weight. Isocyanate groups (NCO) show a signature peak at 2265cm^{-1} [134]. No peak at 2265 cm^{-1} was detected in any of the IR sample spectra. The absence of an isocyanate indicates that the diisocyanate and PEG monomers fully reacted during synthesis and assures that no residual isocyanate groups remain in the polymer product. It can be seen that there is a clear difference in spectral patterns between the pure PEG spectra and the sample spectra. The PU-SSPCM sample spectra shows two distinct peak that are absent in the pure PEG spectra. This observation indicates that the prepared PU-SSPCM polymer has a different composition from its precursor PEG monomer and verifies that the polymerization of the PEG and diisocyanate monomers.

One of the most noticeable distinctions in the sample IR spectra is the appearance of two distinct peaks between 3300-3450 cm^{-1} and 1695 cm^{-1} -1740cm^{-1}. Polyurethane signature peaks include a amine absorption peak (NH) (3300-3450cm^{-1}) and carbonyl (C=O) peak

(1695cm^{-1}-1740cm^{-1}). [107,131,134,135,157] Therefore, the appearance of IR bands in the amine (NH) and carbonyl (C=O) stretching band region confirms that all samples are polyurethanes.

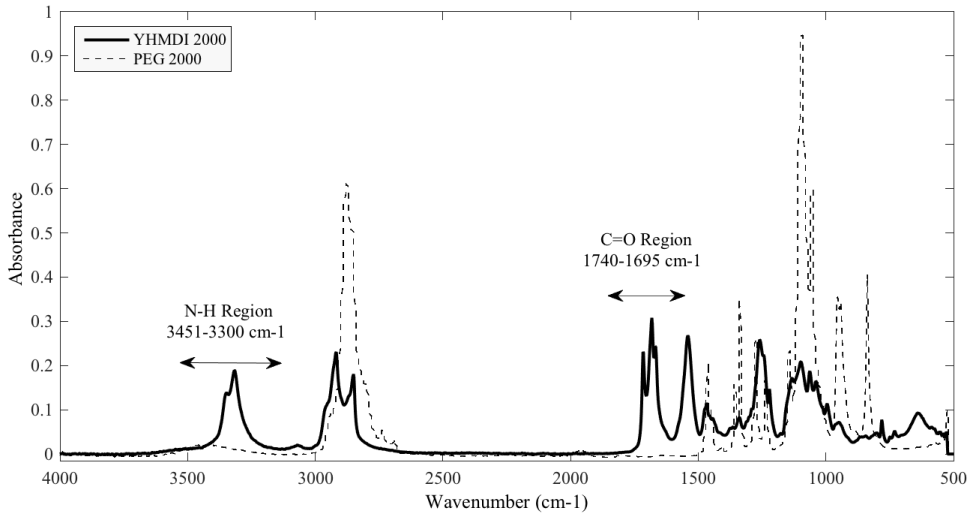

Figure 4.7: FTIR Spectra of YHMDI 2000

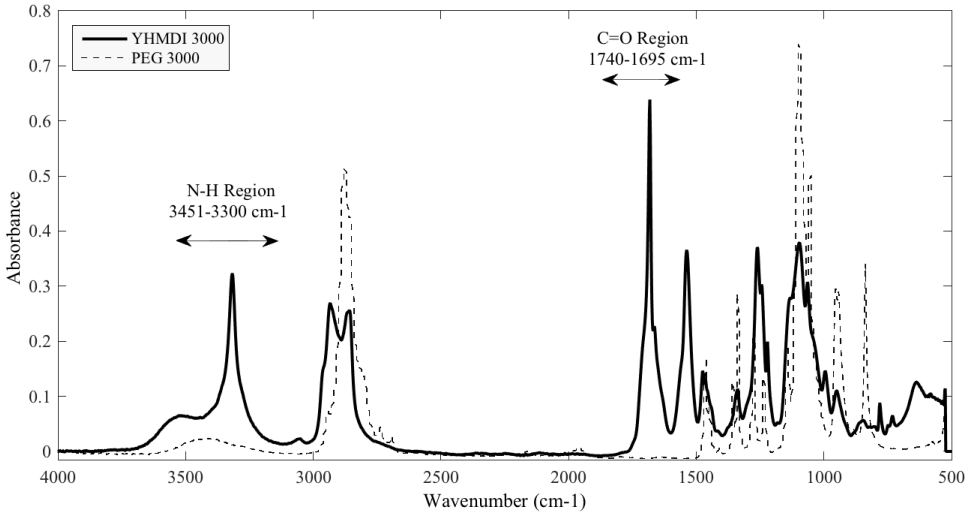

Figure 4.9: FTIR Spectra of YHMDI 3000

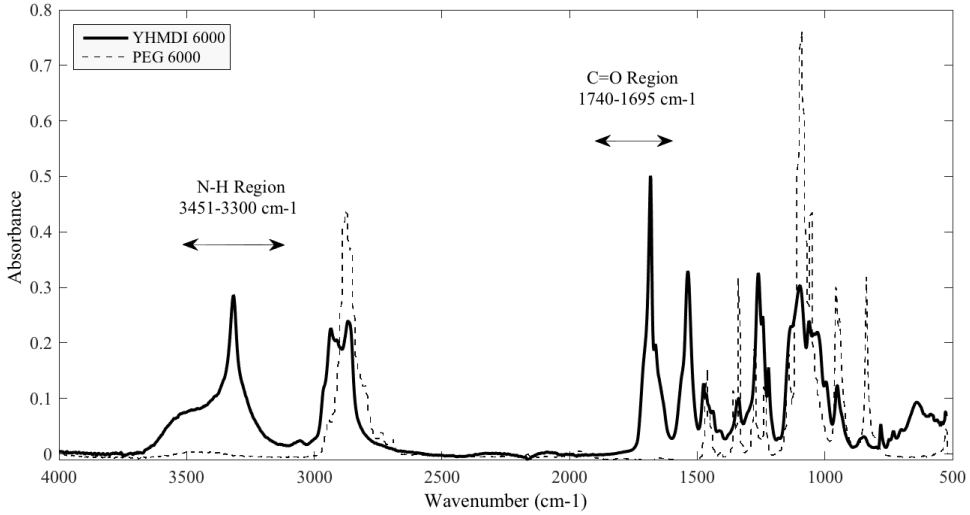

Figure 4.8: FTIR Spectra of YHMDI 6000

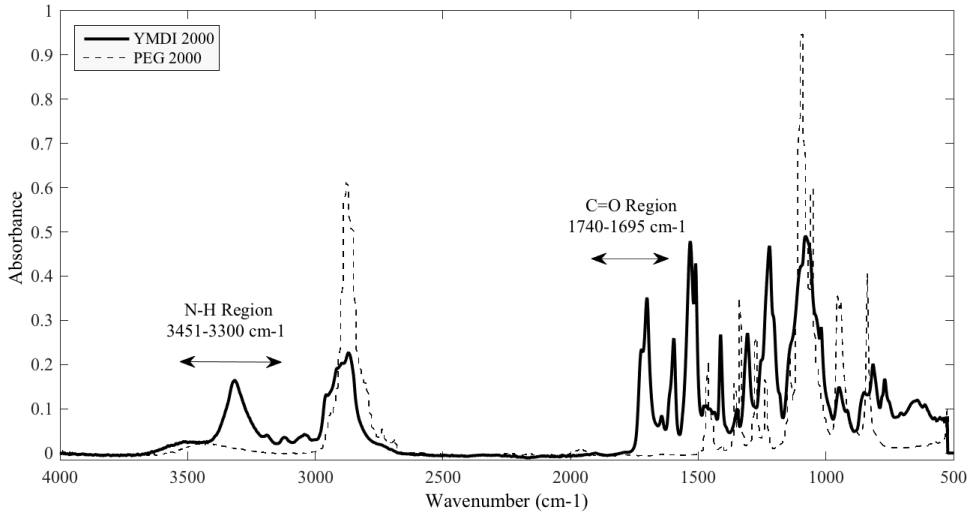

Figure 4.11: FTIR Spectrum YMDI 2000

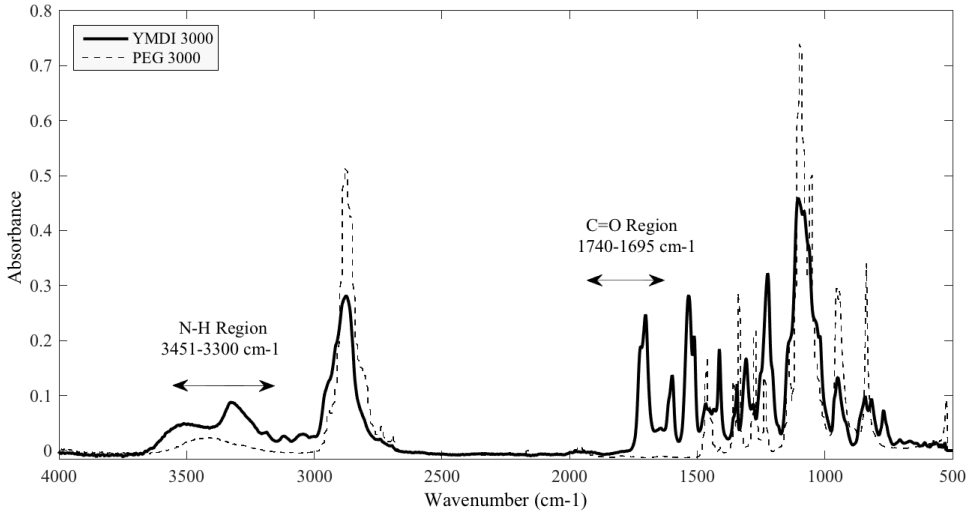

Figure 4.10: FTIR Spectra of YMDI 3000

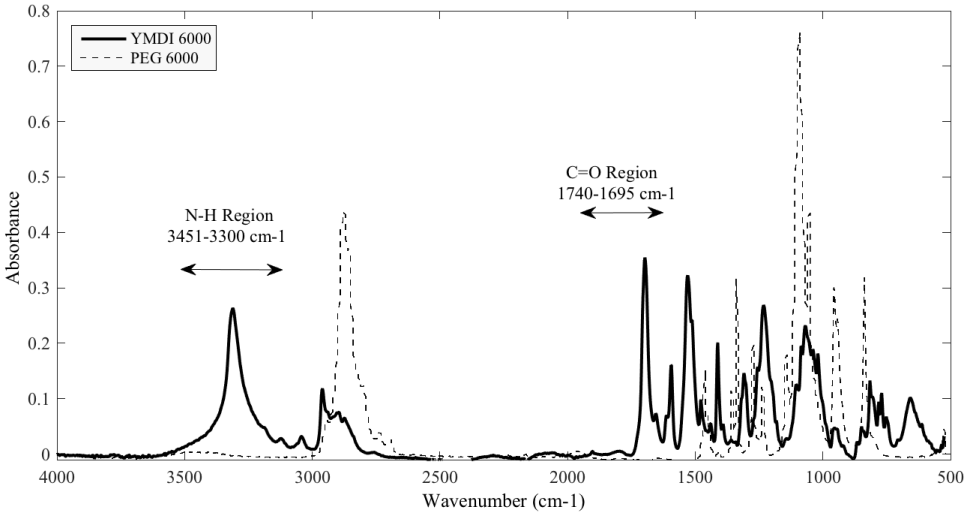

Figure 4.13: FTIR Spectra of YMDI 6000

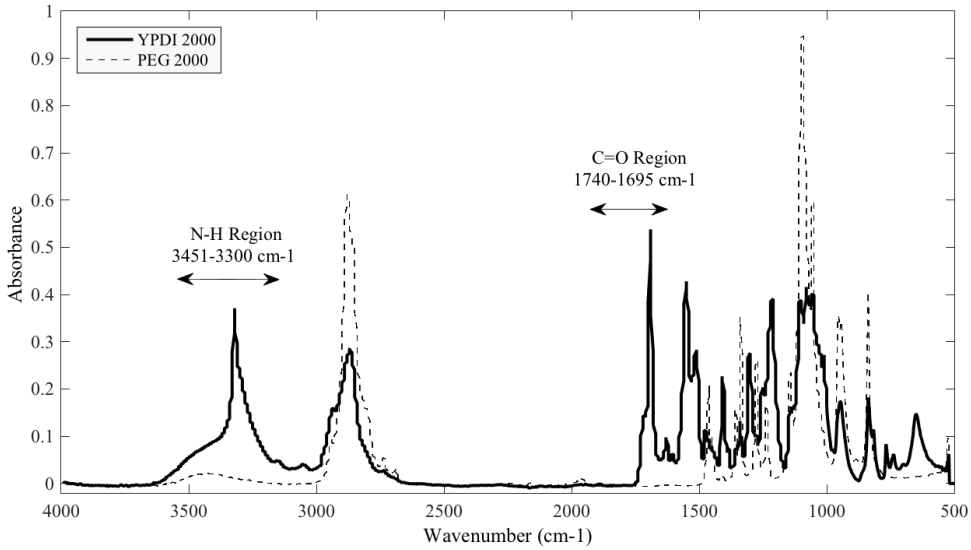

Figure 4.12: FTIR Spectra of YPDI 2000

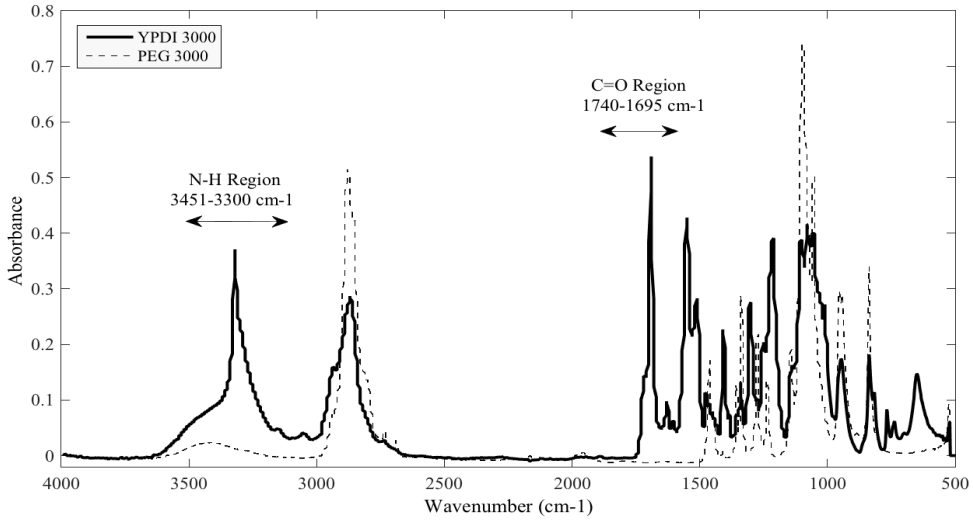

Figure 4.15: FTIR Spectra of YPDI 3000

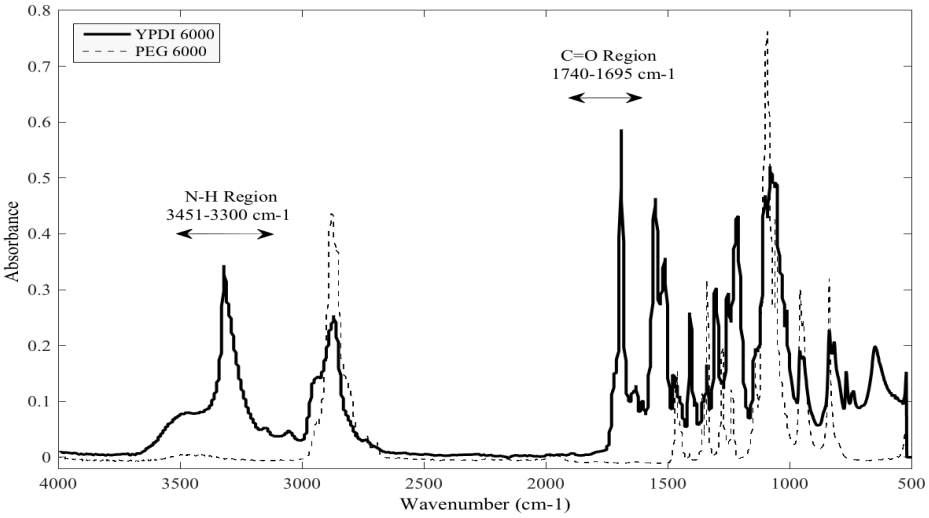

Figure 4.14: FTIR Spectra of YPDI 6000

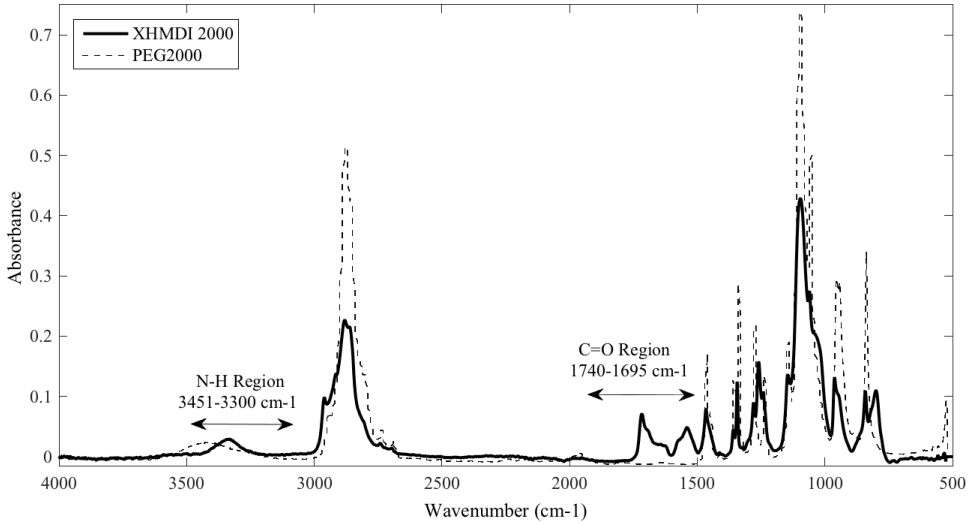

Figure 4.17: FTIR Spectra of XHMDI 2000

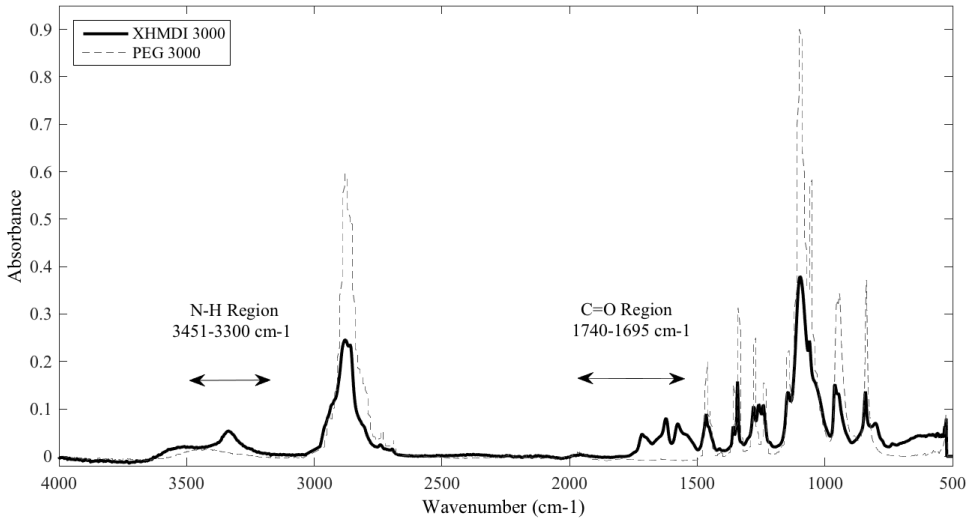

Figure 4.16: FTIR Spectra of XHMDI 3000

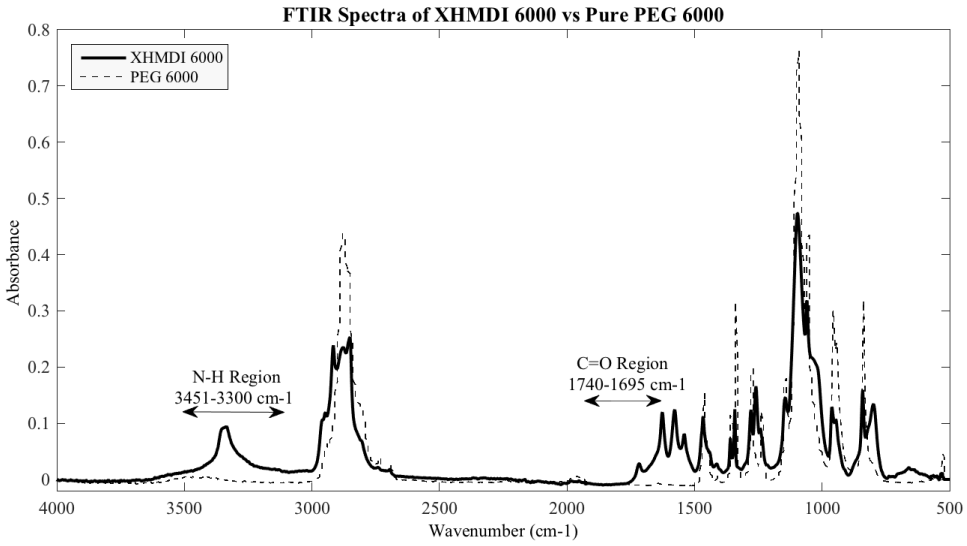

Figure 4.19: FTIR Spectra of XHMDI 6000

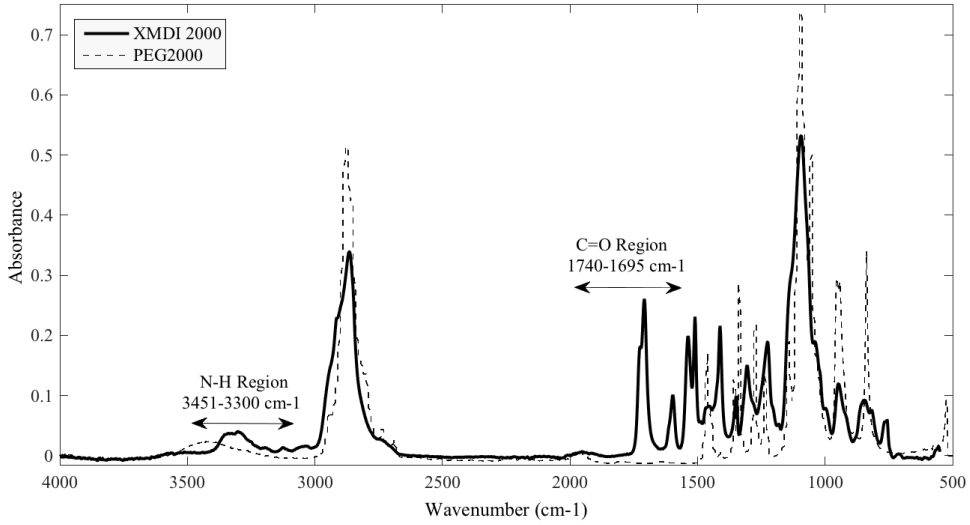

Figure 4.18: FTIR Spectra of XMDI 2000

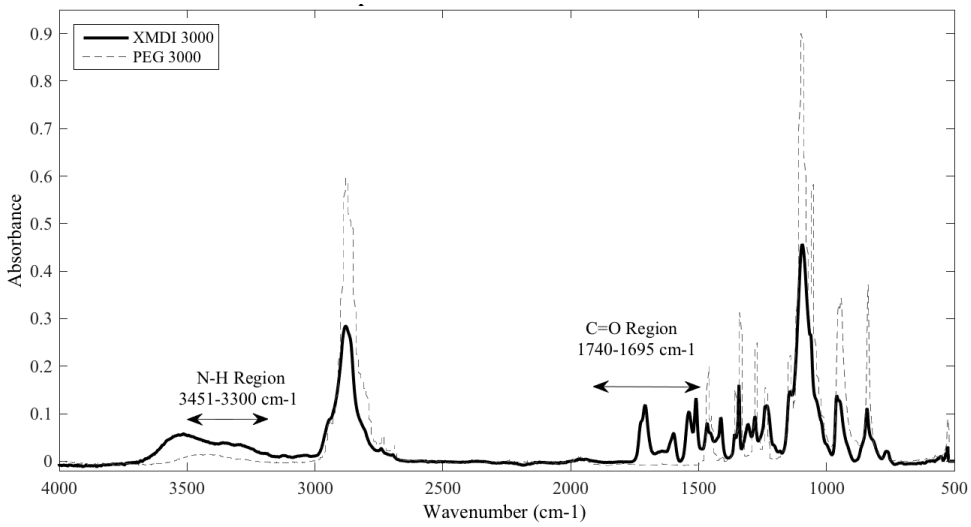

Figure 4.21: FTIR Spectra of XMDI 3000

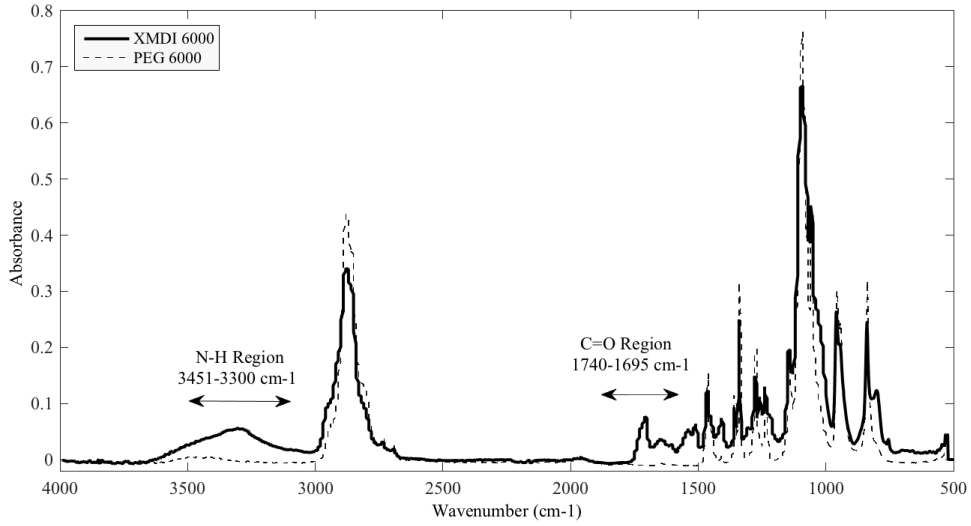

Figure 4.20: FTIR Spectra of XMDI 6000

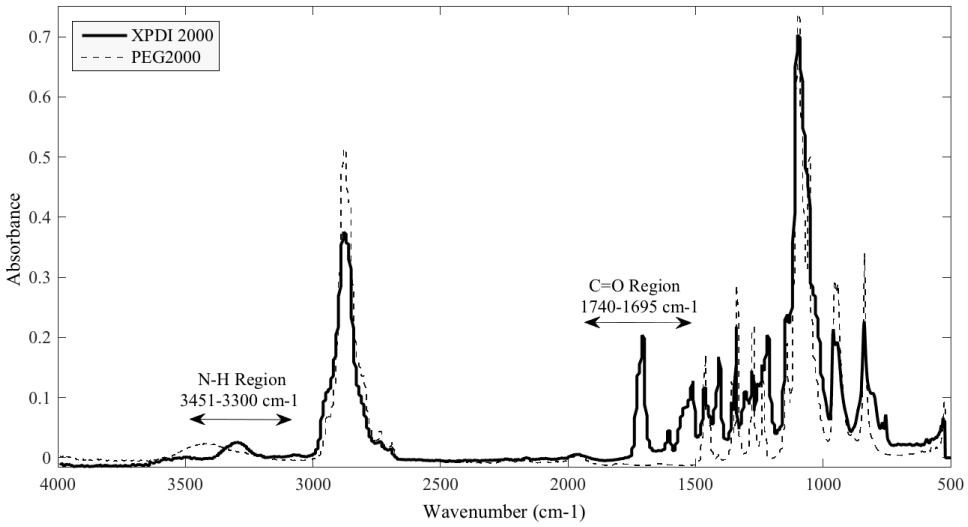

Figure 4.22: FTIR Spectra of XPDI 2000

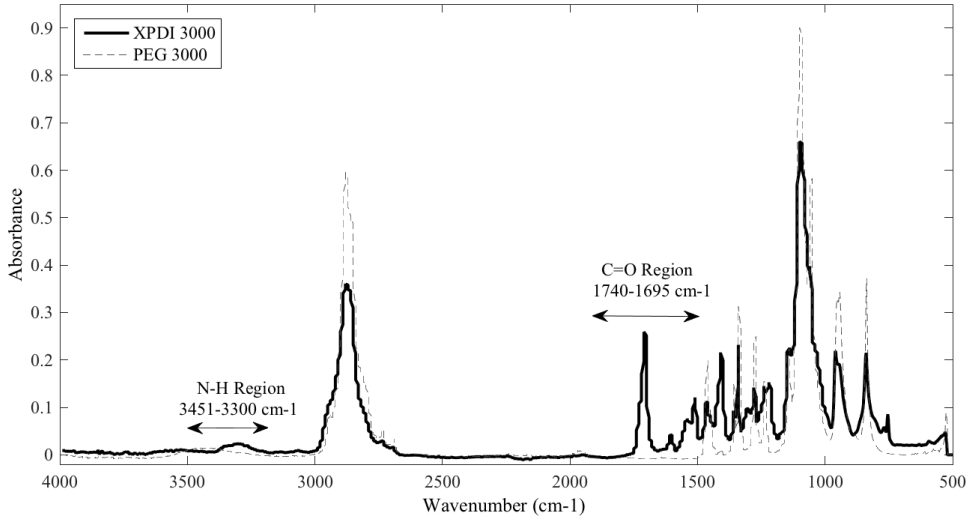

Figure 4.23: FTIR Spectra of XPDI 3000

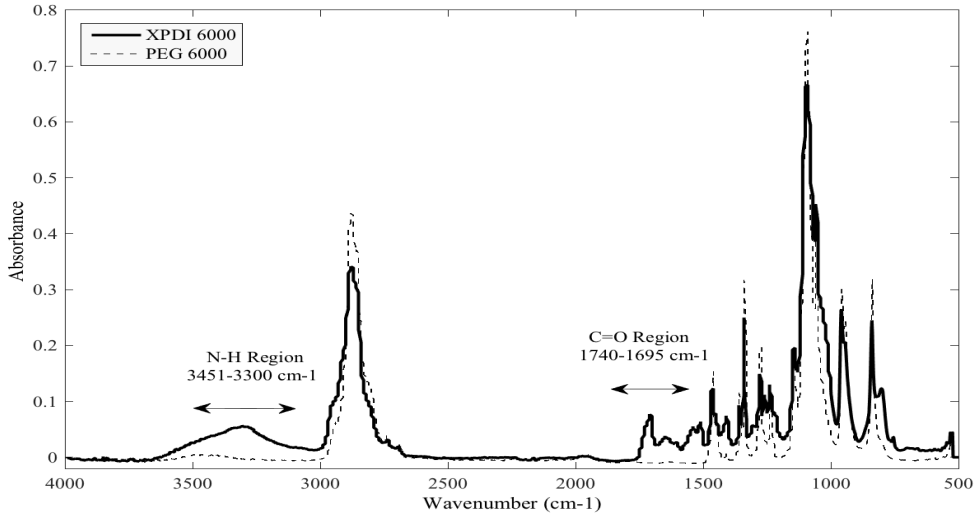

Figure 4.24: FTIR Spectra of XPDI 6000

Table 4.3: Signature Main IR Peaks observed for Polyurethane polymers[6]

Wavelengths of Absorption Bands				
–N=C=O (diisocyanate)	2275 cm^{-1}	2250 cm^{-1}	1350 cm^{-1}	
–NH–COO–(urethane)	1640 cm^{-1}	1610 cm^{-1}	1650 cm^{-1}	1680 cm^{-1}
C=C (in benzene)	800 cm^{-1}	1610 cm^{-1}	1500 cm^{-1}	
Aromatics	3030 cm^{-1}	1600 cm^{-1}	1500 cm^{-1}	
–OH (hydroxyl)	3200 cm^{-1}	3400 cm^{-1}		
C–O–C (ether)	1150 cm^{-1}	1070 cm^{-1}		
$ArNH_2$ (aromatic amine)	1350 cm^{-1}	1250 cm^{-1}		
$AlNH_2$ (aliphatic amine)	1280 cm^{-1}	1180 cm^{-1}		

Distinguish Chemically Cross-linked Network Structure from Physically Cross-link by

Table 4.4: Main NH and C=O peaks

XPCM Sample	N-H (cm^{-1})	C=O (cm^{-1})	YPCM Sample	N-H (cm^{-1})	C=O (cm^{-1})
XMDI 2000	3310	1713	YMDI 2000	3315	1701
XMDI 3000	3321	1709	YMDI 3000	3327	1703
XMDI 6000	3329	1709	YMDI 6000	3311	1697
XHMDI 2000	3320	1717	YHMDI 2000	3316	1716, 1682
XHMDI 3000	3326	1716	YHMDI 3000	3317	1682
XHMDI 6000	3315	1715	YHMDI 6000	3317	1687
XPDI 2000	3302	1709	YPDI 2000	3324	1695
XPDI 3000	3302	1709	YPDI 3000	3324	1722, 1694
XPDI 6000	3305	1710	YPDI 6000	3323	1693

Figure 4.7- Figure 4.24 compares the IR spectra of XPCM and Y-PCM according to PEG molecular weights. The main NH and C=O stretching bands peaks observed for the XPCM sample set and YPCM samples set are listed in Table 4.2. On average, the set of YPCM samples displayed peaks between 3311-3327 cm^{-1} in the amine (NH) region and 1682-1723 cm^{-1} in the carbonyl (C=O) region. For the set of XPCM samples, NH peaks were observed between 3302 and 3329cm^{-1} and C=O peaks appeared around 1709 and 1717$cm^{-1.}$ Consistency in NH and C=O peak frequency observed for both sample sets, provides a good indication that all of the samples in the XPCM set have the same cross-link network structure and all of the samples in the Y-PCM set have the same cross-link network structure.

Use of FTIR Analysis to Distinguish XPCM network structure from YPCM.

Further analysis by FTIR was used to confirm that the two samples sets have different cross-linked network structures and additionally verify that XPCM's chemically cross-linked networks is a result of allophanate branching and not by the formation of urea linkages.The formation of urea linkages would happen if moisture was present in the reaction system. Polyurethane elastomers with urea linkages show a distinct carbonyl stretching peak at 1630 cm^{-1} and an amine stretching peak at 3260 cm^{-1}.[157] For all XPCM IR spectra, no carbonyl peak at 1630cm^{-1} was detected in any of the IR XPCM sample spectra. Therefore, it may be confirmed that XPCM samples are chemically cross-linked with allophanate linkages.

Allophanate identification is one method by which a XPCM chemically cross-linked sample can be distinguished from a physically cross-linked Y-PCM sample. Kopusov identified the signature bands of allophanate in aromatic-isocyanate-based polyurethanes to be 3300, 1695, 1280, and 1310 cm^{-1}.[131]According to Kopusov, the use of FTIR analysis for allophanate identification by these signature bands is complicated and difficult to distinguish because they are often masked by bonded NH and C=O groups of the urethane groups.[131] Therefore, the appearance a allophanate spectrum is not a reliable method for the identification of allophanate linkages. Instead, a alternative method based on a study by Kontou was used to distinguish the network structure of the XPCM sample set from the Y-PCM sample set. Kontou used IR analysis to track the changes in spectroscopic properties of a series of polyurethane materials prepared with a NCO/OH ratio from 0.9 to 1.2.[136]

Comparison of Spectral Perturbations demonstrated by NH and C=O IR Bands

It is well-known that the changing distribution of hydrogen bonding in the hard and soft domain of polyurethanes can be studied by IR spectroscopy [128] [107]. Different hydrogen bonded systems display a set of spectral perturbations in terms of band peak frequency, peak shape, peak intensity, and peak bandwidth. For example, thermoset polyurethanes are chemically cross-linked so they have only one type of hydrogen bonding, whereas the physical cross-links of thermoplastic polyurethanes can have multiple types of hydrogen bonding. Therefore, thermoplastic and thermoset polyurethanes exhibit different sets of spectral perturbations detectable by IR spectroscopy. It is known from the literature that a homogeneous, rather than a heterogeneous phase morphology is demonstrated by the introduction of chemical cross-links. Therefore, the introduction of chemical cross-links may be characterized by a homogeneous dispersion of hard domains in the soft matrix.

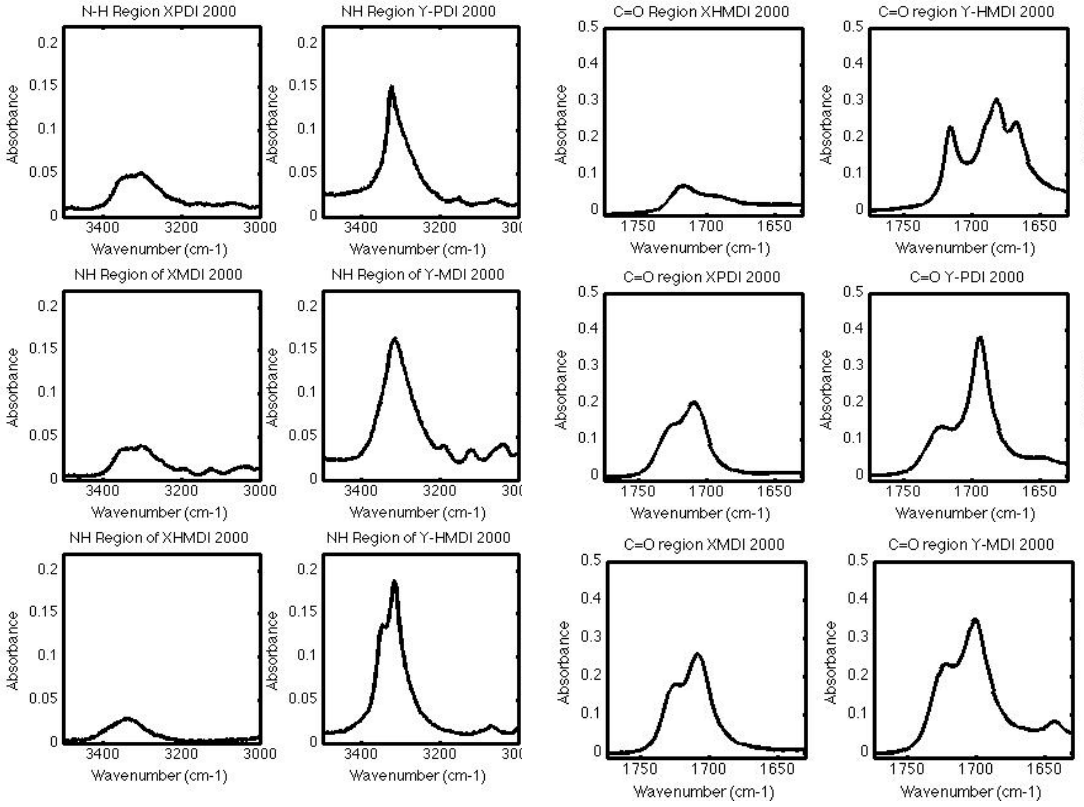

Figure 4.25: NH and C=O IR bands of XPCM and YPCM samples exhibit different types of hydrogen bonding.

From the differences in hydrogen bonding between N-H and C=O groups, IR spectrum of a thermoplastic polyurethane elastomer could be distinguished from a thermoset polyurethane elastomer. This gave sufficient information about the network formed [4,6,7,10] For thermoset elastomers, IR bands with a narrow distribution of H-bonding peaks, and a lower shift in frequency with respect to the "free" N-H peak absorbance area.[136]Figure 4.26 highlights the differences in spectral properties observed, between the hydrogen bonded amine and carbonyl stretching band modes of the XPCM and Y-PCM sample sets. From this comparison, a difference in peak shape, intensity and broadness is realized. For peak shape, symmetrical and narrow NH and C=O peaks were mostly

observed for samples in the XPCM set. On the other hand, NH and C=O peaks observed for Y-PCM samples were broad, contained multiple peaks, and appeared asymmetrical. With regards to the shape of the peak, the Y-PCM IR spectra show a shoulder peak around 3450 cm^{-1}adjacent to the NH peak at 3323 cm^{-1}. This is commonly seen for segmented polyurethanes, as the NH and C=O stretching region contains separate infrared bands attributed to "free" and hydrogen bonded NH and C=O groups. Free "disordered" hydrogen bonds display a frequency around 3450cm^{-1} and bonded "ordered" hydrogen bonds in the NH region appear at ~3330 cm^{-1}. The appearance of a shoulder indicates a mix of free and bonded NH groups in the sample. The same is seen for the carbonyl C=O stretching region. Generally, the band at 1736cm^{-1} is assigned to the "free" C=O, while 1704cm^{-1} is assigned to the hydrogen bonded C=O stretch, appearing as a shoulder.[157] Polyethylene glycol is a polyether therefore; it is certain that only urethane C=O groups participate in hydrogen bonding. Broad or multiple peaks in the NH and C=O regions appear as a result of multiple types of hydrogen bonding. [61,107] The broad peaks observed for the Y-PCM samples indicate the presence of hard segment physical cross-links. The XPCM sample peaks in the NH and C=O region appear narrow and symmetrical. According to Kontou[136] demonstrated that thermoset exhibit sharp and symmetrical NH and C=O stretching bands because they have only one type of hydrogen-bonding.

The C=O stretching band of Y-HMDI 2000 and X-HMDI 2000. Unlike other samples, a multiplet peak is observed for Y-HMDI 2000. There is a noticeable difference in peak broadness between the C=O multiplet peak seen for Y-HMDI2000 and the C=O peak

seen for X-HMDI 2000. An explanation for the broader peaks observed for the Y-PCM sample is that it is thermoplastic and has multiple Infrared bands for different types of hydrogen bonding, whereas, the XPCM samples which are thermoset polymers only have 1 type of bonding. It can be seen that peak intensity is much more prominent for Y-PCM than XPCM samples.

Peak frequency and peak broadness were also analyzed to characterize the differences in spectral properties between XPCM and Y-PCM samples. The absorbance areas of the main peaks in the NH and C=O regions were measured using Ominic software to examine differences in peak broadness. The area of the NH and C=O absorbance curves for chemical and physical cross-linked samples are summarized in Table 4.5. The absorbance area of the NH and C=O stretching peak for chemically cross-linked polyurethanes is lower, compared to the absorbance area of the thermoplastic polyurethane. This result is consistent with Kontou's findings.

Table 4.5: Absorbance Area to indicate broadness

XPCM Sample	*N-H*	*C=0*	*YPCM Sample*	*N-H*	*C=0*
XMDI 2000	5.631	9.4058	YMDI 2000	20.2918	15.3380
XMDI 3000	10.9430	4.6630	YMDI 3000	16.5770	10.6555
XMDI 6000	1.7025	2.9567	YMDI 6000	26.6092	11.9218
XHMDI 2000	3.8722	3.2416	YHMDI 2000	17.641	14.7163
XHMDI 3000	7.5168	2.9873	YHMDI 3000	30.0221	20.8278
XHMDI 6000	11.8360	1.9531	YHMDI 6000	33.7092	17.7499
XPDI 2000	2.5423	7.2566	YPDI 2000	32.8549	14.8420
XPDI 3000	3.7499	7.7265	YPDI 3000	37.6974	14.4096
XPDI 6000	12.8428	3.8094	YPDI 6000	39.3035	18.0712[1]

[1] The absorbance areas of the main peaks in the N-H and C=O regions were measured using Ominic software to examine differences in peak broadness

According to Table 4.3, it is evident that PEG molecular weight has no effect on the frequency wavenumber. However, Figure 4.26 reveals there is relationship between NH and C=O peak intensity and PEG molecular weight is evident. XPCM 2000 shows greater peak intensity in the N-H and C=O regions compared to XPCM 6000. As for XPCM 2000 and XPCM 3000, only a small difference is seen between peak intensities because they are closer in molecular weight. Nonetheless, it is evident that the peak intensity increases with PEG molecular weight. It is reasonable to suppose that XPCM 2000 peak absorbance is higher because it has a higher cross-link density; thus more allophanate-urethane linkages are present, compared to XPCM 6000. Results from the previous section gave evidence that XPCM has the highest cross-link density.

A relationship between PEG molecular weight and peak intensity could be not seen. The absorbance for the 40% HS PCM sample series, shows relatively, the same peak intensities.

FTIR Conclusion

The appearance of distinct peaks in the NH and C=O stretch region verified that all of the samples are polyurethanes. Overall the spectral characteristics observed for XPCMs were low peak intensity, symmetrical shape, small frequency shift, and lower absorbance area. This set of spectral perturbations suggests that XPCM samples exhibit lower hydrogen bonding strength than YPCM samples. The majority of YPCM samples displayed NH and C=O IR bands with shoulder peaks or were observed as a multiplet. Given that hydrogen bonds are responsible for manifesting heterogeneous morphologies, this indicated the XPCM samples are homogeneous and the YPCM samples are heterogeneous. The characteristic spectral properties observed for the chemically cross-linked PUs and physically cross-linked PUs corroborate with Kontou.[136] this result confirmed branching between polyurethane chains occurred as a result of excess isocyanate groups reacting with urethane groups. Therefore, this was sufficient evidence to conclude that all XPCM samples are chemically cross-linked and that all Y-PCM samples are physically cross-linked.

4.3.3. RESULTS FROM ANALYSIS OF THERMAL STABILITY BY TGA

For the utility of PU-SSPCM in building applications the PCM material must be thermally stable at high enough temperatures to endure melt processing. Thermo-

gravimetric analyses (TGA) was used to monitor the degradation of a family of thermoset (XPCM) and thermoplastic (YPCM) PU-SSPCM samples.[23]

TGA scans were collected in air at 20˚C/min up to 400℃. Figure 4.28, Figure 4.26, Figure 4.27 & Figure 4.29 shows the TGA results generated for YPDI, YMDI, and YHMDI thermoplastic PU-SSPCM prepared with PEG 2000, 3000, and 6000 g/mol. At 200˚C, virtually all samples remained stable. All of the YPCM thermoplastic samples showed no sign of degradation until temperatures rose to 250˚C and then showed rapid degradation. However, a few samples showed the appearance of mass loss during initial heating. In Figure 4.26, YMDI 2000 displayed a mass loss of 8.414% at 200˚C. Generally, weight loss less than 10% is not considered significant. Typically, a slight mass change during initial heating will appear due to the loss of solvent. Therefore, this can be attributed to residual DMSO-MBK solvent in the bulk polymer. Therefore, this confirms that all of the thermoplastic PCMs are able to endure melt processing and Thermal degradation is characterized by three temperatures: The onset of degradation (T_0), the midpoint of degradation (T_I), and final decomposition temperature (T_{II}). The onset degradation temperature signifies the beginning of thermal decomposition of more than 10% weight loss. For YPDI 2000, 3000, and 6000 the onset degradation temperature appeared at 296.94˚C, 291.02˚C, and 299.96˚C, respectively. The onset of degradation for YHMDI 2000, 3000 and YMDI 2000, 3000 occurred at 257.71˚C, 270.51˚C and 284.55˚C, 278.23˚C, respectively. YHMDI 6000 and YMDI 6000 were only analyzed up to 250˚C. Information on the thermal degradation properties above 200˚C was not pertinent for this study. Therefore, only the thermal degradation properties of a selected

group of thermoplastic PU-SSPCM were analyzed to 400˚C for a more detailed study. According to Figure 4.26- 4.7, all of the YPCM samples did not start decomposition until temperature higher than 250˚C. DSC method parameters used in this study include an initial heat step, in which the family of YPCM thermoplastic samples are heated to 250˚C. From this data we are certain the sample will not decompose when heated to a homogeneous melt state.

The family of XPCM thermoset sample demonstrated impeccable thermal stability. All of the XPCM samples remained stable up to 400˚C. TGA curves of XPDI, XHMDI, and XMDI 3000 are depicted in Figure 4.29, This series of XPCM samples were chosen for detailed study. It can be seen that The plateau in %weight loss continues on until 400˚C without fully degrading. From these results it is clear all of the XPCM samples are thermally stable above 200˚C.

Comparatively, the thermoplastic YPCM samples demonstrated a lower degradation temperature, which means that XPCMs have greater thermal stability. The percentage of total mass loss observed from onset temperature to 400˚C for YHMDI-2000 and -3000 was 78.71% and 64.08%, which is higher than %mass loss observed for YMDI- (30.6%) and YPDI-2000 (49.6%). The difference between initial degradation temperature and final decomposition was greater for the XPCM samples. These results indicate thermoset PU-SSPCMS have a wider processing temperature range, which is important for the fabrication of PU-SSPCMs.

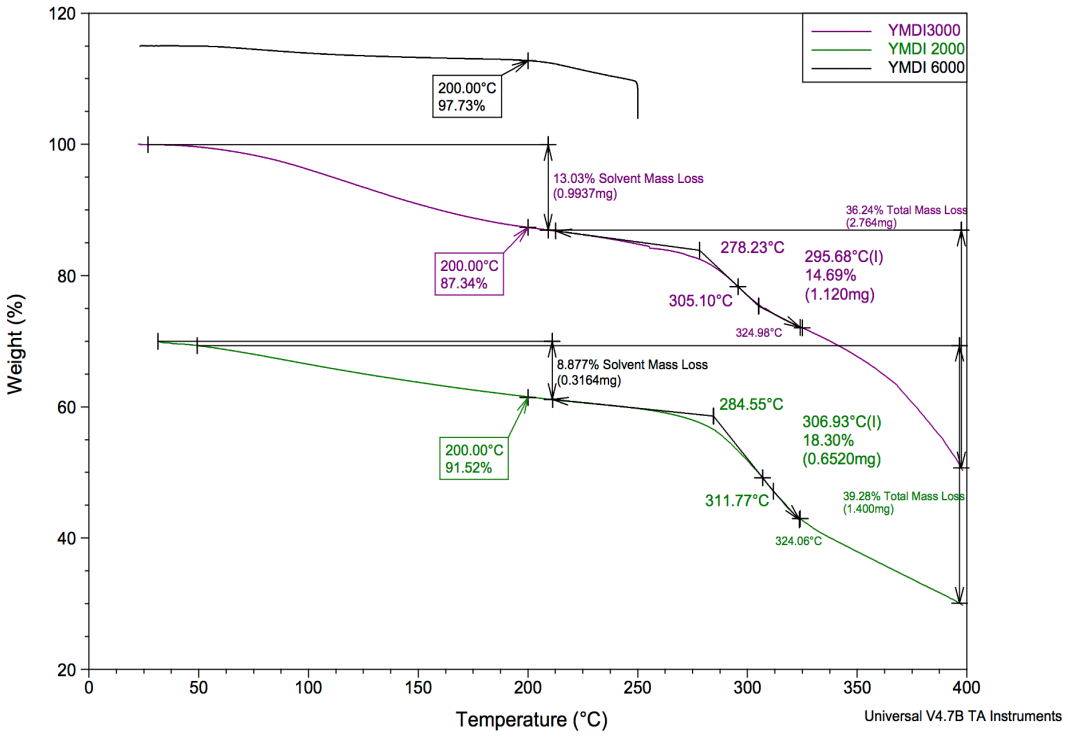

Figure 4.26: TGA Scans of YMDI -2000, 3000, & 6000.

In the literature, it has been documented that at high temperatures, polyurethanes undergo degradation first via decomposition of urethane bonds, followed by breakage of the soft segment phase.[23] Such degradation process could be easily monitored by thermo-gravimetric analyses (TGA). This would explain the slight drop that appears in the initial step for YPCM samples prepared with PEG 2000.

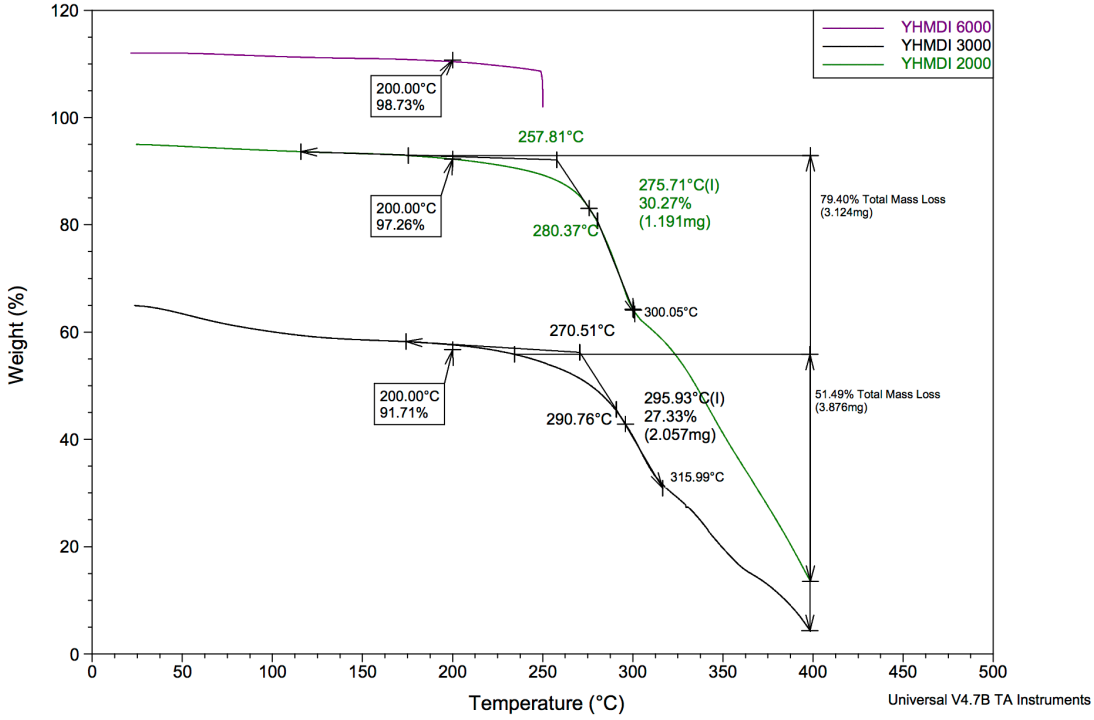

Figure 4.27: TGA Scans of YHMDI 2000, 3000, & 6000

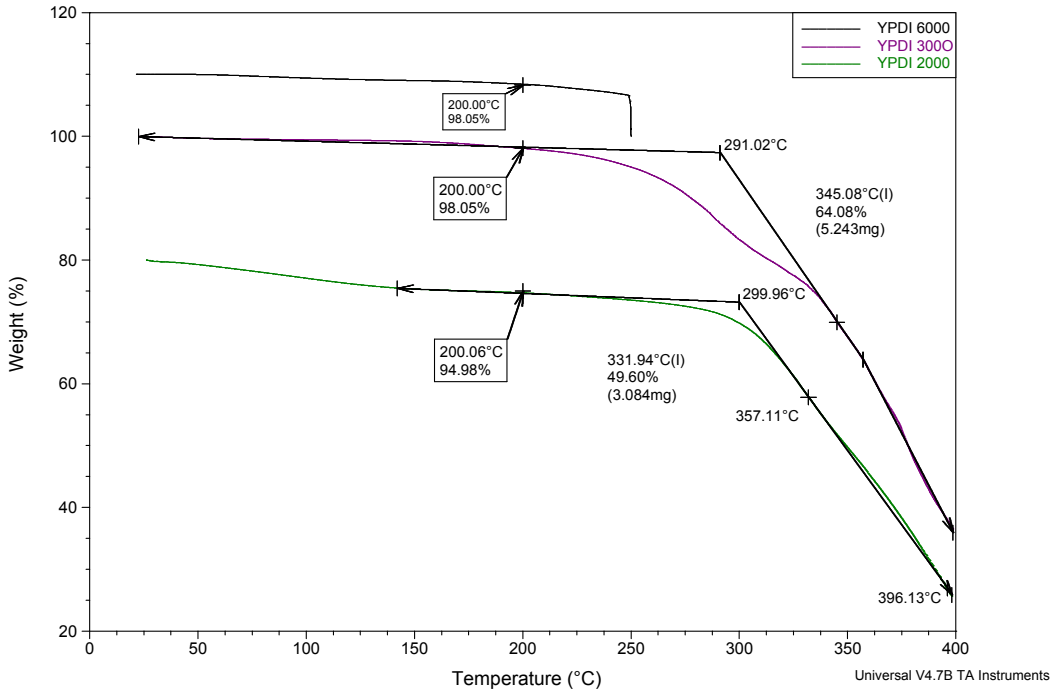

Figure 4.28: TGA Scans of YPDI -2000, 3000, & 6000

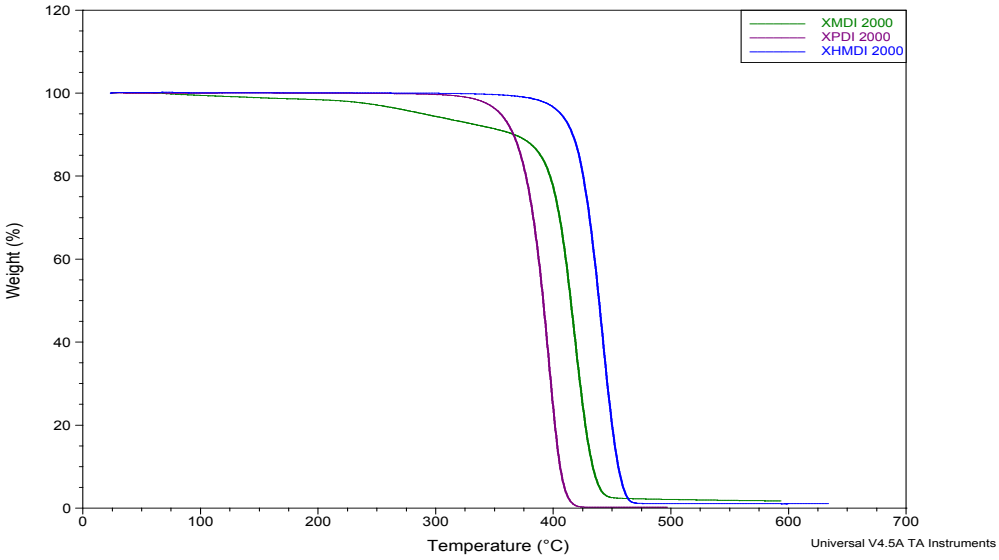

Figure 4.29: TGA scans of XHMDI, XMDI, and XPDI prepared with PEG M_n= 3000 g/mol

4.3.4. POLAR OPTICAL MICROSCOPY

Polar Optical Microscopy (POM) was employed to study crystalline morphology. Images were taken at 20X magnification, accompanied by a hot stage to visually observe the crystalline structure of the synthesized PU-SSPCM samples before and after the phase transition temperature.

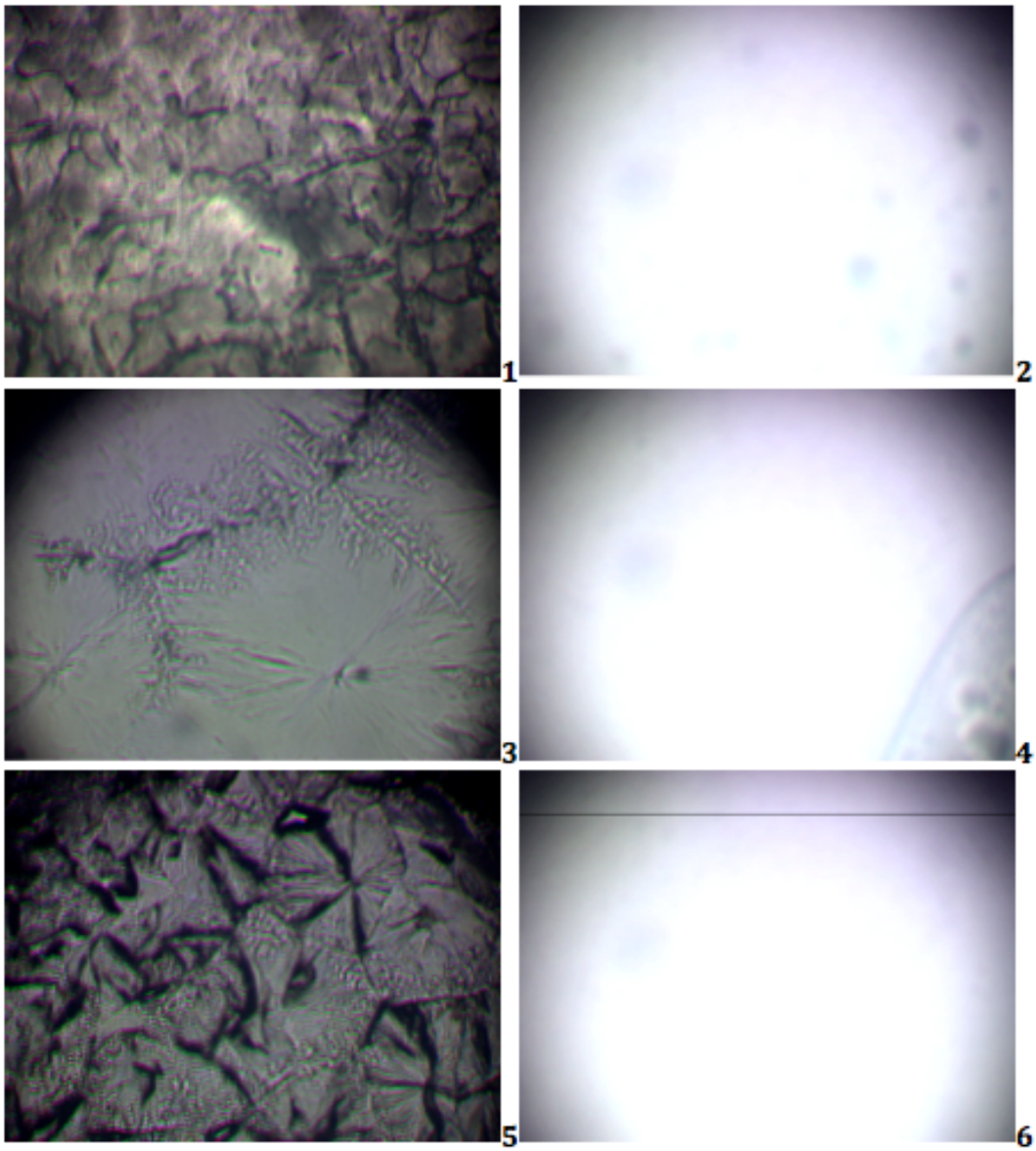

[1] PEG M_n= 2000 g/mol at 25˚C
[2] PEG M_n= 2000 g/mol at 100˚C
[3] PEG M_n= 3000 g/mol at 25˚C
[4] PEG M_n= 3000 g/mol at 100˚C
[5] PEG M_n= 6000 g/mol at 25˚C
[6] PEG M_n= 2000 g/mol at 25˚C

Figure 4.30: POM Images of Pure PEG M_n= 2000, 3000, 6000 g/mol

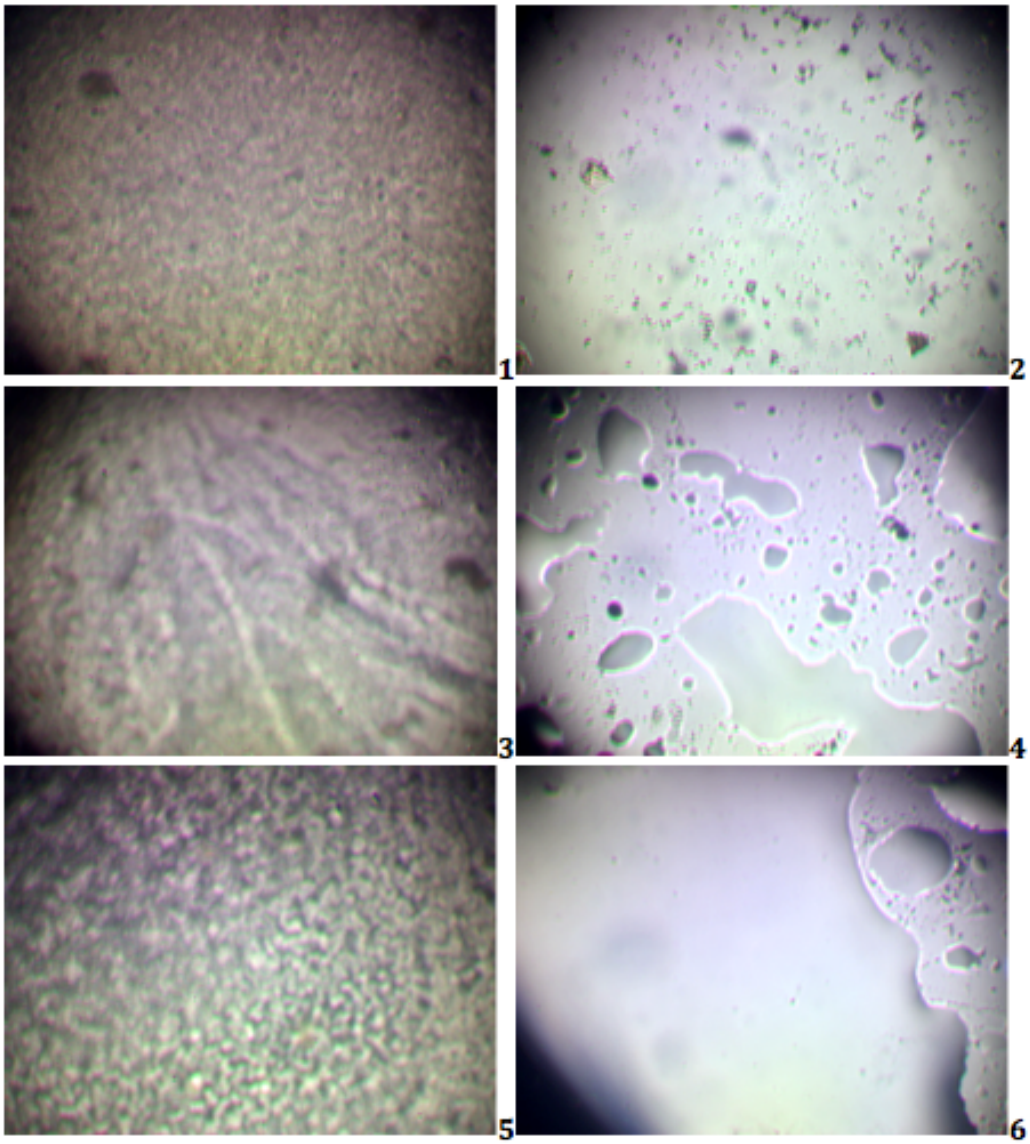

[1] YHMDI M_n= 2000 g/mol at 25˚C
[2] YHMDI M_n= 2000 g/mol at 100˚C
[3] YHMDI M_n= 3000 g/mol at 25˚C
[4] YHMDI M_n= 3000 g/mol at 100˚C
[5] YHMDI M_n= 6000 g/mol at 25˚C
[6] YHMDI M_n= 2000 g/mol at 25˚C

Figure 4.31: POM images of YHMDI PEG M_n= 2000, 3000, 6000 g/mol

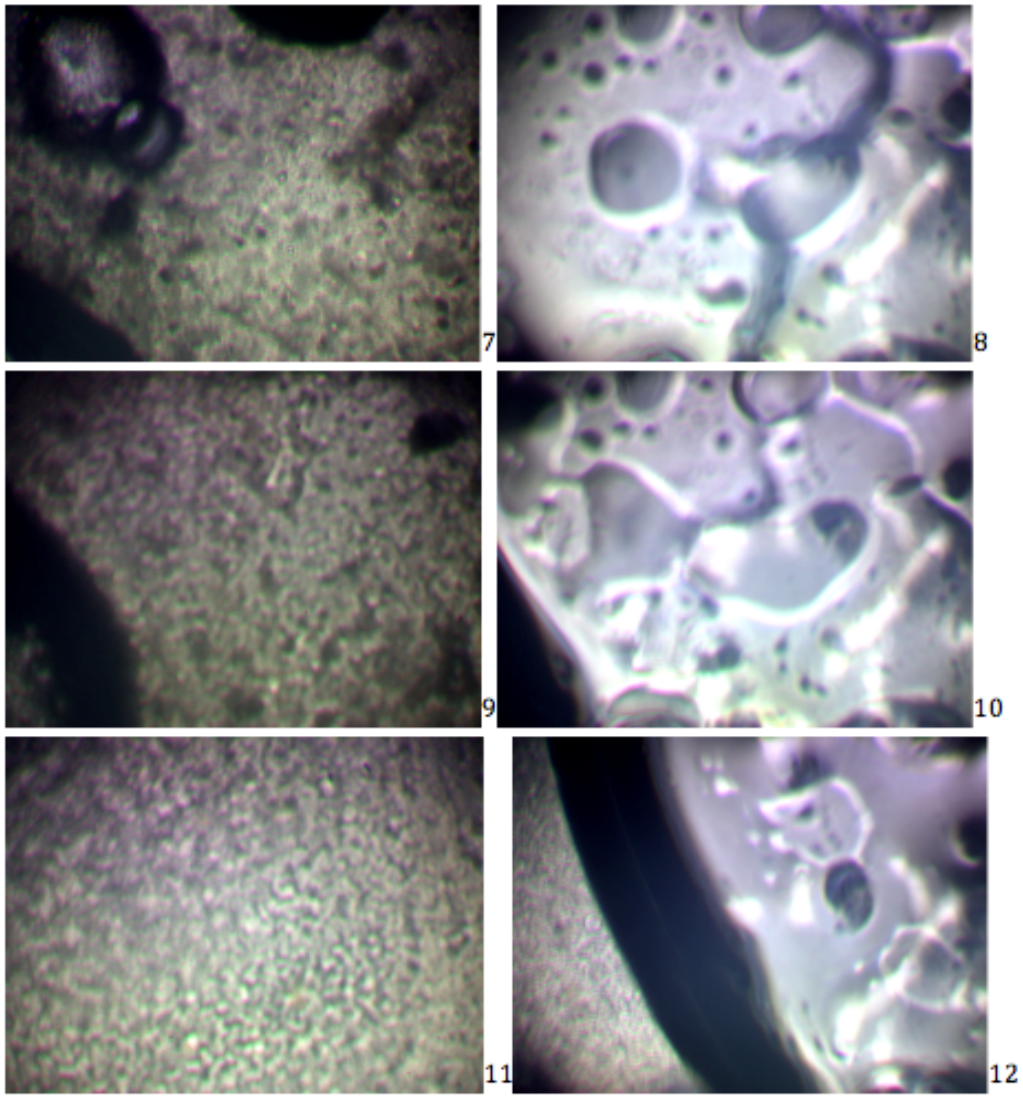

[7] YPDI 2000 at 25°C
[8] YPDI 2000 at 200°C
[9] YPDI 3000 at 25°C
[10] YPDI 3000 at 200°C
[11] YPDI 6000 at 25°C
[12] YPDI 6000 at 200°C

Figure 4.32: POM Images of YPDI PEG M_n= 2000, 3000, 6000 g/mol

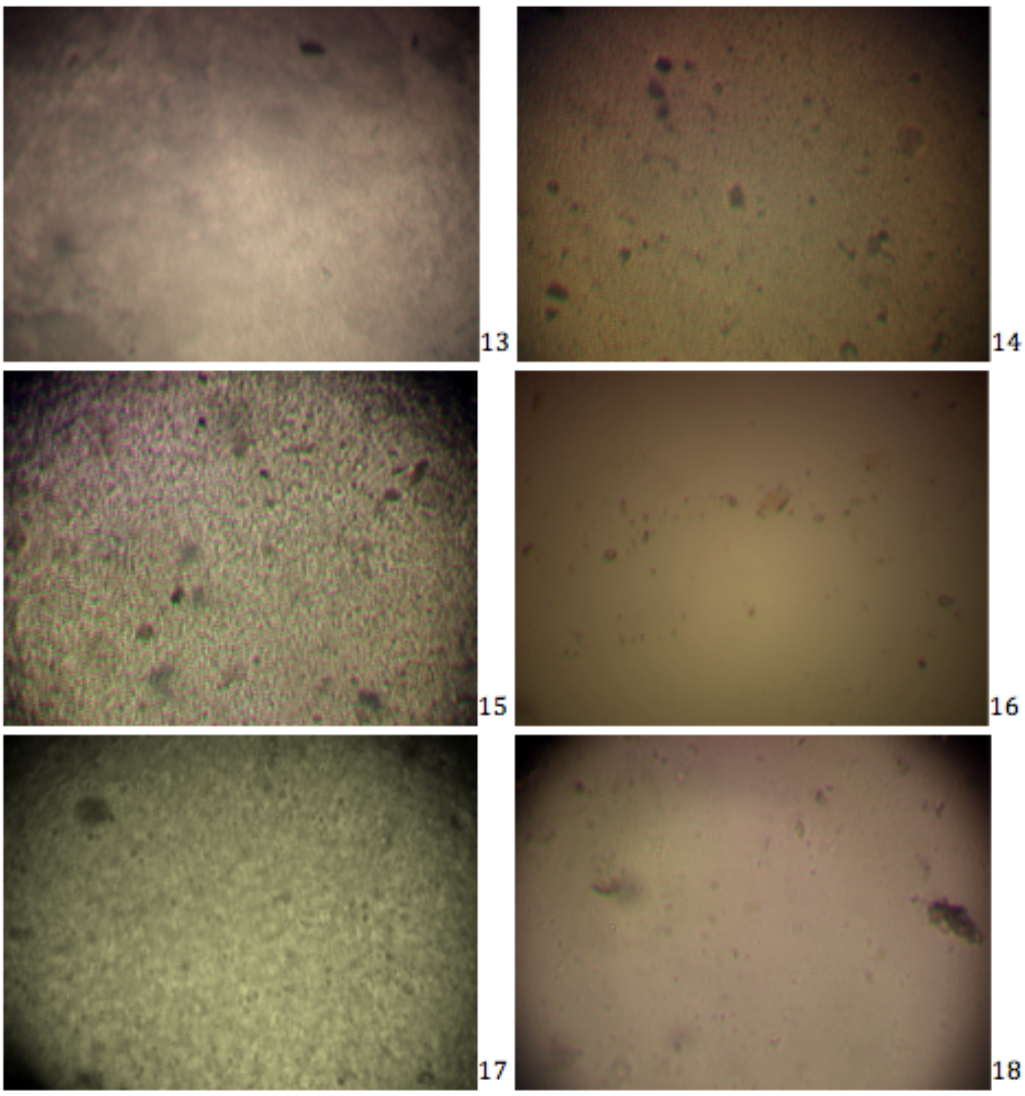

[13] YMDI 2000 at 25°C
[14] YMDI 2000 at 250°C
[15] YMDI 3000 at 25°C
[16] YMDI 3000 at 250°C
[17] YMDI 6000 at 25°C
[18] YMDI 6000 at 250°C

Figure 4.33: POM Images of YMDI PEG M_n= 2000, 3000, 6000 g/mol

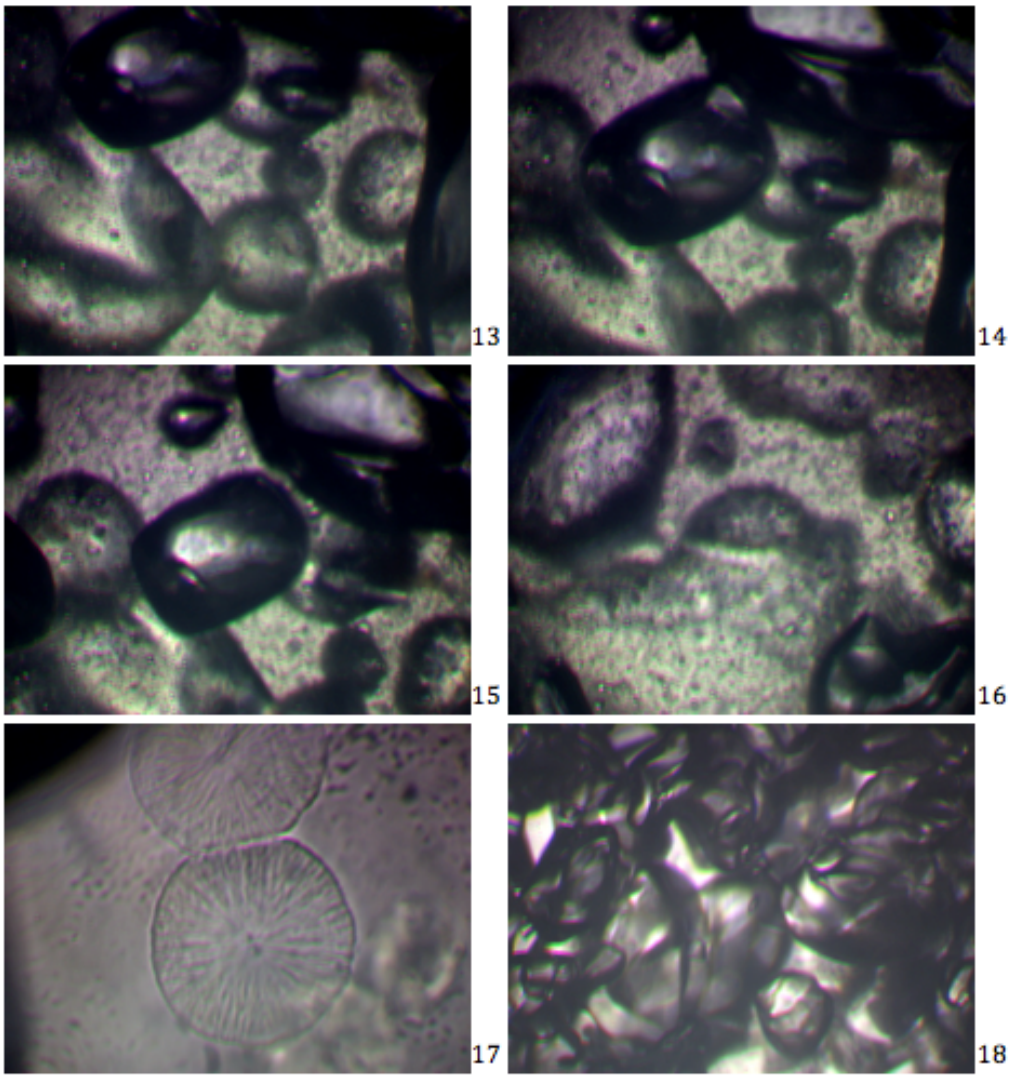

[13] XMDI 2000 at 25°C
[14] XMDI 2000 at 250°C
[15] XMDI 3000 at 25°C
[16] XMDI 3000 at 250°C
[17] YMDI 6000 at 25°C
[18] XMDI 6000 at 250°C

Figure 4.34: POM Images of XMDI M_n= 2000, 3000, 6000 g/mol

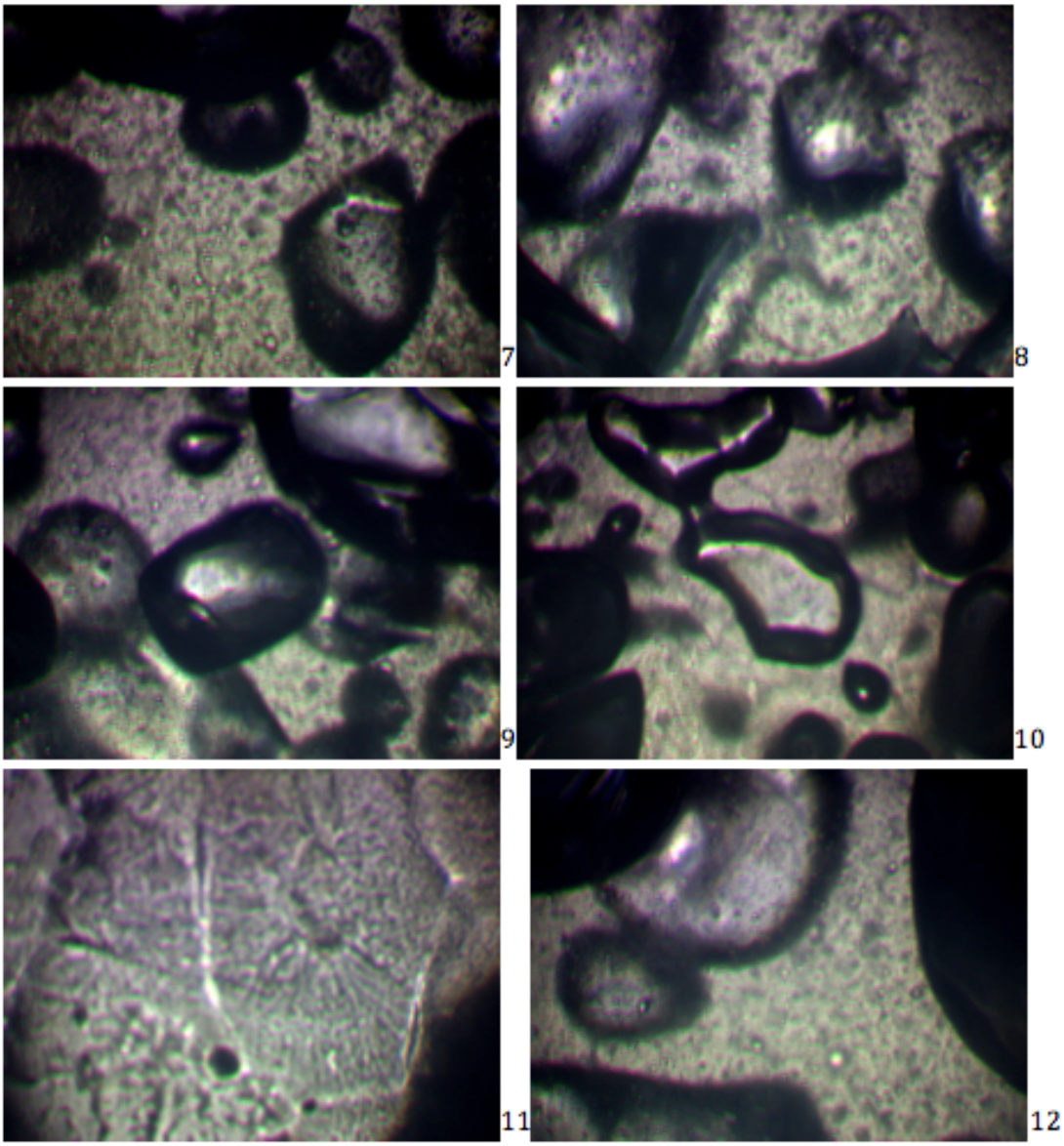

[7] XHMDI 2000 at 25°C
[8] XHMDI 2000 at 200°C
[9] XHMDI 3000 at 25°C
[10] XHMDI 3000 at 200°C
[11] XHMDI 6000 at 25°C
[12] XHMDI 6000 at 200°C

Figure 4.35: POM Images of XHMDI PEG M_n= 2000, 3000, 6000 g/mol

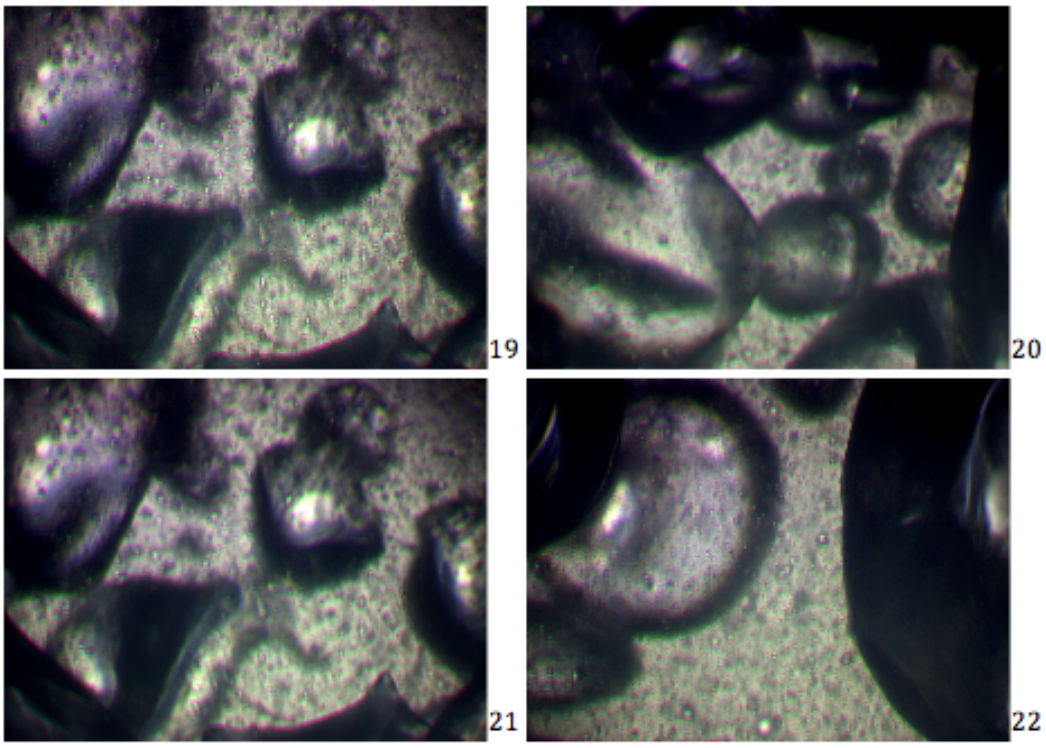

[19] XPDI 2000 at 25°C
[20] XPDI 2000 at 250°C
[21] XPDI 3000 at 25°C
[22] XPDI 3000 at 250°C

Figure 4.36: POM Images of XPDI PEG M_n= 2000, 3000 g/mol

In Figure 4.30 (1-6), the POM images of pure PEG M_n= 2000, 3000, 6000 g/mol are shown at room temperature (21˚C) and at 70˚C. In The POM images taken at 70˚C the PEG polymer is completely transparent, which indicates that the PEG melted. It can be seen in Figure 4.31, Figure 4.32, & Figure 4.33 the thermoplastic Y-PCM samples, when the image turned from cloudy to transparent, as the sample was heated, it signified that the HS crystallites that form the physically cross-linked network had melted. It can be assumed that at this point the Y-PCM sample has reached its homogeneous melt state thereby, all HS domain order has been destroyed. It was observed that all of the sample were transparent at 250˚C. This indicated the samples will be in a homogeneous melt state during DSC experiments, which is necessary for controlling the degree of phase separation in the Y-PCM samples.

It can be seen in Figure 4.34, Figure 4.35 & Figure 4.36 thermoset X-PCM samples, it is expected that the opposite behavior be observed. At no point should the sample become transparent because thermosets cannot be melted. The fact that this was not observed for any of the X-PCM samples confirms that all of them are thermosets and are comprised of a chemically cross-linked network.

Figure 4.35 (7-12) shows the POM images of X-HMDI at room temperature (21˚C) and at 250˚C. The cloudy image observed at 250˚C implies that the sample remained in the amorphous state at temperatures dramatically higher than the melting temperature of pure PEG. This confirms that the sample exhibited a solid-to-solid phase transition.

According to Figure 4.33, the POM images shown for Y-MDI, the sample began to burn around 250˚C, before homogeneous melt was obtained. Therefore, we could not confirm

whether Y-PCM samples prepared with MDI were thermoplastic, using POM analysis; however, results from FTIR analysis showed similar spectral characteristics with the other thermoplastic samples tested.

In the IR results, Peaks were observed. Furthermore, the spectral characteristics observed for X-MDI sample series were 3303 cm-^{1}and 1710 cm^{-1} in the NH and CO regions, respectively. The apparent difference in spectral properties with X-MDI samples, which are known thermosets, and the consistency with known thermoplastic samples provides sufficient evidence confirming that the Y-MDI samples (Y-MDI-2000, 3000, and 6000) are thermoplastic, and that the physical cross-links formed by hydrogen bonding between linear urethane hard segments is responsible for its solid framework. Although s the Y-MDI samples remain grey at 250˚C, we are certain this is not due to allophanate chemical cross-links. According to the TGA results shown in Figure 4.26, a significant decomposition occurs when the samples are heated above 250˚C. Therefore, the sample degrades before a homogeneous melt is obtained. This occurrence is mentioned in previous PU literature and remains a problem for erasing thermal history.[40,101,137]

4.3.5. THERMAL ANALYSIS BY DSC

DSC Analysis was used to evaluate the thermal energy stored and released by a PEG PCM polymer in a thermoset and in a thermoplastic polyurethane-SSPCM system.

First heat Run

First heat run DSC curves for thermoset samples XMDI 2000, XPDI 2000, and XHMDI 2000 are shown in Figure 4.31. These samples were selected for a more detailed study. Initial heat run DSC Curves for thermoplastic Y-HMDI, Y-PDI and Y-MDI samples are displayed in Figures 4.32-4.34. The appearance of two melting peaks at <100C (I) and >100C (II) can be seen in the initial heat curves for most of the Y-PCM samples. This confirms that these are thermoplastic materials and also suggests that a level of phase separation is present in the samples. In literature, the DSC curves for regular thermoplastic PU materials display multiple endotherms. Generally, the peak observed at temperatures >100˚C (I) is attributed to the melting thermal transition of the PEG PCM phase. The melting peak observed at elevated temperatures above >100˚C (II) is related to the disruption of an ordered structure appearing in the hard phase and to the micro-phase mixing of the SS and HS. In most cases, similar peaks that match the signature peaks observed for regular linear PU materials were observed in the Y-PCM initial heat curves shown in Figure 4.40. However, in contrast the same peaks were not observed for the sets of XPCM samples (See Figure 4.39). Only one prominent melting peak was observed, which indicates only one phase is present in the samples. Therefore, it is evident from the difference in DSC curves, that the PU-SSPCMs with chemical cross-links have a different phase morphology than the PU-SSPCMs with physical cross-links.

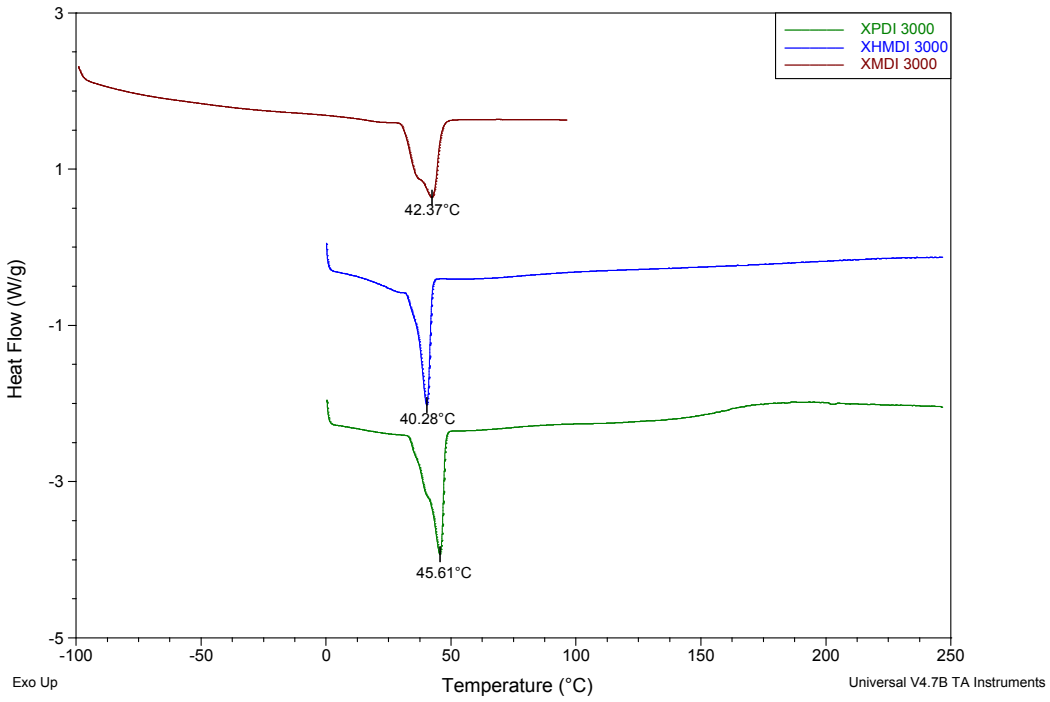

Figure 4.37: DSC Initial Heat run from XMDI3000, XPDI 3000, XHMDI 3000

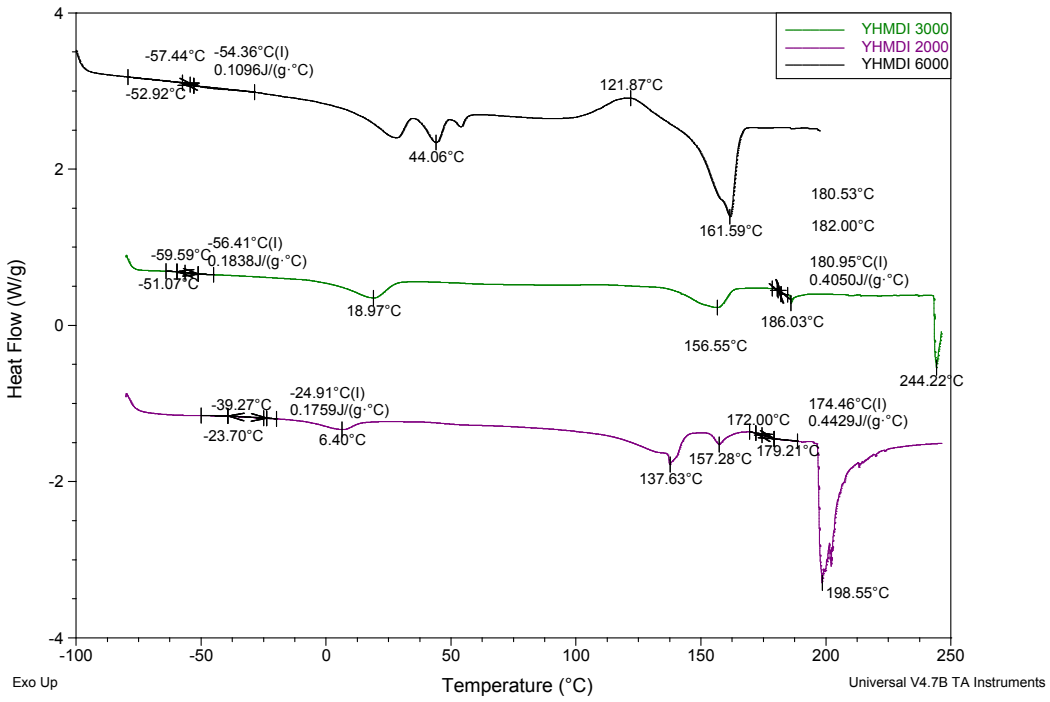

Figure 4.38: DSC Initial Heat runs from series of YHMDI 2000, 3000, & 6000

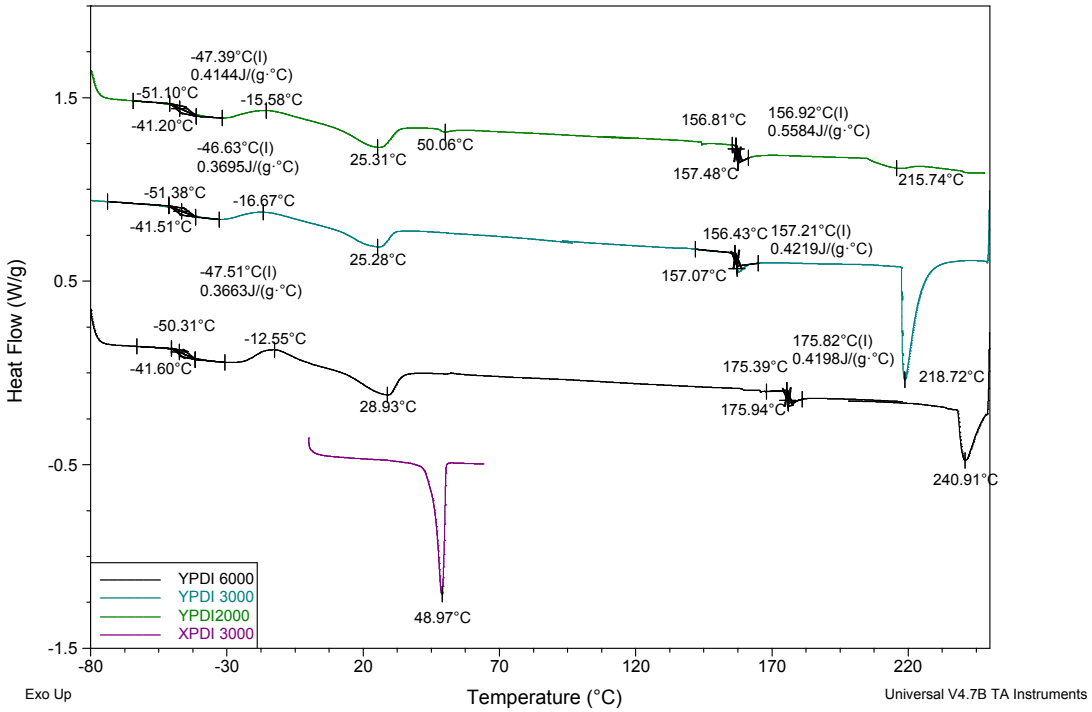

Figure 4.39: DSC Initial Heat run from series of YPDI 2000, 3000, & 6000, and XPDI 3000

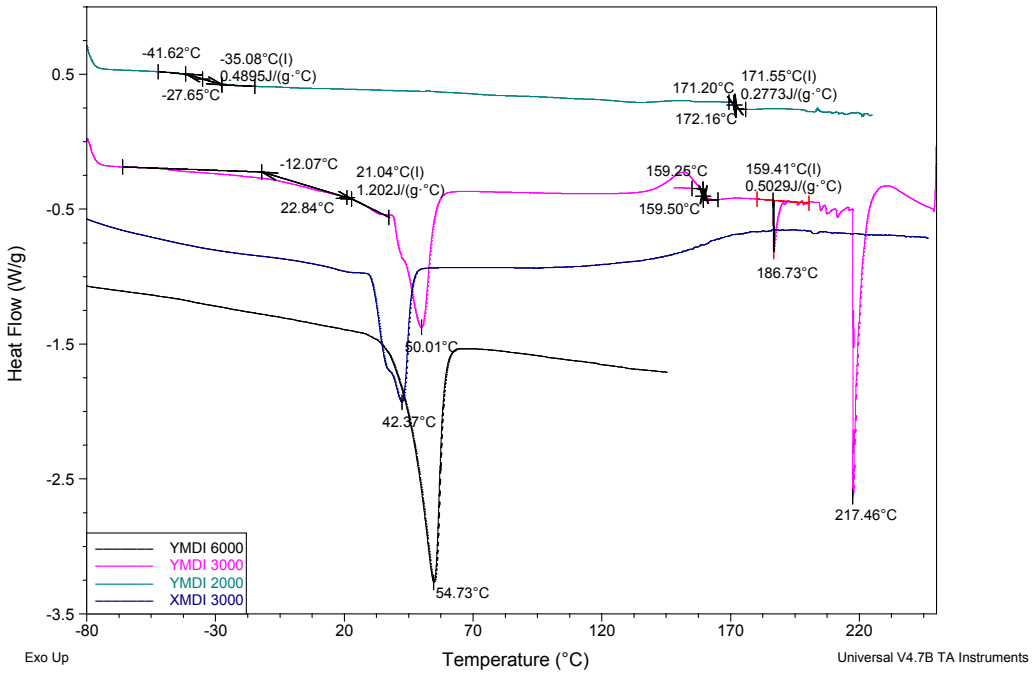

Figure 4.40: DSC Initial Heat run from series of YMDI 2000, 3000, & 6000, and XMDI 3000

DSC – Evaluation of PCM Domain Thermal Energy Storage Properties

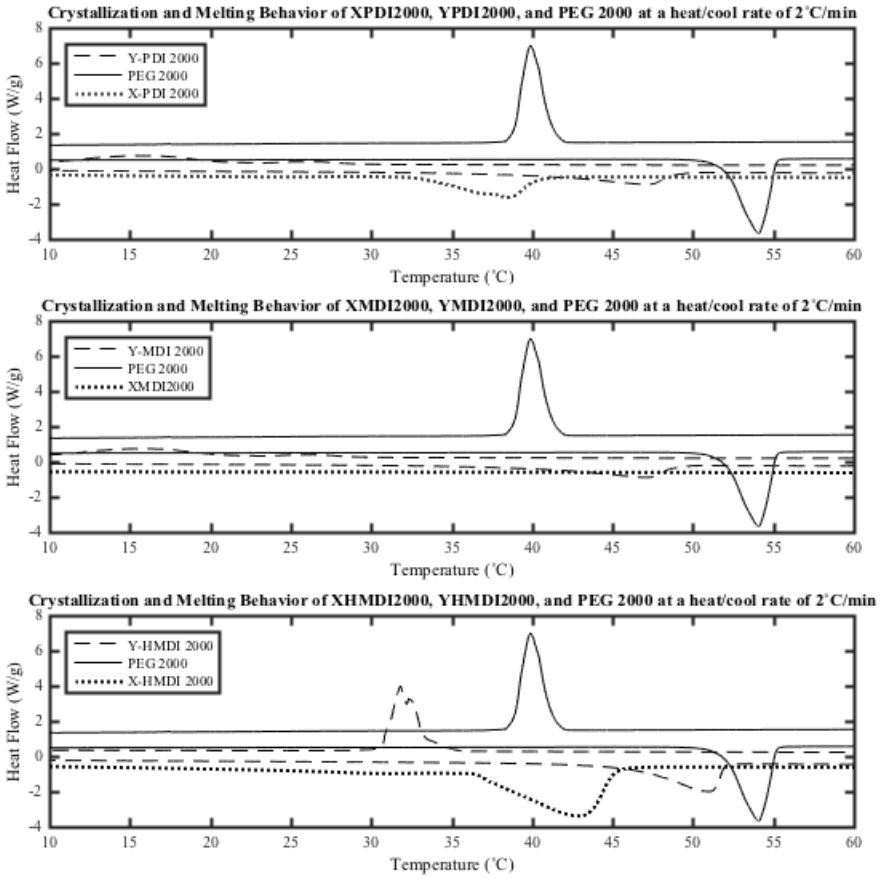

Figure 4.41: Crystallization and Melting Behavior of XPCM 2000 samples overlaid with YPCM 2000 samples prepared with same diisocyanates and pure PEG M_n= 2000 g/mol

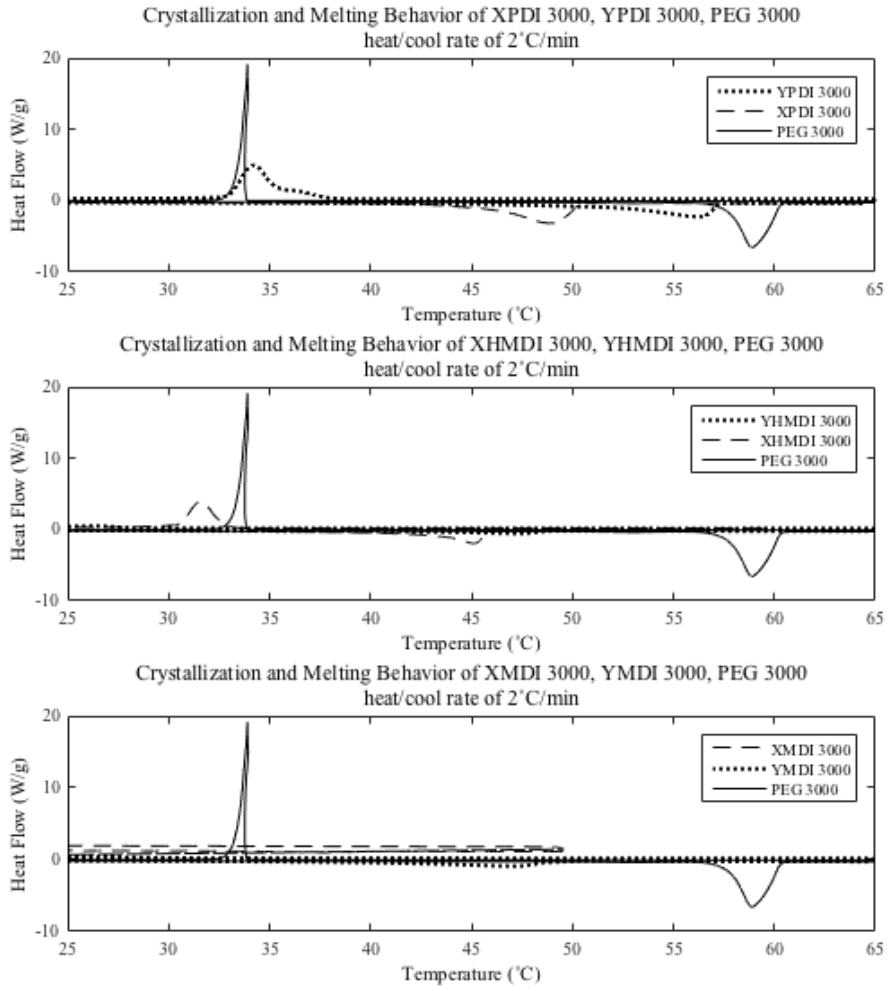

Figure 4.42: Crystallization and Melting Behavior of XPCM 3000 samples overlaid with YPCM 2000 samples prepared with same diisocyanates and pure PEG M_n= 3000 g/mol

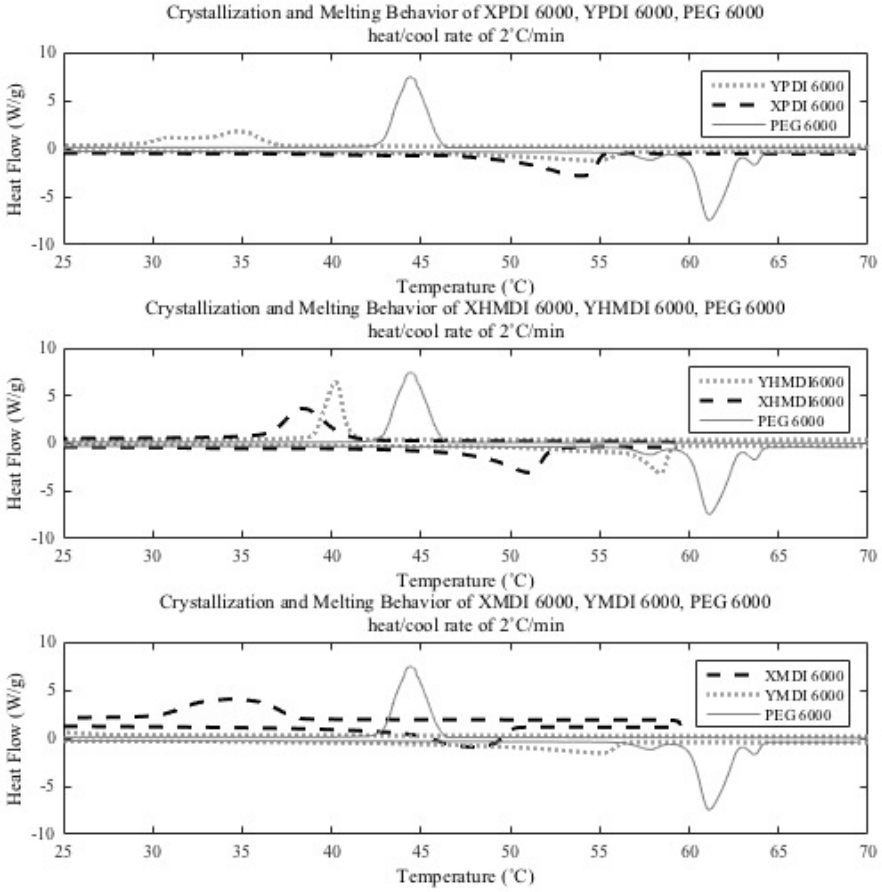

Figure 4.43: Crystallization and Melting Behavior of XPCM 6000 samples overlaid with YPCM 2000 samples prepared with same diisocyanates and pure PEG M_n= 6000 g/mol

DSC curves in Figures 4.35-4.37 show the melting and crystallization behavior of the PEG component of thermoset XPCM samples and thermoplastic Y-PCM samples overlaid with pure PEG, according to respective diisocyanate and PEG molecular weights. The melting and crystallization curves illustrates the storage and release of thermal energy as the PCM PEG polymer transitions between phase states. According to Figures 4.35- 4.37, the pure PEG endo and exothermic peaks were much greater in

intensity and were observed at higher crystallization and melting temperature. The reduction in peak intensity and phase transition temperatures is a result of the urethane HS chain end restrictions on the PEG PCM polymer chain mobility. This observation verified that the PCM PEG chain is attached to a HS urethane group. The magnitude in which crystallization and melting curves dropped in intensity and shifted to lower temperatures indicates the strength of HS chain end restrictions.[34] The HS chain end effect can be quantified by $|\Delta H| = |\Delta H_m^\circ - \Delta H_m|$.

Table 4.6 lists the phase change characteristics of all XPCM and YPCM samples (melt enthalpy (ΔH_m J/g) values and corresponding melting ($T_m^\circ C$) and crystallization ($T_c^\circ C$) temperatures). All values were obtained by standard DSC evaluation. T_m and T_c correspond to the peak melting and crystallization temperature and is the maximum peak temperature at which melting and crystallization occurs. Enthalpy heat of fusion (ΔH_m) was calculated by integrating exothermic and endothermic peak area using TA analysis software. X_c represents the percentage of crystalline PEG PCM polymer chain segments that exhibit latent heat storage properties. The X_c% was calculated based on ΔH_m values using the following equation: $X_c(\%) = (\Delta H_{m\text{-}PCM}/\Delta H^0_{m\text{-}PEG})*100$; where for 100% crystalline PEG, pure PEG ΔH_m was used as ΔH^0_m. ΔH^0_m values for pure PEG was obtained using the same heating and cooling rate as PEG PCM. It was important to compare enthalpy values of PCM PEG to pure PEG obtained from the same method. All enthalpy values were measured on the second heat step.

The comparison of endothermic and exothermic peaks between XPCM and YPCM samples reveals the distinct differences between their melting and crystallization behavior.

Table 4.6: Summary of Thermal Energy Storage Properties

	[a]T_m (°C)	[b]ΔH_m (J/g)	[c]X_c (%)
PEG M_n= 2000 g/mol	54.07	165.30	100%
X-HMDI 2000	43.05	49.16	29.74%
Y-HMDI 2000	51.02	39.31	21.63%
X-PDI 2000	38.63	33.08	20.01%
Y-PDI 2000	47.97	38.87	23.51%
X-MDI 2000	--	--	--
Y-MDI 2000	--	--	--

	[a]T_m (°C)	[b]ΔH_m (J/g)	[c]X_c (%)
PEG M_n= 3000 g/mol	57.73	169.40	100%
X-HMDI 3000	45.17	64.74	38.22%
Y-HMDI 3000	50.81	52.95	31.26%
X-PDI 3000	48.97	81.97	48.39%
Y-PDI 3000	56.32	54.08	33.25%
X-MDI 3000	38.52	50.61	29.88%
Y-MDI 3000	47.06	37.53	22.15%

	[a]T_m (°C)	[b]ΔH_m (J/g)	[c]X_c (%)
PEG M_n= 6000 g/mol	61.13	179.20	100%
X-HMDI 6000	51.12	71.66	39.99%
Y-HMDI 6000	58.38	55.58	31.02%
X-PDI 6000	54.02	104.80	58.48%
Y-PDI 6000	56.32	41.24	23.01%
X-MDI 6000	42.37	67.88	37.88%
Y-MDI 6000	55.04	47.19	26.33%

[a]Phase Transition Temperature (°C),

[b]Enthalpy (J/g)

[c] Percent Crystallinity (%)

The percentage of the PEG soft chain able to crystallize was calculated by %Xc is percent crystallinity. To calculate X_c% The ΔH_m measured for pure PEG was used as the

standard enthalpy of fusion, $\Delta H^0_{m,}$ to calculate percent crystallinity. X_c% values can be used to approximate the size of the crystalline region. Therefore, it can be said that the bar graph shown in Figure 4.47 compares the size of the crystalline region in the samples that are chemically cross-linked and the samples that are physically cross-linked for analogous XPCM and YPCM samples (same diisocyanate and PEG molecular weight components). According to Figure 4.47, it can be seen the comparison of reveals that in most cases X_c% values were higher for the chemically cross-linked XPCM than their physically cross-linked YPCM counterpart. This indicates the the HS chain end effect was less prominent for chemical HS cross-links. It can be seen that in addition to the nature of the HS cross-link, the composition of the HS and PEG molecular weights also plays a factor in influencing PCM crystallization.

This is a systematic study, therefore the main research focus in this chapter is on the relationship between PCM PEG thermal energy storage properties and the nature of the HS cross-link. Even so, it is evident other factors related to the diisocyanate and PEG molecular weight impact thermal energy storage properties. These other relationships will be discussed here.

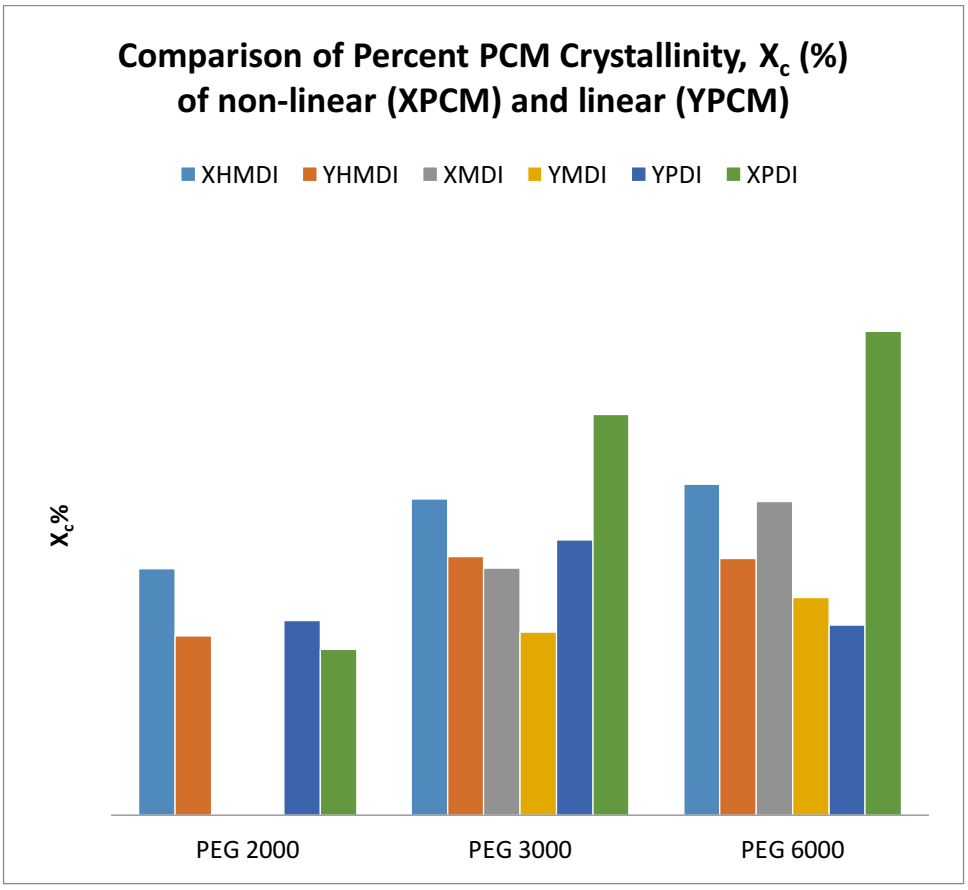

Figure 4.44: Comparison of Xc% Percent Crystallinity of PEG PCM polymer of all XPCM and YPCM samples with respect to diisocyanate HS component and PEG molecular weight.

.

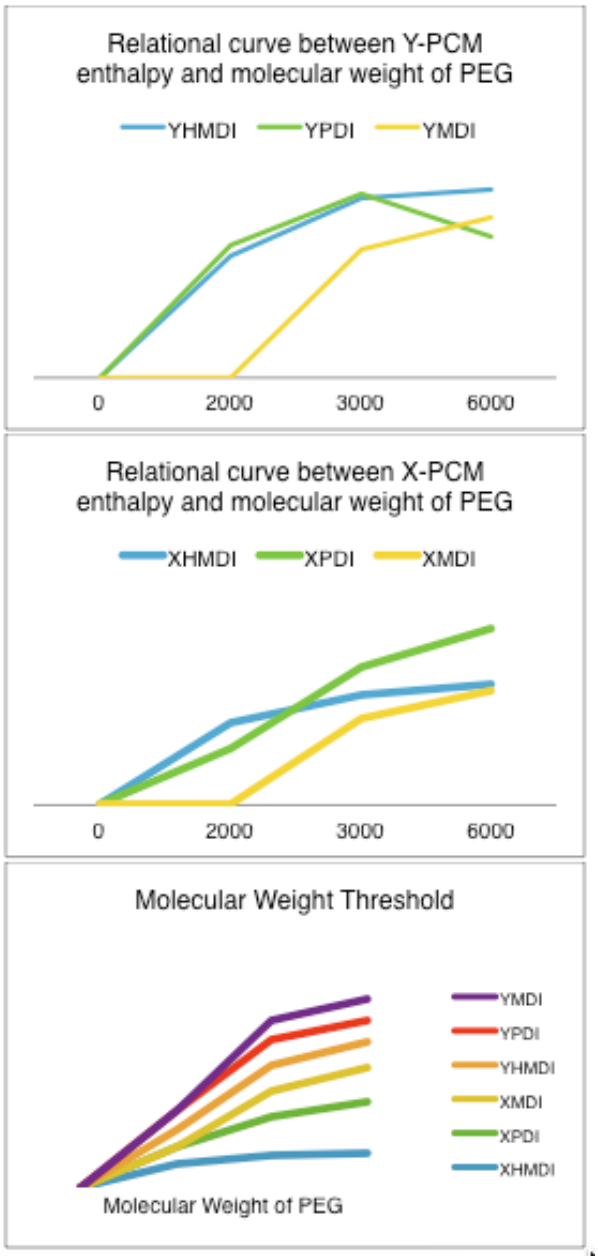

Figure 4.45: Line Plot compares melt enthalpy with PEG molecular weight of PEG

Figure 4.48 illustrates the relationship between melt enthalpy, PEG molecular weight, diisocyanate compositions, and cross-link nature. It is clear from the line plot that melt enthalpy increases proportionally with increasing molecular weight. However, it can be

seen that there is a markedly larger change in melt enthalpy from PEG 2000 to 3000, compared to the change in enthalpy from PEG 3000 to PEG 6000. In Figure 4.48 from 3000 to 6000 g/mol , the line plot shows a plateau in melt enthalpy and phase transition temperature. This was odd and unusual considering the difference in molecular weight between PEG 2000 and 3000 is much less than the difference between PEG 3000 and PEG 6000, which is why a larger jump in enthalpy would be expected. Similar behavior has been observed in previous literature and is known as a molecular weight threshold. Jiang[25] and Alkan both discussed the molecular weight threshold in their research. In Jiang's study[27] on PEG/CDA SSPCM, the phase transition temperature and enthalpy showed little variation for molecular weights above 6000, while lower molecular weight PEG displayed a significant change in thermal characteristics.

Alkan reported a similar result; a small increase in enthalpy for the PU-SSPCMs prepared with 6,000 g/mol PEG. Jiang[25] attributed this behavior to the different crystal structures formed by PEG with a molecular weight greater than 4000 g/mol. Beech describes why molecular weights less than 3700 g/mol will crystallize by extended chain folding, and molecular weights greater than 4000 g/mol will crystalize in both extended-chain and chain folding, and how this causes a plateau in enthalpy. According to Beech, when chains begin to fold, the interfacial free energy decreases by 1kcal. For molecular weights from 1000 to 6000, if there is a narrow distribution, they will crystallize by extended chain and the interfacial energy increases from 1-3kcal. When the molecular weight of the PEO chain equals or is greater than 6000g/mol, less variation in melting temperature is seen because the interfacial energy is decreasing, while PEO chains with molecular

weights from 1000 to less than 6000 that can only crystallize by extended-chain, increase by 1 kcal.

Y-HMDI 6000 ΔHm was 20.45J/g and for Y-HMDI 2000, ΔH_m was 39.31 J/g. In previous literature, typically, as PEG molecular weight increases, ΔH_m increases. However, the opposite result seen in this case was due to the molecular weight threshold. Alkan's results showed a similar behavior with the SSPCM samples prepared with HMDI. Due to its linear structure, HMDI has the ability to assume multiple conformations and create less restriction upon PEG chain mobility.[34] Thus, less of a steric effect is observed for HMDI samples, and a higher SS crystallinity value is observed. However, HMDI 6000 shows a decline in %SS crystallinity and this is because PEG is too long and forms entanglements. According to previous literature, a decline in %SS crystallinity is observed for PEG molecular weights greater than 4000 g/mol.[25,93] This is known as molecular weight threshold. Pielichowski[138] evaluated PEG as a latent heat thermal energy storage using differential scanning calorimetry (DSC) techniques. The results showed an increase in heat of melting with an increase in molecular weight, except for PEG 20,000. When the PEG chain becomes too long and entanglements occur, it disrupts crystallization. Consequently, a lower enthalpy value is observed.[27,138-140]

In addition to PCM molecular weight and HS cross-link nature it is evident that diisocyanate composition also plays a major role in limiting PCM crystallization. Based on the data listed in Table 4.6, HMDI 3000 showed higher ΔH_m values than PDI 3000, and MDI 3000.

MDI, the largest of the three diisocyanates studied, exhibited the smallest ΔH_m values. The DSC curves for X-MDI 2000 and Y-MDI 2000 are presented in Figure 4.41. Interestingly, no endothermic/exothermic peaks were observed for these samples. This implies that no crystallization occurred of the PEG PCM polymer occurred. However, the DSC curves for X-MDI 3000 and Y-MDI 3000 clearly show two endothermic and exothermic peaks (shown in Figure 4.42). This suggests that PEG 2000 g/mol is below the critical molecular weight and when below this chain length, DSC can no longer detect crystallinity because most of the PEG chain is disturbed by cross-link steric hindrance.[27,87] This would imply that a critical minimum chain length is necessary for PCM crystallization to occur. However, endothermic and exothermic DSC curves were observed for X-HMDI 2000, Y-HMDI 2000, X-PDI 2000, and Y-PDI 2000. Because these PU-SSPCM samples exhibit crystallization activity with PEG 2000 g/mol, only just not with MDI, provides evidence that 1) the critical molecular weight is dependent on diisocyanate and 2) the composition of diisocyanate plays a strong role in soft segment crystallinity due to varying steric hindrance. [27,87]

Based on these findings it is evident the composition of the diisocyanate strongly impacts PEG crystallization. In the bar graph (Figure 4.47) and DSC curves, a relationship between the size of the HS diisocyanate and enthalpy %PEG crystallinity may be realized. For both thermoset and thermoplastic sets of samples, the enthalpy values observed for MDI, the largest of the three diisocyanates studied, were significantly less than PU-SSPCM samples prepared with PDI, and even more so, when compared to HMDI samples. With HMDI being the smallest diisocyanate studied, it seems likely to

assume that the smaller the size of the diisocyanate, the higher the enthalpy values observed.

4.4.CONCLUSION

Through FTIR, the identification of hydrogen bonding between N-H and C=O groups gave sufficient information to distinguish a non-homogeneous network from a homogeneous one [102,141-143]

DSC results showed that in most cases X_c% was higher for XPCM than YPCM samples. This suggested that the HS chain end effect is stronger for HS physical cross-links than HS chemical cross-links. It may be speculated, that the reason why XPCM demonstrated higher X_c% is connected to its homogeneous morphology. For heterogeneous morphologies, when HS phases are dispersed in the soft phase matrix, the hard segment acts as an impurity and disrupts the crystallization of soft segment chains.[37,42,97] Whereas, in a homogeneous phase morphology the HS cross-link is immobile and evenly dispersed throughout the PCM matrix.[86] Therefore, in a homogeneous phase morphology SS crystallization is never limited or disrupted by any additional factor, but for a heterogeneous morphology a higher degree of phase separation would lead to less dispersed HS phases in the soft phase to disrupt SS crystallization. Therefore, SS crystallization can vary in heterogeneous morphologies, but will always be the same in thermoset homogeneous morphologies. Based on this theory that different levels of phase domain organization will exhibit different limitations on PCM crystallization, outside of the limiting effects of HS chain restrictions could explain why significant differences in

X_c% was observed for Y-HMDI, Y-MDI, and Y-PDI. The HS diisocyanate and its molecular structure dictates the rate of phase separation and the ability for the HS to form hydrogen bonds. Thus, although all YPCM samples were cooled at the same rate from a homogenous melt, the level of phase separation present in the YPCM samples was different for the samples prepared with PDI, MDI and HMDI. Buckley [100] conducted X-ray scattering (SAXS) and wide-angle X-ray scattering (WAXS) experiments demonstrating that different chemical compositions of thermoplastic PUs caused not only a variation in the degree of phase separation, but also SS crystallinity. However, this is only speculation the scope of this work only considered thermoplastic physically cross-linked PU-SSPCMs with 40% HS weight content, cooled at 20˚C /min, therefore the findings of this study are not sufficient evidence to make this claim. Furthermore, owning to the fact that the relationship between the level of phase mixing and PCM crystallization has yet to be defined, this reasoning is merely an inference. However, it is planned to investigate this relationship in future work.

Overall this work demonstrated that the nature of the cross-link is an important factor, which should be taken into consideration in the further development of novel PU-SSPCM materials. Nonetheless, not only through this work did we determine the relationship between cross-link nature and heat storage capacity, we also found that the molecular structure of the diisocyanate and degree of phase separation are other possible factors governing heat storage capacity.

Overall, the results corroborate with previous literature;[27,30,34] Although the scope of this chapter does not consider degree of phase separation, the following chapters will further

investigate the potential relationship between degree of phase separation and heat storage properties by varying HS content and cooling regime. In future work, instead of using allophanate branches to introduce a 3-D chemically cross-linked network using a tri-functional or polyfunctional chain extender would be interesting.

Chapter 5 : HEAT STORAGE CAPACITY AND DIISOCYANATE STRUCTURAL FEATURES

5.1. INTRODUCTION

The factors that influence the structure of a polyurethane include segment compatibility, segment length, overall composition, molecular weight, intra-segment or inter-segment interactions, such as hydrogen bonding, and the crystallization of both the hard and soft segments. It has been shown that the mobility of the central portion of the soft segment (SS) chains in model networks is higher than that of the outer SS chain segments[37,51]. The difference in chain mobility is a result of Hard Segment (HS) cross-links steric constrictions that restrict the movement of nearby SS chain units, so that this portion of the SS chain can no longer crystallize. This phenomenon is known as the HS chain end effect. A similar effect has been observed in other model cross-linked polymer networks, and this effect is known as the Steric effect, the Disruptive effect, and/or the Drag effect [51,55,87,90,144,145] The impact of the chain-end effect can be realized by the size of the non-crystalline amorphous region or the magnitude to which the size of the crystalline region is reduced from its pure state. For PU-SSPCM materials, there has been some evidence indicating that the ratio of the non-crystalline PEG PCM chain region is related directly to the composition of its HS component, which can be varied by the different structural moieties of diisocyanate[34]. The component of polyurethanes may be aliphatic, aromatic, ether, ester, urethane, and urea groups, offering a wide range of polarities and hydrogen-bonding possibilities, which should promote miscibility or at least strong interfacial bonding[121].

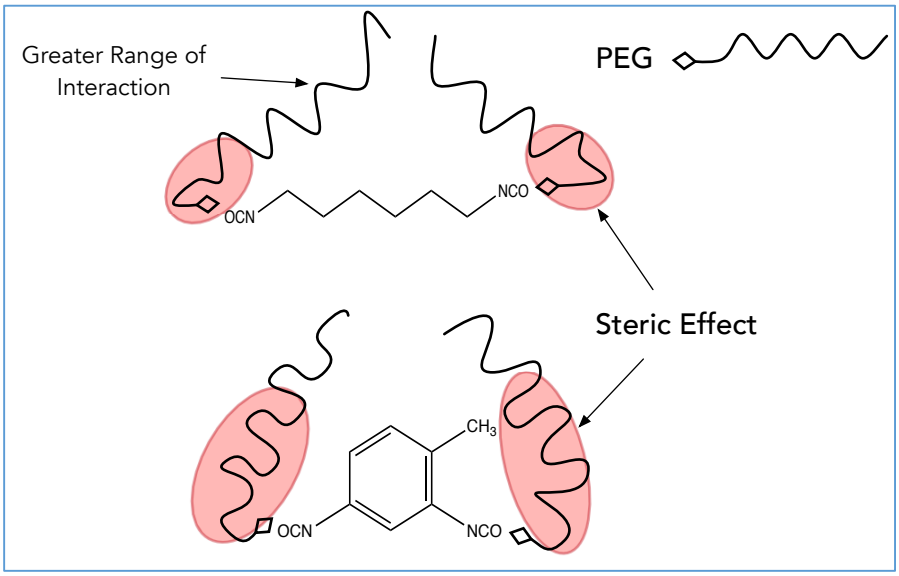

Figure 5.1: Range of interaction between PEG chains as a result of the size of the diisocyanate

Alkan[34] investigated a family of PU-SSPCMs that were derived from different diisocyanate monomers and found a connection between the diisocyanates' compositions and their thermal energy storage properties. In his study, he characterized the thermal energy storage properties of three sets of PU-SSPCMs varied by three types of diisocyanate components, and PEG molecular weights of M_n = 1000, 6000, and 10,000 g/mol. Alkan found that the PU-SSPCMs he prepared with an aliphatic diisocyanate showed higher enthalpy values than the other two PU-SSPCMs that were prepared with aromatic PU-SSPCMs. He also found that, of the two aromatic PCMs he made, the one with the smaller aromatic diisocyanate exhibited slightly higher enthalpy values. Alkan attributed this behavior to the steric effects created by the HS and claimed that there was a correlation between the structure of the diisocyanate component and the number of nearby PEG chain units prevented from participating in crystallization. This relationship

can be seen in Figure 5.1 for diisocyanates with larger structural features. It takes more PEG chain units to move around the HS, thus the range of the interactions between the PEG PCM polymer chains is much less. However, the range of the interactions is much greater than that of a PEG chain attached to a smaller diisocyanate. This behavior is illustrated in Figure 5.1. Furthermore, Alkan observed a difference in enthalpy values between the PCM prepared with diisocyanates with variable geometries, which is associated with HS. Alkan thought that the flexibility and rigidity of the diisocyanates also contributed to the range of interaction between the PCM chains. Aliphatic diisocyanates can assume multiple conformational arrangements, so they are very flexible and can move with the PCM chains, allowing greater interaction. However, aromatic diisocyanates are more rigid because they do not have the ability to assume multiple arrangements. It seems that this rigidity reduces the range of interaction between the PEG chains even more. Thus, smaller crystalline regions were observed for the aromatic PCMs, which explains TDI and IPDI; it seems that, on top of its bulkier structure, the rigidity of the diisocyanate component reduced the range of interactions between the PEG chains even more, which is why smaller crystalline regions were observed for these PU-SSPCMs. Alkan[34] demonstrated that the degree of enthalpy reduction correlated with the size and flexibility of the diisocyanate. Alkan proposed that a larger, more rigid diisocyanate would reduce the range of the interactions between the PEG chains. Thus, for bulkier diisocyanate HS, greater numbers of PEG chain segments are required to go around the diisocyanate. As a result, a smaller portion of the PCM polymer is able to crystallize. Therefore, a reduction in enthalpy is implied due to the smaller crystalline

region, and, subsequently, the overall heat storage capacity is reduced. Alkan's findings indicated that the higher thermal energy storage properties for PU-SSPCMs with a diisocyanate that is small, flexible, and symmetrical affect a lesser portion of attached polymer than rigid, non-symmetrical, bulky polymers.

For conventional PU materials, how the diisocyanate component impacts the extent of the microphase separation, the morphological details of the domains, and their relationships with the final mechanical properties have been studied extensively [128], but, to date, there has not been a study that evaluated how modifying the diisocyanate component affects the thermal properties. However, several studies have measured the response in soft segment crystallinity changes due to varying the diisocyanate.

Steric hindrance restricts rotation around the main chain, and the molecule stiffens. In the absence of crystallinity, intermolecular attractions, or cross-linking, the molecules of the polymer are free to exhibit all of their inherent flexibility, and this unrestricted freedom has major effects on the polymer's properties.

Molecular flexibility depends on the freedom of rotation about the single bonds in the main chain of the polymer molecule; restriction of rotation reduces molecular flexibility. A linear aliphatic chain is fairly free to rotate about its C–C bonds, but it is restricted by the 109° angle between the C–O–C bonds and by the electropositive repulsion between adjacent H atoms, and some energy is required to rotate them past each other. When a $–CH_2–$ is replaced by an oxygen ($–CH_2–O–CH_2–$), rotation around the C=O bond does not bring H atoms into conflict with

each other, so rotation is easier, and the molecule is more flexible; this occurs in polyethers, polyesters, and even polyurethane linkages. When aromatic groups are present, particularly in the main chain, they introduce large, rigid units that greatly reduce molecular flexibility. When the aromatic rings are conjugated with adjacent unsaturated groups in the main chain, the entire conjugated resonating unit becomes much larger, and the stiffening effect is much greater.

Hydrogen bond interaction depends on the structural regularity of the diisocyanate HS component. Hydrogen bonding interactions can be altered by the following structural features: size, symmetry, and variable geometry. These structural features also dictate the rate of phase separation, which directly impacts HS crystallization.[4,5]

Priscariu[1] monitored the rate and degree of phase separation for aliphatic HDI coupled with BDO compared to double aromatic MDI and BDO, and he observed a greater degree of phase separation for the polyurethane with HDI. He attributed HDI's multiple conformational arrangements to introducing greater flexibility to the HS, allowing it to diffuse faster into separate phase domains, thereby obtaining a greater phase separation[4,5]

In a separate study, Prisacariu[1] demonstrated that a diisocyanates' variable geometry can influence the degree of phase separation, and he compared a polyurethane with an MDI-BDO HS to a DBDI HS. DBDI that has a molecular structure that is similar to that of MDI, except that the ethylene bridge between the phenol rings introduces variable geometry into the hard segment. The added internal rotation of this DI around the —CH_2—CH_2—ethylene bridge leads to the appearance of both "anti" and "syn" rotational

conformations. This allows the DBDI HS to adopt a linear conformation, facilitating packing and inter-chain hydrogen bonding.

Figure 5.2 compares the Hard Segments of DBDI differs from PUs with MDI as the rigid MDI HS is intrinsically kinked in shape, reducing its conformational mobility, thereby hindering close packing and hydrogen bond interaction to which only half of the potential hydrogen bonds occurred Because DBDI was able to assume multiple spatial arrangements, it had greater HS mobility, which increased the rate of phase separation, so a greater degree of phase separation was observed for the DBDI polyurethane.

These findings indicate how structural regularity and variable geometry determine the

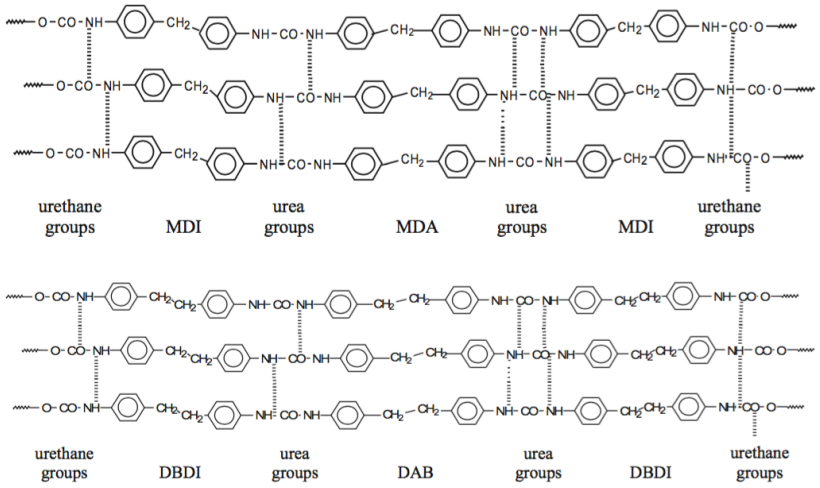

Figure 5.2: A) Hard Segment of a MDI based PUU extended with aromatic DAB B) Hard Segment of a DBDI based PUU extended with aromatic DAB. Adapted from Prisacariu, C. Structural Studies on Polyurethane Elastomers. 2011, 23–60. 8

details of the structure of the phase domain. Seefried[6,7] and others conducted a study that demonstrated how the symmetry of the diisocyanate also strongly influences the extent of phase separation and the structure of the domain. Seefried compared the phase separations of an asymmetric 2,4 TDI and symmetric MDI polyurethane and found that the MDI polyurethane exhibited better phase separation and elastomeric properties because MDI has greater symmetry and bulkiness.[8] Schneider[7] compared asymmetric 2,4 TDI to a symmetric 2,6 TDI polyurethane and found differences in their thermal stability and the extent of phase separations. Sung [146]reported that asymmetrical 2,4 TDI hard segments had an amorphous domain structure, with a glass transition temperature of100 ^{o}C, whereas 2,6 TDI hard segments demonstrated a semi-crystalline structure with a melting temperature of 130 ^{o}C. Sung attributed this difference to 2,4 TDI's head-to-toe isomerism, which led to weak inter-urethane hydrogen bonding.[7] From Prisacariu's, Seefried's[147], and Sung's[146] studies it is apparent that hydrogen bonding ability is the driving force of phase separation. Thus, it may be concluded that diisocyanates that are

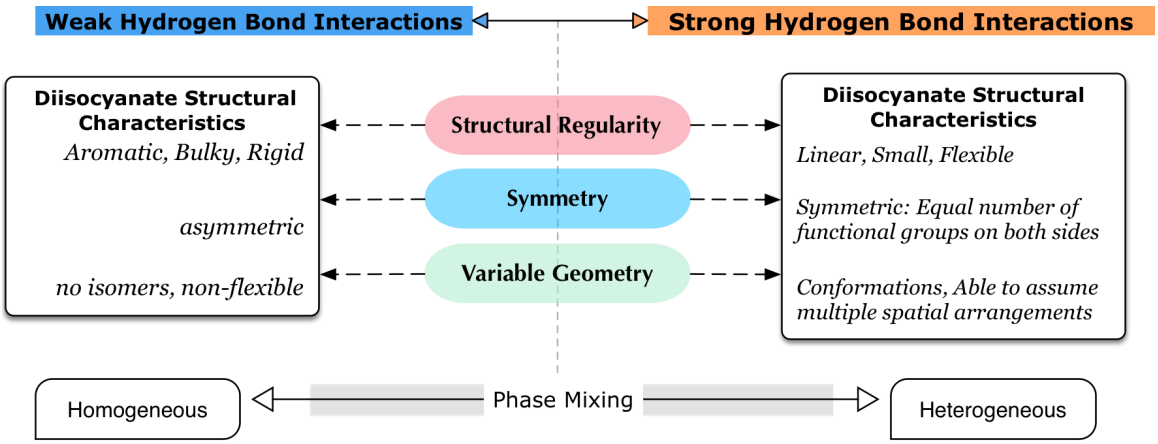

Figure 5.3: Diagram of Diisocyanate Structural Features studied as variables

structurally regular, have a variable geometry, are symmetrical, and form stronger hydrogen bonds will demonstrate a higher degree of separation.[4] The HS structural characteristics that will lead to improved heat storage capacity are unknown. The chain-end effect and the proportions of the non-crystalline PCM chain segments and the crystalline chain segments can be estimated from the enthalpy values demonstrated by the pure PEG PCM component and the pure state PEG enthalpy values. The magnitude to which the sample enthalpy (ΔH_{PCM}) is reduced from its pure state (ΔH_{PEG}) reflects the portion of the PEG PCM chain that is immobilized by the steric hindrance caused by the molecular structure of HS. Therefore, the HS chain end effect can be quantified by the following equation:

Equation 1: Magnitude of the Chain-End effect $|\Delta H| = |\Delta H_{PEG,m} - \Delta H_{PCM,m}|$

Equation 1 shows the difference between the melt enthalpy of the sample, $\Delta H_{PCM,m}$, and the melt enthalpy of pure PEG ($\Delta H_{PEG,m}$). $|\Delta H|$ indicates the number of PEG PCM chain units affected by HS steric constrictions; the sample's enthalpy of melt ($\Delta H_{PCM,\,m}$)

indicates how much heat energy is being absorbed and released, and $\Delta H_{PEG,m}$ indicates the enthalpy of melt of a PEG PCM polymer in its pure state.

In this chapter, the chain-end effect was quantified for a series of linear PU-SSPCM samples prepared with different HS molecular structures. Through the correlation of the chain-end effect with the molecular structure of HS, valuable information was obtained about certain structural characteristics of HS that lead to a configuration in which the least HS steric hindrance is observed. It is expected that less HS steric constrictions would entail the smallest portion of the non-crystalline PEG PCM chain units, which would then provide a higher portion of crystalline PEG PCM chain units, through which maximum TES properties are observed.

Modifications made to the composition of the diisocyanate will alter the hydrogen bonding ability of the urethane HS. Subsequently, changes in D of PS and thermal transitions will occur. The effects of these changes on PCM crystallization are unknown. The diisocyanate components were selected to represent the following diisocyanate structural moieties, i.e., size, structural regularity, rigidity/flexibility, and symmetry. These four structural variables dictate a urethane HS's ability to form hydrogen bonds. The strength of hydrogen bonds is what ultimately determines the degree of phase separation, which determines the final properties. The aim of the present work was to advance this understanding by means of a systematic study of the effects of varying diisocyanate structural moieties of a family of model PU-SSPCMs on PCM domain crystallization and on the resulting properties of thermal energy storage.

The goal of this study was to characterize the chain-end effects observed for diisocyanate structural moieties that alter its structural regularity, symmetry, and variable geometry. The flexibility of the hard segment is controlled by the diisocyanate's conformational arrangements. Thus, latent heat values were measured according to the diisocyanate's degrees of freedom. Latent heat values and phase transition temperature were determined using Differential Scanning Calorimetry (DSC) experiments methods.

Based on the evidence obtained from the literature that addresses conventional polyurethanes and from previous PU-SSPCM findings, it was hypothesized that the HS hydrogen bonding ability will be altered by modifying the diisocyanate component's structural variables, i.e., structural regularity, symmetry, and variable geometry. This, in turn, will produce a series of PU-SSPCM materials with varying degrees of phase separations. It is our hypothesis that the degree of phase separation is the main factor that determines the crystallization behavior of the PCM polymer. From the findings of this work, we ultimately can identify the optimal configuration for a thermoplastic polyurethane-based PCM system that demonstrates thermal energy storage properties by undergoing a solid-to-solid phase transition.

To carry out this investigation systematically, the degree of phase separation and weight percent HS were kept constant in all of the samples, because these factors also have been found to influence PCM crystallinity. By doing so, any changes in thermal energy storage properties can be attributed directly to the diisocyanate component. Polymers were prepared via solution polymerization following the method presented by Lyman[98]. FTIR and NMR analysis techniques were used to confirm that a polyurethane polymer was

formed and that no side reactions interfered with the polymerization. DSC methods were used to identify the thermal energy storage properties of the samples according to their hard segment composition and network structure. TGA was used to evaluate the thermal stability of the samples.

5.2.EXPERIMENTAL

5.2.1. SAMPLE PREPARATION

Chemical Reagents

Six PU-SSPCM polymers with HS components that were varied by diisocyanate monomer were prepared with PCM polymer, PEG M_n = 2000 g/mol, and chain extender 1,4-butane diol (BDO) was prepared. Further details on the reagents used for the synthesis are described in Chapter 3 (pg. 105). In this study, six different diisocyanate monomers were chosen in pairs based on their molecular geometry, i.e., 1,6-diisocyanatohexane (HMDI); 1,12-diisocyanatododecane (DIDD); 1,4-phenylene diisocyanate (PDI); 2,4 tolylene diisocyanate (TDI); 1,3-bis (isocyanatomethyl) cyclohexane (BICH); and 4,4-methylenebis (phenyl isocyanate) (MDI). PU-SSPCM materials were prepared that were composed of two analogous diisocyanate monomers with structural moieties that were opposed in structural regularity, variable geometry, and

Table 5.1: Molar Compositions of Reagents used

	Moles of DI	Moles of PEG	Moles of CE
Y-HMDI	6	1	5
Y-DIDD	8	1	7
Y-TDI	16	1	15
Y-PDI	6	1	5
Y-BICH	8	1	7
Y-MDI	16	1	15

DI - Diisocyanate, CE - Chain Extender

symmetry. These structural variables are known to alter the strength of hydrogen bonding interactions, which causes variable degrees of phase separation between HS and SS. In addition, it was expected that the chain-end effect would vary for different diisocyanates; thus, the magnitude of the reduction in thermal energy storage properties observed for the different PU-SSPCM materials would vary. A list of the diisocyanates and their associated structural moieties are presented in Table 5.3.

Polymerization/ Synthesis

All of the PU-SSPCM samples were fabricated as linear thermoplastic polyurethane polymers composed of 40% hard segment content (%HSC) and 60% PEG PCM (%PCM) content. The procedures followed for the synthesis of all samples considered in this chapter are identical to the two-step synthesis method described in Chapter 3. Polymerization was carried out in round-bottom, 500-mL ChemGlass reaction vessels shown in Figure 3.2: Setup of Reaction vessel used in synthesis of samples; To avoid side reactions, a 50:50 MBK-DMA solution adopted from Lyman's[112] work was used as the reaction medium solution. Prior to the synthesis reaction, the reagents were purged with nitrogen to eliminate excess moisture that could potentially lead to side reactions and reduce yields and molecular weights. These proceedings are described in greater detail in the experimental section in Chapter 3 (page 3105).

Mass of the reagents were added in a 1:1 stoichiometric ratio to obtain a linear polymer with the highest molecular weight. Table 5.1 lists the quantities of reagents that were used.

Sample Nomenclature

A code system for naming each sample was used to keep track of the combinations of monomer constituents that were used. The code system is ordered in the following fashion: [X or Y + Diisocyanate abbreviation + PEG molecular weight- percent hard segment content (%HSC)]. An example of a name based on this code system is YDIDD2000-34 or XPDI 2000. First, the codes refer to the linearity of the sample; X represents thermoset PU-SSPCMs, and Y- designates thermoplastic PU-SSPCMs. All of the samples considered in this chapter were prepared as linear thermoplastic polyurethanes, therefore all of the samples' names begin with 'Y.' The Y is followed by "-" followed by the diisocyanate abbreviation. name, and the number 2000 indicates the molecular weight of the PEG polymer. Table 5.2 provides a list of the samples that were prepared and their associated nomenclature that is used throughout this chapter.

5.2.2. FTIR ANALYSIS

Table 5.2: List of Samples studied

%HS	Diisocyanate	Poly(ethylene glycol) (PEG) Molecular Weight	[Nomenclature]
40%	1,6-Diisocyanatohexane	M_n= 2000 g/mol	Y-HMDI
40%	1,12-Diisocyanatododecane	M_n= 2000 g/mol	Y-DIDD
40%	2,4-Tolylene Diisocyanate	M_n= 2000 g/mol	Y-TDI
40%	1,4-Phenylene Diisocyanate	M_n= 2000 g/mol	Y-PDI
40%	1,3-Bis(isocyanatomethyl)cyclohexane	M_n= 2000 g/mol	Y-BICH
40%	4,4'-Methylenebis(phenyl isocyanate)	M_n= 2000 g/mol	Y-MDI

FTIR analysis with contact ATR techniques was used to confirm that a polyurethane polymer was formed and that no side reactions interfered with the polymerization. A more detailed description of instrumentation, sample preparation and method parameters can be found in the experimental section (See Chapter 3).

5.2.3. THERMAL GRAVIMETRIC ANALYSIS (TGA)

TGA was used to evaluate the thermal stability of the samples. Full descriptions of the test methods and parameters are given in Chapter 3 (page 121).

5.2.4. DSC ANALYSIS OF THERMAL ENERGY STORAGE PROPERTIES AND PHASE MIXING

DSC methods were used to identify the thermal energy storage properties of the samples according its diisocyanate compositions. Further details on sample preparation and instrumentation are given in Chapter 3 (page 112).

The hard and soft PCM domains displayed separate thermal transitions at significantly different temperatures. The crystallization of the HS was observed at much higher temperatures than the PEG PCM chains. The details of the PEG PCM phase domain were affected by HS domain ordering. The scope of this research only pertains to measuring the changes in the TES properties that result from modifying the diisocyanates' structural variables. Any overlapping effects on TES properties resulting from other variables, such as HS ordering, must be eliminated to systematically study the structure-property relationship. A two-part DSC experiment was performed to control the HS ordering in all

of the considered PU-SSPCMs. After the initial heating step, all samples were cooled at the rate of 20 ^{o}C/min to establish the same level of HS ordering in all samples. Afterwards, the samples were cooled and heated at 2 ^{o}C/min from 70 to 0 ˚C and back to 70 ˚C to measure the PU-SSPCMs' heat storage capacities and phase transition temperatures. For evaluating thermal energy storage properties, only the data collected during the second part were relevant, as they represent the phase change performance of the PEG PCM polymer. The data collected during the initial heat step were important for determining the degree of phase separation.

5.3.RESULTS

Synthesis of Samples

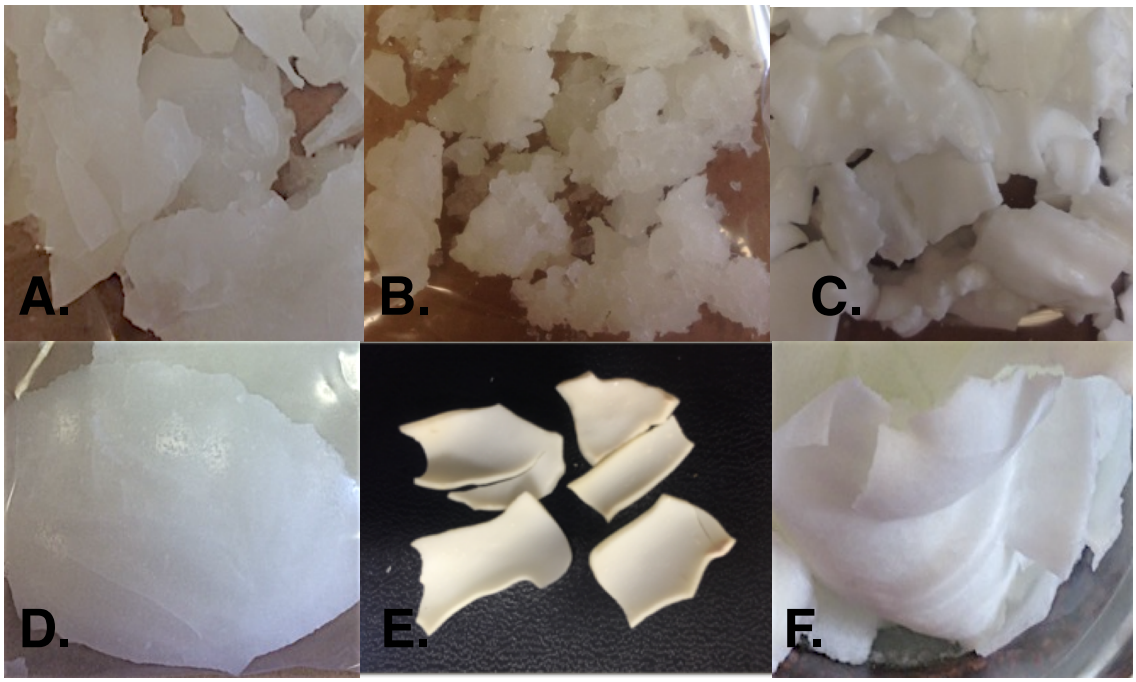

Figure 5.4: Product polymer from synthesis; A) HMDI 2000 B) MDI 2000 C) DIDD 2000 E) TDI 2000 F) BICH 2000

The hard-segment content is about 40 wt % for all polyurethanes. 'A FTIR study has shown that the polymers are polyurethanes and are linear, having neither allophanate groups, nor any indication side reactions interfered with the reaction. This should be noted, since some chemical crosslinks tend to increase the melt viscosity and can influence dramatically the morphology and mechanical properties of block copolymers.

5.3.2. RESULTS FROM FTIR ANALYSIS

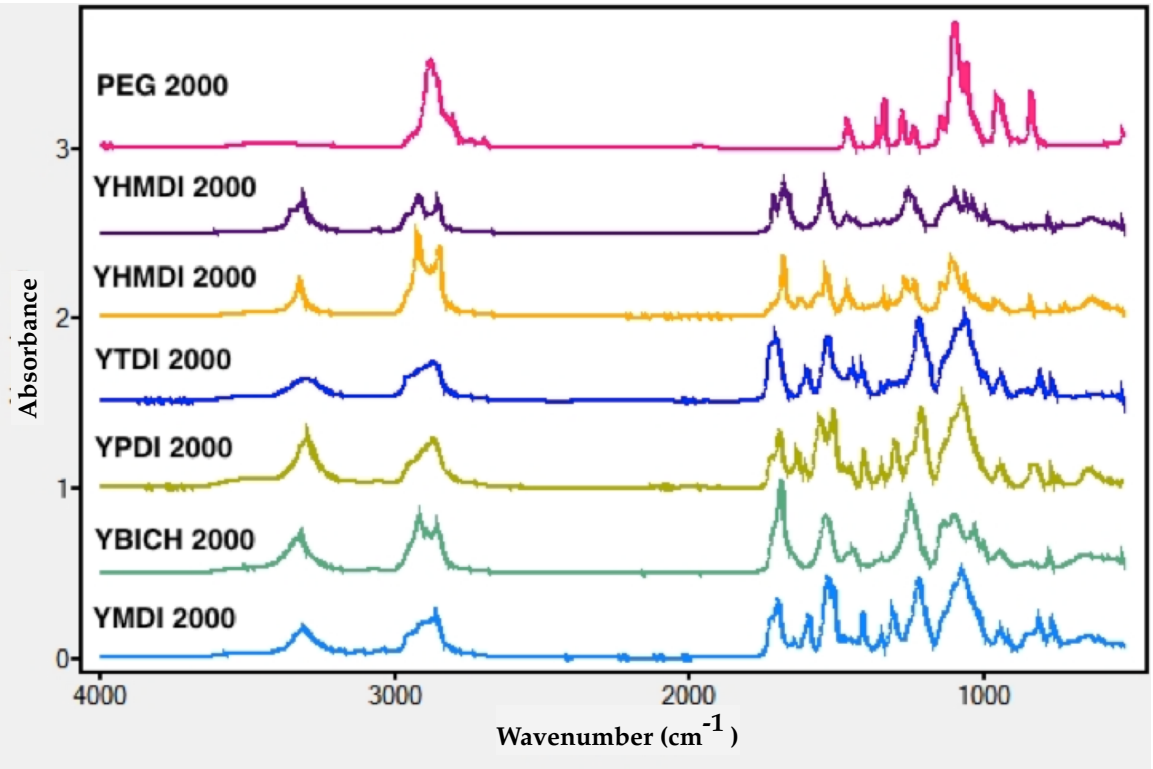

Figure 5.5: FTIR Spectrum of PU-SSPCMs prepared with PEG M_n= 2000 g/mol

FTIR analysis techniques were used to confirm that a polyurethane polymer was formed during the synthesis and that no side reactions interfered with the polymerization. The IR spectra generated from all samples are shown in Figure 5.5. The signature peak frequency of the isocyanate groups is 2265 cm^{-1}. A peak at this frequency was not found in any of the sample spectra. This confirmed that no residual isocyanate groups remained in the product, and it also implies that all of the reagents reacted completely.

Table 5.3: Summary of the N-H and C=O main peaks observed in the IR spectrums shown in Figures 5.5

Sample	N-H (cm^{-1})	C=0 (cm^{-1})
Y-PDI 2000	3324	1695
Y-TDI 2000	3302	1706
Y-DIDD 2000	3328	1682
Y-BICH 2000	3330	1689
Y-MDI 2000	3315	1701
Y-HMDI 2000	3316	1682

Figure 5.5 compares the PCM sample IR spectra with the IR spectrum of pure PEG M_n =2000 g/mol. It can be seen that the PU-SSPCMs displayed a relatively similar spectral patterns. From this comparison, two distinct peaks in the NH and C=O stretch regions were noticed in the sample spectra that were absent in the spectrum of the pure PEG IR. Peaks that appear in the NH and C=O stretching regions, i.e., 3330-3500 and 1680-1740 cm^{-1}, respectively, are of particular interest for polyurethane materials. Therefore, the appearance of distinct absorption bands in the NH and C=O regions provided evidence that a polyurethane polymer was formed as a result of a reaction between isocyanate and hydroxyl groups. Thus, it was concluded that the synthesis was carried out successfully. The main peak frequencies of the PU-SSPCM samples displayed NH and C=O stretching vibrations as listed in Table 5.3.

5.3.3. TGA RESULTS

The TGA curves presented in Figure 5.19 describes the thermal degradation properties of the PU-SSPCM materials listed in Table 5.2. In Figure 5.6, it can be seen that all samples showed no major mass loss (<10%) up to temperatures over 250˚C. This confirmed that all samples had high enough thermal stability to endure DSC experiments and that all solvents from synthesis procedures had evaporated from the polymer. The overlay of TGA curves indicates the samples displayed relatively similar thermal degradation behavior. For the most part, TGA curves displayed characteristics indicating a two-step thermal decomposition had occurred. Generally, SPU materials demonstrate thermal degradation in two steps, where the first step is the degradation of the SS component and the second step is the degradation of the HS component. component[52] Table 5.6 summarizes the thermal degradation properties of the TGA Curves shown in Figure 5.6. For the PU-SSPCMs that displayed a two-step degradation process, the listed onset degradation temperature (T_o) represents the start of degradation of the PEG PCM component and T_{II} is the onset degradation of the HS component. The % mass loss is the percentage of weight lost between T_o and $T_{II.}$ The % Total Loss is the total mass lost from 0 and 400˚C.

According to Table 5.4, of all the PU-SSPCMs considered, the first sample to degrade was YBICH (T_o= 280.54˚C). It can be seen in Figure 5.6, YBICH displayed a two-step degradation process, indicating the HS and SS component degraded at two separate temperatures. Thus, the onset of degradation of the PCM component began at 280.54˚C and ended at 306.53˚C with a mass loss of 32.68%. The onset of the HS component degradation began at 306.53˚C and did not fully degrade before a temperature of 400˚C

was reached. The total %mass loss at 400˚C was 80.32%. On the other hand, YPDI had the highest onset degradation temperature (T_o= 299.64˚C). However, unlike the other samples YPDI did not display a two-step degradation process. At 400˚C, YPDI showed a total %mass loss of only 49.07%.

For the most part all samples displayed an initial mass loss between 32.5% and 42.6%, indicating the % of PEG PCM was in the material. However, for YMDI2000, the onset of degradation was 284.17˚C and ended at 319.5˚C, but only showed a %mass loss of 18.64%. Since this %value was so low, it is suspected that because MDI and PDI are both derived from aromatic diisocyanates they have more rigid structure and possess a higher thermal stability compared to the other samples. Therefore, there may be some overlapping between the decomposition of the PCM and HS component which has may have caused the degradation step of the PCM component to be less. According to literature, thermal stability tends to correlate with molecular rigidity because chemical reaction and degradation depend on molecules moving and meeting each other, and this becomes more difficult when the molecules have less flexibility[121]

Table 5.4: Thermal Degradation Properties from TGA Scans

PU-SSPCM Sample	T_o[a] (˚C)	T_I[a] (˚C)	T_{II}[a] (˚C)	% Mass loss[a]	% Total Mass loss[b]
Y-DIDD 2000	262.46	306.2	315.05	42.58	62.04
Y-HMDI 2000	272.17	290.94	296.44	30.58	78.71
Y-TDI 2000	282.28	320.72	326.42	36.71	52.24
Y-PDI 2000	299.64	331.94	396.13		49.07
Y-BICH 2000	280.54	300.7	306.53	32.68	80.32
Y-MDI 2000	284.17	307.34	319.5	18.64	30.6

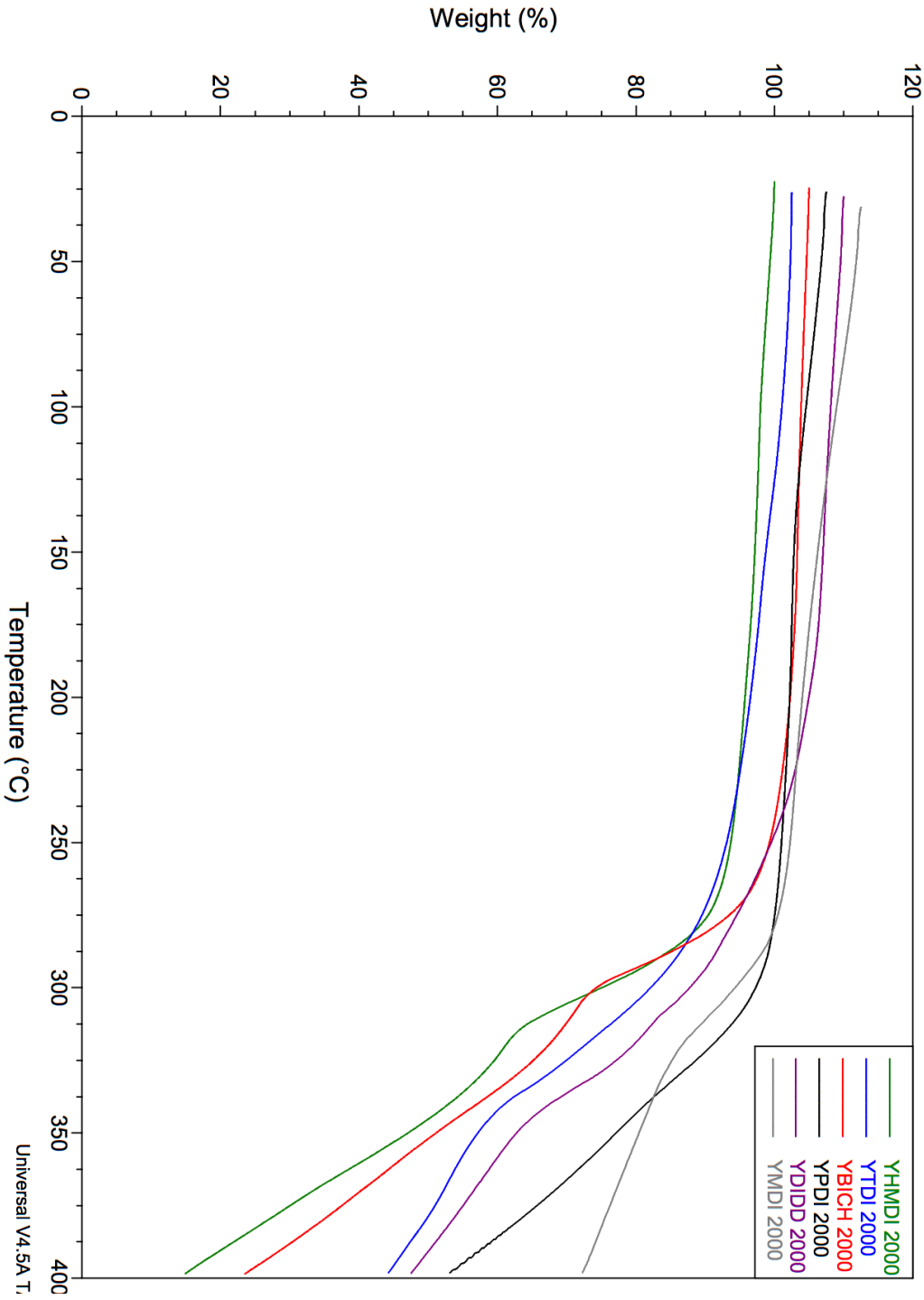

Figure 5.6: TGA scans of all samples

Table 5.5: Summary of PCM Domain Thermal Energy Storage Propertiess

	T_c(°C)	T_m(°C)	ΔH_c (J/g)	ΔH_m (J/g)	X_c
PEG M_n= 2000 g/mol	33.9	54.07	163.3	165.3	100%
Y-DIDD 2000	26.29	48.75	52.4	51.37	30%
Y-HMDI 2000	29.88	47.31	49.36	39.31	48%
Y-TDI 2000	11.32	40.99	27.41	34.5	21%
Y-PDI 2000	21.65	47.06	40.6	40.1	24%
Y-BICH 2000	12.37	49.75	22.48	41.36	25%
Y-MDI 2000	--	--	--	--	--

5.3.4. DIFFERENTIAL SCANNING CALORIMETRY ANALYSIS

DSC methods were used to identify the thermal energy storage properties of analogous materials derived from various diisocyanate monomers with a range of structural moieties suspected of strongly influencing PCM crystallization behavior. Prior to analyzing the phase change properties of the PEG PCM component and initial heat step was performed, during which the glass transition behavior and other information about the phase morphology and the level of phase mixing in the sample was obtained.

After heating to a homogeneous melt state, all samples were cooled at 20˚C/min from 250˚C to 70˚C. Following that the cooling rate was drastically lowered to 2˚C/min. The samples were cooled all the way to 0˚C, and then heated at 2˚C/min up to 70˚C. The phase change change characteristics (melt enthalpy (ΔH_m J/g) values and corresponding melting (T_m˚C) and crystallization (T_c˚C) temperatures, and the Percent Crystallinity X_c) are reported in Table 5.5. T_m and T_c correspond to the peak melting and crystallization temperature and is the maximum peak temperature at which melting and crystallization

occurs. Enthalpy heat of fusion (ΔH_m) was calculated by integrating exothermic and endothermic peak area using TA analysis software. X_c represents the percentage of crystalline PEG PCM polymer chain segments that exhibit latent heat storage properties. The X_c% was calculated based on ΔH_m values using the following equation: $X_c(\%) = (\Delta H_{m\text{-}PCM}/\Delta H^0_{m\text{-}PEG})*100$; where for 100% crystalline PEG, pure PEG ΔH_m was used as ΔH^0_m. ΔH^0_m values for pure PEG was obtained using the same heating and cooling rate as PEG PCM. It was important to compare enthalpy values of PCM PEG to pure PEG obtained from the same method. All enthalpy values were measured on the second heat step.

Comparison of Structural features.

As outlined in the introduction, the diisocyanate structural features structural regularity, variable geometry, and symmetry were selected to be studied in greater detail and determine their connection with PCM domain crystallinity. In order to investigate such a complex relationship, we examined the differences in DSC curves and percent crystallinity values of PU-SSPCMs with opposing diisocyanate structural features. It was predicted that size, symmetry, and rigidity are the main structural variables that would cause the greatest decline in soft segment crystallinity. To analyze this connection, samples were compared with their counterpart's structural features (for example big vs. small, symmetrical vs. non-symmetrical) and analyzed side by side, to isolate the root cause of the soft segment crystallinity decline.

Variable Factor: Structural Regularity varied by size

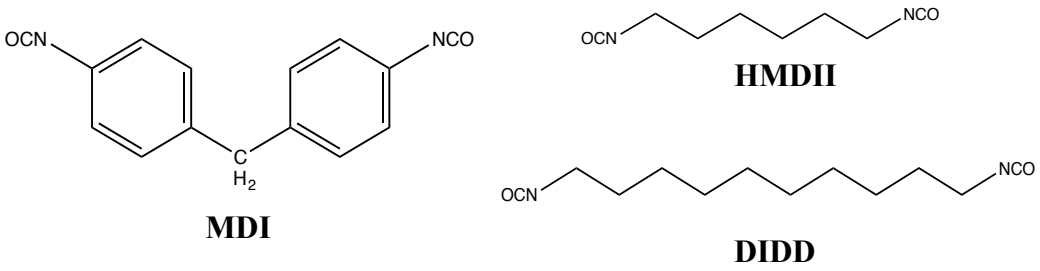

Figure 5.7: Comparison of Molecular structure size of MDI, DIDD, and HMDI

HS structural regularity is the ability to form hydrogen bonds and is varied by strength of hydrogen bond interaction. The strength of hydrogen bond interaction between HS urethane groups depends on the size of the diisocyanate component. (See figure) The strength of hydrogen bond interaction directly impacts HS ordering which influences phase separation properties of polyurethane materials. Therefore, diisocyanate structural regularity of a diisocyanate is strongly connected to determining PU final properties. To investigate the influence of diisocyanate structural regularity on TES properties analogous PU-SSPCMs derived from different size diisocyanate monomers were compared and and analyzed the thermal energy storage properties, accordingly. In this section PU-SSPCMs prepared with MDI is compared to HMDI. In addition to that the thermal energy storage properties of PU-SSPCM prepared with DIDD and HMDI is compared. The comparison of MDI to HMDI reveals the impact a bulky aromatic diisocyanate has on the PEG PCM phase transition compared to a small aliphatic diisocyanate. Whereas, the later compares two sized aliphatic diisocyanates; a smaller

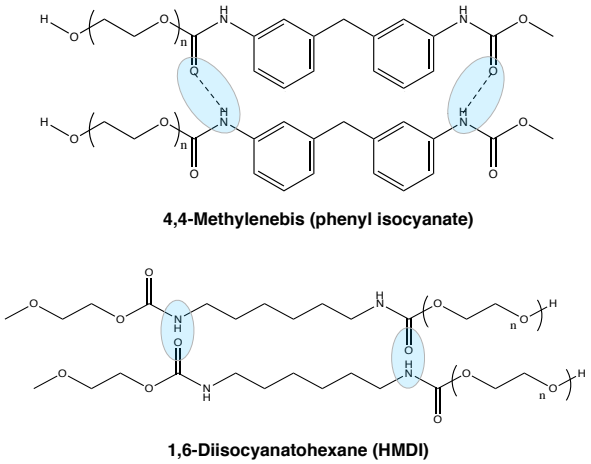

Figure 5.8: Hydrogen Bond interaction of aromatic MDI (top) and aliphatic HMDI (bottom)

diisocyanate HMDI and a larger diisocyanate DIDD. Figure 5.7 illustrates the difference in size between the diisocyanates highlighted in this section.

The DSC curves shown in Figure 5.9, describes the melting and crystallization behavior of MDI and HMDI 3000. It is apparent the two PU-SSPCMs exhibit dissimilar phase transition behavior. HMDI 3000 demonstrated melting and crystallization peaks that were uniform, symmetric and much higher in intensity compared to the melting and crystallization peaks observed for MDI 3000. This result provides evidence that MDI, an aromatic, bulky diisocyanate, exhibits greater steric effects and limited the crystallization of the PEG PCM component to a greater extent than HMDI, a smaller, aliphatic diisocyanate.

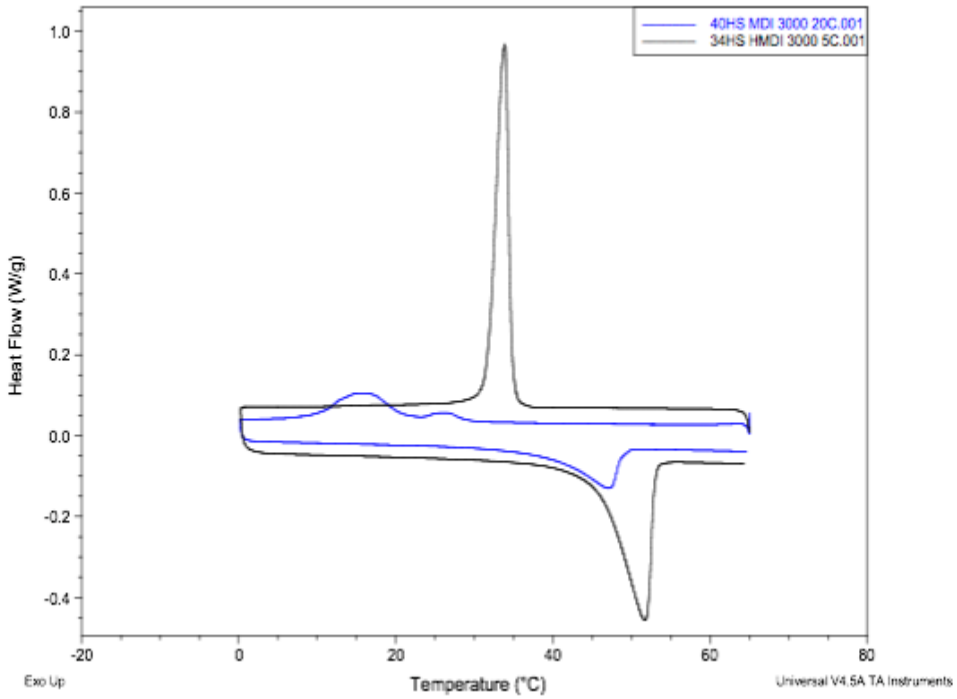

Figure 5.9: DSC Curve of MDI 3000 vs. HMDI 3000

It can be seen for MDI 2000 no soft segment crystallinity because MDI creates a greater confinement effect because it is rigid and bulky compared to HMDI. In addition, the DSC curves obtained from the PU-SSPCMs prepared with MDI and PEG Mn=2000g/mol as the PCM component did not display a endothermic or exothermic peaks. This indicated that the PEG PCM did not exhibit melting or crystallization activity.

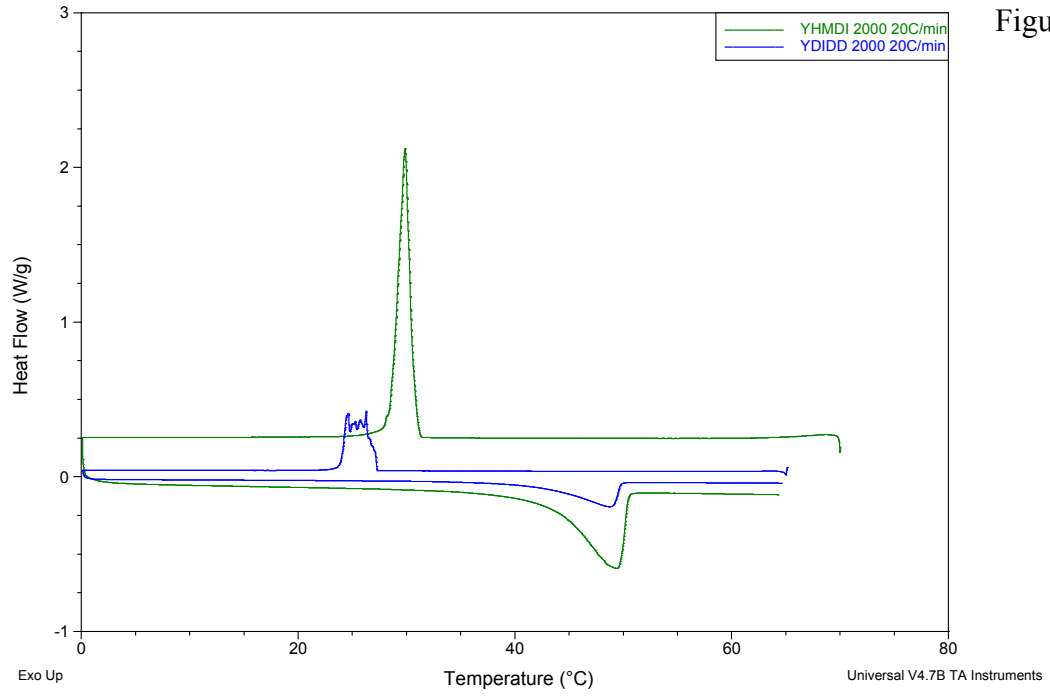

Figure 5.10: DSC Curves of HMDI 2000 and DIDD 2000

Figure 5.12 compares the melting and cooling behavior of aliphatic diisocyanate hard segments, DIDD and HMDI. DSC curves display a multiplet crystallization peak for HMDI and DIDD. DIDD crystallization and melting peak is much more prominent that HMDI. HMDI (T_c = 51.02 ˚C, ΔH_c=39.31 J/g) crystallization was observed at relatively the same temperature as DIDD (T_c = 26.29˚C, ΔH_c=52.40 J/g); however, DIDD was found to have percent crystallinity that was significantly higher than HMDI. The same trend was observed for the melting peak; HMDI (T_m = 47.31˚C, ΔH_m =39.31 J/g) and DIDD (T_m = 48.75˚C, ΔH_m =50.23J/g) showed equivalent melting temperatures (T_m), while DIDD showed a significantly greater percent crystallinity

From the comparison of the DSC Curves collected for aliphatic HMDI-DIDD to the DSC curves obtained for the other PU-SSPCM, it is apparent that only the PU-SSPCM systems

with aliphatic hard segments (HMDI and DIDD) show a multiplet peak. The appearance of a multiplet peak indicates that different sized PEG crystals were formed upon cooling at 1˚C/min. Interestingly, the melting peak was a singular uniform peak and did not show a distribution of peak sizes. The fact that only the samples with aliphatic hard segments displayed this behavior provides insight on the manner in which urethane hard segments with high structural regularity and flexibility. PCMs are only functional thermal regulating devices if they exhibit uniform crystallization and melting, and similar transition temperatures. This finding points to the conclusion that because aliphatic urethane segments exhibit incremental crystallization, the utility of diisocyanates with high structural regularity and high flexibility is not congenial to the functionality of PCMs as a thermal energy storage; even though DSC experiments determined the HMDI and DIDD enthalpy values meet the criteria of a functional thermal energy storage device. However, before ruling out the utility of aliphatic diisocyanates in PU-SSPCMs, the impact of cooling rate on degree of phase separation should be clarified through further investigation.

The difference in enthalpy and T_m between the PU-SSPCMs prepared with bulky and non-bulky diisocyanates indicate there is a connection between diisocyanates structural regularity and thermal energy storage properties. of HMDI (and DIDD) suggests there is a connection with. The fact that on both occasions the larger diisocyanate demonstrated lower $\%X_c$, points to the notion that larger diisocyanates create larger steric effects and limit PEG PCM crystallization to a greater extent than their counterpart. Therefore, it is evident that the chain end effect is more prominent for bulkier, larger diisocyanates.

Furthermore, based on these results it may be concluded that the structural regularity of the HS diisocyanate component can have a significant effect on PU-SSPCM thermal energy storage properties

<u>Structural Variable factor: Symmetry</u>

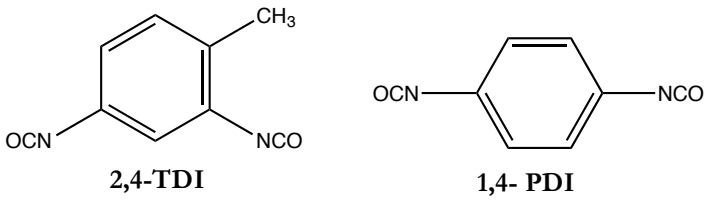

2,4-TDI **1,4- PDI**

Figure 5.11: Molecular structures of asymmetric 2,4-TDI and symmetric 1,4-PDI

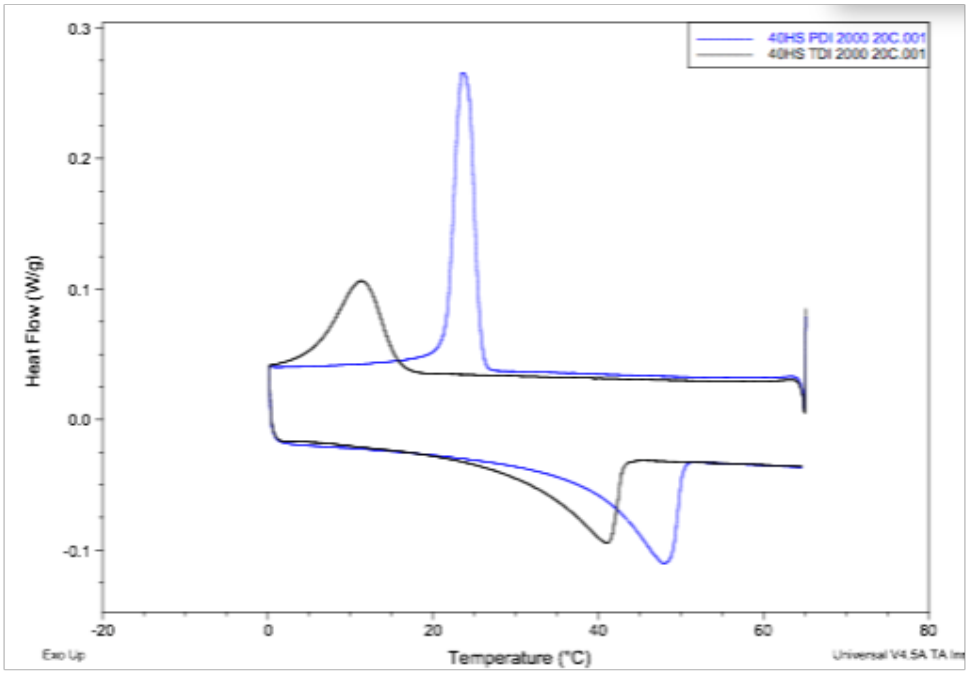

Figure 5.12: DSC Curve Comparison of YPDI and YTDI

Here the symmetry of a diisocyanate and its effect on PEG PCM crystallization and melting was studied. The effect diisocyanates symmetry has on phase morphology and PU mechanical properties has been studied extensively in literature. Unsymmetrical diisocyanates give rise to elastomers with little or no phase separation, whereas the use of symmetrical diisocyanates results in substantial phase separation.[148] This section will analyze the connection between the symmetry of the diisocyanate and PCM domain crystallization. The comparison of DSC curves for symmetric PDI and asymmetric TDI is displayed in Figure 5.11. The comparison of DSC curves highlights the differences in crystallization and melting behavior between a symmetric PDI PU-SSPCM system and an asymmetric TDI PU-SSPCM system.

Figure 5.11 shows dissimilar endothermic and exothermic peaks for both PU-SSPCM systems (Figure 5.24). It is apparent that PDI has a stronger, more prominent crystallization peak than TDI, although they have similar melting peaks. According to Table 5.5, the $\%X_c$ crystallinity and the phase transition temperature were lower than those of PDI. PDI's (T_c = 23.59 ˚C, ΔH_c = 44 J/g) crystallization was observed at a higher temperature than that of TDI (T_c = 11.32 ˚C, ΔH_c = 28.31 J/g). The differences in the crystallization temperatures and enthalpy were not the cause of melting. Melting peaks for PDI (T_m = 47.97 ˚C, ΔH_m = 38.64 J/g) and TDI. Unfortunately, 2,6-TDI, which is truly 2,4-TDI's counterpart as far as symmetry is concerned, was too expensive to obtain a sufficient quantity for this study. So, 1,4-PDI was used as a replacement. PDI is an aromatic and has a relatively similar to 2,4-TDI; except that its isocyanate groups are located at the para positions, which makes the diisocyanate symmetrical. Previous literature has demonstrated 2,4-TDI asymmetric structure offsets HS X stacking, which leads to weaker hydrogen bond interaction. As result, a low level of phase separation was observed for 2,4-TDI polyurethanes.[118,147]close in size, it is evident HS symmetry influences the steric effect and the extent to which SS PEG chain movement is restricted. Symmetrical diisocyanates are more suited for hydrogen bonding. 2-4 TDI asymmetry allows it to only crystallize in a head to toe formation. Consequently, the HS chains are unable to pack as closely, compared to symmetrical 1,4-PDI. These results not only give insight into the notion that symmetric diisocyanates promote PCM crystallization, it also indicates that a higher order of phase separation does as well.

Since both diisocyanate monomers are similar and close in size, it is evident that HS symmetry influences the steric effect and the extent to which SS PEG chain movement is restricted. This finding is in agreement with Schneider's study that found polyurethanes with 2,4 TDI demonstrate weaker mechanical properties, compared to 2,6-TDI. [147]

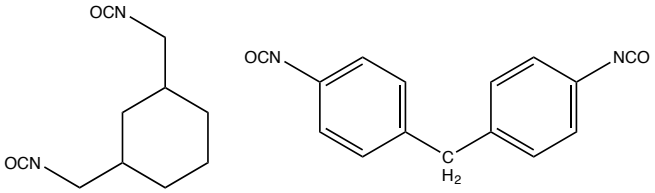

Figure 5.14: Comparison of BICH and MDI Variable Geometry

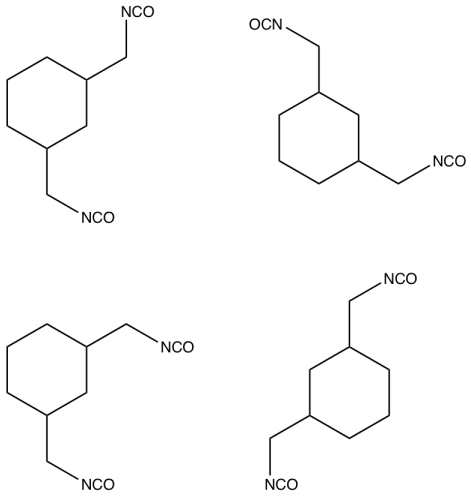

Figure 5.13: BICH conformation arrangements

Variable Factor: Variable Geometry

HS flexibility is varied by the ability of its diisocyanate component to assume different conformational arrangements. Conformation is the shapes or arrangements in three-dimensional space that an organic molecule assumes by rotating carbon atoms, or their substituents around single covalent bonds[121]. Flexible HS have the ability to rearrange its chain structure that facilitates closer packing of the HS groups, and gives rise to stronger hydrogen bond interactions. Previous literature has shown that aliphatic diisocyanates which can assume an unlimited number of spatial arrangements imparts greater flexibility to the hard domain than aromatic diisocyanates. HS flexibility promote the rate and

extent of micro phase segregation. Thus is why polyurethane materials with aliphatic diisocyanates typically exhibit a higher degree of phase separation compared to polyurethanes prepared with aromatic diisocyanate this section the influence a diisocyanates variable geometry has on PEG PCM crystallization is investigated. To study this relationship PU-SSPCMs prepared with BICH an aromatic diisocyanates that can assume four conformations (See Figure 5.13), and MDI an aromatic diisocyanate that cannot assume another conformation. The molecular geometries of BICH and MDI is displayed in Figure 5.14 and the different conformational arrangements of BICH are shown in Figure 5.13. The comparison of the melting and cooling behavior of BICH and MDI is displayed in Figure 5.15. From which, it can be seen the variable geometry of BICH, the methyl group adjacent to the isocyanate and ring structure imparts greater flexibility because it provides an extra degree of freedom that allows BICH to assume multiple conformations. Of the considered diisocyanates in this study, BICH and MDI were the largest in size and have somewhat analogous chemical structures MDI on the other hand does not assume other conformations and is the most rigid of the considered diisocyanates.

According to Figure 5.15 no crystallization or melting behavior was visible for the PU-SSPCM prepared with MDI, while BICH DSC curve showed a broad crystallization and a prominent melting peak. It was found in chapter 4 that PEG M_n =2000g/mol is below the critical molecular weight when prepared with a MDI HS. However, the PU-SSPCM DSC Curves obtained for MDI prepared with PEG 3000 g/mol and 6000 g/mol did display PCM melting and crystallization peaks. However, the DSC curves of BICH

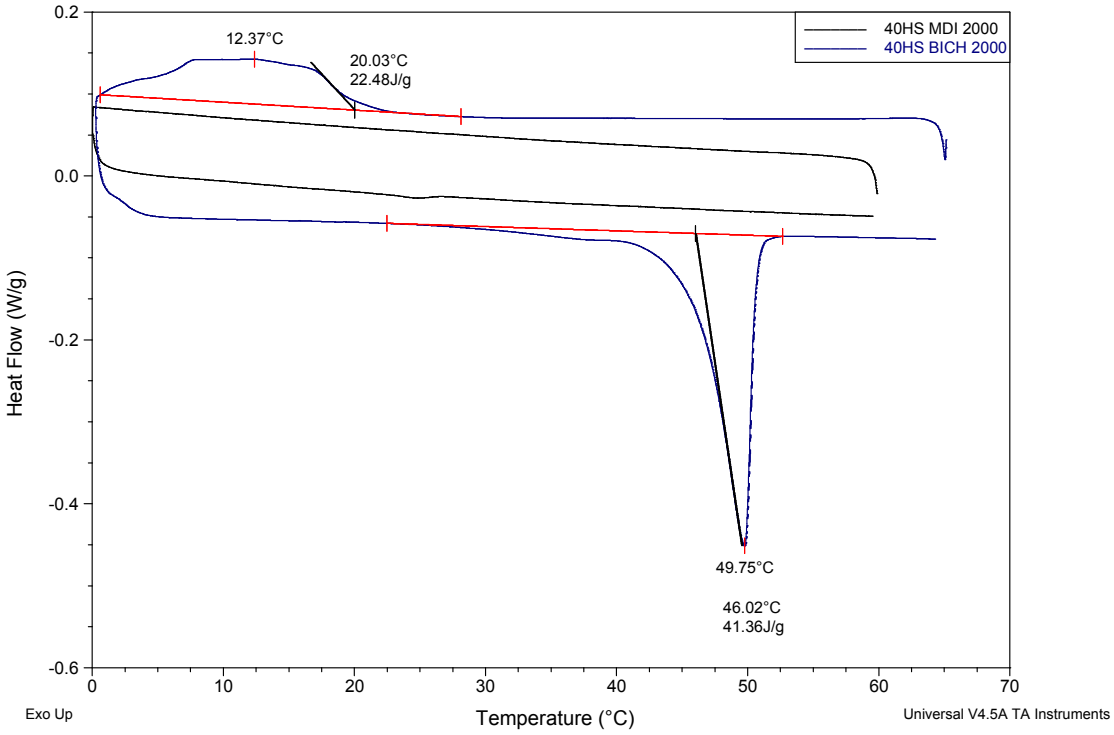

Figure 5.15: Comparison of DSC Curves of MDI 2000 and BICH 3000

prepared with PEG 2000 g/mol did display an endo and exothermic peak. Therefore, a comparison between MDI 3000 and BICH 2000 is shown. This finding adds to the notion that MDI's rigid structure is the source for the inhibition of PEG crystallization and generates a larger steric effect. Nonetheless, the comparison between flexible BICH and rigid MDI does not provide conclusive evidence about the effect variable geometry has upon the crystallization of the PCM polymer.

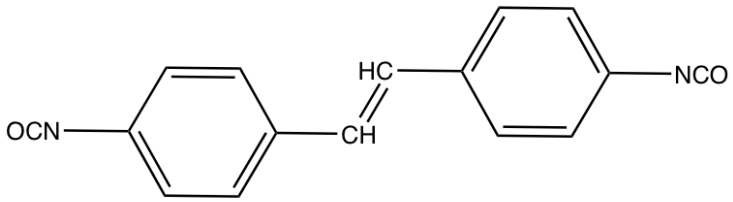

4,4'-dibenzyl diisocyanate (DBDI)

Figure 5.16: Molecular structure of DBDI

To systematically investigate the effect of variable geometry it would have been better to compare MDI to DBDI (See Figure 5.16) DBDI and MDI are double aromatic diisocyanates with almost identical molecular structures except that DBDI has an extra methyl group located in between the aromatic rings. The Ethylene bridge between the phenol rings introduces a variable geometry into the hard segment due to the possibility

of internal rotation of this diisocyanate around the -CH_2-CH_2 ethylene bridge, which leads to the appearance of both "anti" and "syn" rotational conformations (see Figure 5.27). Unfortunately, obtaining DBDI monomer for this research work was not possible. The Romanian laboratory at the Institute of Macro-molecular Chemistry "Petru Poni" Iasi is the only lab known to synthesize this monomer and produce small quantities for personal lab studies and has published papers comparing DBDI to MDI polyurethanes The findings from Prisacariu [54] will be incorporated into this work to supplement this research work's inquiries on HS variable geometry's connection to the crystallization of a PEG PCM polymer.

Fig. 2.4 Extended linear "anti" DBDI position

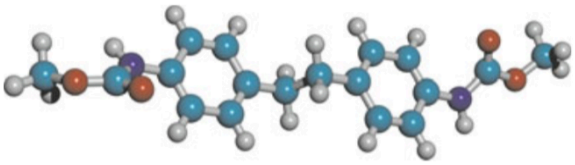

Fig. 2.5 Contorted "syn" DBDI position

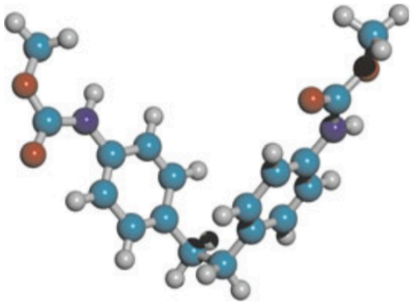

Fig. 2.6 Conventional rigid 4,4-diphenylmethane di-isocyanate (MDI) non-crystallizing

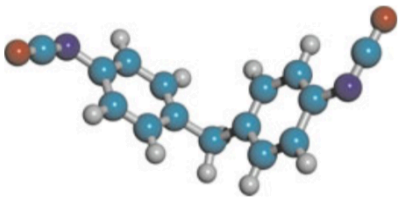

Figure 5.17: Conformational arrangements of DBDI compared to rigid MDI (Source: Prisacariu 2011[47]; Reprinted with permissions from Springer. July 7, 2016.)

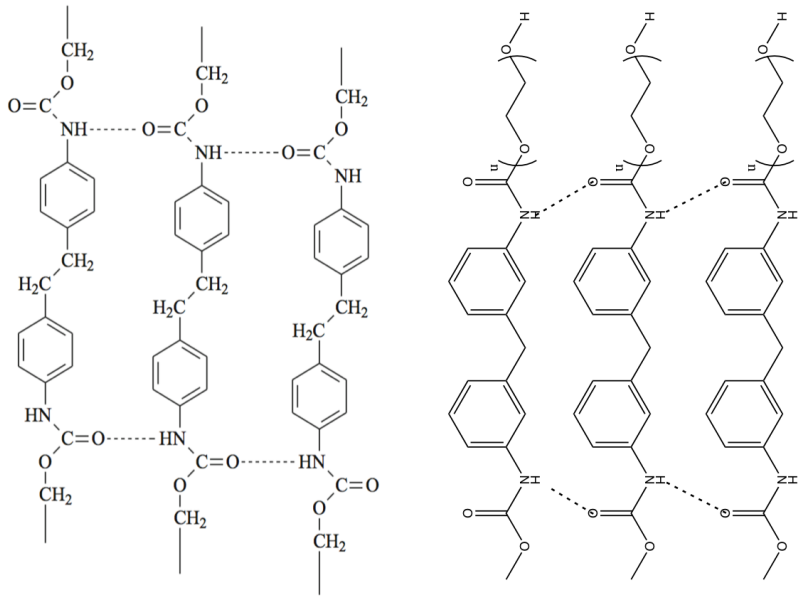

Figure 5.18: Comparison of Chain Stacking Hydrogen Bond Interaction between DBDI (left) and MDI (right)

The results of the papers show that DBDI can adopt a linear conformation, facilitating packing and inter-chain hydrogen bonding. (See Figure 5.18) MDI HS however are intrinsically kinked in shape, reducing conformational mobility and thereby hindering close packing and achievement of hydrogen bonding. In result, PUs with MDIs are not as ordered and as highly crystalline compared to PUs with DBDIs. The primary effect of employing flexible hard segments in PU synthesis was shown to be a closer self-association of HS by hydrogen bonding, which goes along with the previous theme of greater hydrogen bonding that leads to more complete phase separation. The difference in degree of phase separation between DBDI and MDI can best be visualized in the AFM phase images taken by the lab. These images are shown in Figure 5.19. The separation between crystalline and amorphous phases was better observed in the AFM phase contrast images.

In result, PU with MDI are not as ordered and as highly crystalline compared to PU with DBDI. The primary effect of employing flexible hard segments in the PU synthesis was shown to be a closer self-associate of HS by hydrogen bonding. Goes along the previous theme of greater hydrogen bonding that leads to more complete phase separation.

Figure 5.19: Topographical and phase contrast AFM images for freeze fracture surfaces for two analogous materials that differ in the type of diisocyanate a) a PU

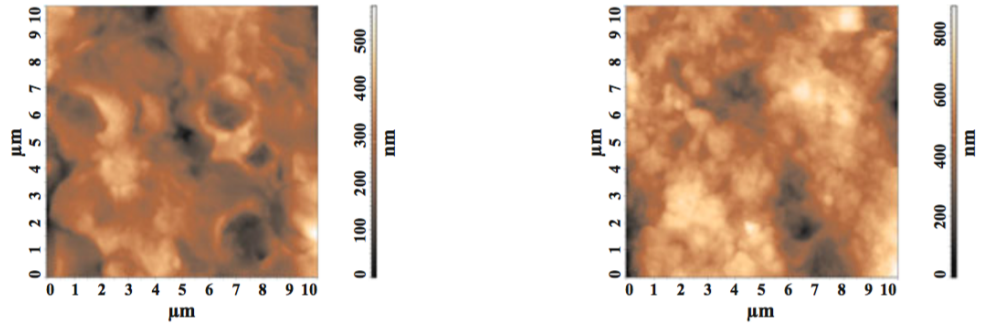

a b

prepared with DBDI:BDO:PTHF; b) a PU prepared MDI:BDO:PTHF with a rigid diisocyanates (Source: Prisacariu 2011: Mrs. I. Stoica, Institute of Macromolecular Chemistry, Petru Poni, Iasi, Romania [41,84]; Reprinted with permissions from Springer. July 7, 2016.)

5.3.5. DSC CURVES OF INITIAL HEAT RUN (GLASS TRANSITION)

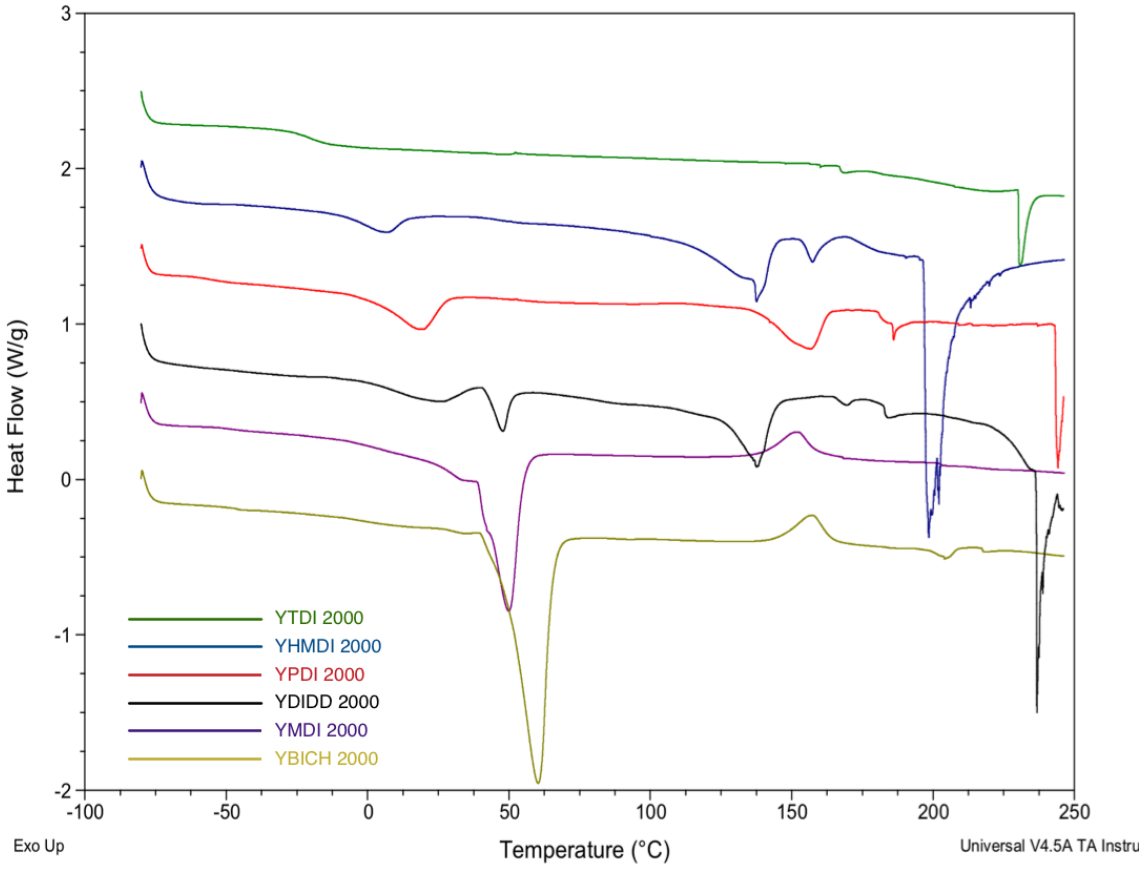

Figure 5.20: Overlay of DSC Curves from initial heating from -80˚C to 250˚C at 20˚C/min.

DSC analysis techniques were utilized to determine the degree of phase separation by measuring the glass transition temperatures (T_g) of the PEG PCM component.

The DSC curves obtained during initial heating from -80˚C to 250˚C at 20˚C/min is presented in Figure 7.6. It can be seen that initial heat DSC curves display multiple endothermic peaks. The appearance of multiple endotherms indicates that separate phase domains are present in the sample. The intensity of these thermal transition signifies the prevalent level of phase mixing in the sample. The following thermal transitions are associated with either PEG PCM chain segments or the diisocyanate HS and were

assigned to specific temperature regions: a) the first thermal transition is a glass transition that is attributed to the cooperative motion of amorphous non-crystalline PEG chain units. This PCM glass transition step appears below 0˚C ($T_{g,SS}$); b) the second transition is a prominent endothermic peak that appears at low temperatures (below 100˚C). This peak is assigned to the melting of ordered PEG PCM chain segments ($T_{m,PCM)}$ <100˚C); c) the third transition is an endothermic peak that may be observed between 100-150˚C. This peak is associated with phase mixed PCM and HS chains ($T_{m,mix}$). The fourth thermal transition is associated with a HS glass transition that is observed above 150˚C ($T_{g,HS}$). The fifth transition is associated with the melting of ordered HS crystallites. This peak is observed at high temperatures between 150˚C-250˚C. The appearance of the series aforementioned of transitions confirms is a signature of phase separation and the intensity of these transitions signifies the level of their presence in the sample[37,129,149]. Therefore, it is apparent in Figure 5.20 that all PU-SSPCM samples displayed multiple endotherms and that the variety in peak intensity shows that the level phase mixing varies with the type of diisocyanates. The thermal properties from the initial heat DSC Curves are summarized in Table 5.6. Measurements of glass transition temperatures were taken at the midpoint of the heat capacity change, and the melting points were taken at the peak maximum of the endotherm.

Approximation of Degree of Phase Separation Based on Tg

No Tg of the PEG PCM component (T_{gPCM}) was visible in the DSC curves for PU-SSPCM samples prepared with aliphatic diisocyanates (HMDI and DIDD). On the other hand, only aliphatic HS showed a HS crystallization peak.

Generally, in DSC analysis of SPU elastomers, the T_g is used to probe the degree of phase separation. The closer the T_g is to its T_g in its pure state, the higher the degree of phase separation. This is because the more phase separated the hard and soft domains are the more they behave like their pure state. This behavior follows the Fox equation (Equation) of a copolymer and follows the Koberstein model.

While ΔH_m is used to interpret the size of the PCM crystalline region, the size of the baseline shift indicates the size of the amorphous region.[37,150,151] The amorphous region is excluded from the PCM crystalline region as it is the outer portion of the PEG PCM polymer nearest to the HS cross-link that is unable to crystallize due to steric hindrance of the diisocyanate. Since the amorphous size and HS steric hindrance are connected, this information may be used to quantify HS steric effects based on diisocyanate structural features.

Table 5.6: Details of Thermal Properties from Initial Heat Step

	PCM Domain $T_{g,PCM}$ (°C)			ΔC_p (J/(g °C)	Endotherms (°C)			$\Delta C_p / \Delta C^\circ_p$
	^aT_g	^bT_g	^cT_g		T_{m1}	T_{m2}	T_{m3}	
PEG 2000		-61.0						
Y-DIDD 2000	-48.96	-44.29	-29.84	0.2327	47.78	137.64	236.76	0.1511
Y-HMDI 2000	-70.96	-69.69	-64.13	0.1591	12.33	157.99		0.1033
Y-TDI 2000	-28.15	-20.86	-14.19	0.6319			230.8	0.4103
Y-PDI 2000	-49.98	-47.73	-43.68	0.2793	18.97	156.55	186.03	0.1814
Y-BICH 2000	-58.79	-54.87	-50.71	0.3086	60.3	157.44	204.05	0.2004
Y-MDI 2000	-43.57	-34.59	-27.01	0.5723				0.3716

The absence of a $T_{g,PEG}$ in aliphatic PU-SSPCM DSC curves indicates little to no amorphous regions exist. Based on this evidence, we may assume that flexible aliphatic HS is the least disruptive to PEG PCM crystallization, and will lead to greater TES properties.

Upon cooling, only HMDI shows an exothermic peak between 150˚C and 250˚C, whereas this was not seen for the other samples. This appearance of such peak demonstrates how much faster smaller aliphatic HS establish HS order, compared to the other HS diisocyanates. On account of the structural moieties that pertain to the HMDI diisocyanate flexibility it can diffuse much more rapidly through the PEG soft segment matrix compared to the other HS diisocyanates considered.

5.3.6. CONCLUSION

Overall, HMDI had the highest variable geometry, as it is able to assume the most conformational arrangements, followed by BICH, and last MDI. The bar graph highlights

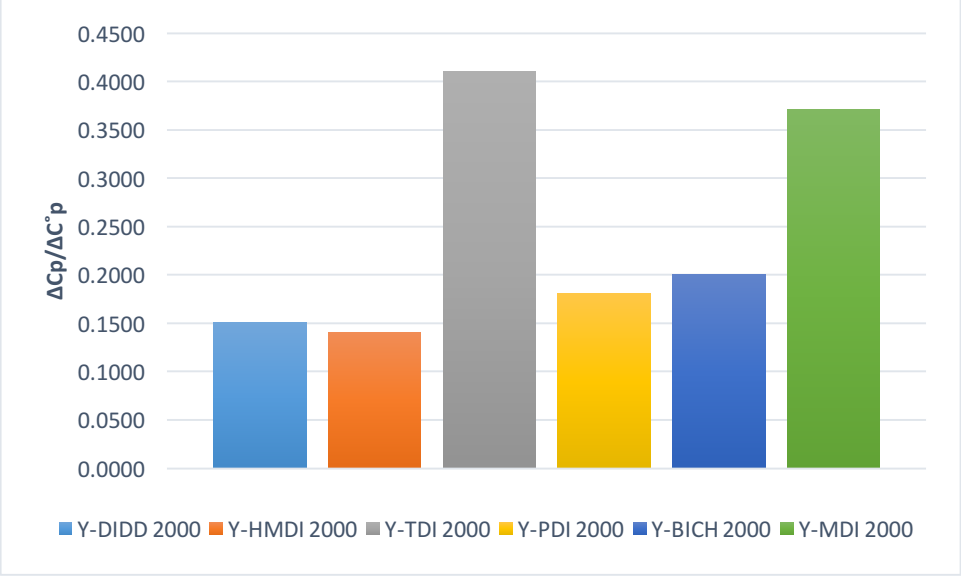

Figure 5.21: Level of Phase Mixing approximated by $\Delta C_p/\Delta C^\circ_p$

an increase in diisocyanate flexibility gave rise to greater thermal energy storage properties. Compared to the other structural factors, not much variation in PEG PCM crystallinity was observed between the PU-SSPCM prepared with symmetric and asymmetric diisocyanates. Due to the fact that all of the other components of the polymer were the same, it is certain that the differences in SS crystallinity are attributed to the structure of the diisocyanate. Initially, it was predicted that the same diisocyanate moieties that inhibit the rate and extent of phase separation: bulky size, rigidity and asymmetric structure would also cause the greatest decline in soft segment crystallinity are. The findings in the study corroborate with this hypothesis. It can be seen in Figure 5.20 that the level of phase mixing varies according to the structural regularity of its diisocyanate component. It is apparent that YTDI 2000 has the highest level of phase mixing followed by MDI. The least phase mixed PU-SSPCM was HMDI and DIDD. This data corroborates with the diisocyanates ability to form hydrogen bonds. This data agrees with the determination of degree of phase separation by FTIR.

Figure 5.21 plots the X_c% vs $\Delta C_p/\Delta C^o_p$ values expressed as a percentage to show how the size of the PCM crystalline region varied with the degree of phase separation. From the comparison of the level of mixing to the percent crystallinity of the PCM, it can be seen that there is no distinctive pattern. A more extensive test method is needed to measure the degree of phase separation present in the sample to compare this.

In conclusion, the findings of this work indicated that diisocyanates that are small and more readily able to crystallize, flexible, and symmetric disrupt a smaller portion of PEG PCM chain segments, compared to diisocyanates that are bulky, rigid and asymmetric.

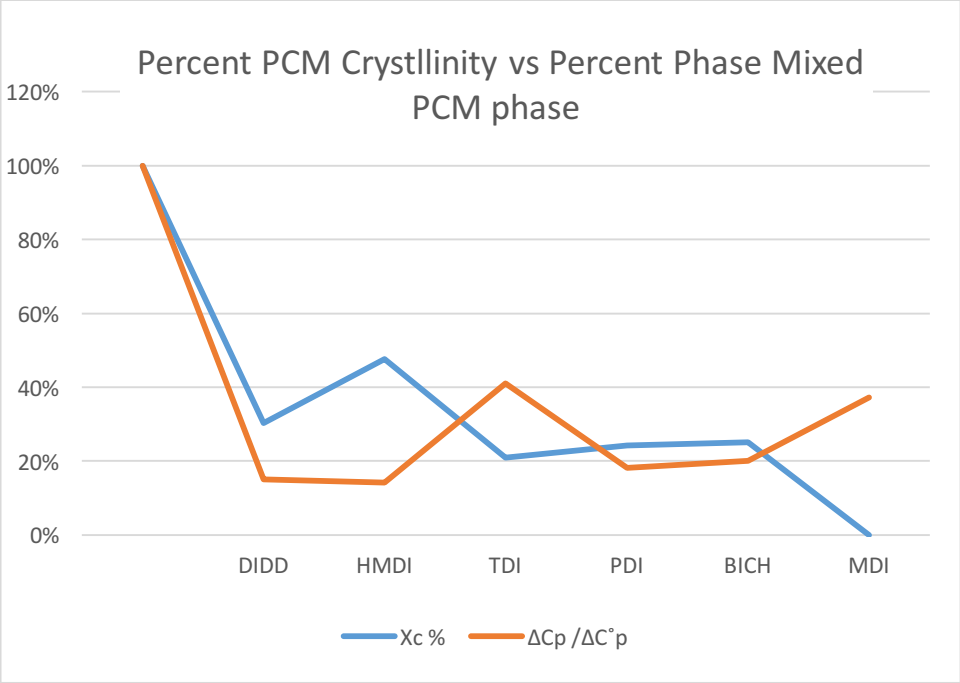

Figure 5.22: Shows the relationship between the degree of phase separation and the size of the PCM crystalline region.

The effect these particular diisocyanate structural features have on thermal energy storage properties originates from the diisocyanates' ability to form hydrogen bonds. However, it is unknown at this time is diisocyanate geometry is the sole factor in determining thermal energy storage properties. The scope of this study focused only on samples cooled at 20˚C/min and prepared with a 40% HS content. It is possible that samples cooled at a different rate or prepared with a different %HSC would demonstrate different TES properties. It is known from literature both variables strongly influence phase separation characteristics.

The following chapters, 6 and 7, will further investigate the potential relationship between the degree of phase separation and heat storage properties by varying HS content and the cooling regime. The SS enthalpy phase change measured in the following chapters will revert back to the enthalpy data in this chapter for a 20˚C/min cooling rate and 40% HS to determine whether modifying either of these factors might introduce significant changes in the heat storage capability. Due to the fact that all of the other components of the polymer were the same, it is certain that the differences in SS crystallinity are attributed to the structure of the diisocyanate.

Chapter 6 THE INFLUENCE of HARD SEGMENT CONTENT ON PU-SSPCM THERMAL ENERGY STORAGE PROPERTIES

6.1. INTRODUCTION

The effects that the proportions of Hard Segment Content (%HSC) and Soft Segment Content (%SSC) have on the final polyurethane properties have been studied extensively for regular polyurethane materials.[28,152] The soft-segment concentration (%SSC) is defined as the ratio of the mass of polyol chains without terminal hydroxyl groups to the total mass of the polymer. And the Hard segment concentration (%HSC) is all the non-polyol components, which is the diisocyanate and chain extender. Usually, both are expressed as a percentage. The %HSC and SSC play major roles in determining the characteristics of the polymer's phase-separated morphology, which ultimately determines its final properties. Polymers with higher HSC% have longer HS chain lengths. Longer HS chain lengths give rise to stronger hydrogen bonding interaction, which then implies stronger physical cross-links. The increase in HS affinity increases the formation of HS phase domain structures, which ultimately leads to a greater degree of phase separation.

According to Koberstein's PU microdomain model, there is a critical HS sequence length for microphase separation, below which HSs are dissolved within the soft microphase or become trapped in it during the formation of the structure.[57] Consequently, this dissolution process increases the glass transition temperature of the soft microphase and degrades the low-temperature response of the material.[129] Abouzahr and Wilkes studied the morphological changes that occur in a series of MDI-based PUs with different HS

fractions.[119] They found that the mechanical properties of the elastomers were defined in four stages, depending on the HSC. Polymers with low HS percentages (<17%) had poorer phase separation and poorer elastomeric properties than polymers with slightly higher %HSC (26%), which showed some phase separation and higher extension, but low hysteresis. As %HSC increased to > 30%, interlocking of the morphology of the HS domain occurred. This led to higher modulus, toughness, and extensibility, but low hysteresis still existed until %HSC rose to 35-40%. At this point, between hard and soft phase domain, an interphase region made of mixed hard and soft phases begins to take shape. At %HSC percentages above 50%, the hard and soft phases invert from HS domains in a soft matrix to soft domains in a HS matrix, and the polymer became a brittle, high modulus plastic.[119] For polymers with low HS concentration (< 30%), only discontinuous HS domains of a micellar nature were observed in the SS solvent-like matrix, especially when the sequence length of the HS was short.[57] However, for PUs with high %HSC (35-40%), the bi-continuous phase morphology clearly was identified. As for PUs with %HSC of 30-33%, continuous soft phase morphology with dispersed hard segments was observed. Typically, PUs with HS around 30% had phase structures that fell between continuous and bi-continuous states. Figure 6.1 shows a schematic representation of the association of the hard segment into domains based on %HSC. Based on Koberstein's model, it is reasonable to speculate that %HSC also would have a strong effect on the thermal energy storage properties. However, in the existing literature related to thermoplastic polyurethane SSPCMs, none of the authors specified the HS

content in the samples they investigated. Therefore, the reported enthalpy values are unreliable and not comparable.

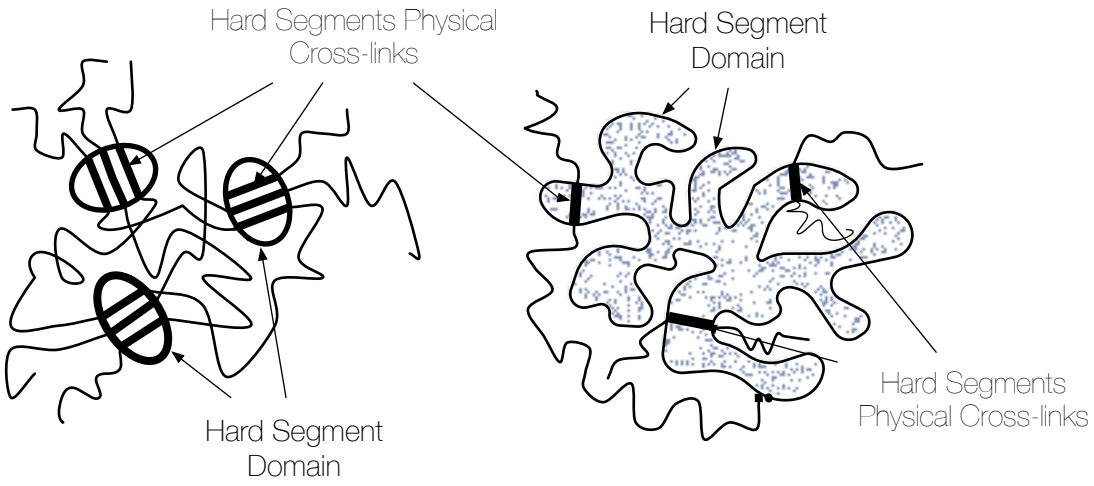

Figure 6.1: Schematic representation of the hard segment association into domains: (a) at low hard segment content; (b) at higher hard segment content

A PU-SSPCM with the highest degree of phase separation would demonstrate two well-defined phase domain structures with one of them composed purely of urethane-rich HS crystallites and the other composed purely of PCM polymer chains (Figure 6.1). Because of the localization of PCM polymer chains and the absence of HS impurities that typically disrupt PCM crystallization, it is inferred that well phase-separated pure PCM phase domains have the greatest opportunity to undergo maximum crystallization. Therefore, based on this assumption, it is likely that higher enthalpy values, as well as better thermal energy storage properties, would be observed for a PU-SSPCM with a high degree of phase separation.

While it is reasonable to conclude that a highly phase-separated morphology would result in maximum enthalpy values, raising the %HSC to increase phase separation implies that decreasing the concentration of the PEG PCM polymer chains could produce a decline in TES properties at the same time. In addition, it was indicated in the previous chapters that larger-sized HS created greater steric constrictions and reduced the range of interaction between PEG chains. It is possible that the chain-end effect would be more prominent in polymers with higher %HSC. This contention between the degree of phase separation and the proportions of the HS and PCM polymer chain segments is investigated in this chapter.

Currently, we do not know whether a continuous soft phase morphology would have more favorable thermal energy storage properties than a bicontinuous phase morphology. In the chapters 4 and 5, it was indicated that the chain-end effect was more noticeable for larger diisocyanate hard segments. This finding gives some indication that longer HS would result in poorer enthalpy values; however, based on Koberstein's model, the %HSC must be above the critical length to observe a solid-to-solid phase transition. Thus, there must be a compromise in the HS concentration, i.e., it must be high enough to maintain a solid framework, and it must be low enough to ensure maximum thermal energy storage properties.

Since it is well known that HS content is a major factor in SPU properties, it is also worthwhile to study the effects that the proportions of %HSC and SSC have on thermal energy storage properties. The purpose of this study was to draw a correlation between the morphology of segmented polyurethane elastomers and thermal energy storage

properties. It is known that the molecular structure of the diisocyanate that makes up the hard segment has a major effect on the degree of phase separation in these types of materials; however, it is unknown whether the degree of phase separation leads to improved thermal energy storage properties. It is known that the sample must possess greater than 40% HS for phase separation to occur.

In this chapter, the thermal energy storage properties of a series of thermoplastic PU-SSPCMs with varying wt% values of HS were studied. The aim of this chapter was to determine how %HSC relates to the crystallization of the PEG PCM polymer. The results in this chapter provide a greater understanding regarding the optimal composition parameters for developing PU-SSPCMs with favorable thermal energy storage properties. PU-SSPCM materials were prepared with 17, 26, 33, and 40% HS content. Information on how the HS content, degree of phase separation, and the phase change enthalpy relate to each other was obtained using DSC techniques. Other analysis techniques, such as FTIR and TGA, were used to provide supplemental information to characterize and interpret the heat storage properties of the SPU-SSPCM materials that were considered. Overall, the goal of this research were to determine the optimal HS content for obtaining a SPU-SSPCM with maximum heat storage properties and to provide new information for future researchers who may be studying and developing novel SPU-SSPCMs.

6.2. EXPERIMENTAL

6.2.1. SAMPLE PREPARATION

In this study, thermoplastic (TPU) PU-SSPCM was the only type of PU-SSPCM considered. Therefore, all of the PU-SSPCMs samples were prepared with the same linear block copolymer chain structure, as shown in Figure 2.8: Schematic of PCM polymer segment and the urethane hard segment (HS). For all of the PU-SSPCMs investigated, poly(ethylene glycol) (PEG) with an M_n = 2000 g/mol was used consistently as the PCM polymer component, and 1,4- butane diol (BDO) was used consistently as the HS chain extender component. For the diisocyanate HS component, three diisocyanates monomers, i.e., HMDI, PDI, and BICH, were selected to make three separate versions of PU-SSPCM polymers. For each version of the PU-SSPCM polymers, a series of samples with varying ratios of HS content (%HSC) and PCM content (%PCM) was prepared

Table 6.1: List of Samples Prepared and Nomenclature

%HSC	HS: DIISOCYANATE COMPONENT	NOMENCLATURE
17%	*1,4-Phenylene Diisocyanate*	**17% PDI**
26%	*1,4-Phenylene Diisocyanate*	**26% PDI**
33%	*1,4-Phenylene Diisocyanate*	**34% PDI**
40%	*1,4-Phenylene Diisocyanate*	**40% PDI**
17%	*1,3-Bis(isocyanatomethyl)cyclohexane*	**17% BICH**
26%	*1,3-Bis(isocyanatomethyl)cyclohexane*	**26% BICH**
33%	*1,3-Bis(isocyanatomethyl)cyclohexane*	**34% BICH**
40%	*1,3-Bis(isocyanatomethyl)cyclohexane*	**40% BICH**
17%	*1,6-Diisocyanatohexane*	**17% HMDI**
26%	*1,6-Diisocyanatohexane*	**26% HMDI**
33%	*1,6-Diisocyanatohexane*	**34% HMDI**
40%	*1,6-Diisocyanatohexane*	**40% HMDI**

(Table 6.1). The following %HSC values were selected to be investigated: 17, 26, 33, and 40% HSC. A code system to name each sample was used to keep track of the combinations of diisocyanates and PEG. The code refers first to the percentage content of the hard segment, and this is followed by the diisocyanate that was used and the molecular weight of the PEG that was used, i.e., *%HSC + Diisocyanate + PEG molecular weight]*. Since all of the samples were prepared with the same PEG molecular weight of M_n = 2000 g/mol, the '2000' part of the name was omitted. All of the PU-SSPCMs that were studied and the nomenclature assigned to each sample are listed in Table 6.1. Further details on the monomer reagents used are provided in Chapter 3, section 3.2. (pages 102-103.)

Fabrication of Considered PU-SSPCMs

The fabrication of all of the samples listed in Table 6.1 was carried out using the same synthesis procedures described previously in section 3.3 (page 109). The hard segment portion of thermoplastic polyurethane elastomers generally is formed by first forming an isocyanate-capped pre-polymer and then building the HS molecular weight with diisocyanate and chain-extending monomers.

A two-step method was selected for the synthesis to increase the likelihood that the polymer product that was formed would have a more organized chain structure, high molecular weight, and low PDI. The two-step method that was used for the reaction is shown schematically in Figure 3.3. A stoichiometric index of I =100 was used in order to obtain polymers with a linear structure. The masses of the reagents used were calculated based on a 1:1 stoichiometric ratio of hydroxyl [–OH] and isocyanate [–NCO] end group. As previously described in section 2.5.2, unbalanced stoichiometric conditions can result

Table 6.2: Molar Compositions used to prepare series of %HSC

[%HSC - DI]	Moles of PEG	Moles of DI	Moles of BDO
17% PDI	1	1	1
26% PDI	1	2.5	1.5
34% PDI	1	4.5	3.5
40% PDI	1	6.5	5.5
17% BICH	1	2	1
26% BICH	1	4	3
34% BICH	1	6	5
40% BICH	1	8	7
17% HMDI	1	1	0.5
26% HMDI	1	2	1
34% HMDI	1	4	3
40% HMDI	1	6	5

in side reactions that prevent the formation of high molecular weight polymers or that could introduce chain branching reactions that would result in a non-linear polymer product. The routes that typical side reactions can take as a result of excess –NCO groups (See Figure 2.38). It was important for the samples that were studied to have the highest possible molecular weight and to have a linear structure. Therefore, to avoid potential side reactions, careful attention was paid to making sure a 1:1 ratio of isocyanate (NCO) and hydroxyl (OH) groups was maintained throughout the reaction.

To synthesize PU-SSPCM polymers with varying proportions of HS content, the molar compositions of diisocyanate and BDO monomers were adjusted to obtain %HSC within the following ranges: [15-17% HSC], [24-26% HSC], [30-34 % HSC], and [40-42% HSC]. To increase the length of the HS component, diisocyanate and BDO reagents were added after the initial pre-polymer formation steps in an alternating fashion to build up the size of the HS component until the desired HS concentrations (%HSC) were obtained. Alternating the addition of the diisocyanates and the BDO reagents allowed the molar ratio of isocyanate and BDO hydroxyl groups to be maintained at a 1:1 stoichiometric ratio. It was important that the ratio of the -NCO and -OH chain extender groups remain balanced during this step to avoid branching. The molar compositions that were used are summarized in Table 6.2.

6.2.2. ANALYSIS AND CHARACTERIZATION OF PU-SSPCMS SAMPLES BY FTIR, TGA, POM

The same experimental parameters described in chapter 3 for analysis by FTIR, TGA, and POM Analysis were used to characterize the prepared PU-SSPCMs (See Chapter 3).

6.2.3. ANALYSIS BY DIFFERENTIAL SCANNING CALORIMETRY (DSC)

See Chapter 3 for further details on the experimental methods. The PEG PCM polymer demonstrated a phase transition between the amorphous and crystalline states at temperatures between 0 and 65 ^{o}C. Based on this range of ambient temperatures, the parameters of the DSC method were used to measure the thermal energy storage properties that were observed for the PEG PCM polymer. First, all of the samples were heated to a homogeneous melt to ensure that all HS ordering was destroyed. After the homogeneous melt was cooled to 65 ^{o}C at a rate of 20 ˚C/min, the samples were cooled and then heated at a rate of 2 ˚C/min. The homogeneous melt step was necessary to destroy any in order in the hard segment of the sample and to establish the same degree of phase separation for all of the samples. This eliminated the possibility of having any discrepancies in the crystallinity of the soft segment due to the organization of the structure of the random domain

6.3. RESULTS

6.3.1. ANALYSIS OF CHEMICAL STRUCTURE BY FTIR ANALYSIS

Confirmation of Synthesis

The chemical structures of the synthesized polymers were analyzed by FTIR spectroscopy, and FTIR spectra were obtained for all samples listed in Table 6.1. An overlay of the IR spectra of the %HSC series of PU-SSPCM samples prepared with BICH, HMDI, and PDI HS is displayed in Figures 6.1, 6.2, and 6.3, respectively. The IR spectra were used to verify that polyurethane polymers were formed during the synthesis and that the polymers had a linear structure. The appearance of a peak at 2965 cm^{-1} was indicative of isocyanate [-NCO] groups.[134] Figures 6.1-6.3 show that no peaks were detected at this location, and the absence of isocyanate and hydroxyl peaks indicated that all of the hydroxyl and isocyanate groups reacted completely and that no residual isocyanates remained in the final precipitate.

Figure 6.2 includes the IR spectra obtained from a PEG homopolymer with an M_n = 2000 g/mol. Different spectral patterns were observed when the PEG IR spectra and the

Table 6.3: Main N-H and C=O peaks observed in sample IR spectra

PU-SSPCM Sample	N-H (cm^{-1})	C=O (cm^{-1})
17% PDI	3310	1713
26% PDI	3321	1709
34% PDI	3329	1709
40% PDI	3320	1717
17% BICH	3326	1716
26% BICH	3315	1715
34% BICH	3302	1709
40% BICH	3302	1709
17% HMDI	3305	1710
26% HMDI	3336	1705
34% HMDI	3316	1716
40% HMDI	3321	1709

sample spectra were compared. Two regions of the FTIR spectrum are of particular interest in SPU, i.e., the strong IR bands that appeared in the C=O stretching vibration region (1685 – 1740 cm^{-1}) and the amine (NH) stretching vibration (3300-3500 cm^{-1}) were indicative of polyurethane materials. Distinct peaks that correspond to the stretching vibrations of C=O and NH were observed for all of the samples that were synthesized. (Figures 6.1, 6.2, and 6.3). Table 6.3 lists the peak frequencies at which the main IR bands appeared in the NH and C=O stretch regions. These results verified that a urethane polymer was formed during the synthesis, and they confirmed that the syntheses of all of the PU-SSPCM samples considered in this chapter were conducted successfully.

Figures 6.1, 6.2, and 6.3 show that the intensities of the NH and C=O peaks increased and the bandwidth decreased as the %HSC in the samples increased. The increases in the intensities of the peaks were associated with an increase in HS ordering. Longer HS chain lengths form stronger interactions, and this produces strongly-bonded, well-organized hydrogen bonds. Thus, we can understand why PU-SSPSCMs have more prominent NH and C=O peaks that are uniform and symmetrical as the %HSC increases.

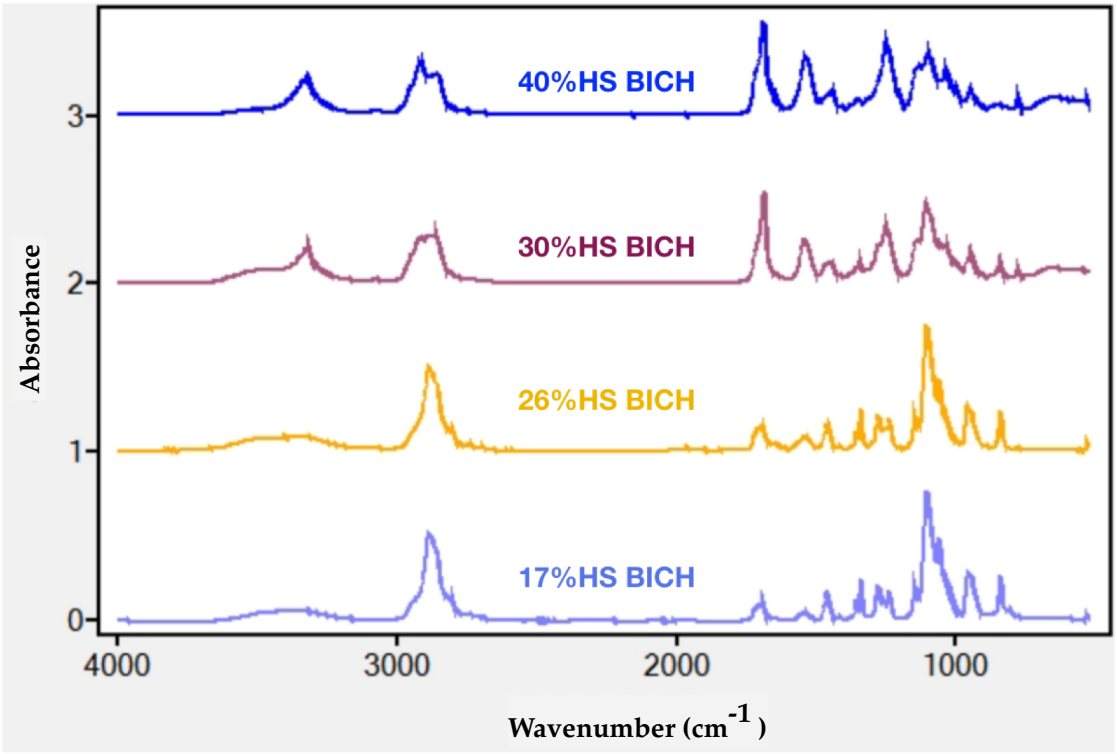

Figure 6.2: FTIR Spectra of 40%, 30%, 26%, and 17% BICH 2000

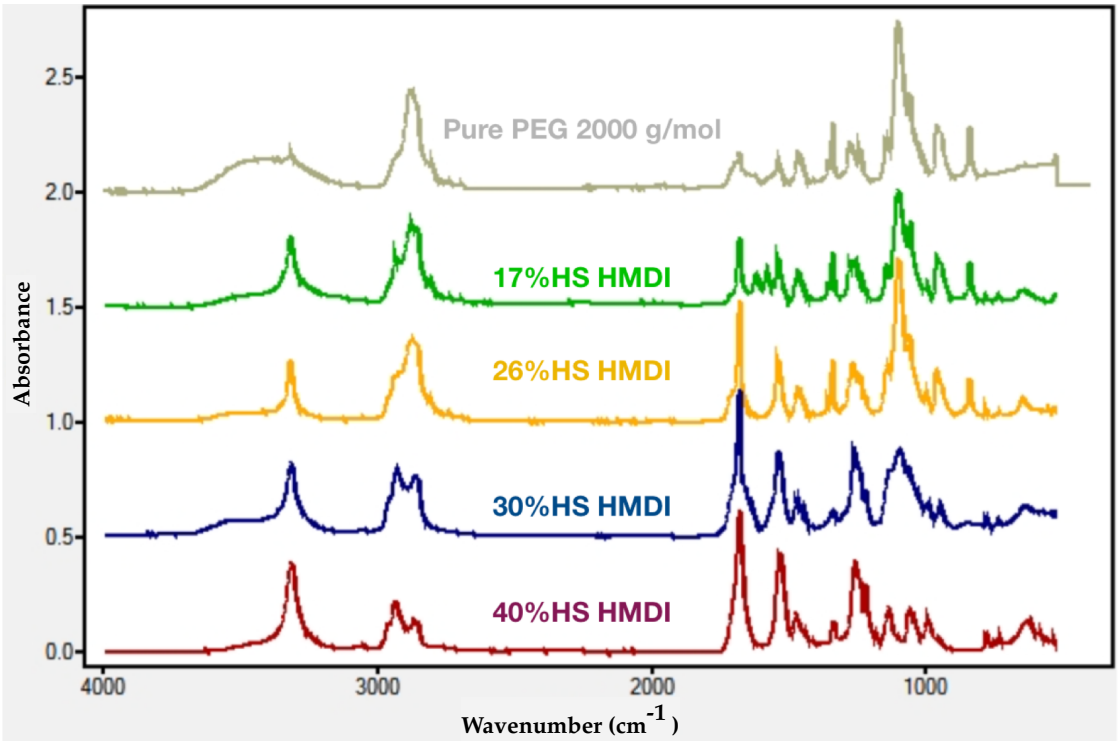

Figure 6.3: FTIR Spectra of 40%, 30%, 26%, and 17% HMDI and Pure PEG 2000g/mol

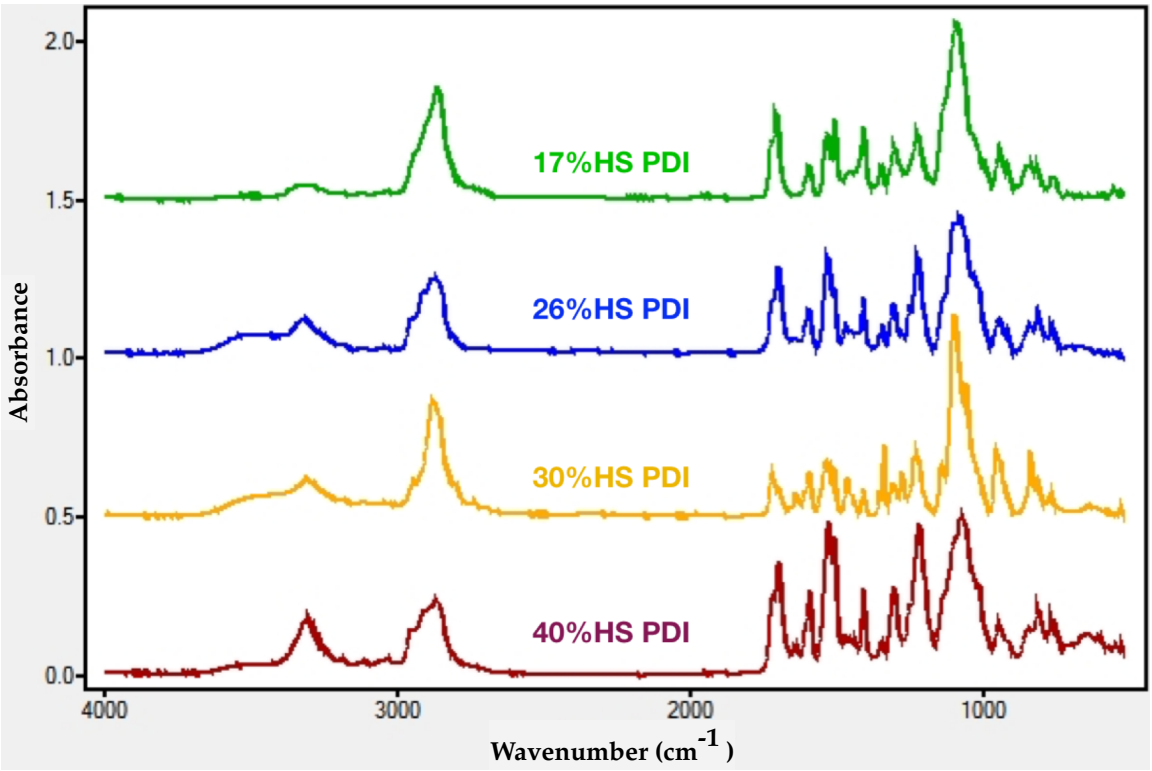

Figure 6.4: FTIR Spectra of 40%, 30%, 26%, and 17% PDI 2000

Approximation of Degree of Phase Separation by FTIR analysis

FTIR Analysis is commonly used to approximate the degree of phase separation in PU materials[61,107,153-156], and the locations the main amine and carbonyl peaks that appeared were used to approximate the degree of phase separation in the samples. Based on reports

Amine (NH) Stretching Vibration Region	non-bonded	3450cm^{-1}	*Carbonyl (C=O) Stretching Vibration Region*	non-bonded	1732 cm^{-1}
	bonded disordered	3340 cm^{-1}		bonded disordered	1705 cm^{-1}
	strongly bonded ordered	3320 cm^{-1}		strongly bonded ordered	1685 cm^{-1}

Figure 6.5: IR Band Vibrations associated with types of Hydrogen Bonding

that are associated with different types of hydrogen bonds.

As indicated by their lower absorbed frequencies, polyurethanes' signature carbonyl and amine IR bands possess restricted vibrational motions, which can be differentiated from those of non-bonded or disordered groups. The shift in the location of the peak frequency provides information about the types of hydrogen bonding that exist in a polyurethane. Thus, identifying shifts in peaks' frequencies is a common method that is used to describe the degree of phase separation in segmented polyurethanes (SPUs)[157].

Carbonyl peaks can be separated into three regions based on the different types of hydrogen bonding[107,157], i.e., carbonyls that are not involved in hydrogen bonding, which generally show peaks near 1732 cm^{-1}; carbonyl groups associated with non-bonded or "disordered" bonds hydrogen bonding are observed at 1708 cm^{-1} and carbonyl peaks observed at 1685 cm^{-1} is attributed to a ordered and strongly hydrogen bonded carbonyl group. that are strongly hydrogen bonded and ordered are observed around 1685cm^{-1}. [107,155,157] However, different HS compositions can cause slight deviations from the peak positions mentioned above.

Table 6.3 indicates that the samples prepared with 30% and 40%HSC had NH peaks below 3320 cm^{-1}, indicating that most of the amine groups in these samples were strongly bonded and ordered. The amine peaks observed at 3450 cm^{-1} were associated with free, non-bonded amines. The PU-SSPCM samples that had amine peaks that were the closest to 3450 cm^{-1} were 17% and 26% PDI, which had peaks at 3321 and 3329 cm^{-1}, respectively, and 17% BICH, which appeared at 3326 cm^{-1}. These locations of these amine peaks indicated that these samples had very low levels of phase separation. However, the C=O peaks of these samples were not in agreement. Overall, all of the

samples displayed relatively similar C=O peaks, which does tell us much about the level of phase mixing in the samples.

The appearance of shoulder peaks is an indicator that phase mixing is prevalent in the sample. Shoulder peaks were observed at slightly higher frequencies, and they were related to the free and non-bonded amine and carbonyl groups. All of the PDI HS PU-SSPCM samples with 26, 30, and 40% HSC had shoulder peaks (Fig. 6.3). The series of samples prepared with an HS BICH showed relatively broad NH peaks due to the overlapping of the free and bonded amine groups (Figure 6.1). Therefore, no distinct shoulder peak could be identified. The appearance of broad peaks suggested that high level of phase mixing was prevalent in the series of HS BICH PU-SSPCMs. For the series of PU-SSPCMs prepared with HMDI HS, only 30% HMDI had a shoulder peak at 3400 cm^{-1}(Fig. 6.2), and 40% HMDI did not show a shoulder peak at all. Therefore, it can be concluded that the numbers of free amines in 17, 26, and 40%HMDI were not significant enough to be detected by DSC. The reason these samples did not display a shoulder peak could be explained in two ways, i.e., 1) 40%HS HMDI had the longest HS length and easily was able to form strong hydrogen bond interactions and 2) the samples prepared with 17 and 26% HSC mostly like had HS lengths that were less than the minimum length required to form hydrogen bonds. Therefore, IR did not detect any amine groups, because the HS was present in the samples at such low concentrations. This also can be seen by the low intensity of the amine and C=O.

6.3.2. THERMOGRAVIMETRIC ANALYSIS (TGA)

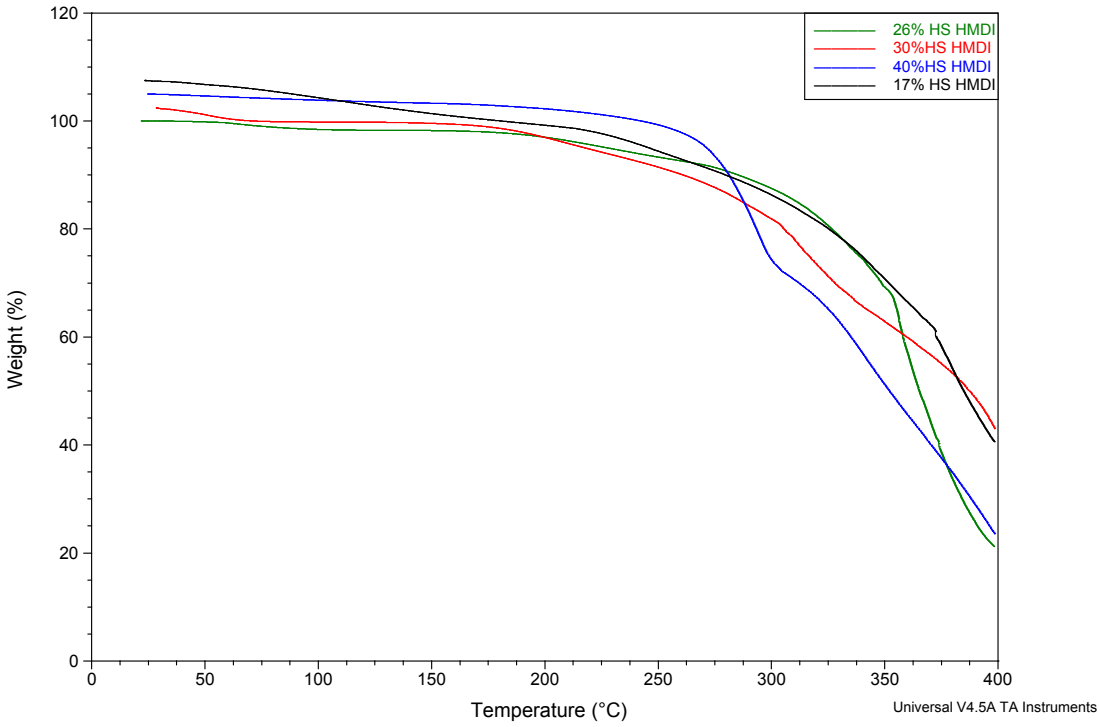

Figure 6.6: Overlay of TGA Scans for 17%, 26%, 33% and 40% HSC prepared with HMDI

The samples listed in Table 6.1 were heated to 400 ˚C at the rate of 20 ˚C/min to measure their thermal stabilities. The TGA curves presented in Figure 6.3 – 6.6, and describe the thermal degradation properties of the PU-SSPCM prepared with HMDI, PDI, and BICH HS diisocyanates, respectively. DSC experiments involve heating samples to a homogeneous melt at 250 ˚C. Details of the degradation temperatures are summarized in Table 6.4. Therefore, prior to conducting DSC experiments, it was important to determine whether the samples would remain thermally stable up to 250 ˚C.

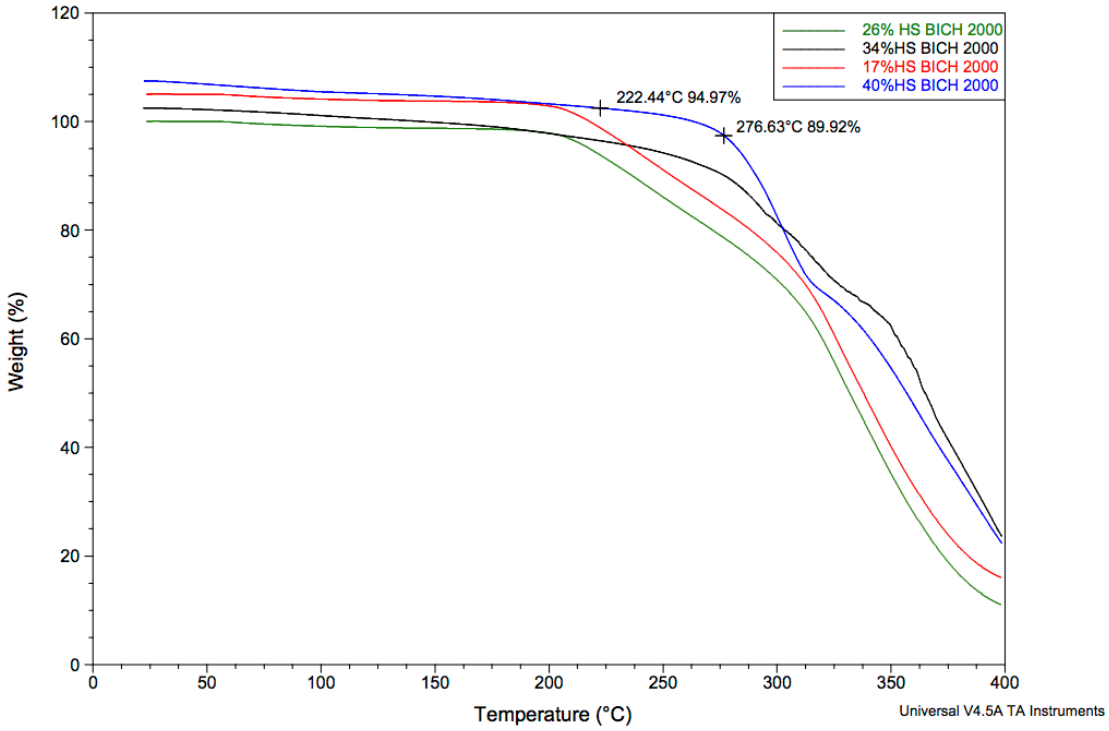

Figure 6.7: Overlay of TGA Scans for 17%, 26%, 33% and 40% HSC prepared with BICH

According to Table 6.4, all of the degradation onset temperatures (T_o) were above 250 ˚C. Therefore, it was concluded that the prepared PU-SSPCM samples were thermally stable at 250 ˚C and could endure the DSC experiments.

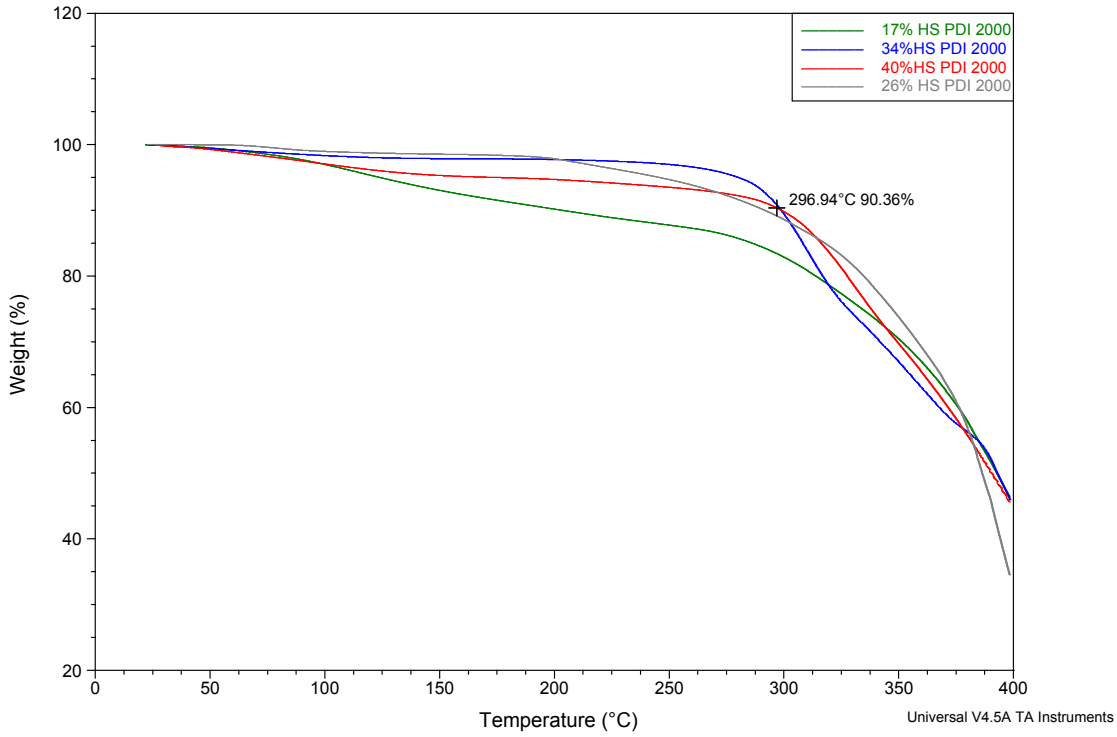

Figure 6.8: Overlay of TGA Scans for 17%, 26%, 33% and 40% HSC prepared with PDI

Table 6.4: Summary of Thermal Degradation Properties from TGA Scans to 400˚C/min

PU-SSPCM Sample	T_o[a] (˚C)	T_I[a] (˚C)	T_{II}[a] (˚C)	% Mass loss[a]	% Total Mass loss[b]
17% PDI	322.06	371.03	377.49	41.41	53.38
26% PDI	293.73	346.31	356.73	41.44	59.64
34% PDI	290.12	310.67	318.83	41.98	54.24
40% PDI	298.43	327.37	332.59	28.05	49.16
17% BICH	202.95	242.78	252.83	22.53	87.85
26% BICH	252	304.63	315.34	31.12	77.43
34% BICH	269.95	291.58	271.95	31.72	73.35
40% BICH	200.1	300.7	306.53	32.68	80.32
17% HMDI	290.29	340.43	351.62	41.19	63.69
26% HMDI	252	304.63	315.34	31.12	77.43
34% HMDI	266.5	292.27	310.04	26.01	54.28
40% HMDI	200.25	290.94	306.43	30.58	78.71

Generally, SPU materials undergo thermal degradation in two steps. The first step is the

degradation of the SS component, and the second step is the degradation of the HS component[52]. Figures 6.4, 6.5, and 6.6 show that, overall, the PU-SSPCMs prepared with 17% HSC and 26% HSC degraded rapidly in one step after reaching the onset degradation temperature. However, the TGA curves for PU-SSPCMs prepared with 30 and 40%HSC showed two distinct degradation steps. These results indicated that the PU-SSPCMs prepared with 30 and 40% HSC have a two-phase morphology, while the PU-SSPCM samples prepared with 17 and 26% HSC have only one phase.

6.3.3. ANALYSIS OF THERMAL PROPERTIES BY DIFFERENTIAL SCANNING CALORIMETRY (DSC)

Melting and crystallization behavior in PCM continuous phase domain

The main aim of this research was to determine the thermal energy storage properties of PU-SSPCMs with varying %HSC and %PCM concentrations. After the PU-SSPCM samples were heated to a homogenous melt, they were cooled at 20 ˚C/min to 70 ˚C. Subsequently, the samples were cooled to 0 ˚C at 2 ˚C/min and then reheated to 70 ˚C at 2 ˚C/min. The TES properties of the PU-SSPCM were approximated from the second cooling and heat cycle at a rate of 2˚C/min.

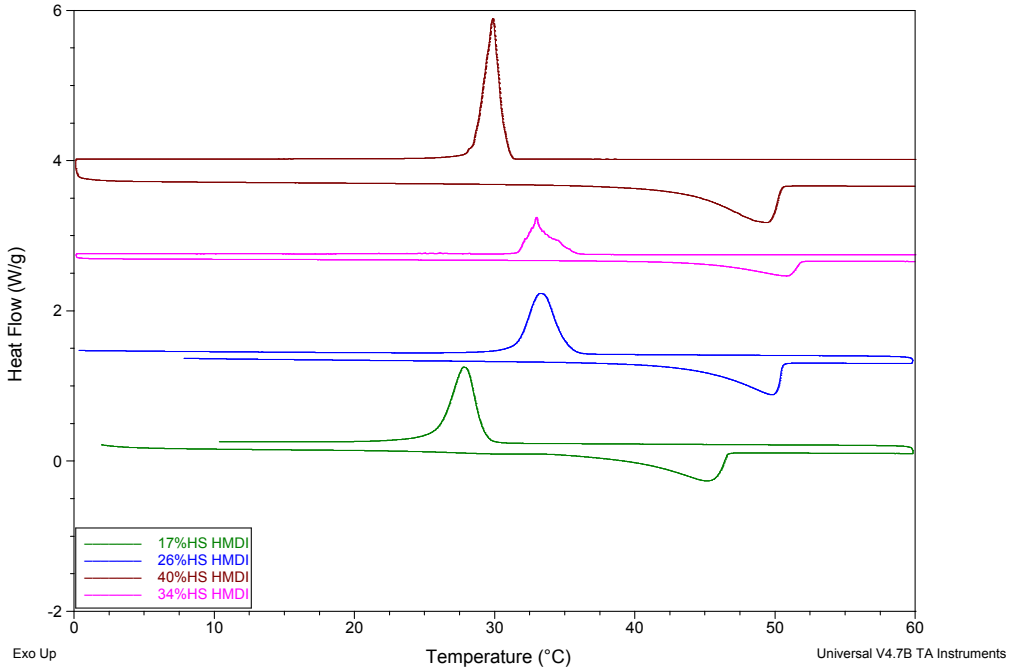

Figure 6.9: DSC Curves of PCM Domain from 17%, 26%, 33%, and 40% HMDI

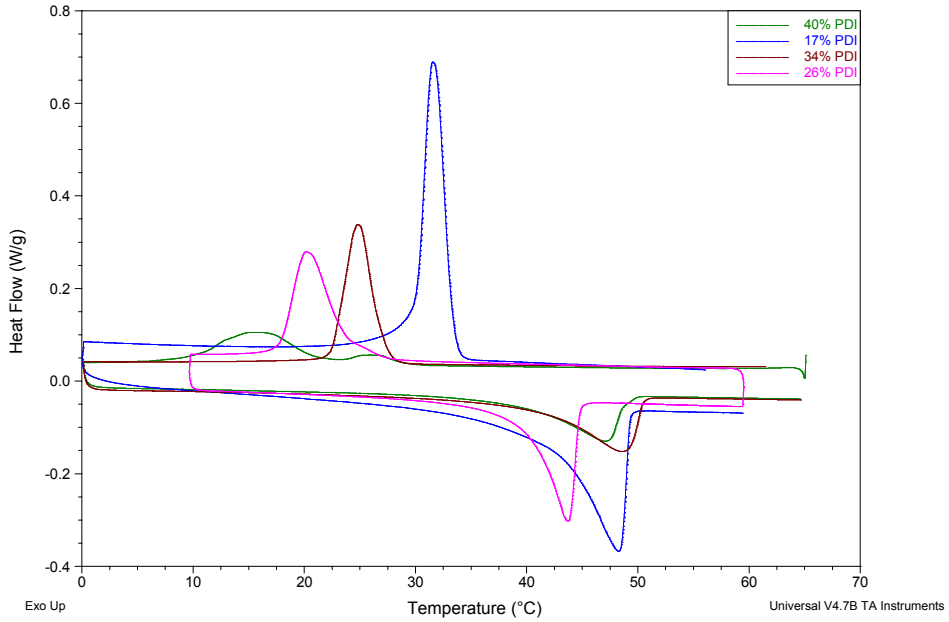

Figure 6.10: DSC Curves of PCM Domain from 17%, 26%, 33%, and 40% PDI

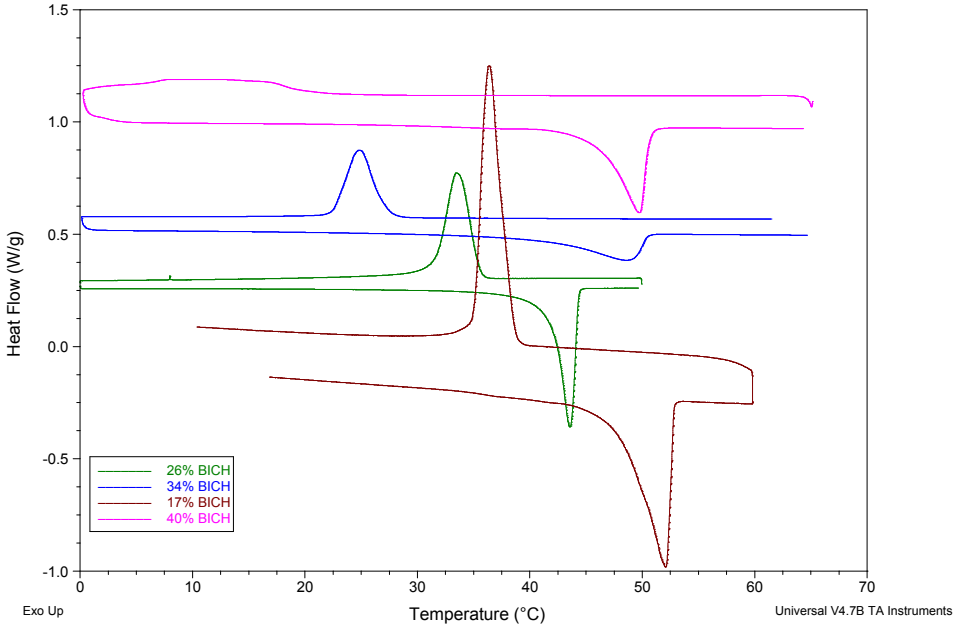

Figure 6.11: DSC Curves of PCM Domain from 17%, 26%, 33%, and 40% BICH

Table 6.5: Phase Change Properties of the PEG PCM Domain

17% HS	T_c (°C)	T_m (°C)	ΔH_m (J/g)	X_c (%)
PDI	40.51	53.88	78.98	48%
BICH	36.36	52.09	147.30	89%
HMDI	27.79	45.15	118.00	71%
26% HS	**T_c (°C)**	**T_m (°C)**	**ΔH_m (J/g)**	**X_c (%)**
PDI	21.95	44.55	55.15	33%
BICH	33.45	43.57	69.66	42%
HMDI	9.75	30.31	50.76	31%
34% HS	**T_c (°C)**	**T_m (°C)**	**ΔH_m (J/g)**	**X_c (%)**
PDI	24.79	48.58	46.34	28%
BICH	12.37	49.75	41.86	25%
HMDI	16.71	38.38	26.74	16%
40% HS	**T_c (°C)**	**T_m (°C)**	**ΔH_m (J/g)**	**X_c (%)**
PDI	16.05	47.06	40.10	24%
BICH	6.77	27.26	19.76	12%
HMDI	22.23	47.31	14.35	9%

The DSC curves shown in Figures 6.8 - 6.10 describe the thermal behavior of the PEG PCM polymer during its solid to solid phase transition as a function of %HSC. The phase transition characteristics that correspond to the crystallization and melting behaviors of the PEG PCM polymer given in Table 6.5. Thermal energy storage properties are defined by phase change enthalpies of crystallization (ΔH_c) and melting (ΔH_m), the phase transition temperatures (T_m, and T_c), and the percent crystallinity, X_c%. These values were used to interpret the crystallization behavior of the PEG PCM polymer and to provide insight concerning how %HSC relates to PU-SSPCM's heat storage capacity. T_m and T_c correspond to the peak melting and crystallization temperature and is the maximum peak temperature at which melting and crystallization occurs and were obtained by standard DSC evaluation. The melting heat of enthalpy, ΔH_m (J/g), describes

the amount of heat absorbed to destroy the ordering of the PEG chain and released to form an ordered crystalline structure. Enthalpy heat of fusion (ΔH_m) was calculated by integrating exothermic and endothermic peak area using TA analysis software. X_c represents the percentage of crystalline PEG PCM polymer chain segments that exhibit latent heat storage properties. The size of this crystalline region is represented by X_c% values, which typically are expressed as a percentage and represent the percent crystallinity of the PEG PCM. X_c% values were calculated based on ΔH_m values using the following equation: $X_c(\%) = (\Delta H_{m\text{-}PCM}/\Delta H^0_{m\text{-}PEG})*100$; where for 100% crystalline PEG, pure PEG ΔH_m was used as ΔH^0_m. ΔH^0_m values for pure PEG was obtained using the same heating and cooling rate as PEG PCM. It was important to compare enthalpy values of PCM PEG to pure PEG obtained from the same method. All enthalpy values were measured on the second heat step.

Reductions in the melt and crystallization properties are caused by the introduction of HS urethane groups to the ends of a PEG PCM polymer chain. The HS restricts the mobility of a portion of the PEG PCM polymer chain, which causes the PCM polymer to become semi-crystalline. This behavior is known as the HS chain-end effect, and the extent to which it affects PEG PCM crystallinity varies with HS composition. Due to the steric hindrance changes introduced by varying %HSC or the chain length of HS, it was predicted that modifying %HSC might provoke changes in the crystallinity (X_c%) of PEG PCM. The DSC melting and crystallization curves in Figures 6.9-6.11 indicate that, as %HSC was varied, there were changes in the intensities of the melt and crystallization peaks and in the phase transition temperature. It can be seen that the melting and

crystallization endotherms and exotherms were less prominent and appear at lower phase transition temperatures than the temperatures observed for PEG M_n = 2000 g/mol in its pure state. Figures 6.9-6.11 show that PU-SSPCM with 17%HSC exhibited much more prominent curves than PU-SSPCM with 40%HSC. This suggests that the end effect limitation of the HS chain on PEG PCM crystallization becomes more dramatic with as %HSC increases.

For the most part, the enthalpy of melt values (ΔH_m (J/g)) given in Table 6.5 indicate that the PU-SSPCMs with higher %HSC had lower ΔH_m values. The ΔH_m values for the three sets of PU-SSPCMs were compared, and the results indicated that the BICH HS produced the lowest enthalpy values and the set of HMDI PU-SSPCMs produced the highest values. Similar behavior was observed in all cases, with little or no sudden changes.

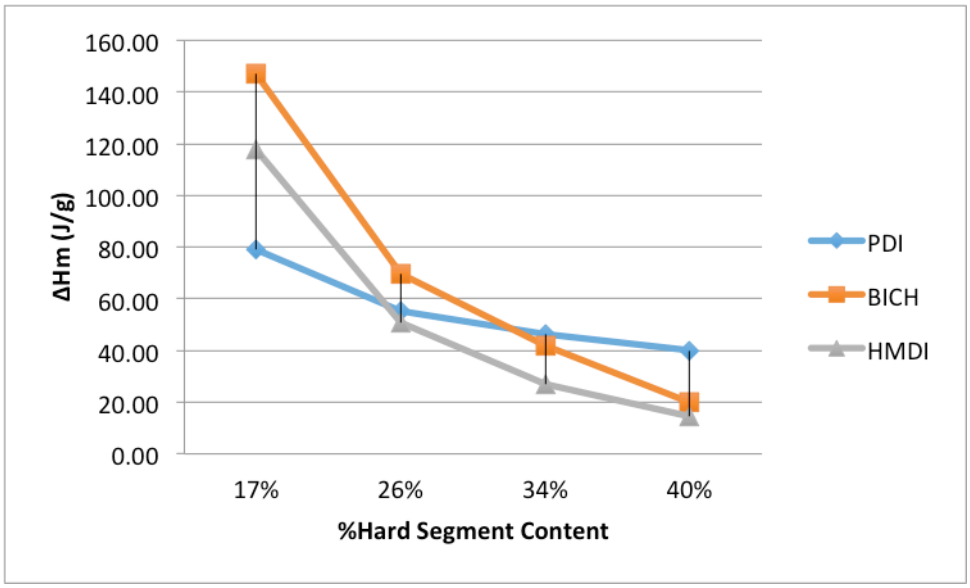

Figure 6.10: Enthalpy vs, %Hard Segment Content

The relationship between ΔH_m values and %HSC is described in Figure 6.9. The curves indicate that the PU-SSPCMs prepared with 17%HSC exhibited higher enthalpy of melt values, while the PU-SSPCMs prepared with 40%HSC demonstrated the lowest. Thus, it can be concluded that a higher %SSC and a lower %HSC lead to greater heat storage capacity because there is a higher concentration of PEG PCM chains

DSC Curves from First Heat Run

Prior to measuring the TES properties in the PCM domain, the DSC experiments included an initial heat step in which the samples were heated from -80 ˚C at 20 ˚C/min to a homogeneous melt (250 ˚C). The thermal behavior during the initial heat step provided information about the samples' phase morphologies. It is known that varying the ratio of %HSC and %SSC will alter the degree of phase separation. The DSC curves

obtained from the initial heating step are shown in Figures 6.13-6.15. According to reports in the literature, the appearance of multiple thermal transitions indicates that a level of phase mixing is present in the sample and may be observed. The level of mixing between the soft and hard phases can be determined based on the temperature at which a thermal transition is observed. Labelled as temperature region T_I, i.e., from -80 to 0 ˚C, a low temperature glass transition occurred that was attributed to the soft phase or the PCM chain. If the sample is semicrystalline, a melting transition can appear between 0 and 100 ˚C (T_{II}). This endotherm is attributed to the melting of ordered PCM soft segments. A melting transition observed between 100 and 150 ˚C (T_{III}) was attributed to phase-mixed PCM soft and hard chain segments. The hard segments may display a glass transition and/or multiple melting transitions between 150 and 250 ˚C (T_{IV}).[53]

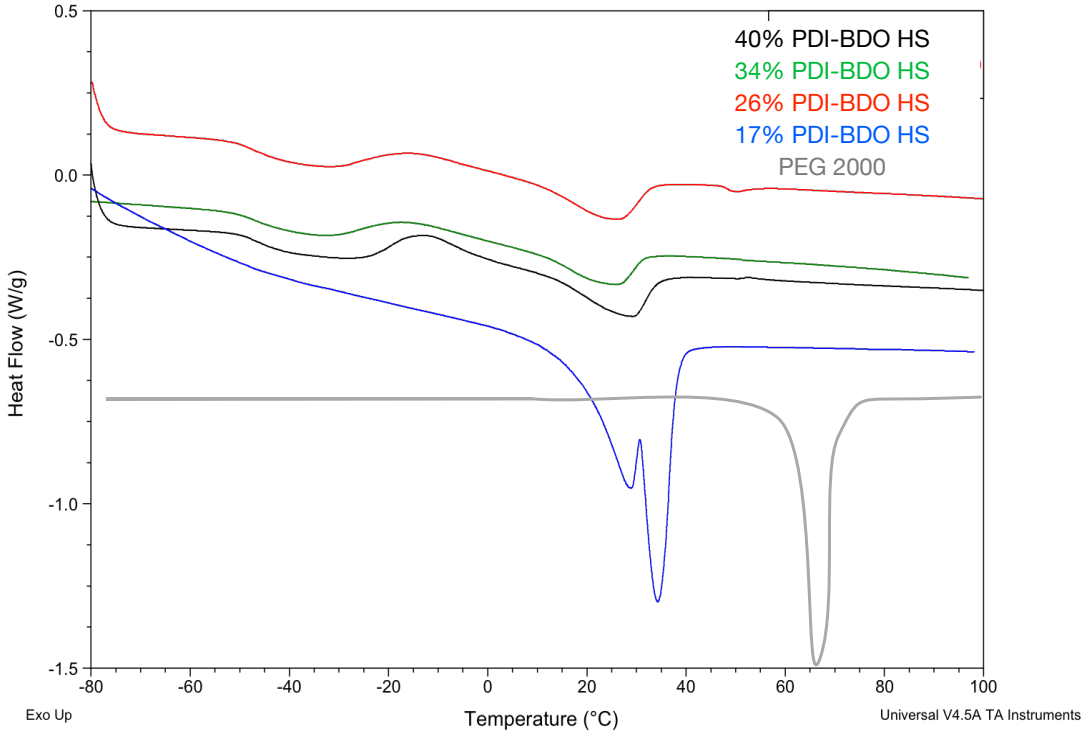

Figure 6.13: DSC Curves from Initial Heat Run of PDI 17%, 26%, 34%, 40%HSC

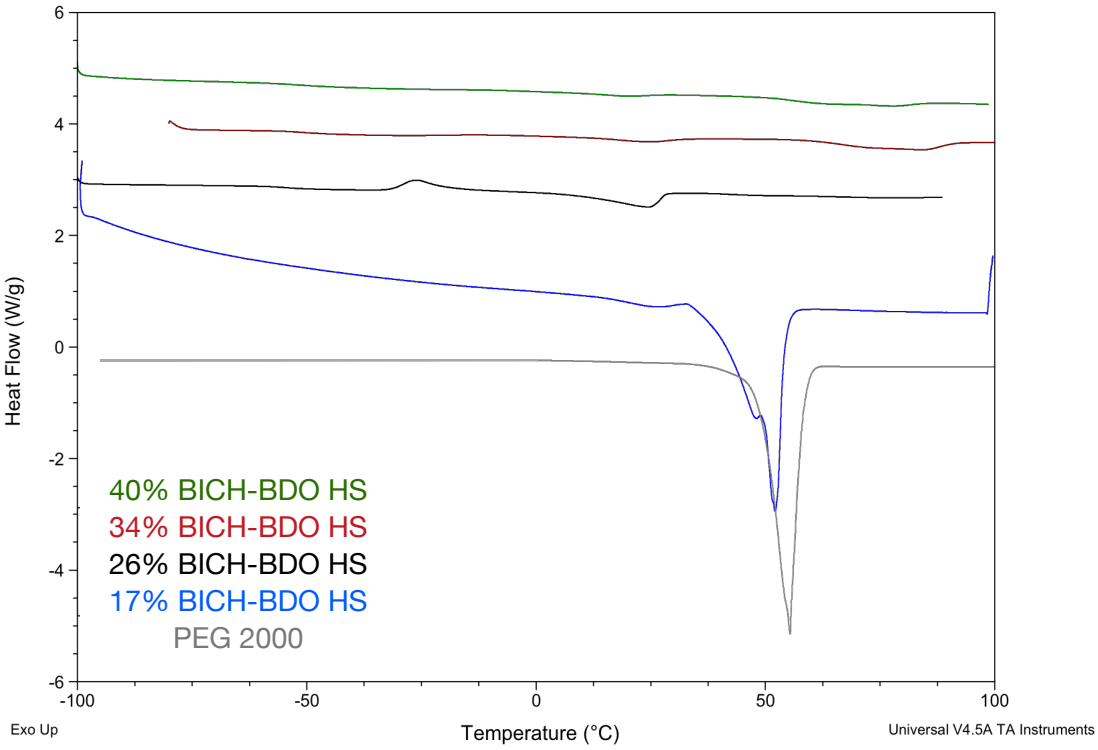

Figure 6.14: DSC Curves from Initial Heat Run of BICH 17%, 26%, 34%, 40%HSC

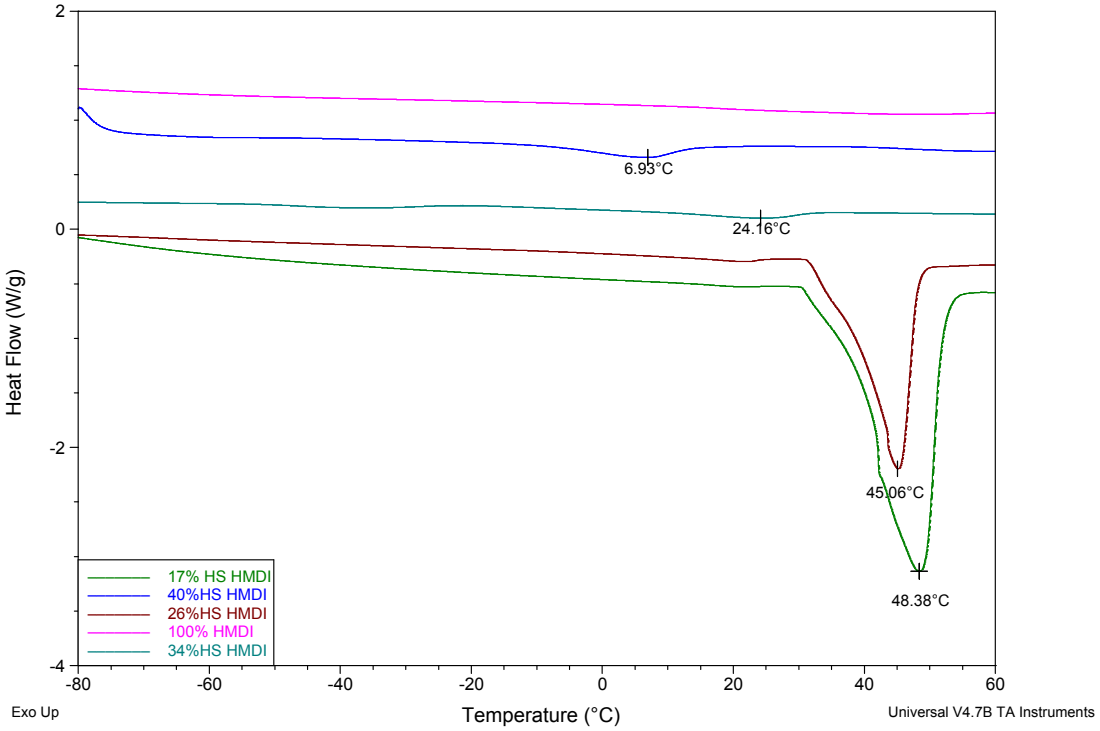

Figure 6.15: DSC Curves from Initial Heat Run of HMDI 17%, 26%, 34%, 40%, & 100% HSC

Table 6.6: Thermal Properties from the Initial Heat Run

	[a]T_g (˚C)	[b]T_g (˚C)	[c]T_g (˚C)	[d]ΔC_p (J/g ˚C)	[e]$T_{I,PCM}$ (˚C)
17% PDI	-78.19	-74.12	-52.13	1.310	34.34
26% PDI	-51.23	-46.49	-42.10	0.3573	26.11
34% PDI	-51.14	-47.39	-41.63	0.3906	25.47
40% PDI	-49.98	-47.73	-43.68	0.2793	28.93
17% BICH	15.32	19.6	20.49	1.045	52.04
26% BICH	6.74	18.6	20.49	0.6204	24.09
34% BICH	4.43	16.22	14.16	0.3494	19.27
40% BICH	-58.79	-54.87	-50.71	0.3086	24.27
17% HMDI	--	--	--	--	48.39
26% HMDI	5.72	17.36	20.95	0.4055	45.06
34% HMDI	-52.29	-46.71	-42.31	0.3622	24.16
40% HMDI	-70.96	-69.69	-64.13	0.1591	6.93

Glass Transition Temperatures [a: Tg -onset, b: Tg midpoint, c: Tg end]

d: ΔCp, baseline shift, size of region of non-crystalline PEG PCM chain units, e: Tm1, first endotherm,

f: $\Delta Cp/\Delta Cp^{\circ}$ level of phase mixing, ΔCp° = 1.54 J/(g˚C) from B. Ellis, Smith, Ray (2009). Polymers—A Proper

It can be seen in Figures 6.12-6.15, that a majority of PU-SSPCMs prepared with %HSC greater than 26% displayed multiple thermal transition. This suggests that there is a level of phase mixing present in these samples. Some variation in the curves between PU-SSPCM %HSC can be seen, which implies that the level of phase mixing in the samples vary with %HSC. An overlay of initial heat curves for a series of HMDI PU-SSPCM prepared %HSC that ranged from 0 to 100% HMDI-BDO HSC is displayed in Figure 6.12. In this figure, the evolution of a two-phase system can be seen. For lower %HSC the curves displayed thermal characteristics that resembled the PEG PCM curve; for higher %HSC high temperature HS endothermic peaks were observed. concentration of HS is varied. The appearance of an endothermic peak between 0 and 70 ˚C was observed in all of the curves except the 100%HS HMDI curve. This endothermic peak was attributed to the melting ordered PEG PCM chain segments.

Details of the initial heat thermal transitions are listed in Table 6.6. It is evident that the glass temperature of the PCM polymer is proportional to the concentration the %HSC. The samples with higher PCM concentrations displayed endothermic peaks at temperatures closer to 65 ˚C, which is the peak transition temperature at which 100% pure PEG PCM homopolymer displayed its melting transition. The DSC Curve for the PU-SSPCMs prepared with 17%HSC demonstrated a melting transition peak similar to the melting peak observed for the PEG homopolymer. Due to the HS chain-end effects, the intensity of the melting peak and the melting temperature decreased as %HSC increased.[9] The sample with 100%HS HMDI displayed only one endothermic peak at150 ˚C. This peak was associated with the destruction of HS ordering. The appearance of one peak implied that this sample had only one phase. Therefore, this confirmed that this sample did not contain any PCM PEG copolymer and was 100% HMDI and BDO HS. The appearance of multiple endotherms indicated that some level of phase separation was present in the sample, and these endotherms are shown in Figures 6.9 - 6.11 for the PU-SSPCMs prepared with 30 and 40%HSC. These DSC results were qualitatively similar to the results obtained in earlier structure-property studies of conventional PU materials[50,140-142].

Based on the data in Table 6.6, higher temperature glass transitions was observed for lower %HSC, while the opposite was observed for 40%HSC PU-SSPCMs, which demonstrated that there were low-temperature glass transitions below 0 ˚C. This suggested that lower %HSC or shorter HS chain lengths had a higher level of phase mixing because the Tg was merged with the hard-phase Tg. Also, considerable

differences in glass transition steps between samples with 17 and 40%HSC are shown in Figures 6.12 - 6.14. It is evident that, for the PU-SSPCM prepared with 17% HSC, the glass transition was broader and more ill-defined. %HSC was increased, the glass transition temperature was lower, and the baseline shift became more prominent. According to the Fox copolymer equation, increasing the HS steric restrictions on the chain mobility of the soft segment polymer chain causes the PU to demonstrate a glass transition at higher temperatures. It also increases the size of the non-crystalline amorphous region and leads to a more prominent baseline shift, ΔCp, at glass transition. Therefore, the broadening of the Tg can be attributed to phase mixing of the HS and PCM soft phases, and this suggests that samples with lower %HSC that were prepared with bulkier aromatic diisocyanates have a higher level of phase mixing than the PU-SSPCMs prepared with greater than 30%HSC and HMDI.

DSC Discussion

Table 6.7: Calculated values for approximating the HS Chain end effect and the confinement effect

	ΔC_p (J/g °C)	$\Delta C_p/\Delta C^\circ_p$	ΔH_m (J/g)	$\lvert\Delta H\rvert$	X_c (%)	$\lvert X_c$ (%)$\rvert$
17% PDI	1.310	0.8506	78.98	86.02	48%	52%
17% BICH	1.045	0.6786	147.30	17.70	89%	11%
17% HMDI	--	--	118.00	47.00	71%	29%
					0%	
26% PDI	0.3573	0.2320	55.15	109.85	33%	67%
26% BICH	0.6204	0.4029	69.66	95.34	42%	58%
26% HMDI	0.4055	0.2633	50.76	114.24	31%	69%
					0%	
34% PDI	0.3096	0.2536	46.34	118.66	28%	72%
34% BICH	0.3494	0.2269	41.86	123.14	25%	75%
34% HMDI	0.3622	0.2352	26.74	138.26	16%	84%
					0%	
40% PDI	0.2793	0.1814	40.10	124.9	24%	76%
40% BICH	0.3086	0.2004	19.76	145.24	12%	88%
40% HMDI	0.1591	0.1033	14.35	150.65	9%	91%

To approximate how the HS chain end effect varies with %HSC or HS length |ΔH| values were calculated. The magnitude of reduction in melt enthalpy values after HS are introduced can be expressed as: |ΔH| = |100% Crystalline PEG - ΔHm,PCM|. Theoretically, |ΔH| can be used to describe the degree to which PEG PCM crystallization is limited by HS chain end effects as it quantifies the portion of non-crystalline amorphous PEG PCM chain. Xc% values represents the PEG PCM polymer percent crystallinity and can be used to describe the size of the crystalline region. Equation 11 These values are given in Table 6.7: |ΔH| is the magnitude difference in the melt enthalpy of between the PU-SSPCM PEG PCM polymer (ΔHm,PCM) and a 100% pure crystalline state (ΔHm, PEG). |ΔH| essentially accounts for the non-crystalline PCM chain segments. Based on |ΔH|, the extent to which the crystallization of a PCM PEG polymer chain in the PCM continuous phase is limited by the HS steric constrictions can be approximated.

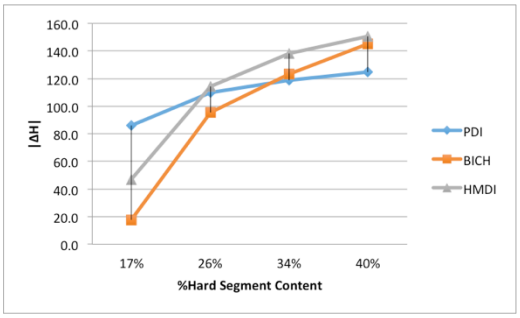

Figure 6.16: HS Chain end effect by |ΔH| vs. %HSC

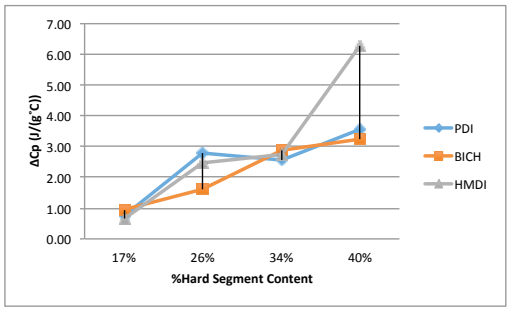

Figure 6.17: Size of PCM non-crystalline region: ΔC_p vs. %HSC

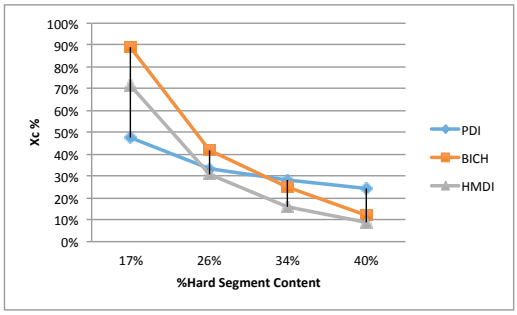

Figure 6.18: Size of PCM Crystalline Region: X_c% vs %HSC

According to the calculated |ΔH| values, the HS chain end effect is more prominent for longer hard segments or greater %HSC. In Figure 6.16, |ΔH| is plotted vs. %HSC to illustrate how the the HS chain end effect relates to %HSC or HS length. Overall, similar

behavior was observed for all PU-SSPCMs with respect to diisocyanate component. It is evident that the HS chain effect is more prominent with increasing %HSC.

PCM chain segments immobilized by phase mixing do not participate in cooperative motion. Therefore, ΔC_p values do not include the phase mixed non-crystalline PCM chains. Because, ΔC_p only represent the non-crystalline PEG chain that are directly affected by HS chain end effects, using ΔC_p value to approximate the HS chain end effect is a more accurate method than using $|\Delta H|$ values, which only accounts for crystalline PCM chains. Because ΔC_p values represent only the PEG PCM chain units restricted by HS chain effects and not immobilized by the HS phase it is theoretically possible ΔCp values could be used to evaluate the chain-end effect

It can be seen in Table 6.5, that with increasing %HSC, ΔC_p values were higher. This indicates that short/longer HS chain lengths exhibit stronger/weaker chain end effects. It can be seen that the crystalline region becomes smaller with increasing %HSC. The opposite is seen for the size of the non-crystalline region; As for ΔC_p, these values increased with higher %HSC, which indicates the size of the PCM non-crystalline amorphous region, increased with higher %HSC.

Assuming X_c% represents the size of the PCM crystalline region, Figure 6.18 illustrates how the size of the crystalline region relates to %HSC. On the other hand; the size of the amorphous region (ΔC_p) relates to %HSC is displayed in Figure 6.. From the comparison of Figure 6.. and Figure 6., it can be seen that the size of the crystalline region and the size of the non-crystalline region are inversely proportional. The increase in the size of the amorphous region suggests that the HS Chain effect is stronger for longer HS

Considering, $|\Delta H|$ and ΔC_p both represent the size of the non-crystalline region, it is evident from the comparison of Figure 6. and Figure 6., the two don't follow identical patterns. While both values show and overall increase with higher %HSC, it is apparent $|\Delta H|$ values deviates from the same path as ΔC_p. The difference in behavior indicates that $|\Delta H|$ is represents not only non-crystalline PCM chain segments hindered by the HS chain end effects, but also the PCM chains that are immobilized because they are dispersed in the hard domain phase. This difference provides compelling evidence demonstrating that PCM crystallization is limited by more than one factor and not just the HS steric restrictions.

Approximation of the degree of phase separation to determine if phase mixing is limiting PCM crystallization

It is known that varying %HSC will dramatically change a PU's phase morphology. However, it is unknown whether phase mixing limits PCM crystallization or whether the limitation on crystallization is only attributed to the HS chain-end effect.

To determine the effects of phase mixing behavior on PCM PEG crystallization, the level of phase mixing was approximated by the ratio between $\Delta C_p / \Delta C^{\circ}_p$. It is evident that the level of phase mixing decreases with higher %HSC. Therefore, it is inferred PEG PCM crystallization is also limited by phase mixing and not just HS restrictions. This result is in corroboration with previous literature. [150] The comparison of the level of phase mixing between the three sets of PU-SSPCMs: BICH, HMDI and PDI PU-SSPCM, it can be seen that each exhibit their own distinct level of phase mixing. Both BICH and PDI PU-

SSPCMs demonstrated higher levels of phase mixing $\Delta C_p/\Delta C°_p$ than HMDI PU-SSPCM. It is likely that since both BICH and PDI are aromatic diisocyanates, they impart greater rigidity to the HS, which will slow down the rate of phase separation. In chapter 5, it was found that PU-SSPCMs HS made with bulkier, aromatic, and structurally irregular diisocyanates tend to exhibit less organized and well-defined phase separated morphologies. Therefore, the results seem to indicate that because BICH molecular structure is bigger and more structurally irregular than PDI, its molecular geometry caused the BICH PU-SSPCM to demonstrate greater phase mixing.

In all three cases, a dramatic change in phase mixing was observed between samples with 17 and 26%HSC. A similar behavior was observed in Figure 6.. A measurable increase in $|\Delta H|$ was observed when %HSC was increased from 17 to 26%. These results strongly seem to suggests that 17% and 26%HSC are below the critical length. Therefore, it could be inferred that the %HSC was below the critical sequence length and this may have this caused select PU-SSPCMs prepared with 17%HSC and 26%HSC to not exhibit a solid-to-solid phase transition. These trends are consistent with the previously discussed initial heating curves, in which the 17%HSC samples showed curves that closely resembled homopolymer. Shorter HS lengths can become trapped in the soft phase that causes to material to behave and exhibit the same properties as its soft polymer component. These results are consistent with the micro domain phase model developed by Koberstein.[36,49] *(*see Figure 6.1*)* Koberstein's model states that when a HS chain length is below the critical HS segment length, the HS will remain dissolved in the soft segment matrix because it is not long enough to form hydrogen-bonded HS crystallites. As a result, the

soft segment chain dominates the PU's final properties[141]. Nonetheless, even though the PU-SSPCMs prepared with 17%HSC and 26%HSC demonstrated extraordinary heat storage capacity, because these samples did not exhibit a solid to solid phase transition, it is not effective and should not be considered.

The comparison of Figure 6.8 to Figure 6.10, which shows how heat storage capacity relates to %HSC indicates both the the level of phase mixing and heat storage capacity decreased with higher %HSC. This pattern of behavior shows that 1) a higher level of phase separation led weaker heat storage capacity and 2) A higher %HSC or HS length also gave rise to weaker thermal energy storage properties. However, on account of the evidence that a second effect limiting PEG PCM crystallization caused by phase mixing is introduced, we cannot yet conclude how the degree of phase separation impacts thermal energy storage properties.

6.4.CONCLUSION

In conclusion, it was found that a greater reduction in enthalpy of melt values was observed in addition to lower percent crystallinity ($\%X_c$). Therefore, from these results it may be concluded that the magnitude to which the chain-end effect impacts thermal energy storage properties is linked to the length of the HS. These results further indicated that higher HS concentration leads to less heat storage capacity and that HS length must be above 26% to demonstrate a solid-to-solid phase transition. Samples prepared with 17% HS content demonstrated exceptional heat storage capacity, however these materials demonstrated a solid-to-liquid phase transition. Therefore, it may be concluded that the

HS length must be above the critical length to demonstrate a solid-to-solid phase transition.

In conclusion, it was found in chapter 4 and 5 that varying chain end effects by the nature of the HS cross-link and HS diisocyanate composition caused a change in final thermal energy storage properties. In this chapter, it was proven the HS chain-end effects can also be varied by %HSC or HS length. DSC results clearly showed that shorter HS lengths limited PCM PEG chain crystallization to a lesser extent than longer or higher %HSC. It was also observed that with varying %HSC, the degree of phase separation present in the samples differed, which caused a change in final thermal energy storage properties. Unlike the previous chapters, which only considered the limitation the HS chain end effect has on PCM crystallization, it was found that the level of phase mixing impacts X_c% the size of the PEG PCM crystalline region, in addition to HS chain end effects. Determination of the direct connection between HS chain-end affect and PCM crystallization as a function of HS chain length lead to the finding of a secondary limiting effect on PCM crystallization brought on by phase mixing. Furthermore, the results also indicated that there is a minimum HS length necessary for the PEG PCM polymer to demonstrate a solid-to-solid phase transition. In addition to that is was found that phase mixing and HS chain end effects both can play a role in determining final thermal energy storage properties

Chapter 7 KINETICS OF HARD SEGMENT CRYSTALLIZATION AND THERMAL ENERGY STORAGE PROPERTIES

7.1.INTRODUCTION

It is known that the degree of phase separation is equally kinetically driven, as it is thermodynamically.[36,55] The development of the hard segment crystalline structure depends on intermolecular interaction between chains and the time allotted for crystallization to occur. Slower cooling rates allow better-packed, more perfect hard segment crystalline to form. Highly crystalline hard segment will enhance the exclusion

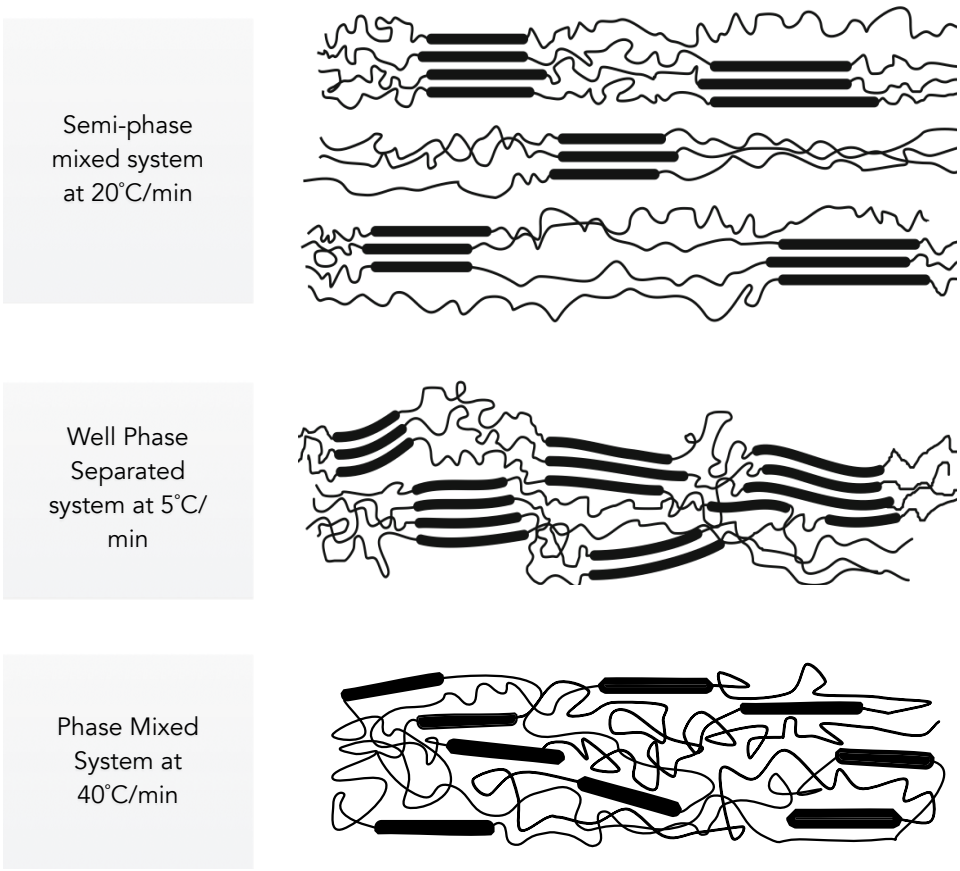

Figure 7.1: Schematic of Phase Morphology after being cooled at 5, 20, and 40 ˚C/min.

of soft segment chains to produce well-defined phase domain structures. [61,63]

In chapters 4, 5 and 6, the variable factors studied were related to HS composition. For the PU-SSPCM samples studied thus far, the kinetics of phase separation was kept constant by cooling all samples at 20˚C/min from 250˚C. This was done in order to study the individual effects of the HS variable factor of interest. Thus far, the results from the previous chapters show that varying the HS composition by its diisocyanate component or by HS concentration does introduce different limitation on PEG PCM crystallization through the HS chain end effect. However, in addition to that it was also observed that the level of phase separation in the sample also varied according to HS compositions. Therefore, it was unclear if the level of phase separation in addition to HS chain end restrictions, plays a role in limiting PCM crystallization. To clarify this, in this chapter the relationship between thermal energy storage properties and the degree of phase separation in PU-SSPCMs was investigated.

A few authors studying conventional polyurethane materials have demonstrated a link between the degree of phase separation and percent soft segment crystallinity. Hood[61] studied the effect of the confinement of hard segment crystallinity on soft segment crystallinity and found that slow cooling rates produced a greater reduction in soft domain crystallinity than quench cooling because the highly crystalline hard segments enhanced the restriction of the motion of the soft segment chain, resulting in fewer active soft segment PEG chains for crystallization. Korley[45] observed lower soft segment crystallinity for polyurethanes with minimal phase mixing between soft segment chains and urethane hard segments. This suggested the primary limitation to SS crystallization is

domain confinement, which inhibits the growth of large, well-ordered SS crystallites. From this literature, it can be assumed that a highly-crystalline hard segment and well-defined phase separation promote the confinement effect, which leads to a greater decrease in the capacity to store thermal energy.

However, Petrovic[37] attributed the limit on crystallization to the HS chain-end effect in a system in which the phases were not mixed. Based on previous claims in the literature, there is a possibility that the confinement effect, also plays a role in limiting PCM crystallization, which then shows that the level of phase separation does play a role in determining the thermal energy storage properties of PU-SSPCMs and should be considered as a main factor in the development of these materials. To the best of our knowledge, the correlation between the degree of phase separation and the thermal energy storage properties exhibited by thermoplastic SSPCMs has yet to be studied. This chapter explores the role that the degree phase separation has in determining the thermal energy storage properties in PU-SSPCMs. Figure 7.1 schematically shows the difference in phase morphologies when cooled at a 5 ˚C/min, 20 ˚C/min, and 40 ˚C/min. The samples cooled at 5˚C/min is expected to have the highest degree of phase separation. It can be seen that in a well-phase-segregated structure that all of the PEG PCM chains are in prime position to align and crystallize since they are localized into one confined area. In s semi- phase mixed, and highly phase mixed structure the presence of HS dispersed in the PCM phase domain acts as an impurity and will disrupt PCM crystallization.[37] Therefore, it is predicted that samples cooled at 5 ˚C/min and will exhibit the best heat storage capacity. However, as phase-segregation increases, the PCM phase domain

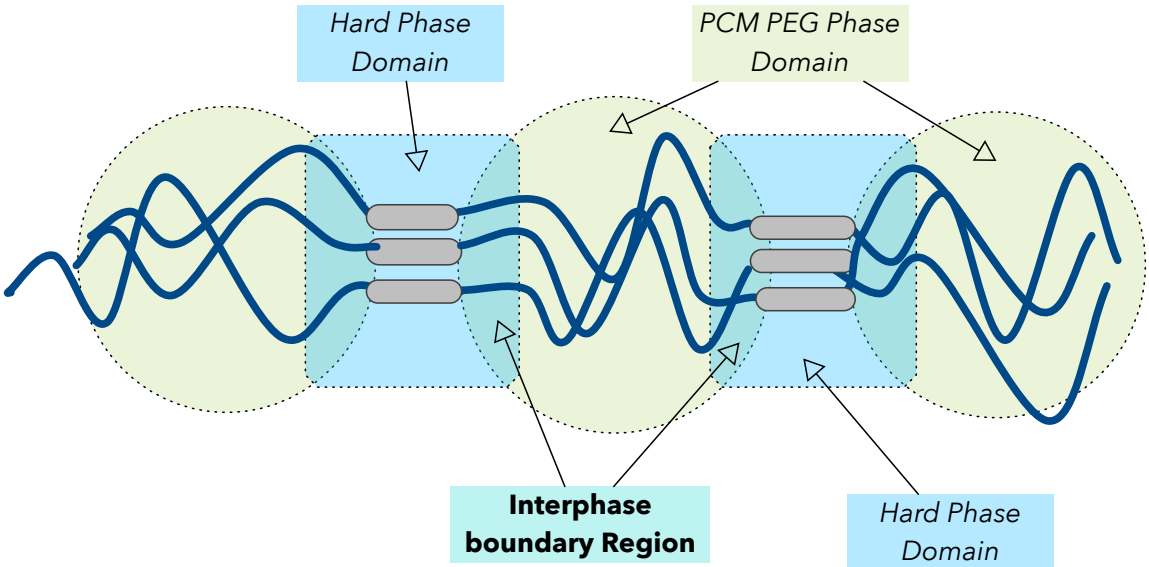

Figure 7.2: Graphic Image represents of the Interphase boundary region between the PCM and Hard Segment Phase.

region. As illustrated in Figure 7.2, the interphase region acts as a boundary region between the hard and PCM continuous phases and consists of the hard and PCM mixed phases. The PCM chain segments dispersed in the interphase region are immobilized by the hard segment chain. However, the dispersed PCM chain segment do not participate in cooperative motion, only the non-crystalline PCM chain segments restricted by the HS chain end can be seen at glass transition[37,52,150]. With the introduction of the non-crystalline PCM chain segments from the interphase region and the non-crystalline PCM chain segments from the HS chain end effects , the limitation on PCM crystallization is doubled, which leads to a greater decline in thermal energy storage properties.

In this chapter, DSC analysis was used to measure the thermal energy storage properties of a PU-SSPCM with a high, semi, and low level of phase mixing. A slow, medium, and fast cooling rates were used control HS crystallization; the perfection of HS crystalline structure directly dictates the degree of phase separation in the sample. From the

information about the confinement effect and how it limits PCM crystallization, and may affect thermal energy storage properties in PU-SSPCMs was obtained.

7.2.EXPERIMENTAL

7.2.1. FABRICATION OF SAMPLES

The samples that were prepared in chapter 5 were used in this study. Therefore, all samples were prepared as linear PU-SSPCMs with 40%HSC. A PEG PCM polymer with a molecular weight of 2000 g/mol was used as the PCM polymer. All samples were prepared by the same fabrication steps that were followed in Chapter 5, and these steps are described in greater detail in Chapter 3. In order to ensure significant confinement of the PEG PCM polymer crystallization, it was necessary to meet three conditions, i.e., a greater volume fraction of HS to SS, a highly-crystalline HS (a HS with a high Tg), and good separation of the HS and SS. The list of samples studied is given in Table 7.1. Because the same samples studied in Chapter 5 were used in this chapter, we know that

Table 7.1: List of Samples Studied

HS Diisocyanate:	[Nomenclature]		
	5°C/min	20°C/min	40°C/min
1,6-Diisocyanatohexane (HMDI)	**HMDI:** 5	**HMDI:** 20	**HMDI:** 40
1,12-Diisocyanatododecane (DIDD)	**DIDD:** 5	**DIDD:** 20	**DIDD:** 40
2,4-Tolylene Diisocyanate (TDI)	**TDI:** 5	**TDI:** 20	**TDI:** 40
1,4-Phenylene Diisocyanate (PDI)	**PDI:** 5	**PDI:** 20	**PDI:** 40
1,3-Bis(isocyanatomethyl)cyclohexane (BICH)	**BICH:** 5	**BICH:** 20	**BICH:** 40
4,4'-Methylenebis(phenyl isocyanate)	**MDI:** 5	**MDI:** 20	**MDI:** 40

the structure and synthesis already have been confirmed by FTIR analysis, and all of these samples demonstrated a solid-to-solid phase transition (Chapter 5).

7.2.2. ANALYSIS OF THERMAL ENERGY STORAGE PROPERTIES BY DSC EXPERIMENTS

A two-part DSC experiment was conducted. The first part involved creating a homogenous melt by heating the sample to homogeneous melt state. The samples were subjected to HS recrystallization at cooling rates of 5, 20, and 40 ^{o}C /min. The medium cool rate of 20 ˚C/min allowed enough time for the samples to establish a level of domain organization, but also some level of phase mixing. A cooling rate of 40 ˚C/min was the closest rate to quench cooling that our DSC instrument could provide.

7.3.RESULTS

The effects of the different cooling rates on the crystallinity of the PCM domain was analyzed. The DSC experiments showed HS crystallization and the subsequent cooling and melting behavior of the PCM polymer after being subjected to slow, medium, and fast cooling regimes of 5, 20, and 40 ˚C/min, respectively. A cooling rate of 40 ˚C/min was the closest rate to quench cooling that the DSC instrument could produce.

7.3.1. DSC CURVES OF PCM DOMAIN

The overlay of DSC curves shown in Figures 7.2-7.7 shows the melting and crystallization behavior of the prepared PU-SSPCM samples cooled at 5, 20, and 40 ˚C/min from a homogeneous melt state. The endothermic and exothermic peaks displayed

were different for each cooling regime in terms of shape, height, and width.

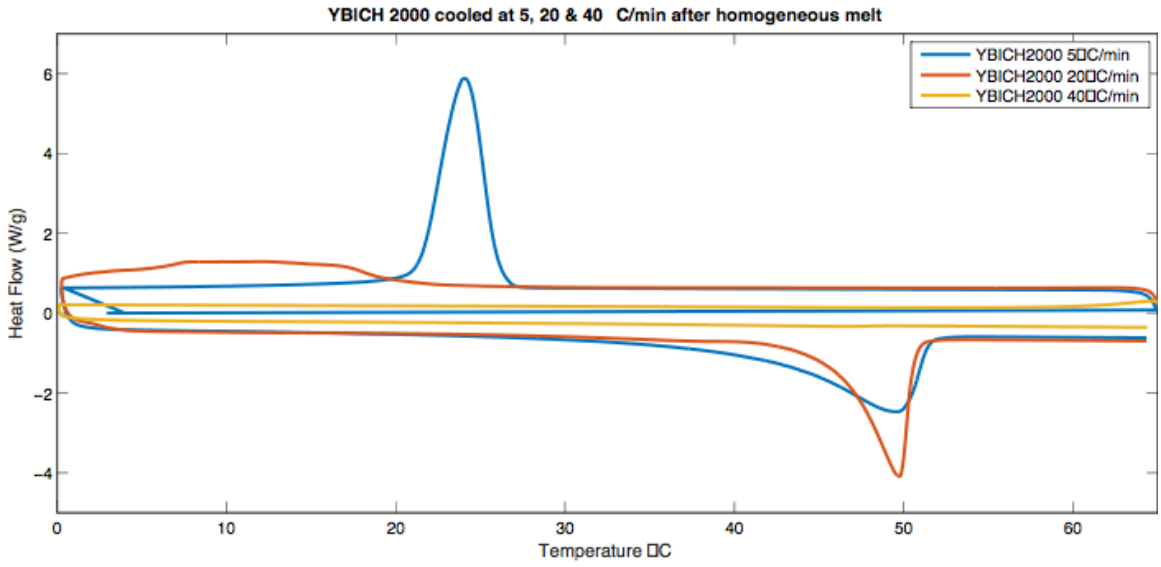

Figure 7.3: DSC Curves showing the melting and crystallization of the PEG PCM domain of YBICH after 5˚C/min, 20˚C/min and 40˚C/min cooling regimes

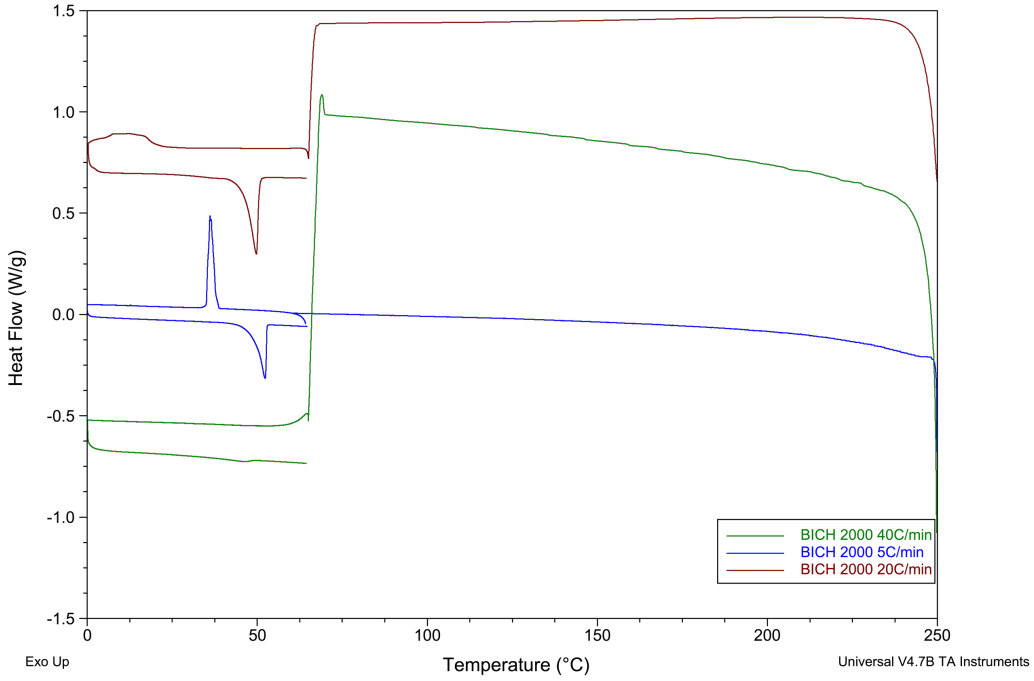

The overlay of DSC curves shown in Figure 7.3 shows the melting and crystallization behavior of the PEG PCM component of Y-BICH PU-SSPCM after cooling at the homogeneous melt rates of 5, 20, , and40 ˚C/min. The shapes, heights, and the widths of the endothermic and exothermic peaks were varied for each cooling regime. A prominent, uniform crystallization peak was observed for the slowest cooling regime (5 ˚C/min). An increase in width and a decrease in intensity were observed as the cooling rate increased to 20 ˚C/min. The opposite pattern was seen in the endothermic peak; the sample cooled at 5 ˚C/min had a weaker endothermic peak than the sample cooled at the medium rate of 20 ˚C/min. The DSC curve for the Y-BICH 2000 sample cooled with the fastest cooling

rate, i.e., 40 ˚C/min, displayed no endothermic or exothermic peak, which indicated that no crystallization or melting behavior occurred.

Slow cooling rates allow more time for the PEG chain to self-associate and organize into a more thermodynamically favorable position to crystallize. Therefore, the prominent crystallization peak observed for Y-BICH cooled at 5 ˚C/min was linked to the higher-ordered PEG chains. Consequently, the broad exothermic peak observed for Y-BICH cooled at 20 ˚C/min could be attributed to the PEG chains having less time to organize.

DSC curves generated for Y-BICH 2000 cooled at 40 ˚C/min displayed no crystallization or melting peaks. At a cool rate of 40 ˚C/min, the melt viscosity increased quite quickly, such that the PEG PCM chain segments and the -[BICH-BDO]- hard segments did not have time to segregate into self-associations, so they remained in a dissolved state in the vitrified polymer matrix.

A cooling rate of 40 ˚C/min allowed the least amount of time for PEG chain ordering. At such a rapid cooling rate, the sample became frozen in a homogeneous, melt-like state in which the PEG chains were miscible with the urethane hard segments. The high degree of phase mixing immobilized and obstructed PEG chain ordering. This explains why no endothermic and exothermic peaks were observed in the DSC curve for Y-BICH cooled at 40 ˚C/min.

However, the melting peaks observed for Y-BICH cooled at 20 ˚C/min and 5 ˚C/min showed the opposite behavior. The endothermic peak observed for Y-BICH cooled at 5 ˚C/min was weaker and broader than the sample cooled at 20 ˚C/min. This suggested that a too-high degree of phase separation could adversely affect PCM crystallization.

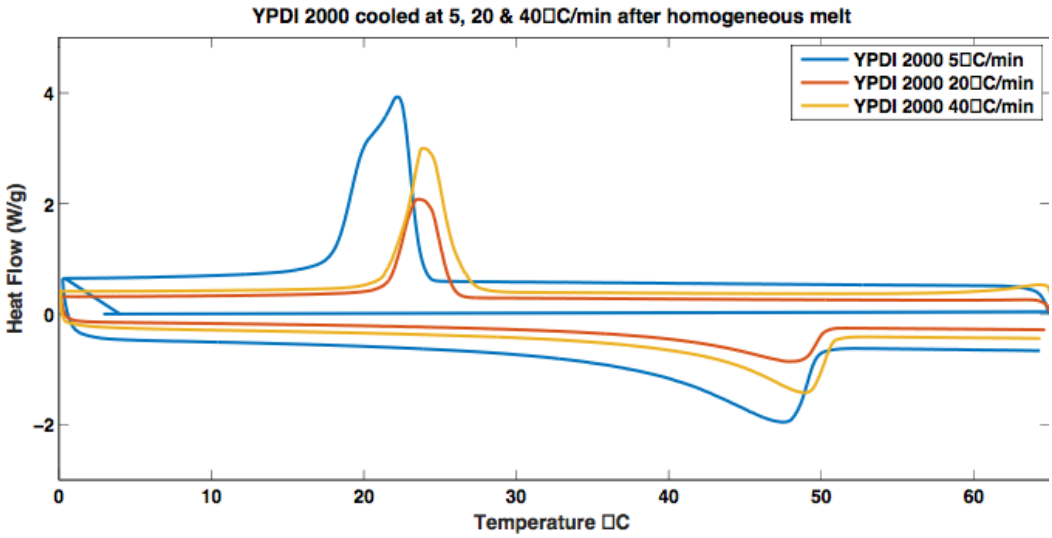

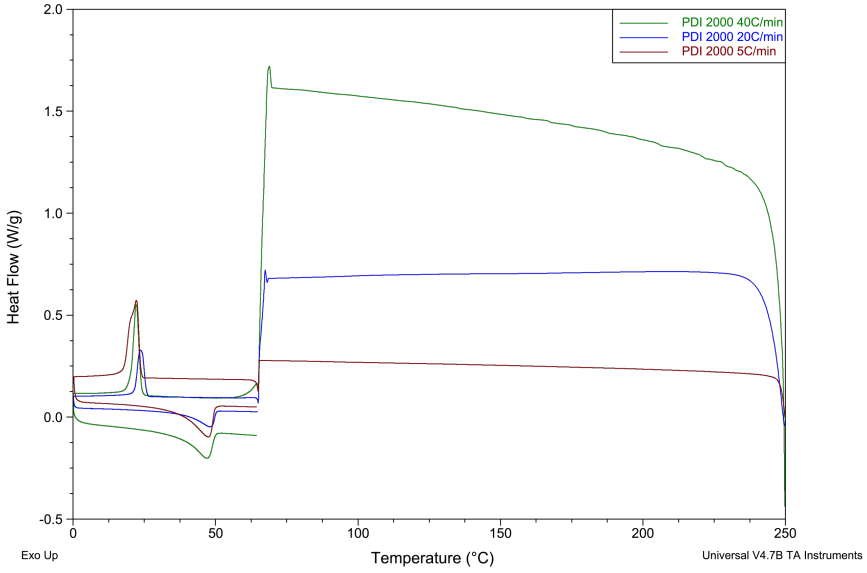

Figure 7.4: DSC Curves showing the melting and crystallization of the PEG PCM domain of YPDI after 5˚C/min, 20˚C/min and 40˚C/min cooling regimes

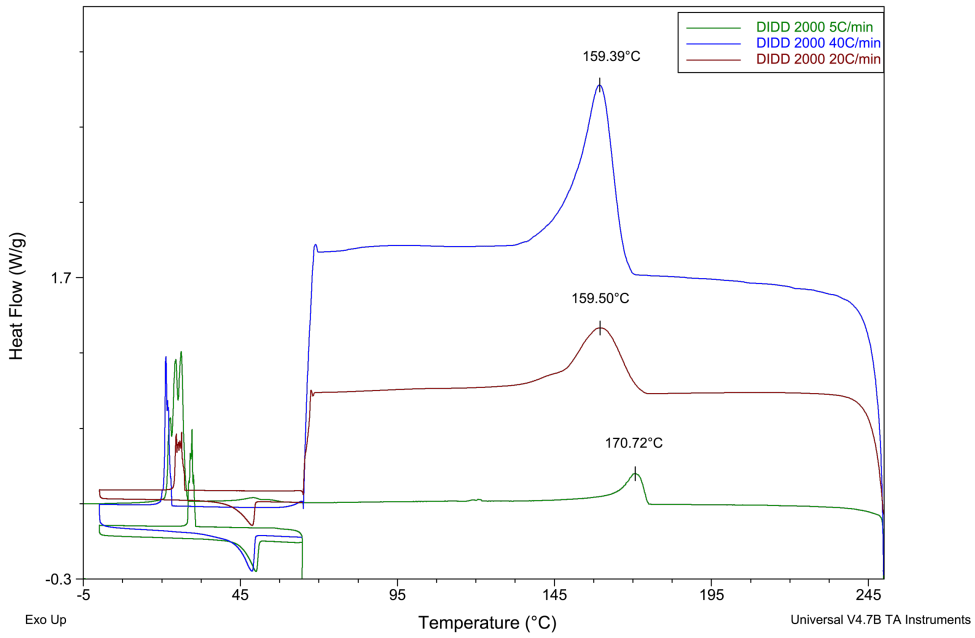

Figure 7.5: DSC Curves showing the melting and crystallization of the PEG PCM phase domain in DIDD PU-SSPCM cooled at 5, 20, and 40 ˚C/min

Figure 7.5 shows the overlay of DSC curves for DIDD PU-SSPCM cooled at 5, 20, and 40 ˚C/min. The comparison of crystallization curves show that the most prominent and uniform crystallization peak was observed at the slowest (5 ˚C /min) and the fastest cooling rates (40 ˚C/min). Contrarily, the opposite was observed for the melting transition. DIDD cooled 20 ˚C/min exhibited the most prominent, and uniform melting peak, followed by DIDD cooled at 5 ˚C/min. The melting transition of DIDD cooled at 40 ˚C/min showed a dramatic decrease in intensity.

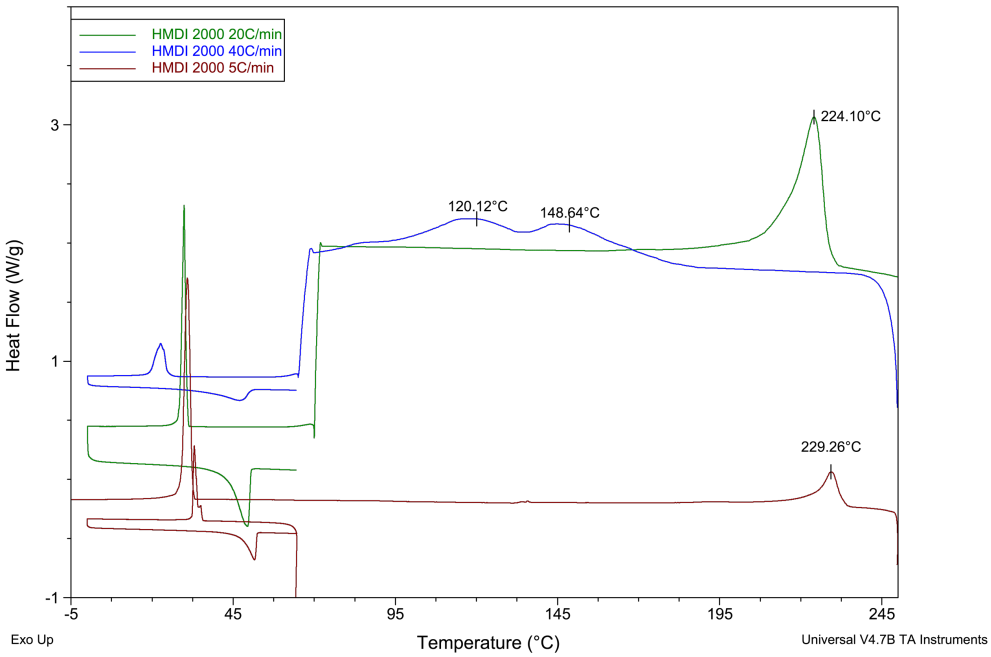

Figure 7.6 DSC Curves showing the melting and crystallization of the PEG PCM domain of YHMDI after 5˚C/min, 20˚C/min and 40˚C/min cooling regimes

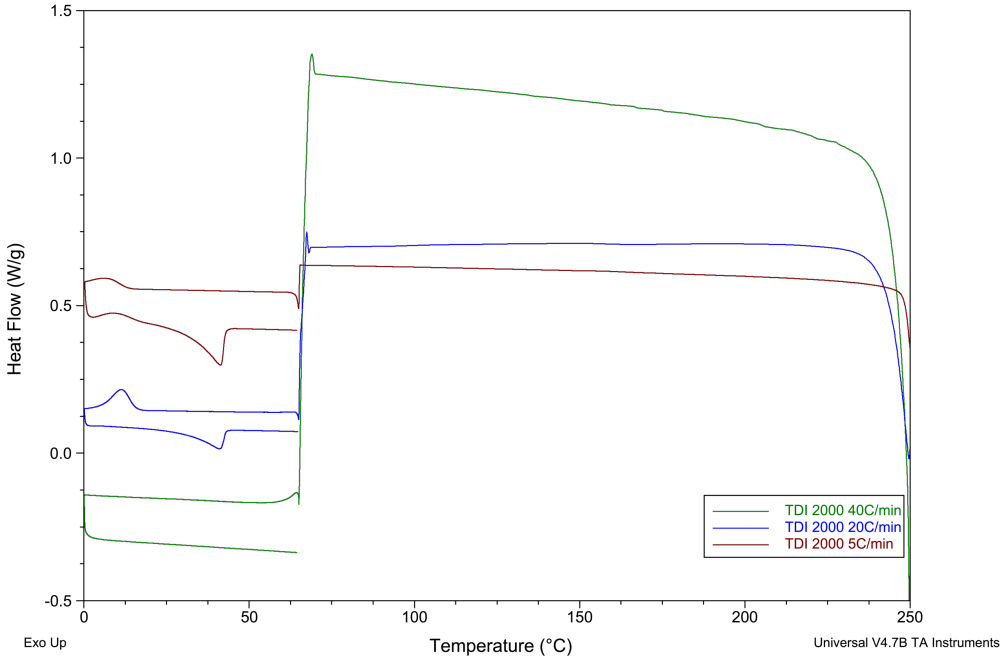

Figure 7.7: DSC Curves showing the melting and crystallization of the PEG PCM domain of YTDI after 5˚C/min, 20˚C/min and 40˚C/min cooling regimes

For Y-TDI 2000, the crystallization peaks observed for the rates of 5 and 20 ˚C/min were both broad, and both displayed low peak intensity (Figure 7.7). The sample runs were programmed to only cool to 0 ˚C, but it was apparent that the TDI sample that was cooled at 5 ˚C/min was not fully crystalized. No crystallization peak at all appeared for the TDI sample cooled at

Table 7.2: Summary of Phase Change Characteristics Following Cooling Regime Treatments

	T_c (°C)	T_m (°C)	ΔH_m (J/g)	X_c (%)
BICH 5°C/min	36.10	52.33	48.55	29%
HMDI 5°C/min	33.04	51.57	49.7	30%
PDI 5°C/min	22.18	47.54	41.29	25%
TDI 5°C/min	7.34	41.37	35.58	22%
DIDD 5°C/min	29.60	49.97	48.44	29%
BICH 20°C/min	6.77	27.26	19.76	12%
HMDI 20°C/min	22.23	47.31	14.35	9%
PDI 20°C/min	16.05	47.06	40.10	24%
TDI 20°C/min	6.77	27.26	19.76	12%
DIDD 20°C/min	26.29	48.75	51.37	31%
BICH 40°C/min	0.00	0	0.00	0%
HMDI 40°C/min	28.61	45.19	49.89	30%
PDI 40°C/min	23.90	48.9	44.48	27%
TDI 40°C/min	0.00	0	0.00	0%
DIDD 40°C/min	21.31	48.69	39.54	24%

40 °C/min, and this explains the absence of an endothermic peak. The TDI sample cooled at 5 °C/min had the most prominent endothermic peak, and it was much narrower than the analogous exothermic peak. The sample that was cooled at 20 °C/min displayed relatively similar exothermic and endothermic peaks. TDI did not follow the trend of the other samples because HS crystallization is limited by its asymmetric structure.

Overall, the cooling regime of 5 °C/min produced endothermic peaks that commonly were much broader than the exothermic peaks. Thus, it was inferred that, since this cooling regime allowed so much time for phase separation to take place, more long range ordering could occur, and this explains the formation of broad endothermic peaks.

The enthalpies of the heat and phase transition temperatures were measured by DSC analysis to estimate the thermal energy storage properties of the PEG PCM polymer. These values are summarized in Table 7.3 for each cooling rate.

According to Table 7.2, The enthalpies of heat values were marginally higher when the sample was cooled at a rate of 20 ˚C/min. The enthalpy of heat and percent crystallinity values when cooled at rates of 40 ˚C/min (49.89 J/g and 30.18%, respectively) and 5 ˚C/min (49.7 J/g and 30.07%, respectively) were about the same. The other aliphatic PU-SSPCM (DIDD) tested also showed higher enthalpy of heat and percent crystallinity when cooled at 20 ˚C/min (51.37 J/g and 31.08%, respectively). However, the same trend was not observed for the samples prepared with aromatic diisocyanates; BICH, PDI, and TDI all demonstrated the highest enthalpy values and percent PCM crystallinity (X_c%) when cooled at 5 ˚C/min.

As shown in Figures 7.2 and 7.5, BICH and TDI cooled at 40 ˚C/min displayed no endothermic or exothermic peaks. This indicate that no PEG PCM chain ordering detectable by DSC occurred, and implies that these samples exhibited zero capacity to store and release heat. It may be presumed that the rapid cooling rate and large, rigid diisocyanate structure were the underlying factors that prevented phase separation, which caused the sample to remain in a miscible, homogeneous state.

The absence of PCM domain crystallization and a melting peak was observed exclusively for aromatic diisocyanate samples cooled at 40 ˚C/min. These results indicated that no HS or PCM chain order occurred. Due to the rapid cooling rate and the rigid aromatic structure, there was not enough time for HS ordering to take place. It was assumed that this sample remained completely immiscible. The fact that all of the samples had their lowest enthalpy of heat and percent crystallinity when cooled at 40 ˚C/min may support the supposition that HS acts as an impurity in poor phase separated systems and disrupts

soft segment crystallization. Unexpectedly, upon cooling, only HMDI and DIDD displayed an HS crystallization peak between 100 and 250 ˚C (Figures 1 and 2). These results proved that the aliphatic HS self-associates to form crystallites much faster than the aromatic HS diisocyanates. The intensity of the HS crystallization peak was decreased when the slower cooling rates were used. The appearance of the HS crystallization peak is proof that these are two-phase materials.

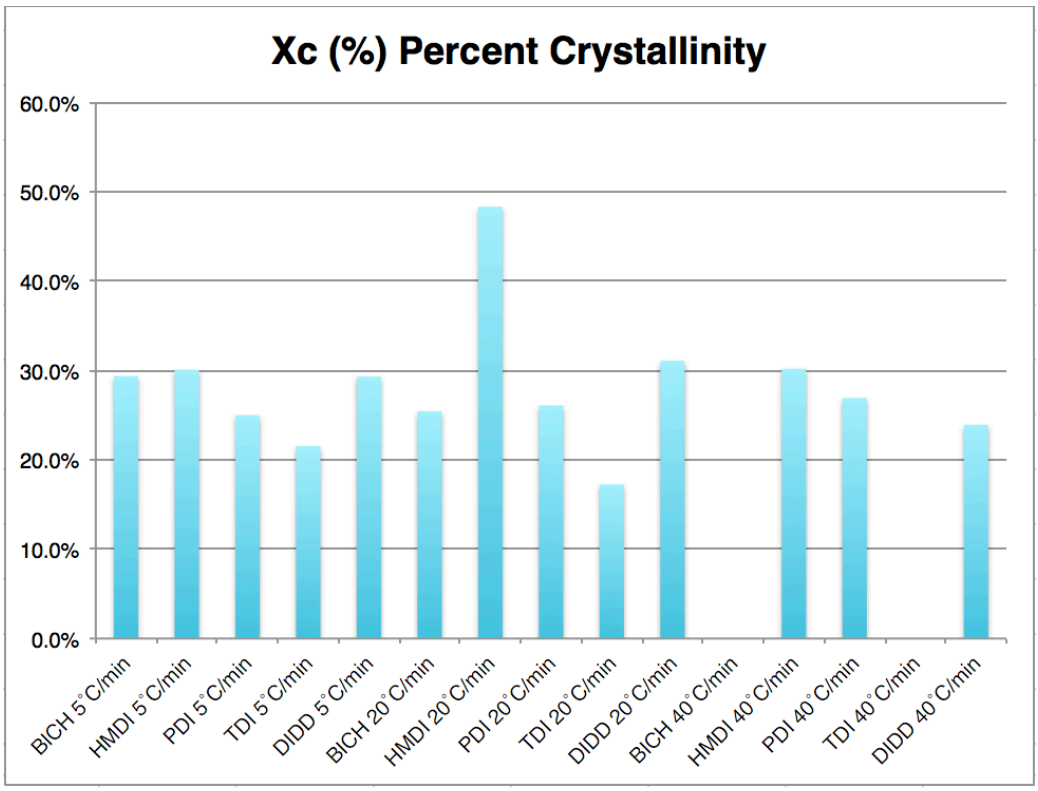

Figure 7.8: Bar graph shows the comparison of Percent Crystallinity values (%X_c) of the PEG PCM Component with respect to Cooling regimes

The thermoplastic SSPCM samples considered in this study were prepared with an aromatic and an aliphatic diisocyanate, and they demonstrated that, even with the same cooling rate, a greater degree of phase separation occurred for the aliphatic hard segment than for the aromatic segment. The flexible nature of the aliphatic diisocyanates

facilitates a more rapid diffusion of the hard segment through the soft matrix. Alternatively, the bulkiness and rigidity of the aromatic diisocyanates result in slower movement, and more time is necessary for the hard segments to self-associate. Hence, with the variation in the degree of phase separation being attributed to the diisocyanate component, it is certain that any changes observed in the measurements of the crystallinity of the soft segment originated solely from the degree of phase separation. The medium cool rate of 20 ˚c/min allowed just enough time for the samples to establish a level of domain organization, but still maintains some phase mixing after the homogeneous melt.

Overall, the cooling regime of 5 ^{o}C/min commonly displayed endothermic peaks that were much broader than the exothermic peaks. It was inferred that, since this cooling regime allows so much time for phase separation to take place, more long range ordering also is taking place, which explains why broad endothermic peaks were observed.

For all of the samples prepared with aromatic diisocyanates (BICH, TDI, and PDI), no exothermic or endothermic peaks were visible (Figs. 7.1, 7.2, and 7.6) when the cooling rate was 40 ˚C/min. The absence of peaks indicated that neither crystallization nor thermal melting processes occurred. This result can be attributed to the fact that the rapid cooling rate did not allow sufficient time for the hard segments to become ordered, and, consequently, PEG PCM chain ordering could not occur, and nitrification was observed instead; the HS and SS remained in a miscible state because the samples were cooled so fast that the thermal incompatibility between block segments did not have time to come into effect. However, the aliphatic samples (HMDI and DIDD) did display exothermic

and endothermic peaks when cooled at 40 ˚C/min. It also should be noted that only the HMDI and DIDD DSC curves showed a hard segment crystallization peak, which appeared for all cooling regimes. This indicated that, even when cooled at such a high rate, some level of HS chain ordering was obtained. These results demonstrated that, even with the same cooling rate, a greater degree of phase separation will be observed for an aliphatic hard segment than for an aromatic hard segment. The flexible nature of the aliphatic diisocyanates facilitates a more rapid diffusion of the hard segment through the soft matrix. Alternatively, the bulkiness and rigidity of the aromatic diisocyanates result in slower movement, and more time is necessary for the hard segments to self-associate. Hence, with the variation in the degree of phase separation being attributed to the diisocyanate component, it is certain that any changes observed in the measurements of the crystallinity of the soft segments are caused solely by the degree of phase separation. The comparison of the set of aromatic samples to the aliphatic samples when cooled at 40 ˚C/min indicated that there must be some level of HS chain ordering for PEG PCM crystallization to occur. From these results, it can be determined that zero thermal energy storage properties are observed for PU-SSPCMs that are completely phase-mixed.

Table 7.2 indicates that, in most cases, the samples had lower enthalpy of heat and lower percentage crystallinity values when cooled at 40 ˚C/min than when they were cooled at 5 or 20 ˚C/min. This supports the supposition that HS acts as an impurity and disrupts soft segment crystallization for systems in which the phases are poorly separated.

The HMDI and DIDD PU-SSPCM samples cooled at 5 ˚C/min were assumed to have the highest degree of phase separation because of their aliphatic structure. HMDI was

expected to have the highest degree of phase separation because it is much smaller than DIDD and can diffuse through the PEG PCM matrix much more rapidly. Decreases in the enthalpy of heat and percent crystallinity values in the samples that were cooled at 5 and 20 ˚C/min were observed exclusively for the HMDI and DIDD PU-SSPCMs. This suggested that the confinement effect limited PEG PCM crystallization and may have had an adverse effect on thermal energy storage properties. These results were in agreement with the results published by Hood and Korley. Conversely, BICH, TDI, and PDI, which were the aromatic PU-SSPCMs, demonstrated higher enthalpy and percentage crystallinity values when cooled at 5 ˚C/min. Thus, the confinement effect was not observed for the aromatic PU-SSPCMs. This may have been due to the fact that the degree of phase separation in these samples did not reach the point at which the confinement of the PEG PCM chains starts to inhibit their crystallization.

The degree of phase separation was measured by the magnitude of increase in enthalpy at T_g, the shift of the PCM glass transition step (T_{gPCM}), the shift of the HS glass transition step ($T_{g,HS}$) hard segments, and by the phase mixing ratio.

Therefore, this demonstrated that SPUs that were synthesized with aliphatic diisocyanates had greater HS flexibility, which leads to greater SS crystallinity. Narrow endothermic and exothermic peaks were observed for the aliphatic PU-SSPCMs (HMDI and DIDD), while broader peaks were observed for the aromatic diisocyanates. This indicated that the PU-SSPCMs with aliphatic diisocyanates produced highly-ordered PEG PCM chain units and had narrow phase transitions. These results were in agreement with the results published by Hood, who reported that the greater flexibility of the hard

segment improved the crystallinity of the soft segment.[61] A narrow phase change favors maximum thermal energy storage. For this reason, we can conclude that aliphatic HS PU-SSPCMs exhibit the most favorable phase change properties for thermal energy storage. This conclusion is based on the facts that the aliphatic HS leads to faster phase separation kinetics and aliphatic diisocyanates have faster phase separation kinetics and more flexible hard segments.

7.3.2. RELATIONSHIP BETWEEN THE CONFINEMENT EFFECT AND DIISOCYANATES OF THE HARD SEGMENT

From these findings, it can be concluded that both the chain-end effect and the confinement effect limit the mobility of the soft-segment chain. We presume that the initial decreases in enthalpy and melting temperature are attributable to the chain-end effect, which is occurring throughout the process, whereas the confinement effect occurs only for highly-phase-mixed systems. However, in non-phase-mixed systems, the HS is dispersed among the PCM polymer chains where it behaves as an impurity and disrupts the ordering of the PCM polymer chains. This is the reason that minimal to no melting or crystallization activity was observed when the cooling rate was 40 ˚C/min.

Based on these results, it is clear that a semi-phase mixed system is the most favorable for obtaining a PU-SSPCM that has maximum thermal energy storage properties. A semi-phase-mixed system does not exhibit the confinement effect and is phase-separated enough that the HS does not obstruct the ordering of the PCM polymer chain.

Chapter 8 CONCLUSION

The findings in Chapter 4,5,6, demonstrate that by modifying the HS composition, this altered the steric hindrance and nature of the HS. As a result, the extent to which the HS restricted PCM PEG polymer chain mobility varied accordingly. Consequently, thermal energy storage properties were affected because PCM crystallinity was suppressed by HS chain-end effects. Therefore, these findings strongly confirm previous predictions made based on the conventional PU structure-property relationships. However, in addition to that other parallel relationships, and behavioral trends were unexpectedly discovered. These trends fall in line with the systematic investigation of the structure property relationships, and should be investigated in further work.

A) It was concluded from Chapter 6, a critical HS length that is greater than >17%-26%HSC is necessary to observe a solid-to-solid phase transition. The result agreed with Koberstein's model, which claims that there is a critical HS length necessary to form physical cross-links, otherwise the material will behave and exhibit properties of the soft macro-diol component. The HS Chain end effect was quantified by $|\Delta H|$ and by ΔCp. Overall both values followed the same trend, however $|\Delta H|$ was more skewed and less consistent. It was clear that ΔCp values were consistent and were perfectly inversely proportional to the crystalline region(ΔH_m). The level of phase mixing approximated by the ratio of |$ indicated that lower %HSC had a higher level of phase mixing. It was found that PU-SSPCMs with higher levels of phase segregation exhibited lower heat storage capacity, which suggested that the confinement effect limits PEG PCM crystallization. On the other hand, the observation of lower enthalpy values could be

attributed to higher %HSC having longer HS chain lengths that reduce the range of interaction between PEG PCM chains. It is unclear which effect is responsible for limiting PCM, therefore the evidence demonstrating the confinement effect was not considered conclusive. A considerable difference in $|\Delta H|$ and ΔC_p values for 30%HSC and 40%HSC would signify that an interphase region is present in the sample. However, only a minimal difference was observed. Camberlain[150]found that ΔC_p method only works with there is definitely phase segregation. Therefore, ΔC_p values for 17% and some 26% samples were invalid. In future work, studying %HS in smaller increments between 30 and 40%HSC to find the sweet spot configuration would be interesting.

B) In chapter 7, the degree of phase separation and the connection between the confinement effect and PCM crystallization was analyzed. Unexpectedly, it was found that slowly (5˚C/min) and quenched (40˚C/min) cooled PU-SSPCMs demonstrated measurably lower enthalpy values than samples cooled at 20˚C/min. This result indicated that a semi-phase mixed PU-SSPCM demonstrates the best heat storage capacity. There results contradicted the initial prediction that a PU-SSPCM with a well-organized high degree of phase separation would exhibit the best heat storage capacity because of the pure phase domains. There was a noticeable difference in the melting and crystallization behavior of the PCM polymer for aliphatic PU-SSPCMs compared to aromatics. Also a HS crystallization peak appeared only for the two aliphatic diisocyanates considered, DIDD and HMDI. This indicated that the aliphatic diisocyanates can rearrange and phase separate at a substantially faster rate than the other diisocyanates. Aromatic PU-SSPCMs cooled at 40˚C/min did not even show a melting or crystallization peak. This indicated

the HS and PCM phase were completely miscible and prevent the crystallization of wither block segment. It was apparent the decline in PCM crystallinity for the samples cooled at 5˚C/min that was attributed to confinement effect. This result proved that a high degree of phase separation will limit PCM crystallization. In future work, it would be interesting to study cooling regimes between 20˚C/min and 40˚C/min to determine the optimal degree of phase separation. Furthermore, the results from chapter 7 demonstrated that not only factors that influence the HS chain-end effect, but also the confinement effect should be taken into account since it was shown that both limit PCM crystallization. Future work|# problem no quantitative theory of the confinement effect. Need to study individual levels.

C) In chapter 5 the results indicated that HS with aliphatic, structurally regular, and symmetric diisocyanate components led to higher enthalpy values and phase transition temperatures.

D) In chapter 4, PU-SSPCMs were prepared with a series of PEG molecular weights. It was found that the phase transition temperatures and enthalpy values were proportional to PEG molecular weight. This result showed that TES properties can easily be tailored by changing the PCM molecular to match a certain temperature condition, which opens up a broad range of potential applications in which these materials potential can be applied. Thus, PU-SSPCMs could be used. However, a molecular weight threshold was observed when PCM PEG MW was increased higher than > 4600-6000 g/mol. Below the molecular weight threshold a marked increase in ΔHm values with higher PEG MW was observed, however after the MW threshold ΔH values plateaued and the change in ΔH

values for higher MW PEG polymer become appreciably less. It was found that above the threshold molecular weight, PEG chains form entanglements that disrupt its crystallization. On the other hand, it was also found that there is a critical molecular weight, or length the PCM polymer chain must be to crystallize. However, the necessary length is dependent on HS composition and its restriction on attached PCM chains. For the PU-SSPCMs prepared PEG 2000g/mol the ones made with MDI and TDI demonstrated zero PCM melting or crystallization behavior. This indicated that PEG 2000 was below the critical length to crystallize and that the HS chain end effect restricted the chain mobility of the entire PCM polymer. It was apparent that due to MDI's bulky, aromatic structure and TDI's aromatic, asymmetric structure that these structural feature exhibit stronger HS chain end effects. It was concluded that diisocyanates with similar structural features should be avoided in order to obtain a PU-SSPCM with maximum thermal storage capacity.

Also, in chapter 4, it was found that non-linear chemically cross-linked PU-SSPCMs demonstrated greater heat storage capacity than the linear physically cross-linked PU-SSPCMs. From Chapter 4 results, it was evident from the results that the extent to which the chain end effect decreases soft segment crystallinity differs not only between chemically and physically cross-linked samples but also between samples prepared with different diisocyanates. However, he linear PU-SSPCMs were all prepared with 40 wt% HS and were cooled at 20˚C/min. In chapters 5-7, it was revealed that factors such as diisocyanate structural features, %HSC, and cooling rate can alter PCM crystallization. Therefore, it is possible modifying these parameters could increase PCM crystallinity to

be higher than non-linear PU-SSPCM. Therefore, it is evident the results from chapter 4 were not conclusive after considering other factors. In future work, it would be interesting to study other types of chemical cross-links such as a multi-functional chain extender.

Slight discrepancies in values are a possibility and are a consequence of synthesis. Obtaining a perfect polymer repetitively is almost impossible. Hence, any values that were slightly skewed were ignored, as long as the general trend was followed. The values obtained for most of the samples were within reasonable ranges. Slight discrepancies in values are a possibility and are a consequence of synthesis.

Overall, it was found that these types of PU-SSPCMs did not meet the criteria necessary to be used effectively in building applications, because such applications would require the PU-SSPCM to exhibit an enthalpy of 100 J/g or higher and demonstrate a phase transition temperature at human-comfort temperatures (18-30 ˚C). The majority of the PU-SSPCMs considered in this work had enthalpy values less than or near 100 J/g, and most of them had phase transition temperatures that were significantly higher than human-comfort temperatures.

Our study is significantly different from prior work because our research approach treats PU-SSPCMs as a polyurethane material that exhibits thermal energy storage properties. Whereas, other literature has focused only on PCM aspect and did not consider the other possible factors that were affecting their results. Our results are encouraging in that it demonstrated the profound impact PU chemical and physical factors can have on a PU-

SSPCMs thermal energy storage properties. Overall, this work exposed the variety of structure-property relationships that can be modified to provide changes in TES properties. It also broadens the possibilities for developing new PU-SSPCMs in the future.

Chapter 9 : References

(1) Zhang, Y.; Zhou, G.; Lin, K.; Zhang, Q.; Di, H. Application of Latent Heat Thermal Energy Storage in Buildings: State-of-the-Art and Outlook. *Building and Environment* 2007, *42* (6), 2197–2209.

(2) Tyagi, V. V.; Buddhi, D. PCM Thermal Storage in Buildings: a State of Art. *Renewable and Sustainable Energy Reviews* 2007, *11* (6), 1146–1166.

(3) Cabeza, L. F.; Castell, A.; Barreneche, C.; de Gracia, A.; Fernández, A. I. Materials Used as PCM in Thermal Energy Storage in Buildings: a Review. *Renewable and Sustainable Energy Reviews* 2011, *15* (3), 1675–1695.

(4) Sharma, A.; Tyagi, V. V.; Chen, C. R.; Buddhi, D. Review on Thermal Energy Storage with Phase Change Materials and Applications. *Renewable and Sustainable Energy Reviews* 2009, *13* (2), 318–345.

(5) Outlast Technologies, Inc. Fabric Coating Composition Containing Energy Absorbing Phase Change Material. US Patent Office May 5, 1997.

(6) van Langenhove, L.; Textile Institute (Manchester, England). *Smart Textiles for Medicine and Healthcare*; CRC, 2007.

(7) ZHAN, Y.; ZHU, P.; ZHAO, X. The Application of Temperature Regulating Textile Using Phase-Changing Material. *Textile Dyeing and Finishing Journal* 2007.

(8) Lencer, D.; Salinga, M.; Wuttig, M. Design Rules for Phase-Change Materials in Data Storage Applications. *Adv. Mater.* 2011, *23* (18), 2030–2058.

(9) Dheep, G. R.; Sreekumar, A. Phase Change Materials—a Sustainable Way of Solar Thermal Energy Storage. In *Energy Sustainability Through Green Energy*; Springer India: New Delhi, 2015; pp 217–244.

(10) Farid, M. M.; Khudhair, A. M.; Razack, S. A. K.; Al-Hallaj, S. A Review on Phase Change Energy Storage: Materials and Applications. *Energy Conversion and Management* 2004, *45* (9-10), 1597–1615.

(11) Morgan, T. World Energy Outlook 2009 Factsheet. 2010, 1–6.

(12) International Energy Agency. *Energy-Efficient Buildings: Heating and Cooling Equipment*; IEA Publications : Paris, 2011; pp 1–56.

(13) DOE, U. S. *Buildings Energy Data Book: 2011*; 2010; Vol. 3, pp 44–55.

(14) Dincer, I.; Rosen, M. A. *Thermal Energy Storage*; Wiley, 2011.

(15) Liu, C.; Li, F.; Ma, L.-P.; Cheng, H.-M. Advanced Materials for Energy Storage. *Adv. Mater.* 2010, *22* (8), E28–E62.
(16) Zalba, B.; Marín, J. M.; Cabeza, L. F.; Mehling, H. Review on Thermal Energy Storage with Phase Change: Materials, Heat Transfer Analysis and Applications. *Applied Thermal Engineering* 2003.
(17) Lai, C.; Chen, R. H.; Lin, C. Y. Heat Transfer and Thermal Storage Behaviour of Gypsum Boards Incorporating Micro-Encapsulated PCM. *Energy & Buildings* 2010.
(18) Kuznik, F.; David, D.; Johannes, K.; Roux, J.-J. A Review on Phase Change Materials Integrated in Building Walls. *Renewable and Sustainable Energy Reviews* 2011, *15* (1), 379–391.
(19) Zhu, N.; Ma, Z.; Wang, S. Dynamic Characteristics and Energy Performance of Buildings Using Phase Change Materials: a Review. 2009, *50* (12), 3169–3181.
(20) Chen, C.; Liu, W.; Yang, H.; Zhao, Y.; Liu, S. Synthesis of Solid–Solid Phase Change Material for Thermal Energy Storage by Crosslinking of Polyethylene Glycol with Poly (Glycidyl Methacrylate). *Solar Energy* 2011, *85* (11), 2679–2685.
(21) Khudhair, A. M.; Farid, M. M. A Review on Energy Conservation in Building Applications with Thermal Storage by Latent Heat Using Phase Change Materials. *Energy Conversion and Management* 2004, *45* (2), 263–275.
(22) Gracia, A. de; Lidia, R.; Castell, A.; Jimenez, M.; Boer, D.; Medrano, M.; Cabeza, L. F. Life Cycle Assessment of the Inclusion of Phase Change Materials (PCM) in Experimental Buildings. *Energy & Buildings* 2010, *42* (9), 1517–1523.
(23) Cao, Q.; Liu, P. Hyperbranched Polyurethane as Novel Solid–Solid Phase Change Material for Thermal Energy Storage. *European Polymer Journal* 2006, *42* (11), 2931–2939.
(24) Li, W.-D.; Ding, E.-Y. Preparation and Characterization of Cross-Linking PEG/MDI/PE Copolymer as Solid–Solid Phase Change Heat Storage Material. *Solar Energy Materials and Solar Cells* 2007, *91* (9), 764–768.
(25) Jiang, Y.; Ding, E.; Li, G. Study on Transition Characteristics of PEG/CDA Solid–Solid Phase Change Materials. *Polymer* 2002, *43* (1), 117–122.
(26) Cao, Q.; Liu, P. Crystalline-Amorphous Phase Transition of Hyperbranched Polyurethane Phase Change Materials for Energy Storage. *J Mater Sci* 2007, *42* (14), 5661–5665.
(27) Jiang, Y.; Ding, E.; Li, G. Study on Transition Characteristics of PEG/CDA Solid–Solid Phase Change Materials. *Polymer* 2002, *43* (1), 117–122.
(28) Su, J.; Liu, P. Effect of Hard and Soft Segments on the Heat Storage Properites of Polyethylene Glycol-Based Polyurethanes. *Acta Polymerica Sinica* 2007.
(29) Xi, P.; Duan, Y.; Fei, P.; Xia, L.; Liu, R.; Cheng, B. Synthesis and Thermal Energy Storage Properties of the Polyurethane Solid–Solid Phase Change Materials with a Novel Tetrahydroxy Compound. *European Polymer Journal* 2012, *48* (7), 1295–1303.
(30) Meng, Q.; Hu, J. A Poly(Ethylene Glycol)-Based Smart Phase Change Material. *Solar Energy Materials and Solar Cells* 2008, *92* (10), 1260–1268.
(31) Su, J.-C.; Liu, P.-S. A Novel Solid–Solid Phase Change Heat Storage Material with Polyurethane Block Copolymer Structure. 2006, *47* (18-19), 3185–3191.

(32) Cao, Q.; Liao, L.; Xu, H. Study on the Influence of Thermal Characteristics of Hyperbranched Polyurethane Phase Change Materials for Energy Storage. *J. Appl. Polym. Sci.* 2010, *115* (4), 2228–2235.
(33) Sarı, A.; Alkan, C.; Biçer, A. Synthesis and Thermal Properties of Polystyrene-Graft-PEG Copolymers as New Kinds of Solid–Solid Phase Change Materials for Thermal Energy Storage. *Materials Chemistry and Physics* 2012, *133* (1), 87–94.
(34) Alkan, C.; Günther, E.; Hiebler, S.; Ensari, Ö. F.; Kahraman, D. Polyurethanes as Solid–Solid Phase Change Materials for Thermal Energy Storage. *Solar Energy* 2012, *86* (6), 1761–1769.
(35) Molecular Mobility and Crystallinity in Polytetramethylene Ether Glycol in the Bulk and as Soft Component in Polyurethanes. *European Polymer Journal* 2011, *47* (11), 2120–2133.
(36) Kosc, M.; Ziabicki, A. Thermodynamics of Crystallization in a Model Polymer Network. *Macromolecules* 1982, *15* (6), 1507–1517.
(37) Petrović, Z. S.; Ferguson, J. Polyurethane Elastomers. *Progress in Polymer Science* 1991, *16* (5), 695–836.
(38) Dickinson, L. C.; Morganelli, P.; Chu, C. W.; Petrovic, Z.; MacKnight, W. J.; Chien, J. C. W. Molecular Motions in Model Network Polymers. *Macromolecules* 1988, *21* (2), 338–346.
(39) Camberlin, Y.; Pascault, J. P. Phase Segregation Kinetics in Segmented Linear Polyurethanes: Relations Between Equilibrium Time and Chain Mobility and Between Equilibrium Degree of Segregation and Interaction Parameter. *Journal of Polymer Science: Polymer Physics Edition* 1984, *22* (10), 1835–1844.
(40) Petrović, Z. S.; Javni, I. The Effect of Soft-Segment Length and Concentration on Phase Separation in Segmented Polyurethanes. *J. Polym. Sci. B Polym. Phys.* 1989, *27* (3), 545–560.
(41) Prisacariu, C. Structural Studies on Polyurethane Elastomers. 2011, 23–60.
(42) Prisacariu, C.; Scortanu, E.; Stoica, I.; Agapie, B.; Barboiu, V. Morphological Features and Thermal and Mechanical Response in Segmented Polyurethane Elastomers Based on Mixtures of Isocyanates. *Polym J* 2011, *43* (7), 613–620.
(43) Abouzahr, S.; Wilkes, G. L.; Ophir, Z. Structure-Property Behaviour of Segmented Polyether-MDI-Butanediol Based Urethanes: Effect of Composition Ratio. *Polymer* 1982, *23* (7), 1077–1086.
(44) Blackwell, J.; Gardner, K. H. Structure of the Hard Segments in Polyurethane Elastomers. *Polymer* 1979, *20* (1), 13–17.
(45) Korley, L. T. J.; Pate, B. D.; Thomas, E. L.; Hammond, P. T. Effect of the Degree of Soft and Hard Segment Ordering on the Morphology and Mechanical Behavior of Semicrystalline Segmented Polyurethanes. 2006, *47* (9), 3073–3082.
(46) Miller, J. A.; Lin, S. B.; Hwang, K.; Wu, K. S. Properties of Polyether-Polyurethane Block Copolymers: Effects of Hard Segment Length Distribution. *Macromolecules* 1985.
(47) Sung, C. P.; Smith, T. W.; Sung, N. H. Properties of Segmented Polyether

Poly (Urethaneureas) Based of 2, 4-Toluene Diisocyanate. 2. Infrared and Mechanical Studies. *Macromolecules* 1980.
(48) Xi, P.; Gu, X.; Cheng, B.; Wang, Y. Preparation and Characterization of a Novel Polymeric Based Solid–Solid Phase Change Heat Storage Material. *Energy Conversion and Management* 2009, *50* (6), 1522–1528.
(49) Liao, L.; Cao, Q.; Liao, H. Investigation of a Hyperbranched Polyurethane as a Solid-State Phase Change Material. *J Mater Sci* 2010, *45* (9), 2436–2441.
(50) Yanshan, L.; Shujun, W.; Hongyan, L.; Fanbin, M.; Huanqing, M.; Wangang, Z. Preparation and Characterization of Melamine/Formaldehyde/Polyethylene Glycol Crosslinking Copolymers as Solid–Solid Phase Change Materials. *Solar Energy Materials and Solar Cells* 2014, *127* (C), 92–97.
(51) Raftopoulos, K. N.; Janowski, B.; Apekis, L.; Pielichowski, K.; Pissis, P. Molecular Mobility and Crystallinity in Polytetramethylene Ether Glycol in the Bulk and as Soft Component in Polyurethanes. *European Polymer Journal* 2011, *47* (11), 2120–2133.
(52) Petrovic, Z. S.; Javni, I. The Effect of Soft-Segment Length and Concentration on Phase Separation in Segmented Polyurethanes. *Journal of Polymer Science Part B: …* 1989.
(53) Martin, D. J.; Meijs, G. F.; Gunatillake, P. A.; McCarthy, S. J.; Renwick, G. M. The Effect of Average Soft Segment Length on Morphology and Properties of a Series of Polyurethane Elastomers. II. SAXS-DSC Annealing Study. 1997, *64* (4), 803–817.
(54) Prisacariu, C.; Scortanu, E.; Stoica, I.; Agapie, B.; Barboiu, V. Morphological Features and Thermal and Mechanical Response in Segmented Polyurethane Elastomers Based on Mixtures of Isocyanates. *Polym J* 2011, *43* (7), 613–620.
(55) Flory, P. J. Thermodynamics of Crystallization in High Polymers. I. Crystallization Induced by Stretching. *J. Chem. Phys.* 1947, *15* (6), 397–408.
(56) Eisenbach, C. D.; Gronski, W. Hydrogen Bonding and Phase Separation in Segmented Polyurethane Elastomers as Studied by 13C NMR Magic Angle Spinning and FT-IR Spectroscopy. *Die Makromolekulare Chemie, Rapid Communications* 1983, *4* (11), 707–713.
(57) Koberstein, J. T.; Galambos, A. F.; Leung, L. M. Compression-Molded Polyurethane Block Copolymers. 1. Microdomain Morphology and Thermomechanical Properties. *Macromolecules* 1992, *25* (23), 6195–6204.
(58) Li, Y.; Gao, T.; Liu, J.; Linliu, K.; Desper, C. R.; Chu, B. Multiphase Structure of a Segmented Polyurethane: Effects of Temperature and Annealing. *Macromolecules* 1992, *25* (26), 7365–7372.
(59) Li, Y.; Gao, T.; Chu, B. Synchrotron SAXS Studies of the Phase-Separation Kinetics in a Segmented Polyurethane. *Macromolecules* 1992, *25* (6), 1737–1742.
(60) Li, Y.; Kang, W.; Stoffer, J. O.; Chu, B. Effect of Hard-Segment Flexibility on Phase Separation of Segmented Polyurethanes. *Macromolecules* 1994.
(61) Hood, M. A.; Wang, B.; Sands, J. M.; La Scala, J. J.; Beyer, F. L.; Li, C. Y. Morphology Control of Segmented Polyurethanes by Crystallization of Hard and Soft

Segments. *Polymer* 2010, *51* (10), 2191–2198.
(62) Hood, M. A.; Wang, B.; Sands, J. M.; La Scala, J. J.; Beyer, F. L.; Li, C. Y. Morphology Control of Segmented Polyurethanes by Crystallization of Hard and Soft Segments. *Polymer* 2010, *51* (10), 2191–2198.
(63) Chu, B.; Gao, T.; Li, Y.; Wang, J.; Desper, C. R.; Byrne, C. A. Microphase Separation Kinetics in Segmented Polyurethanes: Effects of Soft Segment Length and Structure. *Macromolecules* 2002, *25* (21), 5724–5729.
(64) Kośny, J. Overview of Basic Solid–Liquid PCMs Used in Building Envelopes—Packaging Methods, Encapsulation, and Thermal Enhancement. In *PCM-Enhanced Building Components*; Engineering Materials and Processes; Springer International Publishing: Cham, 2015; pp 61–105.
(65) Mehling, H.; Cabeza, L. F. *Heat and Cold Storage with PCM*; Springer Science & Business Media, 2008.
(66) Poudel, N. Towards the Development of Performance Based Guidelines for Using Phase Change Materials in Lightweight Buildings. 2014.
(67) Mehling, H.; Cabeza, L. F. *Heat and Cold Storage with PCM*; Springer Science & Business Media, 2008.
(68) Sharma, A.; Tyagi, V. V.; Chen, C. R.; Buddhi, D. Review on Thermal Energy Storage with Phase Change Materials and Applications. 2009, *13* (2), 318–345.
(69) Tyagi, V. V.; Buddhi, D. PCM Thermal Storage in Buildings: a State of Art. *Renewable and Sustainable Energy Reviews* 2007, *11* (6), 1146–1166.
(70) air, A. S. O. H. R. A. *ASHRAE STANDARD: an American Standard: Thermal Environmental Conditions for Human Occupancy*; 1992.
(71) Kenisarin, M. M.; Kenisarina, K. M. Form-Stable Phase Change Materials for Thermal Energy Storage. *Renewable and Sustainable Energy …* 2012, *16* (4), 1999–2040.
(72) Constantinescu, M.; Dumitrache, L.; Constantinescu, D.; Anghel, E. M.; Popa, V. T.; Stoica, A.; Olteanu, M. Latent Heat Nano Composite Building Materials. *European Polymer Journal* 2010, 1–8.
(73) Towards the Development of Performance Based Guidelines for Using Phase Change Materials in Lightweight Buildings. 2016, 1–323.
(74) Verbeeck, G.; Hens, H. Life Cycle Inventory of Buildings: a Calculation Method. *Building and Environment* 2010, *45* (4), 1037–1041.
(75) Pielichowska, K.; Pielichowski, K. Biodegradable PEO/Cellulose-Based Solid-Solid Phase Change Materials. *Polym. Adv. Technol.* 2010, *22* (12), 1633–1641.
(76) de Gracia, A.; Rincón, L.; Castell, A.; Jimenez, M.; Boer, D.; Medrano, M.; Cabeza, L. F. Life Cycle Assessment of the Inclusion of Phase Change Materials (PCM) in Experimental Buildings. *Energy & Buildings* 2010, *42* (9), 1517–1523.
(77) Liang, X.-H.; Guo, Y.-Q.; Gu, L.-Z.; Ding, E.-Y. Crystalline-Amorphous Phase Transition of Poly(Ethylene Glycol)/Cellulose Blend. *Macromolecules* 1995, *28* (19), 6551–6555.
(78) Li, Y.; Liu, R.; Huang, Y. Synthesis and Phase Transition of Cellulose-Graft-Poly(Ethylene Glycol) Copolymers. *J. Appl. Polym. Sci.* 2008, *110* (3), 1797–1803.
(79) Meng, Q.; Hu, J. A Temperature-Regulating Fiber Made of PEG-Based

Smart Copolymer. *Solar Energy Materials and Solar Cells* 2008, *92* (10), 1245–1252.
(80) Meng, Q.; Hu, J. A Poly(Ethylene Glycol)-Based Smart Phase Change Material. *Solar Energy Materials and Solar Cells* 2008, *92* (10), 1260–1268.
(81) Szycher, M. Chain Extenders. In *Szycher's Handbook of Polyurethanes, Second Edition*; CRC Press, 2012; pp 155–180.
(82) Blackwell, J.; Nagarajan, M. R.; Hoitink, T. B. Structure of Polyurethane Elastomers: Effect of Chain Extender Length on the Structure of MDI/Diol Hard Segments. *Polymer* 1982, *23* (7), 950–956.
(83) Lipatova, T. E.; Ivashchenko, V. K.; Nesterov, A. Y.; Lipatov, Y. S. Study of Mechanisms in the Preparation of Network Polyurethanes. *Polymer Science U.S.S.R.* 1969, *11* (3), 682–687.
(84) Prisacariu, C.; Scortanu, E. Morphology of Polyurethanes Based on the Chain Extender Ethylene Glycol and Aromatic Flexible Diisocyanates, as …. *Rev Roum Chim* 2008.
(85) Cao, Q.; Liu, P. Hyperbranched Polyurethane as Novel Solid–Solid Phase Change Material for Thermal Energy Storage. *European Polymer Journal* 2006, *42* (11), 2931–2939.
(86) Apekis, L.; Pissis, P.; Christodoulides, C.; Spathis, G.; Niaounakis, M.; Kontou, E.; Schlosser, E.; Schoenhals, A.; Goering, H. Physical and Chemical Network Effects in Polyurethane Elastomers. 1992, 144–150.
(87) Qiao, C.; Jiang, S.; Dong, D.; Ji, X.; An, L.; Jiang, B. The Critical Lowest Molecular Weight for PEG to Crystallize in Cross-Linked Networks. *Macromol. Rapid Commun.* 2004, *25* (5), 659–663.
(88) Hoffman, J. D.; Miller, R. L. Kinetic of Crystallization From the Melt and Chain Folding in Polyethylene Fractions Revisited: Theory and Experiment. *Polymer* 1997.
(89) He, Q.; Zhang, W. A Study on Latent Heat Storage Exchangers with the High-Temperature Phase-Change Material. *Int. J. Energy Res.* 2001, *25* (4), 331–341.
(90) Qian, R.; Wu, Z.; Xue, Z.; Yan, R. Length of Chain Segment Motion Needed for Crystallization. *Macromolecular rapid …* 1995.
(91) He, Q.; Zhang, W. A Study on Latent Heat Storage Exchangers with the High-Temperature Phase-Change Material. *Int. J. Energy Res.* 2001, *25* (4), 331–341.
(92) Beech, D. R.; Booth, C.; Pickles, C. J.; Sharpe, R. R. Interfacial Free Energy of Crystals of Low Molecular Weight Poly (Ethylene Oxide). *Polymer* 1972, *13* (6), 246–248.
(93) Qian, R.; Wu, Z.; Xue, Z.; Yan, R. Length of Chain Segment Motion Needed for Crystallization. *Macromol. Rapid Commun.* 1995, *16* (1), 19–23.
(94) Friday, A.; Booth, C. Crystallization of Block Poly (Ethylene Oxide). *Polymer* 1978, *19* (9), 1035–1042.
(95) Castellón, C.; Günther, E.; Mehling, H.; Hiebler, S.; Cabeza, L. F. Determination of the Enthalpy of PCM as a Function of Temperature Using a Heat-Flux DSC-a Study of Different Measurement Procedures and Their Accuracy. *Int. J. Energy Res.* 2008, *32* (13), 1258–1265.
(96) Saiani, A.; Daunch, W. A.; Verbeke, H.; Leenslag, J. W.; Higgins, J. S.

Origin of Multiple Melting Endotherms in a High Hard Block Content Polyurethane. 1. Thermodynamic Investigation. *Macromolecules* 2001, *34* (26), 9059–9068.
(97) Koberstein, J. T.; Galambos, A. F. Multiple Melting in Segmented Polyurethane Block Copolymers. *Macromolecules* 1992, *25* (21), 5618–5624.
(98) Blackwell, J.; Gardner, K. H. Structure of the Hard Segments in Polyurethane Elastomers. *Polymer* 1979, *20* (1), 13–17.
(99) Sperling, L. H. *Introduction to Physical Polymer Science*; John Wiley & Sons, 2015.
(100) Buckley, C. P.; Prisacariu, C.; Martin, C. Elasticity and Inelasticity of Thermoplastic Polyurethane Elastomers: Sensitivity to Chemical and Physical Structure. *Polymer* 2010, *51* (14), 3213–3224.
(101) Marniemi, J.; Parkki, M. G. Radiochemical Assay of Glutathione S-Epoxide Transferase and Its Enhancement by Phenobarbital in Rat Liver in Vivo. 1975, *24* (17), 1569–1572.
(102) Nierzwicki, W.; Wysocka, E. Microphase Separation and Properties of Urethane Elastomers. *J. Appl. Polym. Sci.* 1980, *25* (5), 739–746.
(103) Kothandaraman, H.; Venkatarao, K.; Thanoo, B. C. Preparation, Properties, and Crosslinking Studies on Polyurethane Elastomers. *Polym J* 1989, *21* (10), 829–839.
(104) Szycher, M. Structure–Property Relations in Polyurethanes. In *Szycher's Handbook of Polyurethanes, Second Edition*; CRC Press, 2012; pp 37–86.
(105) Okrasa, L.; Zigon, M.; Zagar, E.; Czech, P.; Boiteux, G. Molecular Dynamics of Linear and Hyperbranched Polyurethanes and Their Blends. *Journal of Non-Crystalline Solids* 2005, *351* (33-36), 2753–2758.
(106) Saunders, J. H.; Frisch, K. C. *Polyurethanes: Chemistry and Technology: Chemistry*; 1964.
(107) Brunette, C. M.; Hsu, S. L.; MacKnight, W. J. Hydrogen-Bonding Properties of Hard-Segment Model Compounds in Polyurethane Block Copolymers. *Macromolecules* 1982, *15* (1), 71–77.
(108) Prisacariu, C. Mechanical Aspects of Polyurethane Elastomers. *Structural studies on polyurethane elastomers* 2011, No. Chapter 4, 103–202.
(109) Vallance, M. A.; Castles, J. L.; Cooper, S. L. Microstructure of as-Polymerized Thermoplastic Polyurethane Elastomers. *Polymer* 1984, *25* (12), 1734–1746.
(110) Prisacariu, C. *Chapter 4: Influence of Soft Segment Molecular Weight and Hard Segment Content on Structure-Property Relationships of Poly(Urethane-Urea)S* ; Springer Science & Business Media: Vienna, 2011.
(111) Prisacariu, C.; Olley, R. H.; Caraculacu, A. A.; Bassett, D. C.; Martin, C. The Effect of Hard Segment Ordering in Copolyurethane Elastomers Obtained by Using Simultaneously Two Types of Diisocyanates. 2003, *44* (18), 5407–5421.
(112) Lyman, D. J. Polyurethanes. I. the Solution Polymerization of Diisocyanates with Ethylene Glycol. *Journal of Polymer Science* 1960, *45* (145), 49–59.
(113) Bayer, O.; Muller, E.; Petersen, S.; Piepenbrink, H. F.; Windemuth, E. New Types of Highly Elastic Substances, Vulcollans. *Rubber Chemistry and Technology* 1950, *23* (4), 812–835.

(114) Martin, D. J.; Meijs, G. F.; Gunatillake, P. A. The Effect of Average Soft Segment Length on Morphology and Properties of a Series of Polyurethane Elastomers. II. SAXS-DSC Annealing Study. *Journal of applied ...* 1997, *62* (9), 1377–1386.
(115) Chu, B.; Gao, T.; Li, Y.; Wang, J.; Desper, C. R. Microphase Separation Kinetics in Segmented Polyurethanes: Effects of Soft Segment Length and Structure. *Macromolecules* 1992.
(116) Li, Y.; Gao, T.; Chu, B. Synchrotron SAXS Studies of the Phase-Separation Kinetics in a Segmented Polyurethane. *Macromolecules* 1992, *25* (6), 1737–1742.
(117) Vipin. Studies on Synthesis & Characterization of Thermoplastic Polyurethane-Urea Copolymers, University of Pune, 2009, pp 1–193.
(118) Bonart, R. *FTIR Investigation of the Influence of Diisocyanate Symmetry on the Morphology Development in Model Segmented Polyurethanes*; B2 (1), 1968.
(119) Abouzahr, S.; Wilkes, G. L.; Folkes, M. J. *Processing, Structure and Properties of Block Copolymers*; Essex: Elsevier, 1985.
(120) Szycher, M. Isocyanate Chemistry. In *Szycher's Handbook of Polyurethanes, Second Edition*; CRC Press, 2012; pp 87–134.
(121) Michael Szycher, P. D. *Szycher's Handbook of Polyurethanes, Second Edition*; CRC Press, 2012.
(122) Lyman, D. J. Polyurethanes. I. the Solution Polymerization of Diisocyanates with Ethylene Glycol. *Journal of Polymer Science* 1960, *45* (145), 49–59.
(123) Dusek, K. Theory of Network Formation by Additional Crosslinking of Polyurethanes Due to Biuret and Allophanate Formation. *Polymer Bulletin* 1987, *17* (5), 481–488.
(124) Dusek, K.; Spirkova, M.; Havlicek, I. Network Formation of Polyurethanes Due to Side Reactions. *Macromolecules* 1990, *23* (6), 1774–1781.
(125) Joshi, V. P. Studies on Synthesis & Characterization of Thermoplastic Polyurethane Urea Copolymers. 2009.
(126) Dusek, K.; Spirkova, M.; Havlicek, I. Network Formation of Polyurethanes Due to Side Reactions. *Macromolecules* 1990, *23* (6), 1774–1781.
(127) Buckley, C. P.; Prisacariu, C.; Caraculacu, A. Novel Triol-Crosslinked Polyurethanes and Their Thermorheological Characterization as Shape-Memory Materials. *Polymer* 2007, *48* (5), 1388–1396.
(128) Prisacariu, D. C. Mechanical Aspects of Polyurethane Elastomers. In *Structural studies on polyurethane elastomers*; Springer Vienna: Vienna, 2011; pp 103–202.
(129) Prisacariu, C.; Prisacariu, C. DSC Polyurethane Elastomers Priscariu. 2014, 1–29.
(130) Bayer, O.; Muller, E.; Petersen, S. New Types of Highly Elastic Substances, Vulcollans. *Rubber Chemistry ...* 1950.
(131) Kopusov, L. I.; Zharkov, V. V. Spectral Studies on the Structure of Polyurethane Elastomers. *J Appl Spectrosc* 1966, *5* (1), 95–97.
(132) Dusek, K.; Spirkova, M.; Havlicek, I. Network Formation of Polyurethanes Due to Side Reactions. 1990, *23* (6), 1774–1781.
(133) Szycher, M. Basic Concepts in Polyurethane Chemistry and Technology. In

Szycher's Handbook of Polyurethanes, Second Edition; CRC Press, 2012; pp 13–36.
(134) Silverstein, R. M.; Webster, F. X.; Kiemle, D. *Spectrometric Identification of Organic Compounds, 7th Edition*; Wiley Global Education, 2005.
(135) Badger, R. M.; Bauer, S. H. Spectroscopic Studies of the Hydrogen Bond. II. the Shift of the O[Single Bond]H Vibrational Frequency in the Formation of the Hydrogen Bond. *J. Chem. Phys.* 1937, *5* (11), 839.
(136) Kontou, E.; Spathis, G.; Niaounakis, M.; Kefalas, V. Physical and Chemical Cross-Linking Effects in Polyurethane Elastomers. *Colloid & Polymer Sci* 1990, *268* (7), 636–644.
(137) Hood, M. A.; Wang, B.; Sands, J. M.; La Scala, J. J.; Beyer, F. L.; Li, C. Y. Morphology Control of Segmented Polyurethanes by Crystallization of Hard and Soft Segments. *Polymer* 2010, *51* (10), 2191–2198.
(138) Pielichowski, K.; Flejtuch, K. Differential Scanning Calorimetry Studies on Poly(Ethylene Glycol) with Different Molecular Weights for Thermal Energy Storage Materials. *Polym. Adv. Technol.* 2003, *13* (10-12), 690–696.
(139) Ding, E. Y.; Jiang, Y.; Li, G. K. Comparative Studies of the Structures and Transition Characteristics of Cellulose Diacetate Modified with Polyethylene …. *Journal of Macromolecular Science* 2001, *40* (6), 1053–1068.
(140) Guo, Y.-Q.; Lclc, X.-H. L. The Miscibility of Cellulose-Polyethylene Glycol Blends. *J. of Macromolecular Sc., Part B* 1999, *38* (4), 439–447.
(141) Li, Y.; Ren, Z.; Zhao, M.; Yang, H.; Chu, B. Multiphase Structure of Segmented Polyurethanes: Effects of Hard-Segment Flexibility. *Macromolecules* 1993.
(142) Brunette, C. M. Brunette 1982. 2001, 1–7.
(143) Brunette, C. M.; MacKnight, W. J. Brunette, Hau, Mac Knight. 2001, 1–7.
(144) Cima, L. G.; Lopina, S. T. Network Structures of Radiation-Crosslinked Star Polymer Gels. *Macromolecules* 1995.
(145) Peppas, N. A.; Merrill, E. W. Crosslinked Poly(Vinyl Alcohol) Hydrogels as Swollen Elastic Networks. *J. Appl. Polym. Sci.* 1977, *21* (7), 1763–1770.
(146) Sung, C. S. P.; Schneider, N. S. Structure-Property Relationships of Polyurethanes Based on Toluene Di-Isocyanate. *J Mater Sci* 1978, *13* (8), 1689–1699.
(147) Schneider, N. S.; Sung, C. S. P. Transition Behavior and Phase Segregation in TDI Polyurethanes. *Polymer Engineering & Science* 1977, *17* (2), 73–80.
(148) Aitken, R. R.; Jeffs, G. *Thermoplastic Polyurethane Elastomers Based on Aliphatic Diisocyanates: Thermal Transitions*; Polymer, 1977.
(149) Seymour, R. W.; Cooper, S. L. Thermal Analysis of Polyurethane Block Polymers. *Macromolecules* 1973, *6* (1), 48–53.
(150) Camberlin, Y.; Pascault, J. P. Quantitative DSC Evaluation of Phase Segregation Rate in Linear Segmented Polyurethanes and Polyurethaneureas. *Journal of Polymer Science Part A: Polymer Chemistry* 1983, *21* (2), 415–423.
(151) Saiani, A.; Daunch, W. A.; Verbeke, H.; Leenslag, J. W.; Higgins, J. S. Origin of Multiple Melting Endotherms in a High Hard Block Content Polyurethane. 1. Thermodynamic Investigation. *Macromolecules* 2001, *34* (26), 9059–9068.
(152) Peebles, L. H. Hard Block Length Distribution in Segmented Block Copolymers. *Macromolecules* 1976, *9* (1), 58–61.

(153) Eisenbach, C. D.; Gronski, W. Hydrogen Bonding and Phase Separation in Segmented Polyurethane Elastomers as Studied by 13C NMR Magic Angle Spinning and FT-IR Spectroscopy. *Die Makromolekulare Chemie, Rapid Communications* 1983, *4* (11), 707–713.
(154) Seymour, R. W.; Estes, G. M.; Cooper, S. L. Infrared Studies of Segmented Polyurethan Elastomers. I. Hydrogen Bonding. *Macromolecules* 1970, *3* (5), 579–583.
(155) Coleman, M. M.; Skrovanek, D. J.; Hu, J.; Painter, P. C. Hydrogen Bonding in Polymer Blends. 1. FTIR Studies of Urethane-Ether Blends. *Macromolecules* 1988, *21* (1), 59–65.
(156) and, J. M.; Painter, P. A Comparison of Hydrogen Bonding and Order in a Polyurethane and Poly(Urethane−Urea) and Their Blends with Poly(Ethylene Glycol). *Macromolecules* 2007, *40* (5), 1546–1554.
(157) Mattia, J.; Painter, P. A Comparison of Hydrogen Bonding and Order in a Polyurethane and Poly(Urethane−Urea) and Their Blends with Poly(Ethylene Glycol). *Macromolecules* 2007, *40* (5), 1546–1554.

An important question for future studies is to determine, in future work the use of SAXS techniques to probe morphological changes and correlate that to the thermal energy storage properties. This experiment would allow the visualization of the changes that occur in the morphology and how that influences thermal energy storage capacity. Furthermore, this information would reveal more information on the impact the degree of phase separation has on the crystallization of the PEG PCM chains.

Chapter 10 EMBODIED ENERGY OF MICROENCAPSULATED PCM

EMBODIED ENERGY OF MICRO-ENCAPSULATED N-ALKANE PHASE CHANGE MATERIALS BY LIFE CYCLE ASSESSMENT

Claire K. Poh, Niraj Poudel, Vincent Y. Blouin

Clemson University

Abstract

Microencapsulated Phase Change Materials (mPCM) are incorporated into thermal insulation to enhance building energy performance. Most research studies have found that mPCM integrated into building wall envelopes (i.e. gypsum board) bring notable savings in energy consumption and reduction in peak hour loads (Kosny). The results of these studies were based solely on the energy consumed or saved during the operational phase. A narrow outlook on environmental concerns is provided in the results when considering only the operational energy of the system. Life Cycle Analysis (LCA) evaluates environmental concerns associated with all stages of a products life from "cradle to grave". The embodied energy or energy consumed manufacturing mPCM measures up considerably to the amount of energy saved by mPCM. Meaning, a net gain in energy

won't be seen for several years. This paper employed LCA to investigate the microencapsulation process and measure the amount of energy used to manufacture mPCM. The Athena Impact Estimator Software (4.1) was used to predict the number of pay back years for mPCM, integrated in a 12" by 12" block of gypsum, to attain net gain in energy. The results of this study provide insight into the broader energy implications of mPCM as an energy-saving technology for buildings.

I. Introduction

Organic Phase Change Materials (PCM) can be used as a thermal energy storage system to enhance the performance of thermal insulation within a building envelope. Phase change materials have the capability of absorbing and releasing thermal energy to reduce or eliminate heat transfer within a room, enough so that the temperature remains within a stabilizing range. During the time the PCM is absorbing or releasing heat, it undergoes a change in phase and stores or releases latent heat in response to changes in environmental temperatures. The amount of heat that can be stored in PCM is directly related to the heat of fusion of the material, which was approximately 151kJ/kg for the microencapsulated paraffinic material used in this research. During this heating process PCM can be effectively recharged by a source of heat. This property can be harnessed to increase the comfort level of a building.

The content of this paper evaluates the amount of energy consumed over the entire life cycle of mPCM. The energy used to encapsulate n-octadecane was quantified for three microencapsulation methods, all of which used a insitu-polymerization technique to

coacervate relatively the same amount of n-octadecane. Three different microencapsulation methods were studied to determine if different microencapsulation methods encompass drastically dissimilar embodied energies. The concept of Life Cycle Assessment, which is considering the energy consumed over the entire life cycle, inspired this study and is used to evaluate mPCM as a sensible energy-saving technology. Life Cycle inventories were utilized to quantify the embodied energy of all starting materials. Energy is either heat energy or work energy. For each step in the microencapsulation process, the heat and work energy of the system was tabulated and summed with the embodied energy of the starting materials to calculate the total embodied energy. This paper uses the software EnergyPlus to estimate the energy saved by mPCM during the operation stage. The software Athena Impact Estimator was used to determine to embodied energy per kg of gypsum wallboard and other materials that make up the building envelope.

II. Life Cycle Assessment

The goal of the US Green Building Council is to reduce the carbon footprint of buildings and become more sustainable. Therefore, the knowledge of the environmental impact of a building's material components is necessary. Life cycle assessment (LCA) is a method that allows us to systematically break down any manufactured item into its components and their subsidiaries industrial processes and thoroughly measure its environmental impact from beginning of production to disposal also known as “cradle to grave”.

(Goleman, 2009) Finding out the embodied energy of a product will reveal if it has any hidden environmental impacts. The hidden impacts, in terms of energy consumption, for mPCM will expose the fact that mPCM as a thermal energy storage has a negative gain and how many years till a net gain is achieved.

A LCA study conducted in Spain revealed that when taking into account the embodied energy of encapsulated paraffin PCM there is an adverse impact on the total energy consumption of a building. (Gracia, et al., 2010) An energy audit of the subsidiary processes that formulate paraffin(n-octadecane) mPCM was performed in this paper. Presuming that the embodied energy of mPCM is measurably greater than the energy saved by mPCM during the operation phase, the intended benefit of using PCM as Thermal Energy Storage in a building is not as beneficial as it appears in other studies that consider only the operation phase.

Life Cycle Inventory (LCI) data used in this study is based off of statistical data that represent the way of life in that region. The LCI data employed in the Spanish study is not interchangeable with LCA studies outside of that region due to the differences in way of life and building structure. The standard of living in the United States is different from Europe; Americans differ in the way they heat their homes, the materials used to build their homes, the average size of the American home is typically larger than the average European home, the structure of the energy grids in the United States is set up differently, the variety of goods imported and where the US imports/exports from also differs from Europe. This is called the regional effect in LCA, meaning only local variables such as land use, climate, etc., are considered. The regional effect plays a big role in the accuracy

of an LCA model.

Life Cycle Assessment takes into account various categories of environmental impacts. Global warming potential, Gross Energy Requirement, Ozone Depletion Potential, Acidification Potential, Eutrophication Potential, and Photochemical Ozone Creation are the 6 impact categories LCA appraises a system's total environmental damage with. However, every LCA model considers only impacts relative to the subject of the LCA study and its use. The objective of this study is to determine how viable PCM is in terms of energy. Therefore this paper will focus solely on the Gross Energy Requirement (GER) Impact category, which indicates the total primary energy resource consumption (direct+indirect+ feedstock) (Boustead and Hancock). The other impact categories aren't considered in this paper because the information these categories gather is not relevant to the overall objective of this paper and the functional unit of the LCA study conducted.

III. Analysis of Micro-Encapsulation Process

In accordance with this paper; the microcapsules of n-octadecane of study was developed and manufactured by Microtek labs. Do to proprietary rights, it is unknown the microencapsulation method used by Microtek. There is a myriad of microencapsulation methods, therefore it is impossible to determine the exact method used. Microencapsulation is considered an art form. (USA Patent No. 6703127, 2004) No universal recipe exists for the microencapsulation process. The parameters chosen for each method is relative to the system and only through optimization can the appropriate parameters be determined. Typically, the method used most to microencapsulate is to

disperse droplets of PCM into an aqueous solution and using techniques, such as coacervation, interfacial polymerization, and in-situ polymerization a wall or shell will form around the droplets of PCM. (USA Patent No. 6703127, 2004) Using Melamine and formaldehyde as the monomers to form the aminoplast as the shell of the microcapsules is well-known in the art (USA Patent No. 7442410, 2008). IR spectra results tell us the wall-forming material is a melamine-formaldehyde resin. The Microtek patent for the invention of the macroencapsulation of PCM describes an in-situ polymerization technique used to carry out complex coacervation. (USA Patent No. 6703127, 2004)Therefore, it is reasonable to assume Microtek uses the same technique to produce their mPCM product. For this reason, insitu-polymerization is the only complex coacervation technique studied in this paper.

The insitu polymerization technique takes advantage of the reaction of cationic and anionic polymers within an aqueous solution. The two reactions that take place when Urea reacts with formaldehyde are

(1) H2N-CO-NH2 +CH2O -> H2N-CO-NH-CH2OH

This is an addition reaction, where the formaldehyde pulls hydrogen off the amine group to form methylol.

(2) H2N-CO-NH-CH2OH + H2N-CO-NH-CH2OH -> H2N-CO-NH-CH-HN-CO-NH-CH2OH + H2O.

This condensation reaction occurs by the OH group of methylol and a H of amine forming a methylene bridge between the amine groups of two urea molecules, forming a urea-polymer chain. (Rochmadi & Wahyu, 2010)

Eventually cross-linking of the two polymers will occur and a film of the urea-formaldehyde polymer will form at the interface of the emulsion bubbles, forming the microcapsule shell.

Since there is a myriad of ways to encapsulate PCM using the insitu-polymerization technique, one can't assume the energy consumed for one method is equivalent to the energy consumed for another method. For this reason, this paper evaluates the energy consumption of three in-situ polymerization microencapsulation methods to verify the final value of energy consumed.

a. Database information

The National Renewable Energy Laboratory (NREL) and its partners came together and created the U.S. Life-Cycle Inventory (LCI) Database, a publicly available database designed to help LCA practitioners answer questions about environmental impact. (U.S. Life-Cycle Inventory Database, 2010)The U.S. Life-Cycle Inventory (LCI) database contains data modules that quantify the material and energy flows into and out of the environment for common unit processes. All data entered into the database must follow a data protocol based on ISO 14048 standards. (U.S. Department of Energy , 2009)

In this paper the values for the embodied energy of the starting materials were obtained from a database of Life Cycle Inventories. It is favorable to have results that reflect the system as accurately as possible so all of the LCIs that were available in the U.S. LCI database were preferred. LCIs in the U.S. database are based on U.S. conditions and standards. The data compiled in the U.S. LCI database contain data that reflect the

chemicals manufactured in the U.S., followed US standards, and operate on the same type of electricity grid. Unfortunately, the U.S. LCI database has yet to encompass all products/chemicals, therefore those starting materials not found were obtained from the EcoInvent database.

The U.S. LCI database project was first initiated in 2003 (U.S. Department of Energy , 2009), thus it is in its' early stages because it hasn't had the time or the backing to develop to the level of the European LCI database (i.e. EcoInvent). Projects like EcoInvent has had time to cultivate a support group of industry partners and in return has acquired a wider variety of data modules. Although it is more favorable to use LCI data based on U.S. standards, using other countries' LCI databases is still a better estimation of a unit processes' "cradle to gate" energy consumption than none at all. More than likely the data from other countries' databases won't yield a huge difference in the final result.

b. Quantifying energy of system

The total amount of energy required to manufacture mPCM transpires from the energy consumed to produce the starting chemicals and the amount of energy inputted into the system during the emulsification and encapsulation unit processes. A Life Cycle Inventory database was used to specify the embodied energy of the starting materials. The work energy inputted into the system includes the way of mixing (mechanical stirring, pressure, homogenization, ultrasonic, centrifugation) and the amount of thermal energy added to heat the system with a direct relationship to the duration of the process.

All calculations in this paper assume the system is a closed system; no exchange of matter (movement of molecules across the boundary of the system and surroundings) but some exchange of energy (heat, work, friction, radiation). Heat energy and work energy are the two forms of energy. A distinction between the two is heat is the exchange of thermal energy from a hot to a cold body and work energy involves the net directed movement of matter from one location to another. The energy of a system will change if heat is transferred to or from the system or work is done by the system. Heat and work are the only forms of energy transferred between a closed system and its' surroundings, this demonstrates the first law of thermodynamics and can be quantified by the equation:

(1) $E_2 - E_1 = q + w$

The thermal energy inputted into the system can be described in terms of energy input by the amount of heat required to raise the system to the specified temperature and the amount of heat to be added to maintain the system at this temperature (USA Patent No. 6703127, 2004)The amount of energy added to the system was calculated using the equation;

(2) $Q=mc\Delta T$.

No system is 100% efficient, overtime heat from the system is lost to its surroundings. For all calculations it is assumed 1/12 of heat is lost per hour. The amount of heat the solution must add to maintain a constant temperature is added to the final total of energy consumed for each process.

The mechanical energy inputted into the system was calculated by the power imparted by the stirrer to the fluid. This value is characterized in terms of the pumping flow rate and

velocity head produced. The amount of power inputted into the system was determined by equation (2), the equation for power consumption. (Puel, Briancon, & Fessi, 2006)

(2) $P=N_p p_c N^3 D_A^5$

N_p, power number

P_c, density of continuous liquid phase (kg m^{-3})

N, the agitator rotational velocity (s^{-1})

D_A^5, diameter of the agitator (m)

Values for the Reynolds number (Re) were based on the parameters used for a microencapsulation process done in a ½ liter vessel. For now, this is the best assumption for these calculations. Process can be found on pg. 162 .in the book Microencapsulation: Methods and Industrial applications. (Puel, Briancon, & Fessi, 2006)

i. Process 1

The first method analyzed in this paper is based off U.S. Patent # 7,442,410. (USA Patent No. 7442410, 2008)This invention provides a method that uses melamine-formaldehyde as the shell material. The coacervation mechanism of this method takes place using an in-situ condensation technique. The melamine-formaldehyde resin *form a viscous phase called the complex coacervate that exists in equilibrium with a dispersant or emulsifier. Water immiscible droplets of n-octadecane (the phase change material) are stirred into*

the system as the core material to form an emulsion mixture. The emulsion is composed of 30 grams of the core material, n-octadecane. Monomers; 1.5g of polypropylene glycol with an average MW > 400 and .1g of polyisocyanate (TDI). These monomers act as dispersants by reacting with the free amino groups on melamine. Prior research has observed that paraffinic compounds with various alkane chain lengths are difficult to emulsify uniformly due to their low surface tension. (USA Patent No. 7442410, 2008). TDI and polypropylene glycol modify the polymer surface so that satisfactory emulsification can occur and the pre-condensate of melamine-formaldehyde will be easily deposited around the core material to form the first outer layer of the shell. *A suspension or dispersed fluid is necessary to ensure that the reaction can take place at the interface of all the n-octadecane droplets simultaneously, resulting in similar properties for the particles. (* ALF LAMPRECHT,)

The emulsion is prepared by mixing 3 solutions. (See figure 1). Solution One contains a protective colloid, which is a polymer with at least one anionic functional group and is prepared to act as the vehicle for the emulsion. Method one uses poly(styrene-alt-maleic anhydride) (p(SMA) or TA) as the colloid material. p(SMA) is commonly used because it is preferable to use a polymer with carboxylic groups. (USA Patent No. 7442410, 2008) Adequate quantities of p(SMA), usually 1.5-2.5 %wt with respect to the core material. In method one, 2.5g of p(SMA) was dissolved in 57.5g of water. Solution Two is the suspension fluid. TDI and polypropylene glycol are dissolved in the core component material at a temperature 5˚C higher than the melting point of the core material. The

melting temperature of n-octadecane, is 28˚C, therefore the monomers in method one are dissolved at 33˚C.

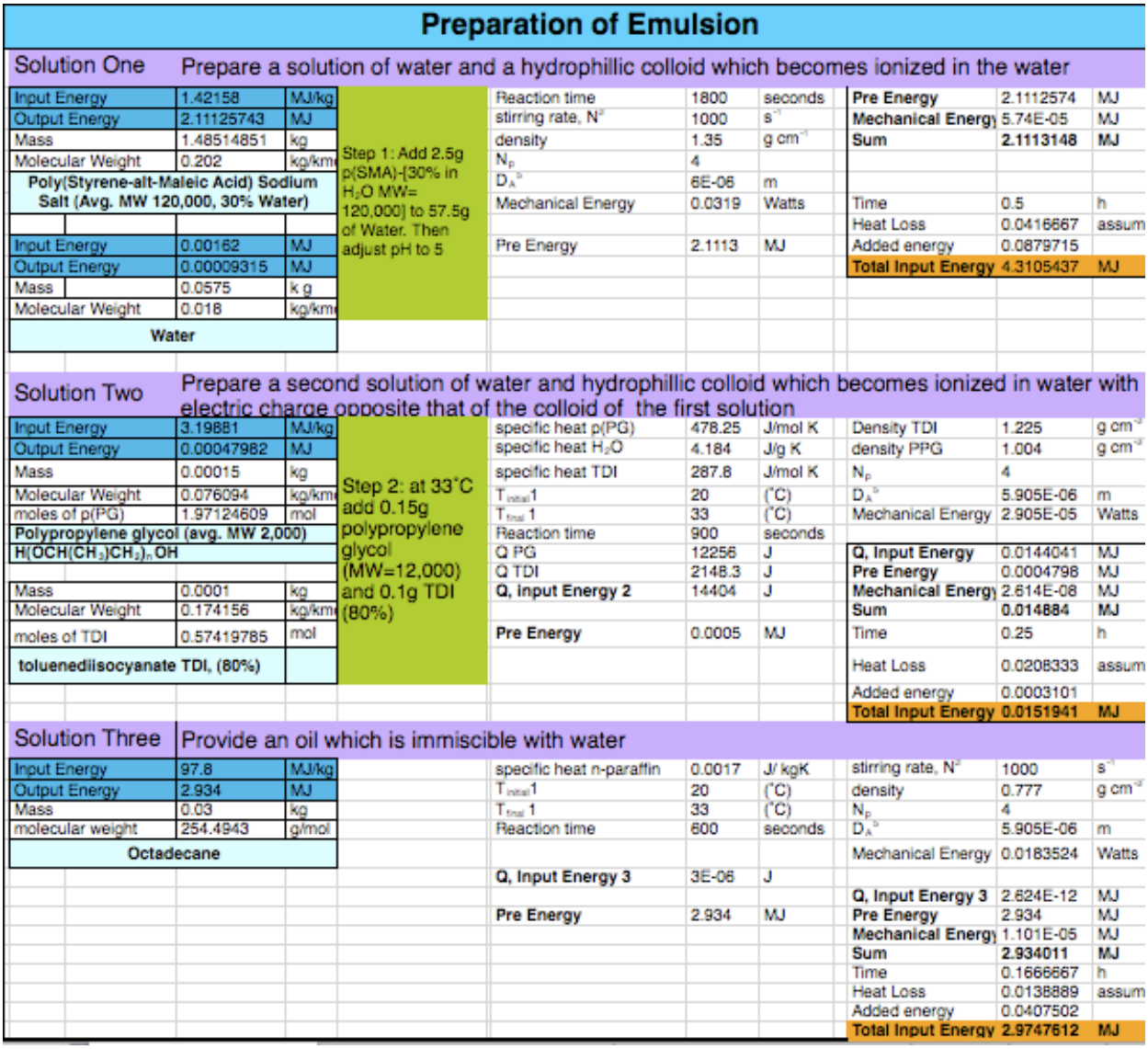

Preparation of Emulsion

Solution One — Prepare a solution of water and a hydrophillic colloid which becomes ionized in the water

Input Energy	1.42158	MJ/kg
Output Energy	2.11125743	MJ
Mass	1.48514851	kg
Molecular Weight	0.202	kg/km
Poly(Styrene-alt-Maleic Acid) Sodium Salt (Avg. MW 120,000, 30% Water)		
Input Energy	0.00162	MJ
Output Energy	0.00009315	MJ
Mass	0.0575	k g
Molecular Weight	0.018	kg/km
Water		

Step 1: Add 2.5g p(SMA)-[30% in H_2O MW= 120,000] to 57.5g of Water. Then adjust pH to 5

Reaction time	1800	seconds	**Pre Energy**	2.1112574	MJ
stirring rate, N	1000	s^{-1}	**Mechanical Energy**	5.74E-05	MJ
density	1.35	g cm^{-3}	**Sum**	**2.1113148**	**MJ**
N_p	4				
D_A	6E-06	m			
Mechanical Energy	0.0319	Watts	Time	0.5	h
			Heat Loss	0.0416667	assum
Pre Energy	2.1113	MJ	Added energy	0.0879715	
			Total Input Energy	4.3105437	MJ

Solution Two — Prepare a second solution of water and hydrophillic colloid which becomes ionized in water with electric charge opposite that of the colloid of the first solution

Input Energy	3.19881	MJ/kg
Output Energy	0.00047982	MJ
Mass	0.00015	kg
Molecular Weight	0.076094	kg/km
moles of p(PG)	1.97124609	mol
Polypropylene glycol (avg. MW 2,000)		
$H(OCH(CH_3)CH_2)_nOH$		
Mass	0.0001	kg
Molecular Weight	0.174156	kg/km
moles of TDI	0.57419785	mol
toluenediisocyanate TDI, (80%)		

Step 2: at 33˚C add 0.15g polypropylene glycol (MW=12,000) and 0.1g TDI (80%)

specific heat p(PG)	478.25	J/mol K	Density TDI	1.225	g cm^{-3}
specific heat H_2O	4.184	J/g K	density PPG	1.004	g cm^{-3}
specific heat TDI	287.8	J/mol K	N_p	4	
$T_{initial}1$	20	(˚C)	D_A	5.905E-06	m
$T_{final}1$	33	(˚C)	Mechanical Energy	2.905E-05	Watts
Reaction time	900	seconds			
Q PG	12256	J	**Q, Input Energy**	0.0144041	MJ
Q TDI	2148.3	J	**Pre Energy**	0.0004798	MJ
Q, input Energy 2	14404	J	**Mechanical Energy**	2.614E-08	MJ
			Sum	**0.014884**	**MJ**
Pre Energy	0.0005	MJ	Time	0.25	h
			Heat Loss	0.0208333	assum
			Added energy	0.0003101	
			Total Input Energy	**0.0151941**	**MJ**

Solution Three — Provide an oil which is immiscible with water

Input Energy	97.8	MJ/kg
Output Energy	2.934	MJ
Mass	0.03	kg
molecular weight	254.4943	g/mol
Octadecane		

specific heat n-paraffin	0.0017	J/ kgK	stirring rate, N	1000	s^{-1}
$T_{initial}1$	20	(˚C)	density	0.777	g cm^{-3}
$T_{final}1$	33	(˚C)	N_p	4	
Reaction time	600	seconds	D_A	5.905E-06	m
			Mechanical Energy	0.0183524	Watts
Q, Input Energy 3	3E-06	J			
			Q, Input Energy 3	2.624E-12	MJ
Pre Energy	2.934	MJ	**Pre Energy**	2.934	MJ
			Mechanical Energy	1.101E-05	MJ
			Sum	**2.934011**	**MJ**
			Time	0.1666667	h
			Heat Loss	0.0138889	assum
			Added energy	0.0407502	
			Total Input Energy	**2.9747612**	**MJ**

Figure 1: Preparation of Emulsion in Method One.

The first solution is dispersed into the second solution at 33˚C to form the emulsion mixture and droplets of n-octadecane are slowly added. The emulsion is stirred at a rate of 2000rpm for 10-15min to produce oil droplets of 4-5µm. The amount of energy to stir

and heat each solution to the designated temperature is quantified in figure 1 using equations (1), (2), and (3). (See figure 1 for table values for the emulsion mixture)

Preparation of Melamine-Formaldehyde Precondensate

Input Energy	0.81	MJ/kg		specific heat melamine	156.11	J/mol K	density (formaldehy	1.09	g cm^{-3}
Output Energy	0.002916	MJ		specific heat Formaldehyd	36.69	J/mol K	density (Melamine)	1.573	g cm^{-3}
Mass	0.0036	kg		specific heat H_2O	4.184	J/g K	stirring rate, N	1000	s^{-1}
Molecular Weight	0.03003	kg km	Step 1:. 2.5g of Melamine is added to 3.6g of 37% Formaldehyde solution and 5g of Water. At 70˚C, stir system at 600rpm for 1 hour.	$T_{initial}$1	20	(˚C)	N_p	4	
Moles of Formaldehyd	0.11988012	mol		T_{final} 1	70	(˚C)	D_A	5.905E-06	m
aq. Formaldehyde (35-39%)							Mechanical Energy	0.0371536	Watts
Input Energy	3.2	MJ/kg		Reaction time	5400	seconds	**Q, Input Energy**	0.0018605	MJ
Output Energy	0.008	MJ					**Mechanical Energy**	0.0002006	MJ
Mass	0.0025	kg					**Pre-Energy**	0.0109241	MJ
Molecular Weight	0.12612	kg km		Q1 Melamine	154.72	J			
moles of Melamine	0.01982239	mol		Q1 Formaldehyde	659.76	J	**Sum**	**0.0129852**	**MJ**
Melamine				Q1 Water	1046	J			
					=		Time	1.5	h
Input Energy	0.00162	MJ/kg		**Q, Input Energy**	1860.5	J	Heat Loss	0.0833333	assum
Output Energy	0.0000081	MJ					Added energy	0.0016232	MJ
Mass	0.005	kg	Step 2: Cool system to 33˚C	**Pre-Energy**	0.0109	MJ	**Total Input Energy**	**0.0146084**	**MJ**
Molecular Weight	0.018	kg/mo							
Water									

Figure 2: Preparation of Melamine-Formaldehyde Pre-Condensate for Method One

Mixing melamine, formaldehyde and water in a molar ratio of 1:3 forms the precondensate solution. The system is heated to 70˚C and stirred at 600rpm for an hour and a half to enhance the formation of the pre-condensate. (See figure 2 for values of energy input) The molar ratio of melamine to formaldehyde is important to microencapsulation. A low melamine ratio will cause the precondensate to be too hydrophilic, therefore a high molar ratio of melamine should be employed for satisfactory deposition of the precondensate onto the droplets of n-octadecane. (Xing, Li, & Newton, 2008)

Figure 3: Emulsification Step for Method One

Emulsification & Encapsulation			
Add n-Octadecane solution (solution 3) to p(SMA) solution (solution 2) at 31-33˚C. Stir system at 2,0000 rpm for 10-15 min	**Energy Pre-condensate**	0.014608365	MJ
	Energy solution One	4.310543698	MJ
	Energy solution Two	0.01519408	MJ
	Energy solution Three	2.974761164	MJ
	Reaction time	900	secon
	$T_{initial}$ 1	20	(˚C)
	T_{final} 1	33	(˚C)
	stirring rate, N^2	37037.03704	s^{-1}
	density	1.35	g cm^{-3}
	N_p	4	
	D_A^5	5.9049E-06	m
	Mechanical Energy	1.18098	Watts
	Pre-Energy Step 1	7.315107308	MJ
	Mechanical Energy	0.001062882	MJ
	Sum	**7.31617019**	**MJ**
	Time	0.25	h
	Heat Loss	0.020833333	assum
	Added energy	0.152420212	
	Total Input Energy	**7.468590402**	**MJ**
After 15 minutes decrease stir rate to 400-600 rpm	Reaction time	900	secon
	stirring rate, N^3	1000	s^{-1}
	density	1.35	g cm^{-3}
	N_p	4	
	D_A^5	5.9049E-06	m
	Mechanical Energy	0.03188646	Watts
	Mechanical Energy	2.86978E-05	MJ
	Sum	**2.86978E-05**	**MJ**
	Time	0.25	h
	Heat Loss	0.020833333	assum
	Added energy	5.97871E-07	
	Total Input Energy	**2.92957E-05**	**MJ**
	Total Emulsion Energy	7.468619698	MJ

During the emulsification step the prepared precondensate solution is stirred into the emulsion at a mild rate of 400-600rpm. It is important to not stir the mixture too vigorously to prevent hindering the deposition of the precondensate onto the oil droplets. The temperature of the encapsulation mixture is raised to 70-80˚C to facilitate the encapsulation process by initializing the condensation reaction for 1-5 hours. The amount of thermal energy added to heat the system to 80*C is quantified in figure 3. The amount of work put into the system to mechanically stir the emulsion was calculated in figure 3.

Drying and Hardening of Capsule Shell					
specific heat melamine	156.11	J/mol K	stirring rate, N	1000	s^{-1}
specific heat Formaldehyde	36.69	J/mol K	density	1.35	g cm^{-3}
specific heat H_2O	4.184	J/g K	N_p	4	
specific heat p(PG)	478.254519	J/mol K	D_A	5.9E-06	m
specific heat n-paraffin	1.712	J/g K	Mechanical Energy	0.03189	Watts
		J/mol K			
$T_{initial}$	33	°C			
T_{final}	80	°C	Emulsion Energy	7.46862	MJ
Reaction time	18000	sec	Mechanical Energy	0.00057	MJ
Total Mass			Input Energy	0.00241	MJ
Q n-paraffin	2413.92	J	**Sum**	**7.47161**	**MJ**
Q_{Total} Input Energy	0.00241392	MJ	Time	5	h
			Heat Loss	0.41667	assum
			Added energy	3.11317	MJ
			Total Energy Consumed	**10.5848**	**MJ**

Figure 4: Encapsulation Step for Method One.

All emulsions are typically made in a stirred reactor. Mechanical stirring facilitates fluid motion and creates an environment that allows the core material (n-octadecane) when suspended in a continuous phase to undergo two types of forces, that act in opposite direction resulting in the formation of paraffin droplets

Equation (2) and (3) were used to quantify the energy input for each step in the process. Assuming a closed system equation (1) was used to quantify the total amount of energy consumed for each step and the entire process. The heat energy (Q), mechanical energy (W), and pre-energy stemmed from the starting materials or previous step were summed together and the total amount of energy consumed from “Cradle to gate” (shown in figure 4) for method one was found to consume 11.0897 MJ to produce 30g of mPCM.

c. Process 2

The second microencapsulation method analyzed in this paper uses the insitu polymerization as the complex coacervation technique to prepare microcapsules of n-octadecane using a urea-melamine-formaldehyde copolymer as the shell of the capsule.(Xing-Xiang Zhang, 2004)

Preparation of Urea-Melamine-Formaldehyde Pre-Polymer

Input Energy	0.81	MJ/kg
Output Energy	6.422E-06	MJ
Volume	19.5	mL
Molecular Weight	0.03003	kg kmol^{-1}
Moles of Formaldehyd	0.000264	kmol
aq. Formaldehyde (35-39%)		
Input Energy	3.2	MJ/kg
Output Energy	0.0224	MJ
Mass	0.007	kg
Molecular Weight	0.12612	kg kmol^{-1}
moles of Melamine	0.056	mol
Melamine		
Input Energy	0.00162	MJ/kg
Output Energy	0.0000324	MJ
Volume	20	mL
Mass	0.02	kg
Molecular Weight	0.018	kg/mol
Water		
Input Energy	9.202	MJ/kg
Output Energy	0.0130668	MJ
Mass	0.00142	kg
Molecular Weight	0.0591667	kg kmol-1
mole	0.024	mol
Urea		

Mixture was prepared by mixing 19.5mL of formaldehyde, 7 g of Melamine, 1.42g of Urea, and 20 mL of Water.

The pH of the mixture was adjusted to 8-8.5 with Triethanolamine and stirred at 65˚C

specific heat melamine	156.11	J/mol K
specific heat Formaldehyd	36.69	J/mol K
specific heat H_2O	4.184	J/g K
specific heat urea	13900	J/mol K
$T_{initial}$ 1	20	(˚C)
T_{final} 1	65	(˚C)
Reaction time	1800	seconds
Q1 Melamine	314.72	J
Q1 Formaldehyde	1.3076	J
Q1 Water	3765.6	J
Q1 Urea	3002.4	J
	=	
Q, Input Energy	7084	J
Pre-Energy	0.0355	MJ
Volume Ratio		
Urea	0.2	
Melamine	0.8	
Formaldehyde	3	

density (formaldehyde)	1.09	g cm^3
density (Melamine)	1.573	g cm^3
density (Urea)	1.335	g cm3
stirring rate, N^3	1000	s^{-1}
N_p	4	
D_A^{5}	5.905E-06	m
Mechanical Energy	0.0371536	Watts
Q, Input Energy	0.007084	MJ
Mechanical Energy	6.688E-05	MJ
Pre-Energy	0.0355057	MJ
Sum	**0.0426566**	**MJ**
Time	0.5	h
Heat Loss	0.0833333	assum
Added energy	0.0017774	MJ
Total Pre-polymer Ene	**0.0444339**	**MJ**

Figure 5: Preparation of Urea-Melamine-Formaldehyde Pre-Polymer For Method Two

The pre-polymer solution consists of the copolymer urea-melamine-formaldehyde in a molar ratio of 0.2:0.8:3. It was prepared by mixing g of Urea, 19.5mL of formaldehyde (37%), 7g of melamine and 20mL of distilled water. The pH of this pre-polymer solution was adjusted to 8.5 by adding triethanolamine and stirred at 65˚C until the suspension became transparent.

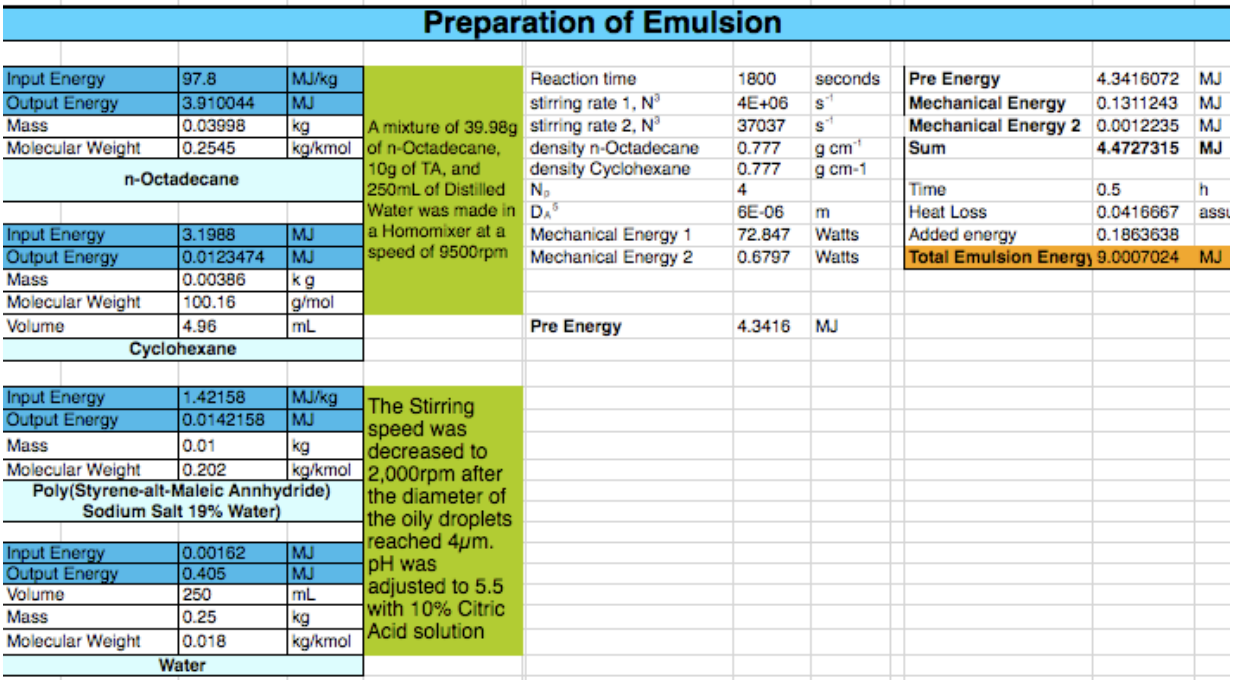

Preparation of Emulsion

Input Energy	97.8	MJ/kg
Output Energy	3.910044	MJ
Mass	0.03998	kg
Molecular Weight	0.2545	kg/kmol
n-Octadecane		
Input Energy	3.1988	MJ
Output Energy	0.0123474	MJ
Mass	0.00386	k g
Molecular Weight	100.16	g/mol
Volume	4.96	mL
Cyclohexane		
Input Energy	1.42158	MJ/kg
Output Energy	0.0142158	MJ
Mass	0.01	kg
Molecular Weight	0.202	kg/kmol
Poly(Styrene-alt-Maleic Annhydride) Sodium Salt 19% Water)		
Input Energy	0.00162	MJ
Output Energy	0.405	MJ
Volume	250	mL
Mass	0.25	kg
Molecular Weight	0.018	kg/kmol
Water		

A mixture of 39.98g of n-Octadecane, 10g of TA, and 250mL of Distilled Water was made in a Homomixer at a speed of 9500rpm

The Stirring speed was decreased to 2,000rpm after the diameter of the oily droplets reached 4μm. pH was adjusted to 5.5 with 10% Citric Acid solution

Reaction time	1800	seconds
stirring rate 1, N^3	4E+06	s^{-1}
stirring rate 2, N^3	37037	s^{-1}
density n-Octadecane	0.777	g cm^{-1}
density Cyclohexane	0.777	g cm-1
N_0	4	
D_A^5	6E-06	m
Mechanical Energy 1	72.847	Watts
Mechanical Energy 2	0.6797	Watts
Pre Energy	4.3416	MJ

Pre Energy	4.3416072	MJ
Mechanical Energy	0.1311243	MJ
Mechanical Energy 2	0.0012235	MJ
Sum	**4.4727315**	**MJ**
Time	0.5	h
Heat Loss	0.0416667	ass
Added energy	0.1863638	
Total Emulsion Energy	9.0007024	MJ

Figure 6: Preparation of Emulsion for Method Two.

The phase change material to be used as the core material was prepared by mixing 39.98g of n-octadecane, 3.86g of cyclohexane at a volume ratio of 91.2:8.8, 10g of poly(styrene-alt-maleic anhydride) (pSMA) was added as an emulsifier to 250 mL of distilled water to form an aqueous dispersant solution.

Emulsification & Microencapsulation			
	Energy Pre-polymer	0.04443392	MJ
	Energy Emulsion	9.00070243	MJ
The pre-polymer solution is added to the emulsion in droplets, while the emulsion was stirred at a speed of 2000rpm	***Mass of Mixture***	*40*	*g*
	Specific heat n-octadeca	*224*	*J/g*
	Q, Emulsion	*0.00896*	*MJ*
	Reaction time	10800	seconds
	$T_{initial}$ 1	65	(˚C)
	T_{final} 1	65	(˚C)
	stirring rate, N^3	37037.03704	s^{-1}
	density of UMF pre-polym	1.38	g cm^3
	N_p	4	
	D_A^5	5.9049E-06	m
	Mechanical Energy 1	1.207224	Watts
After all the pre-polymer is added. The emulsion is stirred for a further 2 hours	Reaction time	5400	seconds
	stirring rate, N^3	37037.03704	s^{-1}
	density	0.777	g cm^3
	N_p	4	
	D_A^5	5.9049E-06	m
	Mechanical Energy 2	0.6797196	Watts
The pH of the emulsion was adjusted to 9 with 50% wt Triethanolamine solution. The emulsion was cooled to 25˚C, filtered and washed with distilled water	**Pre-Energy Step 1**	9.04513635	MJ
	Mechanical Energy 1	0.013038019	MJ
	Mechanical Energy 2	0.003670486	MJ
	Sum	**9.058174369**	**MJ**
	Time	3	h
	Heat Loss	0.083333333	assume
	Added energy	2.264543592	
	Total Input Energy	**11.32271796**	**MJ**

Figure 7: Emulsification Step for Method Two.

The emulsifier solution was added to the phase change material solution in a homomixer and stirred at a speed of 9500rpm to make an emulsion. Once the diameters of the oily droplets were smaller than 4µm, and the stirring speed was decreased to 2000 rpm and the pH was adjusted to 5.5 with 10-wt% solution of citric acid. The cyclohexane inside the microcapsule was removed after drying the microcapsules are heat-treated for 30 min at 160˚C in a vacuum oven.

Drying and Hardening of Capsule Shell							
The cyclohexane was removed from inside the microcapsule by heat treating the capsules at 160˚C for 30 minutes inside a vaccum oven untill constant weight was achieved	ΔvapH Cyclohexane	32	kJ/mol	Q heat treatment	0.16649	MJ	
	mol cyclohexane	0.0385	mol	Emulsion Energy	11.3227	MJ	
	$T_{initial}$	25	˚C	SUM	11.489	MJ	
	$T_{final\ 3}$	160	˚C				
				Time	0.5	h	
	Reaction time	1800		Heat Loss	0.041667	assu	
				Added energy	0.478717	MJ	
	Q heat treatment	166.49	kJ	Total Energy Consumed	11.96792	MJ	
	Emulsion Energy	11.323	MJ				

Figure 8: Removal of Cyclohexane for Method 2.

The same equations and same assumptions used in method one to quantify the total amount of energy consumed was used in method two. As shown in Figure 8, the amount of energy used to produce approximately 40 g of mPCM was 12.96374 MJ.

d. Process 3

The third method this paper refers to is described in the paper Mechanism of microencapsulation with Urea Formaldehyde polymer. (Rochmadi & Wahyu, 2010)This method prepares mPCM through insitu-polymerization using a two-step method.

aq. Formaldehyde (35-39%)		
Input Energy	0.81	MJ/kg
Output Energy	0.1672	MJ
Mass	0.20642	kg
Molecular Weight	0.03003	kg mol^{-1}
Mol	0.11988	mol

Urea		
Input Energy	9.202	MJ/kg
Output Energy	1.10424	MJ
Mass	0.12	kg
Molecular Weight	0.12612	kg mol^{-1}
mole	0.95147	mol

Water		
Input Energy	0.00162	MJ/kg
Output Energy	0.00081	MJ
Mass	0.5	kg
Molecular Weight	0.018	kg/mol

Pre-polymer					
specific heat urea	13900	J/mol K	density (formaldehyde	1.09	g cm^{3}
specific heat Formaldehyde	36.69	J/mol K	density (Urea)	1.335	g cm^{3}
specific heat H_2O	4.184	J/g K	stirring rate, N^{3}	1000	s^{-1}
$T_{initial}$ 1	20	(˚C)	N_p	4	
T_{final} 1	70	(˚C)	D_A^{5}	6E-06	m
Reaction time	3600	second	Mechanical Energy	0.032	Watts
Q Formaldehyde	219.9	J	Q, Input Energy	0.766	MJ
Q Urea	7E+05	J	Mechanical Energy	1E-04	MJ
Q Water	1E+05	J	Pre-Energy	1.271	MJ
	=		Sum	2.038	MJ
Q_{tot} Input Energy 1	8E+05	J			
			Time	1	h
Pre Energy	1.271	MJ	Heat Loss	0.083	assu me
			Added energy	0.17	MJ
			Total Input Energy	2.207	MJ

Figure 9: Preparation of the Pre-polymer for Method 3.

In the first step a high rotation speed homogenizer is used as a stirrer to disperse and emulsify g of n-octadecane in a Urea-Formaldehyde resin. The Urea-formaldehyde resin was prepared in basic conditions to promote a soluble methylol urea. 120g of Urea and 225mL of 37% Formaldehyde were mixed together in a three neck flask, equipped with a mechanical stirrer, reflux condenser and water bath. Adding 1M NaOH adjusted the pH of the solution to 8-8.5. The system was heated to and maintained at 70˚C for 1 hour. After an hour the solution was cooled and diluted to a concentration of 042g/mL with 500mL of distilled water.

Emulsion Step

Octadecane		
Input Energy	97.8	MJ/kg
Output Energy	3.1916	MJ
Mass	0.0326	kg
molecular weight	0.2545	kg/kmol

Distilled Water 2		
Input Energy	0.0016	MJ
Output Energy	0.0003	MJ
Mass	0.2143	k g
Molecular Weight	0.018	kg/mol

Urea-Formaldehyde Resin (Step 1)		
Volume of Solution	150	mL
UF Resin Conc.	0.42	g/mL

UF Resin Conc.	0.00042	kg/mL	stirring rate, N^3	1.8E+07	s^{-1}
UF Pre-polymer Soln	0.000294	kg/mL	density UF pre-polymer	1.38	g cm^3
mass octadecane	0.032634	kg	N_s	4	
Mass UF Pre-polymer Solution	0.063	kg	D_s^3	5.9E-06	m
Volume of Distilled Water	214.2657143	mL	**Mechanical Energy**	572.891	Watts
Total Mass	0.095634	kg			
Specific Heat, paraffin	0.001712	J/kgK	**Q, input energy**	8.2E-09	MJ
Reaction time	900	secon	**Mechanical Energy**	0.5156	MJ
$T_{ins}1$	20	(˚C)	**Pre-Energy, Step 1**	2.20745	MJ
$T_{sol}1$	70	(˚C)	**Pre-Energy water**	0.00035	MJ
Q, input energy	0.00818627	J	**Pre-Energy Octadecane**	3.19161	MJ
			Sum	**5.91501**	**MJ**
Pre-Energy, Step 1	2.207454434	MJ			
Pre-Energy water	0.000347143	MJ	Time	0.25	h
Pre-Energy Octadecane	3.1916052	MJ	Heat Loss	0.02063	
			Added energy	0.12323	
			Total Input Energy	**6.03824**	**MJ**

Figure 10: Emulsion Step for Method Three.

Before the Urea-formaldehyde resin and the n-octadecane was heated in a water bath to 50-70˚C and emulsified together in a homomixer at a rotation speed of 15600 rpm. After 50 minutes of stirring the homogenizer is replaced with a helical-type stirrer.

Microcapsule Shell Formation					
$T_{emulsion}$	70	(˚C)	stirring rate, N^3	4.62963	s^{-1}
T_{final}	25	(˚C)	density, pre-polymer	1.38	g cm^{-3}
Specific Heat, paraffin	0.00171	J/kgK	N_p	4	
Reaction time	21600	second	D_A^5	5.9E-06	m
Total Mass	0.09563	kg	**Mechanical Energy**	0.00015	Watts
Pre-energy, Step 2	6.03824	MJ	**Pre-energy, Step 2**	6.03824	MJ
			Mechanical Energy	3.3E-06	MJ
			Sum	**6.03824**	**MJ**
			Time	6	h
			Heat Loss	0.5	
			Added energy	3.01912	MJ
			Total Input Energy	**9.05736**	**MJ**

Figure 11: Microcapsule Shell Formation for Method 3.

The shell of the microcapsule is formed in step two. During this step, a 10% citric acid solution is added to adjust the pH to 3. Low pH (acidic conditions) is necessary to facilitate the reaction of urea with formaldehyde. The helical stirrers are set at a stirring speed of 100rpm and this process was run for 3-6 hours at a constant temperature. After the 3-6 hours the capsules are cooled for an hour. The product is then filtered with distilled water and then dried at 40˚C.

Filter and dry at 40˚C						Dry in Oven at 100˚C					
$T_{initial}$	25	(˚C)	**Pre-energy, step 3**	9.057361337	MJ	$T_{initial}$	40	(˚C)	**Q n-paraffin**	0.0098	MJ
T_{final}	40	(˚C)	**Q Input Energy**	0.002455881	MJ	T_{final}	100	(˚C)	**pre-energy, step 4**	9.8148	MJ
Reaction time	3600	sec	**Sum**	**9.059817218**	**MJ**	C_p paraffin	1.712	J/gK	**Sum**	**9.8246**	**MJ**
C_p n-octadecane[2]	1.71	J/g K				Total Mass	95.63	g	Time	1	h
Total Mass	95.6	g	Time	1	h	**Q n-paraffin**	9824	J	Heat Loss	0.0833	assu
Q Input Energy	2456	J	Heat Loss	0.083333333					Added energy	0.8187	MJ
			Added energy	0.754984768	MJ	**pre-energy, step 4**	9.81	MJ	**Total Energy Consumed**	**10.64**	**MJ**
Pre-energy, step 3	9.06	MJ	**Total Input Consumed**	**9.81**	**MJ**						

Figure 12: Drying of Microcapsules for Method Three.

The same equations used to calculate energy in method 1 are used to calculate energy in method 2. The total energy consumed for to produce approximately 32 g of PCM using method 3 was 10.64 MJ.

e. Comparison

i. The results of this paper convey the three-encapsulation methods consume relatively the same amount of energy to encapsulate approximately 30-40g of n-octadecane. This verifies that all n-octadecane mPCMs have reasonably equivalent embodied energies. Therefore, provided that the mPCM of interest is n-octadecane, it can be assumed that the payback for integrating mPCM into gypsum wallboard will be fairly the same no matter what microencapsulation process was used to manufacture the mPCM.

ii. Operational Inputs. (Niraj)

a. Operational energy of mPCM embedded into gypsum wallboard.

IV. Discussion

a. Summary of results

Method	Total Energy Consumed		Mass of PCM	
1	10.585	MJ	30	g
2	11.968	MJ	39.98	g

3	10.64	MJ	32.6	g
Average	11.06433333	MJ	34.19333333	g

Table 1: Final Energy Consumed for all three Methods

The results of this study demonstrate that the embodied energy of all the starting materials, except n-octadecane, contribute very little to the final value of energy used. Therefore, we can assume that altering the starting chemicals, besides n-octadecane, will not have a significant effect on the final value of energy consumed. Future research may entail studying natural polymers as an alternate to synthetic polymers, as a way to develop a more sustainable process.

The findings of this study also imply that the emulsion step and the duration of the emulsion step is the significant driver of energy use in the microencapsulation process. A way to reduce energy use would be to reduce the length of time the emulsion step is carried out.

b. Analysis of payback period

The Athena Software determined that the embedded energy of a 12’ by 12’ block of gypsum is 5 MJ per ft^2. The average mass of PCM of the three microencapsulation methods was 34.19g of n-octadecane. Assuming 34.19g of PCM requires 11.0643MJ. Which corresponds to 30% PCM and 70% gypsum by volume, that is 64.94MJ per ft^2.

Using PCMs density of 0.6g/cm^3 200.6g of PCM is used in 12ft gypsum drywall. To produce 200g of PCM, it will take 69 MJ of energy to make a 12" by 12" block of gypsum-PCM drywall. Thus, the added embedded energy due to the added PCM is about 69 – 1.5 = 67.5MJ. Provided that the latent heat of fusion PCM is 151 kJ/kg, which would be 100% efficiency performance and the PCM is activated 200 days per year. Based on a PCM-enhanced 12' by 12' block of gypsum figures it was estimated the pay back would be 10.75 years.

Based on a PCM-enhanced 12'ft by 12' ft. block of gypsum drywall with 30% PCM and 70% gypsum by volume it was found it would take ~69.0 MJ of energy to produce 200g of mPCM. Provided that the latent heat of fusion PCM is 151 kJ/kg, which would be 100% efficiency performance and the PCM is activated 200 days per year it was estimated the payback would be around 10.75 years.

Acknowledgements

Thank you to my advisor, Dr. Vincent Blouin and my group members Niraj Poudel, and Celia Cui Wong.

References

(Davis, Hart, Work, & Virgallito, 2004)

(Goleman, 2009)

(Gracia, et al., 2010)

(Puel, Briancon, & Fessi, 2006)

(Rochmadi & Wahyu, 2010)

(U.S. Department of Energy , 2009

(U.S. Life-Cycle Inventory Database, 2010)

(Xing, Li, & Newton, 2008)

(Xing-Xiang Zhang, 2004)

Chapter 11 : Appendix

Appendix I: From figure 1.1 (1.1.4)

Buildings Energy Data Book: 1.1 Buildings Sector Energy Consumption *March 2012*

1.1.4 2010 U.S. Buildings Energy End-Use Splits, by Fuel Type (Quadrillion Btu)

	Natural Gas	Fuel Oil (1)	LPG	Other Fuel(2)	Renw. En.(3)	*Site* Electric	*Site* Total	*Site* Percent	Primary Electric (4)	Primary Total	Primary Percent
Space Heating (5)	5.14	0.76	0.30	0.10	0.54	0.72	7.56	37.0%	2.24	9.07	22.5%
Space Cooling	0.04					1.92	1.96	9.6%	5.94	5.98	14.8%
Lighting						1.88	1.88	9.2%	5.82	5.82	14.4%
Water Heating	1.73	0.13	0.07		0.04	0.54	2.51	12.3%	1.67	3.63	9.0%
Refrigeration (6)						0.84	0.84	4.1%	2.62	2.62	6.5%
Electronics (7)						0.81	0.81	3.9%	2.49	2.49	6.2%
Ventilation (8)						0.54	0.54	2.6%	1.66	1.66	4.1%
Computers						0.38	0.38	1.9%	1.19	1.19	2.9%
Cooking	0.39		0.03			0.21	0.63	3.1%	0.64	1.06	2.6%
Wet Cleaning (9)	0.06					0.33	0.38	1.9%	1.01	1.06	2.6%
Other (10)	0.30	0.01	0.30	0.05	0.02	0.89	1.58	7.7%	2.76	3.45	8.6%
Adjust to SEDS (11)	0.68	0.25				0.44	1.37	6.7%	1.35	2.28	5.7%
Total	**8.35**	**1.14**	**0.70**	**0.15**	**0.59**	**9.49**	**20.43**	100%	**29.39**	**40.33**	100%

Note(s): 1) Includes distillate fuel oil (1.06 quad) and residual fuel oil (0.08 quad). 2) Kerosene (0.04 quad) and coal (0.07 quad) are assumed attributable to space heating. Motor gasoline (0.05 quad) assumed attributable to other end-uses. 3) Comprised of wood space heating (0.42 quad), biomass (0.11), solar water heating (0.04 quad), geothermal space heating (less than 0.01 quad), solar photovoltaics (PV) less than 0.02 quad), and wind (less than 0.01 quad). 4) Site-to-source electricity conversion (due to generation and transmission losses) = 3.10. 5) Includes furnace fans (0.42 quad). 6) Includes refrigerators (2.36 quad) and freezers (0.26 quad). Includes commercial refrigeration. 7) Includes color television (1.02 quad) and other office equipment (0.81 quad). 8) Commercial only; residential fan and pump energy use included proportionately in space heating and cooling. 9) Includes clothes washers (0.10 quad), natural gas clothes dryers (0.06 quad), electric clothes dryers (0.60 quad) and dishwashers (0.31 quad). Does not include water heating energy. 10) Includes residential small electric devices, heating elements, motors, swimming pool heaters, hot tub heaters, outdoor grills, and natural gas outdoor lighting. Includes commercial service station equipment, ATMs, telecommunications equipment, medical equipment, pumps, emergency electric generators, combined heat and power in commercial buildings, and manufacturing performed in commercial buildings. 11) Energy adjustment EIA uses to relieve discrepancies between data sources. Energy attributable to the residential and commercial buildings sector, but not directly to specific end-uses.

Source(s): EIA, Annual Energy Outlook 2012 Early Release, Jan. 2012, Summary Reference Case Tables, Tables A2, Table A4, Table A5, and Table A17; EIA, National Energy Modeling System (NEMS) for AEO 2012 Early Release, Jan. 2012; EIA, Supplement to the Annual Energy Outlook 2012 Early Release, Jan. 2012, Table 32; BTS/A.D. Little, Electricity Consumption by Small End-Uses in Residential Buildings, Aug. 1998, Appendix A for residential electric end-uses; BTS/A.D. Little, Energy Consumption Characteristics of Commercial Building HVAC Systems, Volume II: Thermal Distribution, Auxiliary Equipment, and Ventilation, Oct. 1999, p. 1-2 and 5-25 - 5-26; EIA, Annual Energy Outlook 1998, Dec. 1997, Table A5, p. 108-109 for 1995 ventilation; and BTP/Navigant Consulting, U.S. Lighting Market Characterization, Volume I, Sept. 2002, Table 8-2, p. 63.